

**STUDIES ON TRANSITION METAL CHELATES OF
SOME TRIDENTATE AROYLHYDRAZONES**

*Thesis submitted to
Cochin University of Science and Technology
in partial fulfillment of the requirements
for the award of the degree of
Doctor of Philosophy
Under the Faculty of Science*

by

BIBITHA JOSEPH



**Department of Applied Chemistry
Cochin University of Science and Technology
Kochi 682 022**

November 2014

Studies on Transition Metal Chelates of some Tridentate Aroylhydrazones

Ph. D. Thesis under the Faculty of Science

Author:

Bibitha Joseph

Research Fellow, Department of Applied Chemistry

Cochin University of Science and Technology

Kochi 682 022

India

Email: bibithajosephbj@gmail.com

Research Advisor:

Dr. M.R. Prathapachandra Kurup

Professor

Department of Applied Chemistry

Cochin University of Science and Technology

Kochi 682 022

India

Email: mrp@cusat.ac.in

Department of Applied Chemistry

Cochin University of Science and Technology

Kochi 682 022

India

November 2014

Front cover: Molecular structure of $[\text{NiL}^1(\text{H}_2\text{O})_2]_2$

*“My God is my protection,
and with him I am safe.”*

(2 Samuel 22:3)



To Holy Mother Mary.....



Phone Off. 0484-2862423
Phone Res. 0484-2576904
Telex: 885-5019 CUIIN
Fax: 0484-2577595
Email: mrp@cusat.ac.in
mrp_k@yahoo.com

Department of Applied Chemistry
Cochin University of Science and Technology
Kochi 682 022, India

Dr. M.R. Prathapachandra Kurup
Professor

20-11-2014

Certificate

*This is to certify that the thesis entitled “**Studies on Transition Metal Chelates of some Tridentate Aroylhydrazones**” submitted by **Ms. Bibitha Joseph**, in partial fulfillment of the requirements for the degree of Doctor of Philosophy, to the Cochin University of Science and Technology, Kochi-22, is an authentic record of the original research work carried out by her under my guidance and supervision. The results embodied in this thesis, in full or in part, have not been submitted for the award of any other degree. All the relevant corrections and modifications suggested by the audience and recommended by the doctoral committee of the candidate during the presynopsis seminar have been incorporated in the thesis.*

M.R. Prathapachandra Kurup
(Supervisor)

Declaration

I hereby declare that the work presented in this thesis entitled “**Studies on Transition Metal Chelates of some Tridentate Aroylhydrazones**” is entirely original and was carried out independently under the supervision of **Prof. M.R. Prathapachandra Kurup**, Department of Applied Chemistry, Cochin University of Science and Technology and has not been included in any other thesis submitted previously for the award of any other degree.

20-11-2014
Kochi-22

Bibitha Joseph

Acknowledgement

First and foremost, I thank God Almighty for the blessings He has bestowed upon me and for giving me the strength and wisdom to achieve this dream. I thank Holy Mother Mary and all saints for solacing me when I was depressed and frustrated during the course of my studies. It is to their intercession I attribute my success.

This doctoral thesis is in its current form due to the assistance and encouragement of several people. It is a pleasure to express my sincere thanks to all those who helped me for the success of this study and made it an unforgettable experience. It has been a great privilege for me to work under the guidance of Prof. (Dr.) M.R. Prathapachandra Kurup, Department of Applied Chemistry, CUSAT. I express my heartfelt gratitude to my supervising guide Prof. (Dr.) M.R. Prathapachandra Kurup. Words are insufficient to appreciate my teacher for his whole hearted involvement, inspiration and constant support during the entire period of research work. I especially thank him for the exemplary guidance, monitoring, constant encouragement, understanding, care and empathy.

I express my sincere thanks to former Heads, Prof. K. Girish Kumar who is my doctoral committee member and Prof. K. Sreekumar for their encouragement and support. I am very much thankful to Dr. N. Manoj, Head, Department of Applied Chemistry, CUSAT for the support and cooperation during the period of this work. I am thankful for the support received from all the teaching and non-teaching staff of the Department of Applied Chemistry, CUSAT.

I am indebted to all the staff of SAIIF, Kochi, IIT Madras, IIT Bombay and IPC, IISc, Bangalore for the services rendered for sample analyses. I am thankful to the Council of Scientific and Industrial Research, New Delhi, India for the financial assistance.

I am grateful to Rev. Dr. Vincent Joseph, Principal, Nirmala College, Muvattupuzha for his support and encouragement. I place my special thanks to Sr. Celine George K.,

Head of the Department and all faculty members of the Department of Chemistry, Nirmala College, Muvattupuzha for their support and advice.

The working atmosphere in my research lab has been inspiring and enjoyable during all these years and I cannot imagine ever working in a nicer atmosphere than we had. Thank you all my friends in inorganic lab for all the unforgettable golden moments. I am grateful to my seniors, Dr. Seena E.B., Dr. Sheeja S.R., Dr. Binu Varghese, Dr. Reena T.A., Dr. Nancy Mathew, Dr. Neema Ani Mangalam and Dr. Renjusha S., who helped me a lot in the beginning years of my research. I thank from the depth of my heart the teacher fellows Dr. Jessy Emmanuel, Dr. Annie C.F., Dr. Marthakutty Joseph, Dr. Laly K. and Dr. K. Jayakumar for their valuable care, help and attention. My special thanks are due to Dr. Roji J. Kunnath and Dr. M. Sithambaresan for their valuable advices and fruitful discussions. Special word of gratitude to Dr. Jinsa Mary Jacob and Nisha for creating a good ambience to do the work and for clarifying my doubts. Thank you so much for your love, care and advices. My deep gratitude and sincere thanks to my junior lab mates, Ambili, Aiswarya, Mridula, Sreejith, Nithya, Vineetha, Sajitha, Lincy, Daly and Fousia for their support and love. I wish to express special thanks to Asokan sir, Yamuna miss, Vishnupriya, Anju and Reshma for their encouragement and help.

I am extremely fortunate to have such caring and loving parents, Mr. Joseph Mathew and Ms. Chinnamma Joseph. My dream of completing this work would not have been blossomed without their wholehearted support, sacrifice and prayers. They deserve special mention for providing me with all the opportunities to explore my potentials and pursue my dreams ever since I was a child. I thank God Almighty for blessing me with such affectionate parents.

With great pleasure, I would like to give special thanks to my soul mate Gilson for the mental strength, support, prayers, patience and encouragement throughout my research studies. His support and motivation helped me to become strong and capable to complete this thesis. My little daughter Isabel, the most precious gift in my life... I express my deep sense of love to you, my dear. Though not deliberately, she missed my love, care and affection during this period.

I express my sincere thanks to papa and mummy for their blessings, affection and support during my study. I am very much indebted to Bibin chetai, Sibi and Alexia for the love, confidence, encouragement and sustained support during this work. I also express my feeling of gratitude to Jasmine chechi, Bineetta and their family for their love, encouragement and prayers during my research period. My aunt also encouraged me a lot and showered her love and affection enabling me to complete this work successfully.

I am extremely grateful to all my teachers and well wishers. Finally, I would like to thank everybody who was behind the fulfillment of my thesis.

Above all, I praise God, the almighty for providing me this opportunity and granting me the capability to proceed successfully.

Bibitha Joseph

Preface

In recent years, the interest in coordination chemistry of aroylhydrazones has been increased due to their various binding modes towards transition metal ions and wide range of applications. Aroylhydrazones have been extensively investigated due to their chelating capabilities and pharmacological properties. They have recently been identified as molecules for nonlinear optics. There is currently a considerable effort to develop new materials with large nonlinear optical properties because they provide valuable information for the structural analyses and for their practical use in optoelectronic devices. Aroylhydrazones and their transition metal complexes are very promising compounds in this field and their crystal structures and spectral investigations are well desirable. In order to investigate the interesting coordinating properties of hydrazones, complexes with different types of ligand environments are essential. So in the present work we chose four different aroylhydrazones as principal ligands. Introduction of heterocyclic bases like 1,10-phenanthroline, 2,2'-bipyridine, pyridine and 3-picoline leads to the syntheses of mixed ligand complexes which can cause different bonding, spectral properties and geometries in coordination complexes. This thesis is an attempt to explore the chelating behavior and second order nonlinear optical properties of some ONO and ONN donor hydrazone systems.

The work embodied in this thesis was carried out by the author in the Department of Applied Chemistry, CUSAT, Kochi, during the period 2009-2014. The thesis is divided into nine chapters. Chapter 1 deals with the general introduction of aroylhydrazones, their coordination diversity and various applications. The objectives of the present work and the various physico-chemical techniques employed for the characterization of aroylhydrazones and their complexes are also included in this chapter. Chapter 2 describes the syntheses and characterization of four aroylhydrazones. Chapters 3-8 delineate

the syntheses and characterization of oxidovanadium(IV), cobalt(II), nickel(II), copper(II), zinc(II), cadmium(II) and dioxidomolybdenum(VI) complexes derived from the hydrazones under study. Chapter 9 portrays the second order nonlinear optical studies of synthesized aroylhydrazones and some of their transition metal complexes. A brief summary and conclusion of the work is also included in the last part of the thesis.

Contents

Chapter-1

A BRIEF OUTLINE ON AROYLHYDRAZONES.....	01 - 23
1.1 Introduction.....	01
1.2 Aroylhydrazones.....	02
1.3 Coordination diversity of aroylhydrazones.....	05
1.4 Applications of hydrazones.....	09
1.4.1 Hydrazones in nonlinear optics.....	09
1.4.2 Biological potential of hydrazones and their metal chelates.....	10
1.4.3 Analytical applications.....	12
1.4.4 Catalytic applications.....	13
1.5 Scope and objectives of the present work.....	13
1.6. Physical measurements.....	15
1.6.1 Elemental analyses.....	15
1.6.2 Conductivity measurements.....	16
1.6.3 Magnetic susceptibility measurements.....	16
1.6.4 Infrared spectroscopy.....	16
1.6.5 Electronic spectroscopy.....	16
1.6.6 Mass spectrometry.....	16
1.6.7 NMR spectroscopy.....	17
1.6.8 EPR spectroscopy.....	17
1.6.9 Thermogravimetric analyses.....	17
1.6.10 Single crystal X-ray diffraction studies.....	17
1.6.11 Second harmonic generation studies.....	18
References.....	19

Chapter-2

SYNTHESES, SPECTRAL CHARACTERIZATION AND CRYSTAL STRUCTURES OF SOME AROYLHYDRAZONES.....	25 - 70
2.1 Introduction.....	25
2.2 Experimental.....	27
2.2.1 Materials.....	27
2.2.2 Syntheses of aroylhydrazones.....	27
2.2.2.1 4-Benzyloxy-2-hydroxybenzaldehyde-4- nitrobenzoylhydrazone dimethylformamide monosolvate ($H_2L^1 \cdot C_3H_7NO$).....	28
2.2.2.2 5-Bromo-2-hydroxy-3-methoxybenzaldehyde nicotinoylhydrazone dihydrate methanol monosolvate ($H_2L^2 \cdot 2H_2O \cdot CH_3OH$).....	28

2.2.2.3	4-Diethylamino-2-hydroxybenzaldehyde nicotinoylhydrazone monohydrate ($H_2L^3 \cdot H_2O$)	29
2.2.2.4	2-Benzoylpyridine-4-nitrobenzoylhydrazone (HL^4)	30
2.3	Characterization of aroylhydrazones	30
2.3.1	Elemental analysis	30
2.3.2	Mass spectra	30
2.3.3	Infrared spectra	33
2.3.4	Electronic spectra	36
2.3.5	NMR spectral studies	37
2.3.6	X-ray Crystallography	42
2.3.6.1	Crystal structure of $H_2L^1 \cdot C_3H_7NO$	43
2.3.6.2	Crystal structure of $H_2L^2 \cdot 2H_2O \cdot CH_3OH$	50
2.3.6.3	Crystal structure of $H_2L^3 \cdot H_2O$	55
2.3.6.4	Crystal structure of HL^4	60
	References	67

Chapter-3

SYNTHESES AND SPECTRAL CHARACTERIZATION OF OXIDOVANADIUM(IV) CHELATES OF TRIDENTATE AROYLHYDRAZONES

		71 - 100
3.1	Introduction	71
3.2	Experimental	74
3.2.1	Materials	74
3.2.2	Syntheses of hydrazones	74
3.2.3	Syntheses of VO(IV) complexes	74
3.3	Results and discussion	77
3.3.1	Elemental analyses	78
3.3.2	Molar conductivity and magnetic susceptibility measurements	78
3.3.3	Infrared spectra	78
3.3.4	Electronic spectra	82
3.3.5	Electron paramagnetic resonance spectra	86
	References	98

Chapter-4

SYNTHESES AND SPECTRAL CHARACTERIZATION OF COBALT(II) CHELATES OF TRIDENTATE AROYLHYDRAZONES

		101 - 118
4.1	Introduction	101
4.2	Experimental	103
4.2.1	Materials	103
4.2.2	Syntheses of hydrazones	103
4.2.3	Syntheses of Co(II) complexes	104

4.3	Results and discussion	106
4.3.1	Elemental analyses	106
4.3.2	Molar conductivity and magnetic susceptibility measurements	106
4.3.3	Infrared spectra	107
4.3.4	Electronic spectra	110
4.3.5	Thermogravimetric analyses	113
	References	117

Chapter-5

SYNTHESES, SPECTRAL CHARACTERIZATION AND CRYSTAL STRUCTURE OF NICKEL(II) CHELATES OF TRIDENTATE AROYLHYDRAZONES		119 - 146
5.1	Introduction	119
5.2	Experimental	122
5.2.1	Materials	122
5.2.2	Syntheses of hydrazones	122
5.2.3	Syntheses of Ni(II) complexes	122
5.3	Results and discussion	124
5.3.1	Elemental analyses	125
5.3.2	Molar conductivity and magnetic susceptibility measurements	125
5.3.3	Infrared spectra	126
5.3.4	Electronic spectra	129
5.3.5	X-ray crystallography	132
5.3.6	Thermogravimetric analyses	140
	References	144

Chapter-6

SYNTHESES AND SPECTRAL CHARACTERIZATION OF COPPER(II) CHELATES OF TRIDENTATE AROYLHYDRAZONES		147 - 175
6.1	Introduction	147
6.2	Experimental	149
6.2.1	Materials	149
6.2.2	Syntheses of hydrazones	149
6.2.3	Syntheses of Cu(II) complexes	150
6.3	Results and discussion	152
6.3.1	Elemental analyses	152
6.3.2	Molar conductivity and magnetic susceptibility measurements	152
6.3.3	Infrared spectra	153
6.3.4	Electronic spectra	156
6.3.5	Electron paramagnetic resonance spectra	159
6.3.6	Thermogravimetric analysis	170
	References	173

Chapter-7

SYNTHESES, SPECTRAL CHARACTERIZATION AND CRYSTAL STRUCTURES OF ZINC(II) AND CADMIUM(II) CHELATES OF TRIDENTATE AROYLHYDRAZONES 177 - 211

7.1	Introduction.....	177
7.2	Experimental.....	179
7.2.1	Materials.....	179
7.2.2	Syntheses of hydrazones.....	180
7.2.3	Syntheses of Zn(II) complexes.....	180
7.2.4	Syntheses of Cd(II) complexes.....	182
7.3	Results and discussion.....	184
7.3.1	Elemental analyses.....	184
7.3.2	Molar conductivity measurements.....	184
7.3.3	Infrared spectra.....	185
7.3.4	Electronic spectra.....	189
7.3.5	X-ray crystallography.....	192
7.3.5.1	Crystal structure of [Zn(L ⁴) ₂]-0.5CH ₃ OH·0.5CH ₃ CH ₂ OH (27).....	193
7.3.5.2	Crystal structure of [Cd(HL ⁴)Br ₂]-C ₃ H ₇ NO (32).....	198
7.3.6	Thermogravimetric analyses.....	205
	References.....	209

Chapter-8

SYNTHESES, SPECTRAL CHARACTERIZATION AND CRYSTAL STRUCTURE OF DIOXIDOMOLYBDENUM(VI) CHELATES OF TRIDENTATE AROYLHYDRAZONES 213 - 234

8.1	Introduction.....	213
8.2	Experimental.....	215
8.2.1	Materials.....	215
8.2.2	Syntheses of hydrazones.....	215
8.2.3	Syntheses of MoO ₂ (VI) complexes.....	215
8.3	Results and discussion.....	217
8.3.1	Elemental analyses.....	217
8.3.2	Molar conductivity and magnetic susceptibility measurements.....	218
8.3.3	Infrared spectra.....	218
8.3.4	Electronic spectra.....	220
8.3.5	X-ray crystallography.....	221
8.3.6	Thermogravimetric analysis.....	230
	References.....	233

Chapter-9

**STUDIES ON SECOND ORDER NONLINEAR OPTICAL
PROPERTIES OF AROYLHYDRAZONES AND SOME**

TRANSITION METAL CHELATES 235 - 250

9.1	Introduction.....	235
9.1.1	Theoretical explanation of nonlinear optics.....	236
9.1.2	Second harmonic generation.....	238
9.1.3	Second order nonlinear optical materials.....	239
9.1.3.1	Design of molecules for second order nonlinear optics ...	239
9.1.3.2	Inorganic materials as second order NLO materials.....	242
9.1.3.3	Organic molecules as second order NLO materials.....	242
9.1.3.4	Hydrazones as second order NLO materials.....	243
9.1.4.	NLO measurements.....	245
9.2	Experimental.....	245
9.2.1	Syntheses of hydrazones.....	245
9.2.2	Syntheses of transition metal chelates.....	245
9.2.3	Second harmonic generation studies.....	245
9.3	Results and discussion.....	246
	Conclusion.....	247
	References.....	248

SUMMARY AND CONCLUSION..... 251 - 258

Abbreviation 259 - 260

A BRIEF OUTLINE ON AROYLHYDRAZONES

<i>Contents</i>	1.1	Introduction
	1.2	Aroylhydrazones
	1.3	Coordination diversity of aroylhydrazones
	1.4	Applications of hydrazones
	1.5	Scope and objectives of the present work
	1.6	Physical measurements
		References

1.1. Introduction

Alfred Werner received the Nobel Prize in Chemistry in 1913 for recognition of his work on the linkage of atoms in compounds by which he has thrown new insights on earlier investigations and opened up new fields of research especially in coordination chemistry. The chemistry of coordination compounds is an important and challenging area of modern inorganic chemistry. During the last fifty years, advances in this area have provided development of new concepts and models of bonding and molecular structure, novel breakthroughs in chemical industry and new insights into the functioning of critical components of biological systems. The living system is partially supported by coordination compounds. Chlorophyll, the pigment responsible for photosynthesis is a coordination compound of magnesium. Hemoglobin, the red pigment of blood which acts as oxygen carrier is a coordination

compound of iron. Coordination compounds also find extensive applications in metallurgical process, analytical and medicinal chemistry.

Coordination compounds can have a wide variety of structures depending on the metal ion, coordination number and denticity of the ligands used. Diverse coordination compounds arise from interesting ligand systems containing different donor sites. So the selection of ligands is most important in determining the properties of coordination compounds. A ligand system having electronegative atoms like nitrogen and oxygen increases the denticity and thus enhances the coordination possibilities. The architectural beauty of coordination compounds is due to the interesting ligand systems containing different donor sites say ONO, NNO, NO and NNS. Among the nitrogen-oxygen donor ligands, hydrazones possess a special place due to their ease of synthesis, easily tunable electronic properties, denticity and formation of wide variety of complexes with chemical, structural, biological and industrial importance [1-3].

1.2. Aroylhydrazones

Aroylhydrazones are a class of azomethines having the group $-C=N-N-$ and are widely employed as ligands in coordination chemistry. These ligands are readily available, versatile and can exhibit various denticities and functionalities depending on the nature of the starting materials employed for their preparation. Substituted hydrazones can be obtained by introducing substituted hydrazides and carbonyl compounds. General formula for a substituted aroylhydrazone is shown in Fig. 1.1.

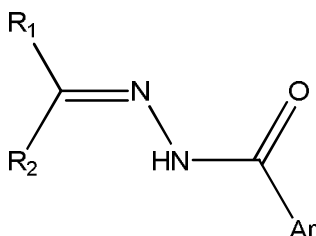


Fig. 1.1. General formula for a substituted aroylhydrazone.

A quick survey of the structure of a hydrazone (Fig. 1.2) reveals that it has (i) nucleophilic imine and amino-type nitrogens, (ii) an imine carbon that has both electrophilic and nucleophilic character, (iii) configurational isomerism stemming from the intrinsic nature of the C=N bond and (iv) in most cases an acidic N–H proton [4]. These structural motifs give the hydrazone group its physical and chemical properties, in addition to playing a crucial part in determining the range of applications it can be involved in.

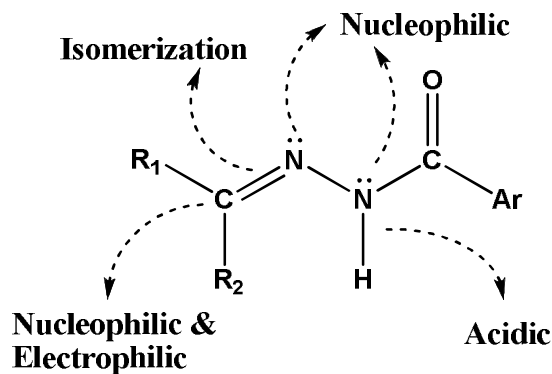


Fig. 1.2. The structural and functional diversity of the hydrazone group.

Hydrazones can be made by three main synthetic pathways, (i) coupling between aryl diazonium salts and β -keto esters or acids, which is also known as the Japp–Klingemann reaction [5], (ii) coupling between hydrazines and ketones or aldehydes [6] and (iii) coupling between aryl halides and non-

substituted hydrazones [7]. Aroyl hydrazones, which are easily formed by the condensation of aromatic hydrazides (aroylhydrazides) with carbonyl compounds are of special interest as ligands, as they offer a combination of amide oxygen and imine nitrogen as donor atoms, the imine nitrogen being involved in the formation of an N–N bond reminiscent of a doubly reduced azo functionality. The electron density of the amide oxygen and imine nitrogen involved in chelation can be controlled by protonation-deprotonation of the amide nitrogen.

Amido-iminol tautomerism occurs readily in hydrazones and has an important role in determining the overall charge on the ligands. Hydrazones generally exist in the amido form in the solid state but in solution they tend to exist as an equilibrium mixture of amido and iminol forms (Fig. 1.3). The amido-iminol equilibrium depends on the nature of the substituents present in the hydrazide moiety, pH of the medium used for reaction and the metal salts employed [8]. Hydrazones can bind to a metal center in the neutral amido or anionic iminolate forms. These ligands, due to their facile amido-iminol tautomerization and the availability of several potential donor sites depending on the nature of the substituents attached to the hydrazone unit, represent good polydentate chelating agents with interesting modes of ligation for a variety of metal ions.

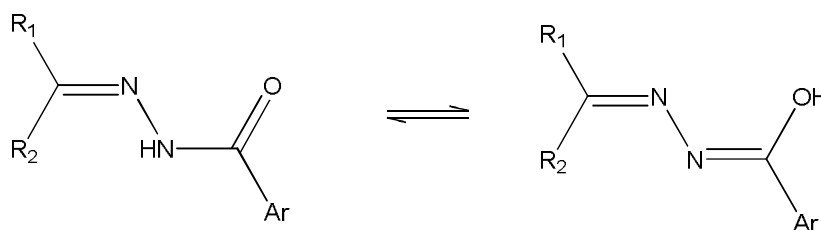
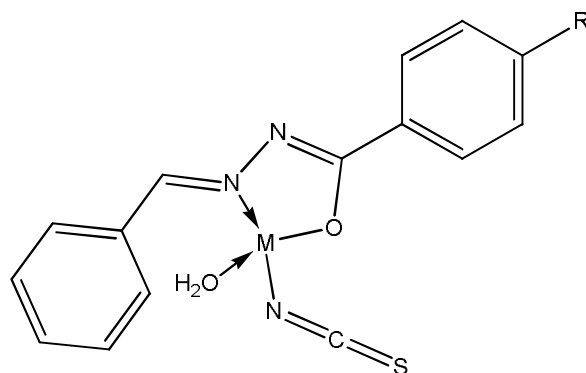


Fig. 1.3. Tautomerism in aroylhydrazones.

1.3. Coordination diversity of hydrazones

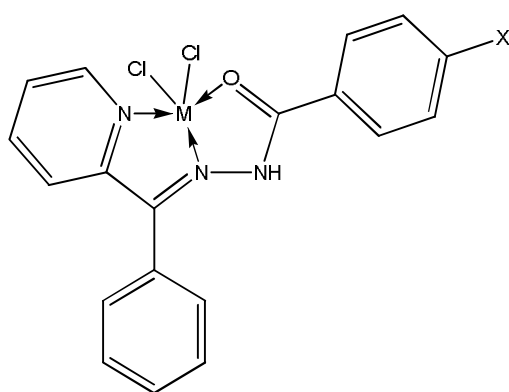
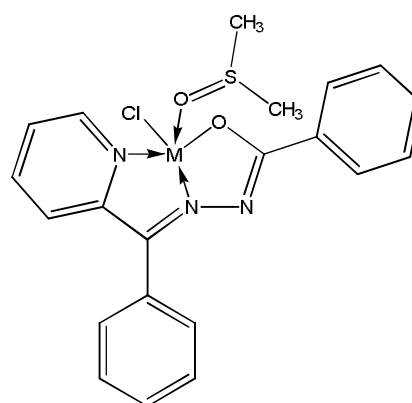
Hydrazones are versatile class of ligands which have been studied for a long time as potential multifunctional ligands with various coordination modes [9-11]. The coordination mode adopted by a hydrazone depends on different factors like tautomerism, reaction conditions, stability of the complex formed and number and nature of the substituents on hydrazone skeleton. Aroylhydrazones, in the absence of side chains with donor atoms are potentially bidentate ligands (Structure I) with the carbonyl O and the azomethine N as possible donor sites [12].



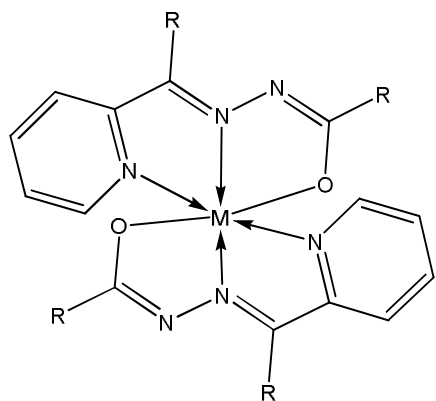
Structure I

Other donor sites may be provided by substituents on hydrazide part as well as on carbonyl part. When the heteroatom in the substituent coordinates to the metal centre, the hydrazone can behave as a tridentate ligand. Moreover, these ligands exhibit amido-iminol tautomerism and can coordinate in either neutral, monoanionic, dianionic or tetraanionic form bearing unusual coordination numbers such as six and seven in some mononuclear or binuclear species [13]. For example, if we take a hydrazone having a pyridine group on the carbonyl part, it can coordinate to the central metal by adopting an NNO coordination mode, either through neutral amido form (Structure II) or through the

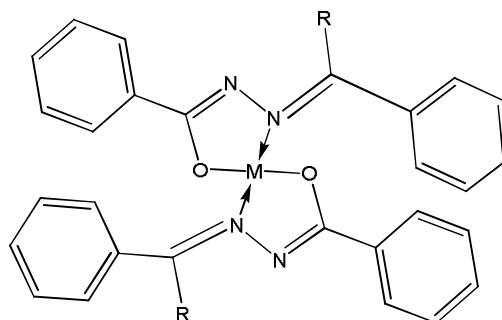
deprotonated iminolate form (Structure III) [14]. Usually in basic solution amide oxygen gets deprotonated and coordinates to the metal centre in the iminolate form where as strongly acidic condition favors compounds formulated with a neutral ligand [15,16]. The lengths of the N–C and C=O bonds are very important indicators of the type of coordination. When hydrazone based ligands coordinate to metal ions in the amido form, the lengths of the HN–C and C=O bonds are around 1.34 and 1.27 Å respectively [17] while their bond lengths in the iminolate form are about 1.28 and 1.34 Å respectively [18].

**Structure II****Structure III**

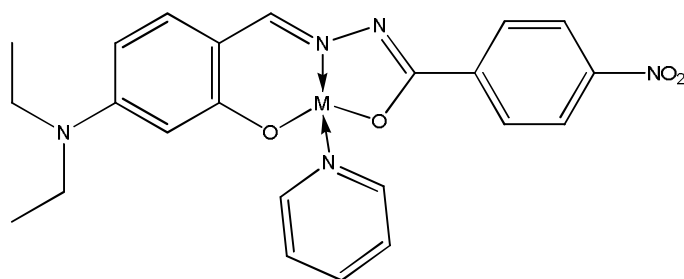
The structural changes of the segment attached to the hydrazone will affect the metal binding of the ligand and exhibit interesting coordination modes with transition metal ions to form octahedral, square planar and tetrahedral complexes (Structure IV-VI) [19-21].



Structure IV

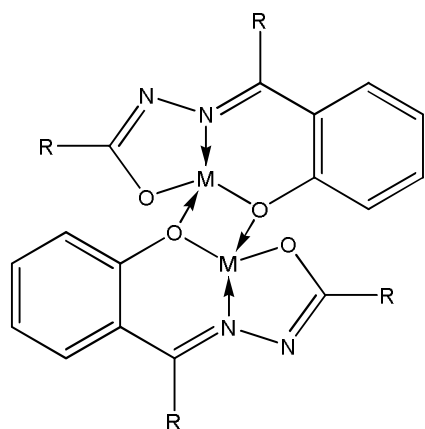


Structure V

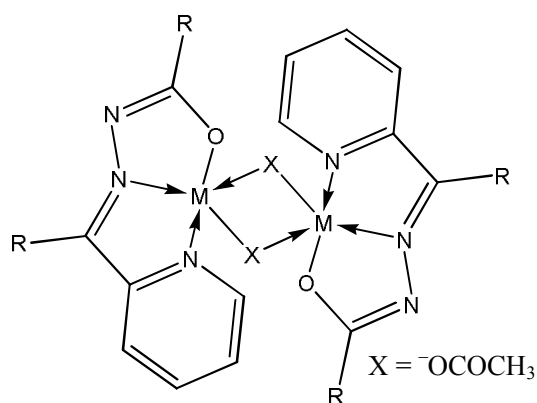


Structure VI

Sometimes hydrazones can form bridged complexes. If the tridentate ONO donor hydrazone possesses a phenolic group, the phenolate oxygen can form a bridge between the metal centers and thus forming dimeric complexes (Structure VII) [22]. Attractive bridging ligands like dicyanamide, azide, acetate ions etc. have attracted great attention in designing dinuclear transition metal complexes (Structure VIII) [23].

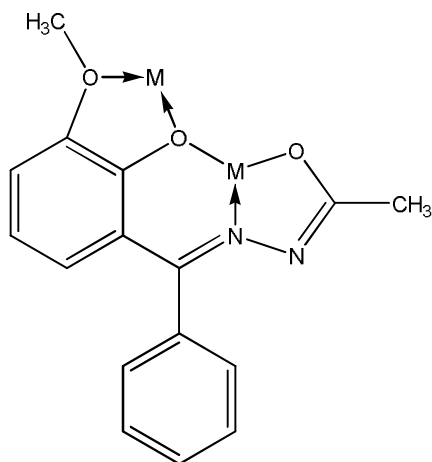


Structure VII



Structure VIII

If the hydrazone contains additional donor sites like $-OMe$ group, the dianionic hydrazone can act as a tetradentate ligand resulting in the formation of multinuclear complexes (Structure IX) [24]. There are cases in which hydrazones form coordination polymers [25]. The coordination modes of hydrazones are of much interest because of the existence of many potential donor sites.



Structure IX

1.4. Applications of hydrazones

The hydrazone functional group is ubiquitous in various fields ranging from organic synthesis, medicinal chemistry and nonlinear optics to supramolecular chemistry and has many applications. The modularity, straightforward synthesis and stability towards hydrolysis of hydrazones can be cited as reasons for their popularity. But in reality it is the functional diversity of this azomethine group which is characterized by the triatomic structure $C=N-N$, that enables its use in various fields.

1.4.1. Hydrazones in nonlinear optics

There is currently a considerable effort to develop new materials with large second order nonlinear optical susceptibilities because of their potential applications in optical signal processing, frequency conversion and in optoelectronics [26-28]. The phenomenon of optical power limiting, a nonlinear optical effect, is interesting due to its application to the protection of eyes and sensitive optical devices from high power laser pulses. Hydrazones have revealed to be an important class of organic crystalline materials exhibiting good NLO activities [29-31]. Nonlinear optical properties shown by hydrazones and their metal complexes offer their use in optoelectronic devices. Compounds which are noncentrosymmetric, planar and properly functionalized with strong electron donating and electron withdrawing groups at the terminal position of a π bridge could exhibit large molecular nonlinearity. One of the methods that have been adopted to improve the nonlinear optical properties of a material is to synthesize organic compounds of the type electron donor-bridge-electron acceptor. The molecules in which donor and acceptor groups are connected at the terminal positions of a π bridge to create highly polarized molecules exhibit

large molecular nonlinearity. It is reported that hydrazones can act as a π bridge for π electron delocalization across the donor-acceptor links. It is possible to tailor materials with large nonlinear optical property through structure modification in hydrazones by introduction of donor/acceptor groups to the bridge. Naseema *et al.* established the influence of donor/acceptor groups on the nonlinear optical properties of some aroylhydrazone derivatives [32]. Cariati *et al.* investigated the second order nonlinear optical properties of copper and palladium complexes of N-salicylidene-N'-aroylhydrazones and found that these complexes have considerable nonlinearity. The use of square planar coordinating metals Cu(II) and Pd(II) could force the organic ligand in a planar conformation so as to maximize conjugation [33].

1.4.2. Biological potential of hydrazones and their metal chelates

Hydrazones and their metal chelates have growing importance because of the wide spectrum of their biological applications like antimicrobial, antiinflammatory, antifungal, antitubercular, and anticancer activities [34-38]. Many researchers have synthesized these compounds as target structures and evaluated their biological activities. In many cases it was reported that metal chelates possess better biological activities than their corresponding ligands [39]. The bio-activity of hydrazones may be due to the presence of multidentate coordination centers and their ability to form stable chelates with essential metal ions which organisms need in their metabolism. It has also been shown that the azomethine N, which has a lone pair of electrons in an sp^2 hybridized orbital is biologically important [40,41]. Hydrazones possessing an azomethine proton $NH-N=CH$ constitute an important class of compounds for new drug development. Pinheiro *et al.* synthesized a series of hydrazone derivatives with significant antitubercular activity [42]. Ajani *et al.* synthesized

2-quinoxalinone-3-hydrazone derivatives with significant antibacterial and antifungal activities [43]. The results showed that this skeletal framework exhibited marked potency as antimicrobial agents.

Cancer still remains a threat to human health as a result of its mortality and morbidity. In the last years, many efforts have been made to develop new strategies for finding safe and effective ways of treating this disease, which includes a better understanding of biological processes involved in cancer cell survival and also the search for more selective and potent chemotherapeutic agents. Hydrazones as well as their complexes are well known for their anticancer properties [44]. Lindgren *et al.* developed benzothiazole hydrazones with high activity against breast cancer [45]. Recently Alagesan *et al.* have examined the cytotoxicity of copper(II) complexes of 2-acetylpyridine benzoyl hydrazone and 2-acetylpyridine thiophene-2-carboxylic acid hydrazone and demonstrated that the complexes possess superior cytotoxicity than that of well-known commercial anticancer drug cisplatin to the tumor cells but are less toxic to the normal cell line and have emerged as potential candidates for further studies [46]. Some hydrazone analogues are found to be potential iron chelating drugs for the treatment of iron overload diseases or genetic diseases such as β -thalassemia. The iron chelator salicylaldehyde isonicotinoyl hydrazone has shown considerable potential to protect cardiac cells by inhibition of both catecholamine oxidation and cardiotoxicity [47,48].

Vanadium compounds are effective for lowering plasma glucose levels in diabetic animals. Hydrazone complexes have been widely used as versatile ligands in coordination chemistry and the interaction of simple vanadium species with these ligands have been extensively investigated in recent years

with respect to their remarkable efficiency as insulin mimetic compounds. A number of oxidovanadium complexes with hydrazone ligands have been reported for their insulin mimetic properties [49]. These observations have guided the development of new hydrazones with various biological activities.

1.4.3. Analytical applications

Hydrazones are extensively used as analytical reagents because they react with metal ions and form colored precipitates or solutions. Since the protonation of amide nitrogen also affects the extent of electron delocalization in the hydrazone backbone, a sharp color change of the ligand and its complexes often accompanies deprotonation and this property has led to search for its possible applications in analytical chemistry for ultra trace determination of metal ions and the development of sensors and acid-base indicators based on such complexes. Jain and Singh reviewed the applications of hydrazones as analytical reagents [50]. The broad range of the chemical and supramolecular reactivities of the hydrazone functional group enables their use in the detection of cations and anions. Chandrasekhar *et al.* studied the spectrophotometric determination of Ni(II) and Cu(II) using diacetylmonoxime isonicotinoyl hydrazone [51]. In 2006, Tong *et al.* reported an “off-on” fluorescent chemosensor for Cu²⁺ based on a rhodamine B-based hydrazone [52]. The acidic nature of the hydrazone N–H group allows the detection of anionic species through H-bond interactions that alter the photophysical properties of the system. These spectroscopic changes make hydrazones ideal for anion sensing applications especially for acetate and fluoride anions [53]. Krishna *et al.* have reported a simple, sensitive and selective spectrophotometric method for the determination of Cd(II) in

biological materials (Cigarette tobacco, Radish flesh and Cabbage) and in alloy samples using cinnamaldehyde-4-hydroxybenzoyl hydrazone [54].

1.4.4. Catalytic applications

Aroylhydrazones and their complexes have attracted considerable attention due to their high synthetic potential in catalysis. It is well known that the use of nitrogen containing ligands leads to an increased catalytic activity [55]. Aroylhydrazone complexes are good candidates for catalytic oxidation studies because of their ability to resist oxidation. Monfared *et al.* have reported catalytic potential of oxido and dioxidovanadium complexes of hydrazone ligand (benzenetricarboxylic acid/benzoylhydrazide) for the oxidation of alkene, alkane and aromatic hydrocarbons using H₂O₂ as the terminal oxidant. Good to excellent conversions have been obtained for the oxidation of most of the hydrocarbons [56]. Mizar *et al.* demonstrated that copper(II) complexes of aroylhydrazones derived from β -diketones can be used as efficient and selective catalysts for the peroxidative oxidation of cyclohexene to cyclohex-2-enol and cyclohex-2-enone under mild conditions [57]. Molecular modeling of the metalloproteins that catalyze certain biochemical processes is one of the major interests of modern coordination chemistry [58]. As simulants of galactose oxidase (GO), a new Cu(II) hydrazone model system of GO using benzyl dihydrazone was synthesized and catalytic experiments confirmed their abilities to enable the aerobic oxidation of benzyl alcohol to benzaldehyde under room temperature [59].

1.5. Scope and objectives of the present work

Hydrazones and their metal complexes have been extensively studied in recent decades due to their attractive structures and topologies as well as their

potential applications in various fields. The ability of aroylhydrazones to form transition metal complexes is a developing area of research and the coordinating properties of hydrazones can be tuned by the appropriate choice of parent aldehyde or ketone and the hydrazide. The properties of the obtained complexes depend very much on the coordination geometries, nature of donor atoms as well as the metal centers. In order to pursue the interesting coordinating properties of hydrazones, complexes with different types of ligand environments are essential. In this perspective, we intend to study the structures and coordination chemistry of some transition metal chelates with four different aroylhydrazones as principal ligands. Introduction of heterocyclic bases like 1, 10-phenanthroline, 2,2'-bipyridine, pyridine and 3-picoline as auxiliary ligands leads to the syntheses of mixed ligand metal chelates which can cause different bonding, spectral properties and geometries in coordination compounds. The selection of 4-benzyloxy-2-hydroxybenzaldehyde-4-nitrobenzoylhydrazone was based on the idea of developing ligand having D- π -A general structure, so that the ligand and metal complexes exhibit NLO activity. Hence it is interesting to explore the coordinating capabilities of the synthesized hydrazones and to study the NLO activity of hydrazones and their metal complexes.

The objectives of our present work includes

- To synthesize some ONO and NNO donor aroylhydrazones.
- To characterize the synthesized aroylhydrazones by different physico-chemical techniques.
- To synthesize different transition metal chelates using the synthesized aroylhydrazones as principal ligands and some heterocyclic bases as coligands.

- To study the coordination modes of different aroylhydrazones in transition metal chelates by using different physico-chemical methods like partial elemental analyses, thermogravimetry and by different spectroscopic techniques.
- To establish the structure of the compounds by isolating single crystals of the compounds and by collecting and refining single crystal X-ray diffraction data.
- To study the second harmonic generation efficiencies of some compounds by Kurtz and Perry technique.

In the present work, four tridentate aroylhydrazones were synthesized and characterized. The molecular structures of these aroylhydrazones were established by single crystal X-ray diffraction studies. The metals selected for the preparation of the complexes are vanadium, cobalt, nickel, copper, zinc, cadmium and molybdenum. The second harmonic generation efficiencies of some of the compounds were studied by Kurtz and Perry powder technique [60].

1.6. Physical measurements

The physico-chemical methods adopted for the present study are discussed below.

1.6.1. Elemental analyses

Elemental analyses of carbon, hydrogen and nitrogen present in all the compounds were done on a Vario EL III CHNS elemental analyzer at the Sophisticated Analytical Instrument Facility, Cochin University of Science and Technology, Kochi-22, Kerala, India. This information is important to determine the purity of synthesized compounds.

1.6.2. Conductivity measurements

The molar conductivities of the complexes in DMF (10^{-3} M) at 298 K were measured using a Systronic model 303 direct reading conductivity meter at the Department of Applied Chemistry, CUSAT, Kochi, India.

1.6.3. Magnetic susceptibility measurements

The magnetic susceptibility measurements of the complexes were carried out on a Vibrating Sample Magnetometer using $\text{Hg}[\text{Co}(\text{SCN})_4]$ as a calibrant at the SAIF, Indian Institute of Technology, Madras.

1.6.4. Infrared spectroscopy

Infrared spectra of the compounds were recorded on a JASCO FT-IR-5300 Spectrometer in the $4000\text{-}400\text{ cm}^{-1}$ range using KBr pellets at the Department of Applied Chemistry, CUSAT, Kochi, India.

1.6.5. Electronic spectroscopy

The electronic spectra of the compounds were recorded in DMF on a Thermo Scientific Evolution 220 UV-Vis Spectrophotometer in the 200-900 nm range at the Department of Applied Chemistry, CUSAT, Kochi, India. The solid state electronic spectra of some complexes were recorded on Agilent Varian Cary 5300 Spectrophotometer at the Sophisticated Analytical Instrument Facility, Cochin University of Science and Technology, Kochi-22, Kerala, India.

1.6.6. Mass spectrometry

Mass spectra of the hydrazones were recorded by direct injection on WATERS 3100 Mass Detector using Electrospray ionization (ESI) technique

designed for routine HPLC-MS analyses at the Department of Applied Chemistry, CUSAT, Kochi, India.

1.6.7. NMR spectroscopy

¹H NMR spectra of hydrazones were recorded using Bruker AMX 400 FT-NMR Spectrometer with deuterated DMSO as the solvent and TMS as internal standard at the Sophisticated Analytical Instrument Facility, CUSAT, Kochi, India.

1.6.8. EPR spectroscopy

The EPR spectra of the complexes in the solid state at 298 K and in DMF at 77 K were recorded on a Varian E-112 spectrometer using TCNE as the standard with 100 kHz modulation frequency, 2 G modulation amplitude and 9.1 GHz microwave frequency at the SAIF, IIT Bombay, India. Some of the EPR spectra are simulated using EasySpin [61].

1.6.9. Thermogravimetric analyses

TG-DTG analyses of the complexes were carried out in a Perkin Elmer Pyris Diamond TG/DTA analyzer under nitrogen at a heating rate of 10 °C min⁻¹ in the 50-700 °C range at the Sophisticated Analytical Instrument Facility, CUSAT, Kochi, India.

1.6.10. Single crystal X-ray diffraction studies

Single crystal X-ray diffraction studies of the compounds were carried out using Bruker SMART APEXII CCD diffractometer equipped with a graphite crystal, incident-beam monochromator and a fine focus sealed tube with Mo K α ($\lambda=0.71073$ Å) as the X-ray source at the SAIF,

Cochin University of Science and Technology, Kochi-22, Kerala, India. The unit cell dimensions were measured and the data collections were performed at 296(2) K. Bruker SMART software was used for data acquisition and Bruker SAINT software for data integration [62]. Absorption corrections were carried out using SADABS based on Laue symmetry using equivalent reflections [63]. The structure was solved by direct methods using SHELXS97 and refined by full-matrix least-squares refinement on F^2 using SHELXL97 [64]. The graphics tools used were ORTEP-3 and DIAMOND version 3.2g [65,66].

1.6.11. Second harmonic generation studies

The second harmonic generation studies of the compounds were studied by Kurtz and Perry powder technique at the Department of Inorganic and Physical Chemistry, IISc, Bangalore. The experimental arrangement for the nonlinear optical studies utilizes a Quanta-Ray DCR II Nd: YAG laser. The sample was illuminated by a laser beam of fundamental wavelength 1064 nm with pulse width of 10 ns and repetition rate 10 Hz. An output signal of 532 nm was measured in a 90° geometry using KDP as the standard.

References

- [1] H.H. Monfared, R. Bikas, P.M. Anarjan, A.J. Blake, V. Lippolis, N.B. Arslan, C. Kazak, *Polyhedron* 69 (2014) 90.
- [2] P. Sudheesh, N.K.S. Narendran, K. Chandrasekharan, *Opt. Mater.* 36 (2013) 304.
- [3] G. Verma, A. Marella, M. Shaquiquzzaman, M. Akhtar, M.R. Ali, M.M. Alam, *J. Pharm. Bioallied Sci.* 6 (2014) 69.
- [4] X. Su, I. Aprahamian, *Chem. Soc. Rev.* 43 (2014) 1963.
- [5] F.R. Japp, F. Klingemann, *Ber. Dtsch. Chem. Ges.* 20 (1887) 2942.
- [6] A.C. Day, M.C. Whiting, *Org. Synth.* 50 (1970) 3.
- [7] V. Lefebvre, T. Cailly, F. Fabis, S. Rault, *J. Org. Chem.* 75 (2010) 2730.
- [8] M. Sutradhar, M.V. Kirillova, M.F.C.G. da Silva, C.M. Liu, A.J.L. Pombeiro, *Dalton Trans.* 42 (2013) 16578.
- [9] M.U. Anwar, A.S. Elliott, L.K. Thompson, L.N. Dawe, *Dalton Trans.* 40 (2011) 4623.
- [10] S. Gao, Z.Q. Weng, S.X. Liu, *Polyhedron* 17 (1998) 3595.
- [11] S. Naskar, M. Corbella, A.J. Blake, S.K. Chattopadhyay, *Dalton Trans.* (2007) 1150.
- [12] M.V. Angelusiu, S.F. Barbuceanu, C. Draghici, G.L. Almajan, *Eur. J. Med. Chem.* 45 (2010) 2055.
- [13] O.A. El-Gammal, F.E. El-Morsy, B. Jeragh, A.A. El-Asmy, *Can. Chem. Trans.* 1 (2013) 277.
- [14] A.A.R. Despaigne, J.G. Da Silva, A.C.M. Carmo, O.E. Piro, E.E. Castellano, H. Beraldo, *Inorg. Chim. Acta* 362 (2009) 2117.

- [15] M.F. Iskander, T.E. Khalil, R. Werner, W. Haase, I. Svoboda, H. Fuess, *Polyhedron* 19 (2000) 949.
- [16] B. Samanta, J. Chakraborty, S. Shit, S.R. Batten, P. Jensen, J.D. Masuda, S. Mitra, *Inorg. Chim. Acta* 360 (2007) 2471.
- [17] H.H. Monfared, M. Vahedpour, M.M. Yeganeh, M. Ghorbanloo, P. Mayer, C. Janiak, *Dalton Trans.* 40 (2011) 1286.
- [18] R. Bikas, H.H. Monfared, L. Sieron, A. Gutierrez, *J. Coord. Chem.* 66 (2013) 4023.
- [19] N.A. Mangalam, S. Sivakumar, M.R.P. Kurup, E. Suresh, *Spectrochim. Acta A* 75 (2010) 686.
- [20] R. Gup, B. Kirkan, *Spectrochim. Acta A* 62 (2005) 1188.
- [21] B.N.B. Raj, M.R.P. Kurup, E. Suresh, *Struct. Chem.* 17 (2006) 201.
- [22] S. Pal, *Proc. Indian Acad. Sci. (Chem. Sci.)* 114 (2002) 418.
- [23] M.C. Vineetha, M. Sithambaresan, J.M. Jacob, M.R.P. Kurup, *Acta Cryst. E* 68 (2012) 1086.
- [24] J. Chakraborty, S. Thakurta, G. Pilet, D. Luneau, S. Mitra, *Polyhedron* 28 (2009) 819.
- [25] M.M. Wang, H. Wang, G.Q. Gan, Y. Qu, H. Chen, Z.D. Lin, *J. Macromol. Sci. A* 49 (2012) 355.
- [26] G. Zhang, T. Liu, T. Zhu, J. Quin, Y. Wu, C. Chen, *Opt. mater.* 31 (2008) 110.
- [27] P.N. Prasad, D.J. Williams, *Introduction to Nonlinear Optical Effects in Molecules and Polymers*, Wiley Interscience, New York, 1991.
- [28] Iwai, T. Kobayashi, H. Fuyra, Y. Mori, T. Sasaki, *Jpn. J. Appl. Phys.* 36 (1997) 276.

- [29] G.A. Babu, R.P. Ramasamy, P. Ramasamy, S. Natarajan, *J. Cryst. Growth* 311 (2009) 3461.
- [30] F.Z. Henari, P.S. Patil, *Optics and Photonics Journal* 4 (2014) 182.
- [31] A.H. Reshak, H. Kamarudin, S. Auluck, *J. Phys. Chem.* 116 (2012) 4677.
- [32] K. Naseema, K.V. Sujith, K.B. Manjunatha, B. Kalluraya, G. Umesh, V. Rao, *Optic. Laser Tech.* 42 (2010) 741.
- [33] F. Cariati, U. Caruso, R. Centore, W. Marcolli, A. De Maria, B. Panunzi, M.A. Roviello, A. Tuzi, *Inorg. Chem.* 41 (2002) 6597.
- [34] B. Hollo, J. Magyari, V.Z. Radovanovic, G. Vuckovic, Z.D. Tomic, I.M. Szilagyi, G. Pokol, K.M. Szecsenyi, *Polyhedron* 80 (2014) 142.
- [35] G.L. Parrilha, R.P. Vieira, A.P. Rebolledo, I.C. Mendes, L.M. Lima, E.J. Barreiro, O.E. Piro, E.E. Castellano, H. Beraldo, *Polyhedron* 30 (2011) 1891.
- [36] E.N. Nfor, A. Husian, F. Majoumo-Mbe, I.N. Njah, O.E. Offiong, S.A. Bourne, *Polyhedron* 63 (2013) 207.
- [37] P. Dandawatea, K. Vemurib, E.M. Khan, M. Sritharan, S. Padhye, *Carbohydr. Polym.* 108 (2014) 135.
- [38] P. Krishnamoorthy, P. Sathyadevi, R.R. Butorac, A.H. Cowley, N.S.P. Bhuvanesh, N. Dharmaraj, *Dalton Trans.* 41 (2012) 6842.
- [39] S.Y. Ebrahimipour, I. Sheikhshoaie, A. Crochet, M. Khaleghi, K.M. Fromm, *J. Mol. Struct.* 1072 (2014) 267.
- [40] T. Sedaghat, M. Yousefi, G. Bruno, H.A. Rudbari, H. Motamedi, V. Nobakht, *Polyhedron* 79 (2014) 88.
- [41] I. Babahan, E.P. Coban, H. Biyik, *Maejo Int. J. Sci. Technol.* 7 (2013) 26.
- [42] A.C. Pinheiro, C.R. Kaiser, T.C.M. Nogueira, S.A. Carvalho, E.F. da Silva, Lde. O. Feitosa, Md. Henriques, A.L. Candea, M.C. Lourenco, M.V. de Souza, *Med. Chem.* 7 (2011) 611.

- [43] O.O. Ajani, C.A. Obafemi, O.C. Nwinyi, D.A. Akinpelu, *Bioorg. Med. Chem.* 18 (2010) 214.
- [44] R.S. Nair, M. Kuriakose, V. Somasundaram, V. Sheno, M.R.P. Kurup, P. Srinivas, *Life Sci.* 116 (2014) 90.
- [45] E.B. Lindgren, M.A. Brito, T.R.A. Vasconcelos, M.O. Moraes, R.C. Montenegro, J.D. Yoneda, K.Z. Leal, *Eur. J. Med. Chem.* 86 (2014) 12.
- [46] M. Alagesan, N.S.P. Bhuvanesh, N. Dharmaraj, *Dalton Trans.* 42 (2013) 7210.
- [47] T. Simunek, C. Boer, R.A. Bouwman, R. Vlasblom, A.M.G. Versteilen, M. Sterba, V. Gersl, R. Hrdina, P. Ponka, J.J. de Lange, W.J. Paulus, R.J.P. Musters, *J. Mol. Cell. Cardiol.* 39 (2005) 345.
- [48] P. Haskova, P. Kovarikova, L. Koubkova, A. Vavrova, E. Mackova, T. Simunek, *Free Radic. Biol. Med.* 50 (2011) 537.
- [49] S.P. Dash, S. Pasayat, S. Bhakat, S. Roy, R. Dinda, E.R.T. Tiekink, S. Mukhopadhyay, S.K. Bhutia, M.R. Hardikar, B.N. Joshi, Y.P. Patil, M. Nethaji, *Inorg. Chem.* 52 (2013) 14096.
- [50] P. Jain, R.P. Singh, *Talanta* 29 (1982) 77.
- [51] K.B. Chandrasekhar, K.H. Reddy, *Indian J. Chem.* 41 (2002) 1643.
- [52] Y. Xiang, A.J. Tong, P.Y. Jin, Y. Ju, *Org. Lett.* 8 (2006) 2863.
- [53] J. Shao, H. Lin, M. Yu, Z.S. Cai, H.K. Lin, *Talanta* 74 (2008) 1122.
- [54] D.G. Krishna, N. Devanna, K.B. Chandrasekhar, *Int. J. Pharm. Bio. Sci.* 1 (2010) 1.
- [55] N. Thilagavathi, A. Manimaran, N.P. Priya, N. Sathya, C. Jayabalakrishnan, *Appl. Organometal. Chem.* 24 (2010) 301.
- [56] H.H. Monfared, S. Kheirabadi, N.A. Lalami, P. Mayer, *Polyhedron* 30 (2011) 1375.

- [57] A. Mizar, M.F.C.G. da Silva, M.N. Kopylovich, S. Mukherjee, K.T. Mahmudov, A.J.L. Pombeiro, *Eur. J. Inorg. Chem.* (2012) 2305.
- [58] E. Kim, E.E. Chufan, K. Kamaraj, K.D. Karlin, *Chem. Rev.* 104 (2004) 1077.
- [59] H. Shi, Y. Yin, *Inorg. Chim. Acta* 421 (2014) 446.
- [60] S.K. Kurtz, T.T. Perry, *J. Appl. Phys.* 39 (1968) 3798.
- [61] S. Stoll, *Spectral Simulations in Solid-State Electron Paramagnetic Resonance*, Ph. D. thesis, ETH, Zurich, 2003.
- [62] SMART and SAINT, Area Detector Software Package and SAX Area Detector Integration Program, Bruker Analytical X-ray; Madison, WI, USA, 1997.
- [63] Bruker, SADABS, APEX2, XPREP and SAINT, Bruker AXS Inc., Madison, Wisconsin, USA, 2004.
- [64] G.M. Sheldrick, *Acta Cryst. Sect. A* 64 (2008) 112.
- [65] L.J. Farrugia, *J. Appl. Cryst.* 45 (2012) 849.
- [66] K. Brandenburg, *Diamond Version 3.2g*, Crystal Impact GbR, Bonn, Germany, 2010.

..........

SYNTHESES, SPECTRAL CHARACTERIZATION AND CRYSTAL STRUCTURES OF SOME AROYLHYDRAZONES

Contents	2.1	Introduction
	2.2	Experimental
	2.3	Characterization of aroylhydrazones
		References

2.1. Introduction

Aroylhydrazones are known to be an important class of nitrogen-oxygen donor ligands because of their variable bonding modes towards transition metal ions and their highly interesting chemical, biological and medicinal properties. These ligands are readily available, versatile and can exhibit various denticities and functionalities depending on the nature of the starting materials employed for their preparation [1-3]. The ease of preparation, increased hydrolytic stability relative to imines and tendency towards crystallinity are all desirable characteristics of hydrazones. Due to these positive traits, hydrazones have been under study for a long time.

Aroylhydrazones play an important role in inorganic chemistry as they easily form stable complexes with most transition metal ions. Literature survey of hydrazone complexes revealed that the coordination behavior

depends on the nature of the substituents and also on the position of the imine group relative to other moieties. Moreover, the proton transfer between hydrazinic N and keto group of hydrazide part results in the formation of iminolic tautomer having new coordination properties [4,5]. The development of the field of bioinorganic chemistry has increased the interest in hydrazone complexes since it has been recognized that many of these complexes may serve as models for biologically important species [6]. Coordination compounds derived from aroylhydrazones have been reported to act as enzyme inhibitors and are useful due to their pharmacological applications [7-10]. These compounds have interesting biological properties such as antiinflammatory, anticonvulsant, antitubercular, antitumor, anti-HIV and antimicrobial activities [11-17]. Hydrazones are important compounds for drug design, catalysis and also for the syntheses of heterocyclic compounds [18-20]. Due to their chelating behavior, hydrazones are used in analytical chemistry as selective metal extracting agents as well as in spectroscopic determination of certain transition metals [21,22]. Also many reports have shown that they are suitable candidates for NLO materials [23]. A large number of π -conjugated molecules have been investigated in the last thirty years for suitability to function as components in hypothetical NLO materials. Aroylhydrazones offer many possibilities to tailor materials with the desired π -electron delocalization through optimization of the microscopic hyperpolarizabilities (molecular engineering) and the incorporation of molecules in a crystalline lattice (crystal engineering) and polymers [24,25].

The above said facts prompted us to synthesize and characterize some metal complexes using aroylhydrazones as the ligand system. We have synthesized four hydrazones using 4-nitrobenzoic hydrazide, nicotinic

hydrazide, 4-benzyloxy-2-hydroxybenzaldehyde, 5-bromo-2-hydroxy-3-methoxybenzaldehyde, 4-diethylamino-2-hydroxybenzaldehyde and 2-benzoylpyridine. In this chapter the syntheses, crystal structures and spectral perspectives of the aroylhydrazones are discussed. The synthesized ligand systems consisting of ONO and ONN donor aroylhydrazones and are given below.

- 4-benzyloxy-2-hydroxybenzaldehyde-4-nitrobenzoylhydrazone dimethylformamide monosolvate ($H_2L^1 \cdot C_3H_7NO$)
- 5-bromo-2-hydroxy-3-methoxybenzaldehyde nicotinoylhydrazone dihydrate methanol monosolvate ($H_2L^2 \cdot 2H_2O \cdot CH_3OH$)
- 4-diethylamino-2-hydroxybenzaldehyde nicotinoylhydrazone monohydrate ($H_2L^3 \cdot H_2O$)
- 2-benzoylpyridine-4-nitrobenzoylhydrazone (HL^4)

2.2. Experimental

2.2.1. Materials

4-Benzyloxy-2-hydroxybenzaldehyde (Sigma-Aldrich), 5-bromo-2-hydroxy-3-methoxybenzaldehyde (Sigma-Aldrich), 4-diethylamino-2-hydroxybenzaldehyde (Sigma-Aldrich), 2-benzoylpyridine (Sigma-Aldrich), nicotinic hydrazide (Sigma-Aldrich) and 4-nitrobenzoic hydrazide (Sigma-Aldrich) were of Analar grade and were used as received. Solvents used were methanol and dimethylformamide.

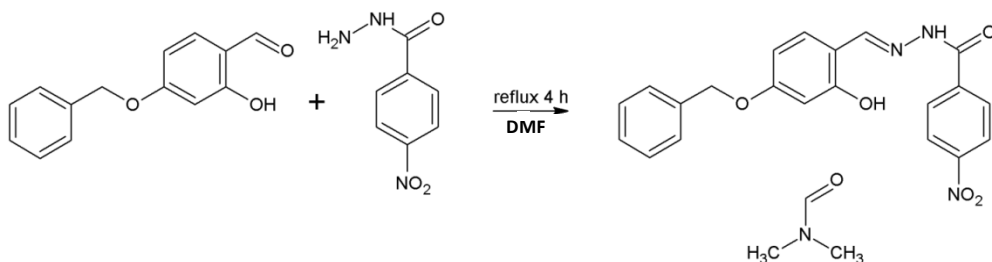
2.2.2. Syntheses of aroylhydrazones

The hydrazones were synthesized by adapting the reported procedure [26,27], namely *via* condensation between appropriate aldehyde/ketone with the respective aroylhydrazide as described below.

2.2.2.1. 4-Benzyloxy-2-hydroxybenzaldehyde-4-nitrobenzoylhydrazone dimethylformamide monosolvate ($H_2L^1 \cdot C_3H_7NO$)

To a solution of 4-nitrobenzoic hydrazide (0.181 g, 1 mmol) in DMF, a solution of 4-benzyloxy-2-hydroxybenzaldehyde (0.228 g, 1 mmol) in DMF was added and the reaction mixture was refluxed for 4 h. after adding two drops of sulfuric acid. On cooling yellow colored crystals were separated, washed with methanol and dried over P_4O_{10} *in vacuo*. Reaction scheme for the synthesis of $H_2L^1 \cdot C_3H_7NO$ is shown below (Scheme 2.1).

$H_2L^1 \cdot C_3H_7NO$: Yield: 79%, M.P.: 220 °C, Elemental Anal. Found (Calcd.) (%): C: 62.01 (62.06); H: 5.27 (5.21); N: 12.12 (12.06).

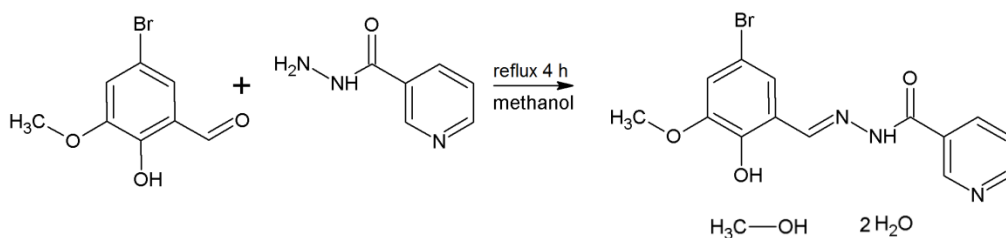


Scheme 2.1. Synthesis of $H_2L^1 \cdot C_3H_7NO$.

2.2.2.2. 5-Bromo-2-hydroxy-3-methoxybenzaldehyde nicotinoylhydrazone dihydrate methanol monosolvate ($H_2L^2 \cdot 2H_2O \cdot CH_3OH$)

A methanolic solution of nicotinic hydrazide (0.137 g, 1 mmol) was refluxed with a methanolic solution of 5-bromo-2-hydroxy-3-methoxybenzaldehyde (0.231 g, 1 mmol) continuously for 4 h. The reaction mixture was kept aside for slow evaporation at room temperature. After 4-5 days, colorless block shaped crystals were formed and carefully separated. The scheme for the reaction is shown below (Scheme 2.2).

$H_2L^2 \cdot 2H_2O \cdot CH_3OH$: Yield: 81%, M.P. : 110 °C, Elemental Anal. Found (Calcd.) (%): C: 43.51 (43.08); H: 4.53 (4.82); N: 10.50 (10.05).

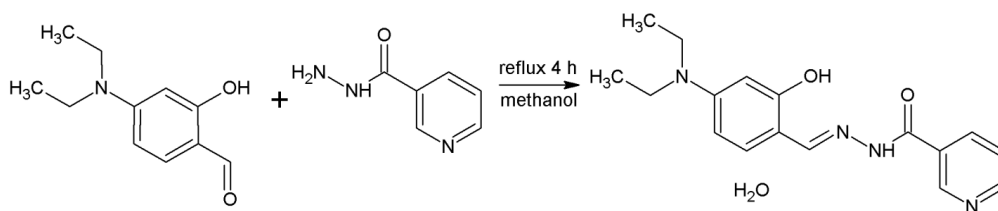


Scheme 2.2. Synthesis of $H_2L^2 \cdot 2H_2O \cdot CH_3OH$.

2.2.2.3. 4-Diethylamino-2-hydroxybenzaldehyde nicotinoylhydrazone monohydrate ($H_2L^3 \cdot H_2O$)

4-Diethylamino-2-hydroxybenzaldehyde nicotinoylhydrazone monohydrate was prepared by refluxing methanolic solutions of nicotinic hydrazide (0.137 g, 1 mmol) and 4-diethylamino-2-hydroxybenzaldehyde (0.193 g, 1 mmol) for 4 h. The formed crystals were collected, washed with few drops of methanol and dried over P_4O_{10} *in vacuo*. The scheme for the reaction is shown below (Scheme 2.3).

$H_2L^3 \cdot H_2O$: Yield: 76%, M.P. : 104 °C, Elemental Anal. Found (Calcd.) (%): C: 61.44 (61.80); H: 6.23 (6.71); N: 16.63 (16.96).

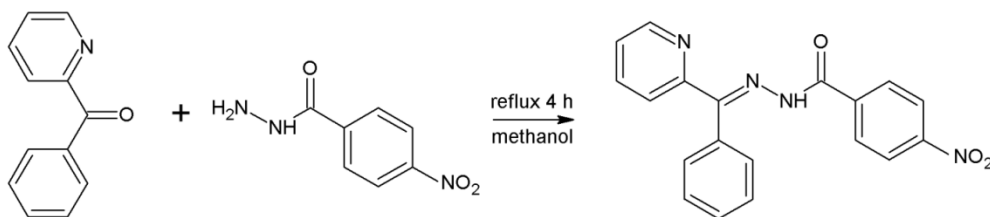


Scheme 2.3. Synthesis of $H_2L^3 \cdot H_2O$.

2.2.2.4. 2-Benzoylpyridine-4-nitrobenzoylhydrazone (HL⁴)

To a methanolic solution of 4-nitrobenzoic hydrazide (0.181 g, 1 mmol), a methanolic solution of 2-benzoylpyridine (0.183 g, 1 mmol) was added followed by one drop of dilute sulfuric acid. The resulting solution was refluxed for 4 h. On cooling colorless block shaped crystals were formed and carefully separated. The scheme for the reaction is shown below (Scheme 2.4).

HL⁴: Yield: 73%, M.P. : 168 °C, Elemental Anal. Found (Calcd.) (%): C: 65.54 (65.89); H: 4.13 (4.07); N: 15.98 (16.18).



Scheme 2.4. Synthesis of HL⁴.

2.3. Characterization of aroylhydrazones

2.3.1. Elemental analyses

C, H, N analyses data of the synthesized aroylhydrazones are given in Section 2.2 which indicate that the compounds are analytically pure.

2.3.2. Mass spectra

Mass spectrometry (MS) is a powerful analytical technique that is used to identify unknown compounds and to elucidate the structure of molecules by measuring the mass-to-charge ratio of charged particles. The electrospray

ionization (ESI) technique was used to measure the m/z ratio of charged particles. MS works by ionizing the compound to generate charged molecules or fragments and measuring their mass to charge ratios. Mass spectrum is a plot of m/z of positive ion fragments versus their relative abundance. Hydrazones, which are formed from the reaction between carbonyl compounds and hydrazides are stable at room temperature but unstable at higher temperatures and have relatively high boiling points. Therefore GC-MS is not easy to apply for hydrazone analysis due to these physical natures. Therefore, LC-MS has been used to analyze these derivatives [28,29]. In the present study, the molecular ion (M^+) peaks at 391.5, 350.2, 312.3 and 346.3 amu for the aroylhydrazones H_2L^1 , H_2L^2 , H_2L^3 and HL^4 respectively indicate the molecular masses of respective aroylhydrazones synthesized (Figs. 2.1-2.4).

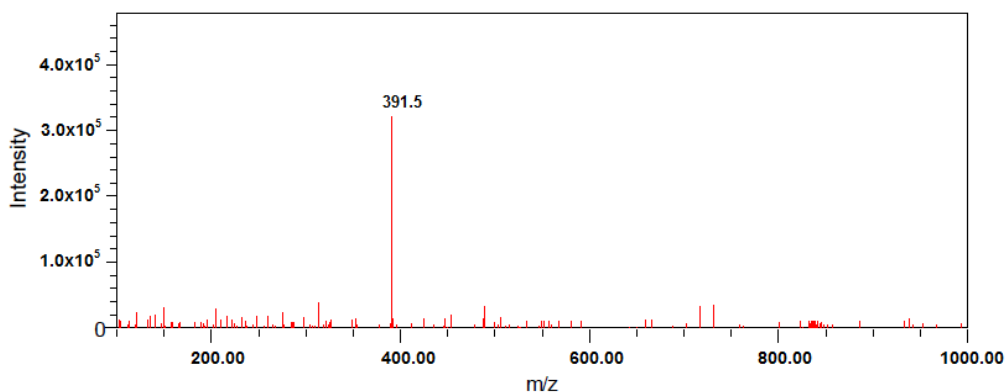


Fig. 2.1. Mass spectrum of H_2L^1 showing molecular ion (M^+) peak.

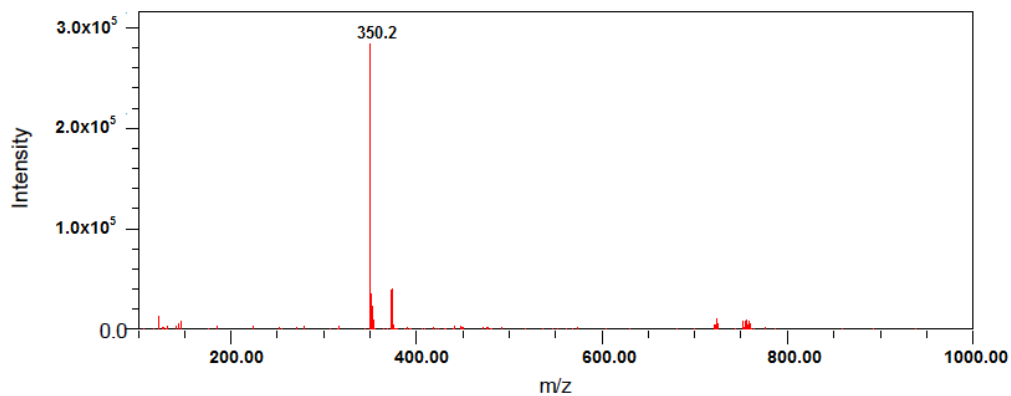


Fig. 2.2. Mass spectrum of H₂L² showing molecular ion (M⁺) peak.

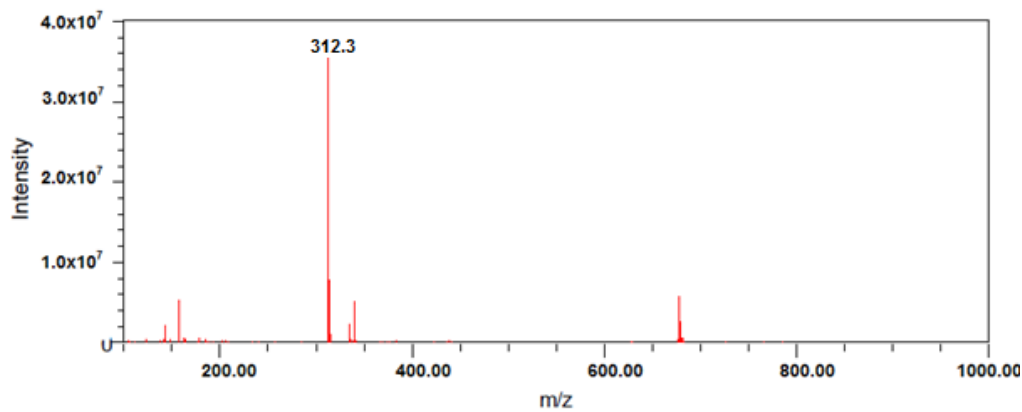


Fig. 2.3. Mass spectrum of H₂L³ showing (M⁺) peak.

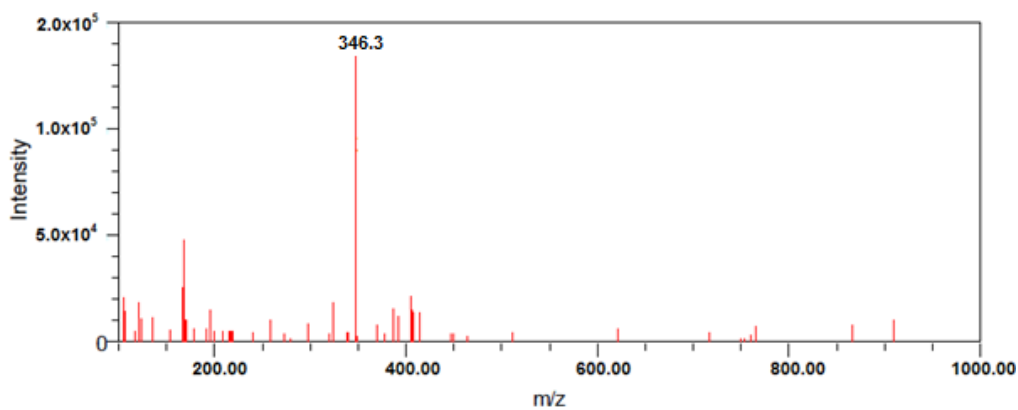


Fig. 2.4. Mass spectrum of HL⁴ showing (M⁺) peak.

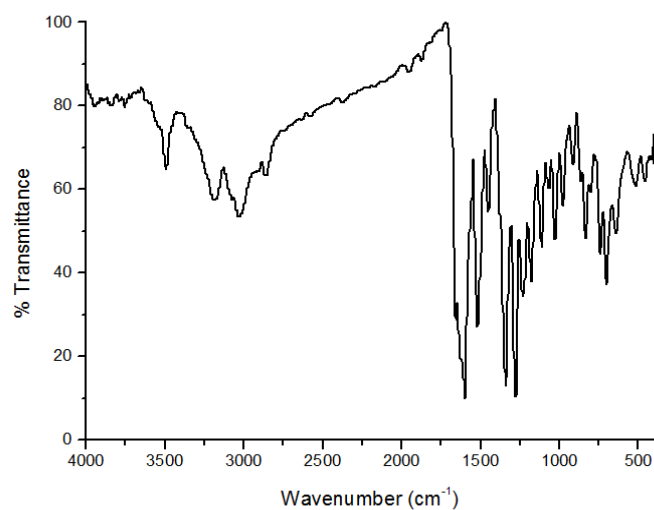
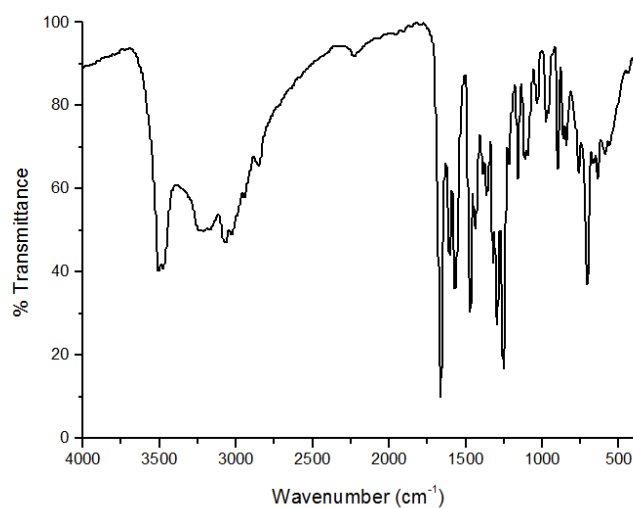
2.3.3. Infrared spectra

Infrared spectra of the aroylhydrazones were recorded on a JASCO FT-IR-5300 spectrometer in the 4000-400 cm^{-1} range using KBr pellets. The significant bands observed in the IR spectra of the aroylhydrazones along with their relative assignments are presented in the Table 2.1. FT-IR spectral data of the compounds are in accordance with their molecular structure.

In the IR spectra of aroylhydrazones, $\nu(\text{C}=\text{N})$ bands are observed in the 1597-1609 cm^{-1} range indicating the condensation of hydrazide and the aldehyde/ketone moiety and it is in agreement with the literature reports of aroylhydrazones [30,31]. In the IR spectra of aroylhydrazones the $\nu(\text{C}=\text{O})$ stretching vibrations are observed at 1661, 1669, 1632 and 1683 cm^{-1} for $\text{H}_2\text{L}^1 \cdot \text{C}_3\text{H}_7\text{NO}$, $\text{H}_2\text{L}^2 \cdot 2\text{H}_2\text{O} \cdot \text{CH}_3\text{OH}$, $\text{H}_2\text{L}^3 \cdot \text{H}_2\text{O}$ and HL^4 respectively suggesting that the hydrazones exist in the amido form in the solid state. This is further supported by medium bands in the 3067-3186 cm^{-1} range due to $\nu(\text{N}-\text{H})$ vibration [32]. The broad absorption bands at 3218 cm^{-1} for $\text{H}_2\text{L}^2 \cdot 2\text{H}_2\text{O} \cdot \text{CH}_3\text{OH}$ and $\text{H}_2\text{L}^3 \cdot \text{H}_2\text{O}$ are due to the $\nu(\text{O}-\text{H})$ stretching mode of lattice water and the decrease in the value is due to the involvement of intermolecular hydrogen bond and this is confirmed by the single crystal X-ray diffraction studies. In all the hydrazones except HL^4 , the sharp bands in the 3377-3505 cm^{-1} range are due to stretching mode of phenolic O-H group. The N-N stretching vibrations are found in the 1102-1127 cm^{-1} region [33,34]. Figs. 2.5-2.8 depict the infrared spectra of the aroylhydrazones.

Table 2.1. The important IR frequencies (cm^{-1}) of aroylhydrazones

Compound	$\nu(\text{C}=\text{N})$	$\nu(\text{C}=\text{O})$	$\nu(\text{N}-\text{N})$	$\nu(\text{N}-\text{H})$	$\nu(\text{O}-\text{H})$
$\text{H}_2\text{L}^1 \cdot \text{C}_3\text{H}_7\text{NO}$	1604	1661	1102	3186	3488
$\text{H}_2\text{L}^2 \cdot 2\text{H}_2\text{O} \cdot \text{CH}_3\text{OH}$	1609	1669	1110	3067	3505
$\text{H}_2\text{L}^3 \cdot \text{H}_2\text{O}$	1603	1632	1127	3075	3377
HL^4	1597	1683	1122	3069	----

**Fig. 2.5. IR spectrum of $\text{H}_2\text{L}^1 \cdot \text{C}_3\text{H}_7\text{NO}$.****Fig. 2.6. IR spectrum of $\text{H}_2\text{L}^2 \cdot 2\text{H}_2\text{O} \cdot \text{CH}_3\text{OH}$.**

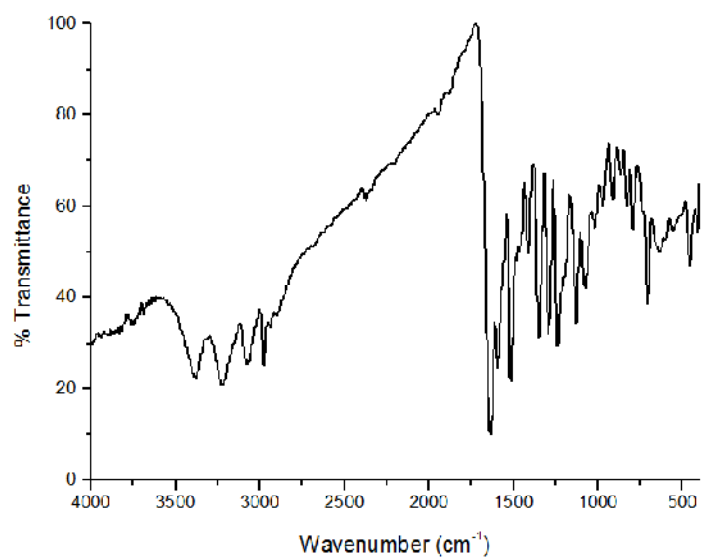


Fig. 2.7. IR spectrum of $H_2L^3 \cdot H_2O$.

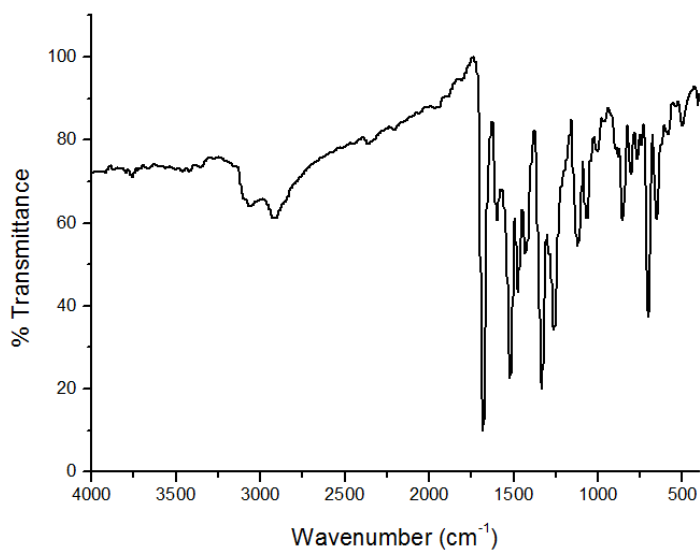


Fig. 2.8. IR spectrum of HL^4 .

2.3.4. Electronic spectra

The significant electronic absorption bands in the electronic spectra of aroylhydrazones recorded in DMF are presented in Table 2.2. Bands in the 27020-36990 cm^{-1} range are attributed to $n \rightarrow \pi^*$ and $\pi \rightarrow \pi^*$ transitions of the benzene ring, imine and carbonyl groups present in them (Fig. 2.9).

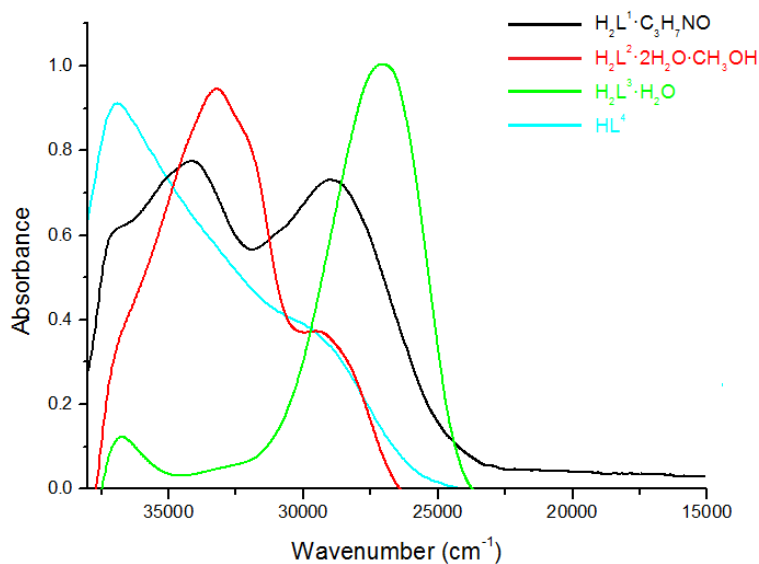


Fig. 2.9. Electronic spectra of aroylhydrazones.

Table 2.2. Electronic spectral assignments (cm^{-1}) of aroylhydrazones

Compound	$n \rightarrow \pi^* / \pi \rightarrow \pi^*$
$\text{H}_2\text{L}^1 \cdot \text{C}_3\text{H}_7\text{NO}$	36990, 34130, 28970
$\text{H}_2\text{L}^2 \cdot 2\text{H}_2\text{O} \cdot \text{CH}_3\text{OH}$	33240, 29350
$\text{H}_2\text{L}^3 \cdot \text{H}_2\text{O}$	36780, 27020
HL^4	36940, 29740

2.3.5. NMR spectral studies

Nuclear Magnetic Resonance (NMR) spectroscopy has become the dominant method of analysis for organic compounds because in many cases it provides a way to determine an entire structure using one set of analytical tests. It is also used in inorganic chemistry and biochemistry where it provides a lot of valuable structural information. The ^1H NMR spectrum provides useful information about the number of different types of hydrogen present in the molecule and their electronic environment.

The ^1H NMR spectrum of the synthesized aroylhydrazones were recorded with $\text{DMSO-}d_6$ as solvent on a Bruker AMX 400 spectrometer and TMS as standard. The ^1H NMR spectrum of $\text{H}_2\text{L}^1 \cdot \text{C}_3\text{H}_7\text{NO}$ is given in Fig. 2.10. The sharp singlet at 12.24 ppm in the downfield region of the spectrum indicates the presence of iminol form of the hydrazone. A singlet with an area of integration one at 11.44 ppm is due to the presence of phenolic proton. Absence of any coupling interactions by protons on neighboring atoms renders singlet peaks for these iminolic and phenolic protons. Upon D_2O exchange these signals are disappeared showing that these two protons are readily exchangeable and confirmed the above assignments (Fig. 2.11). Aromatic protons appear as multiplets at 6.58-8.58 ppm range.

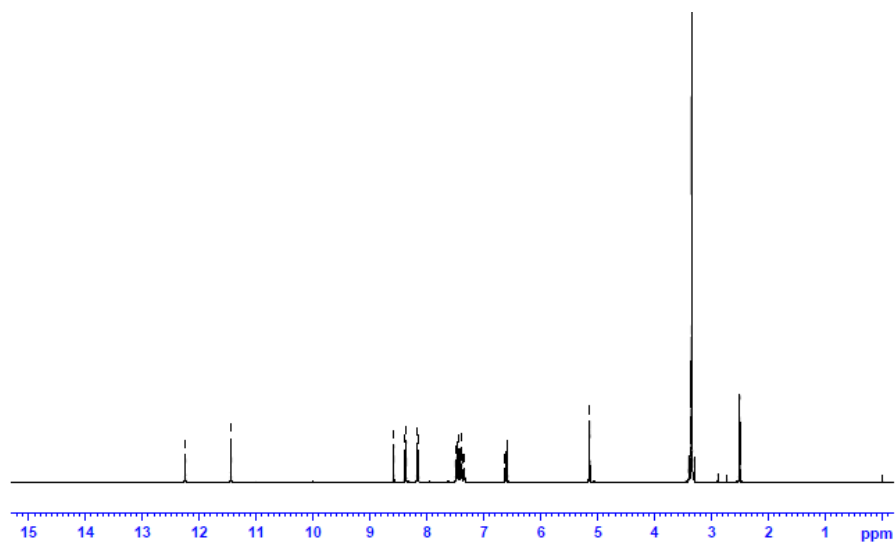


Fig. 2.10. ^1H NMR spectrum of $\text{H}_2\text{L}^1\cdot\text{C}_3\text{H}_7\text{NO}$.

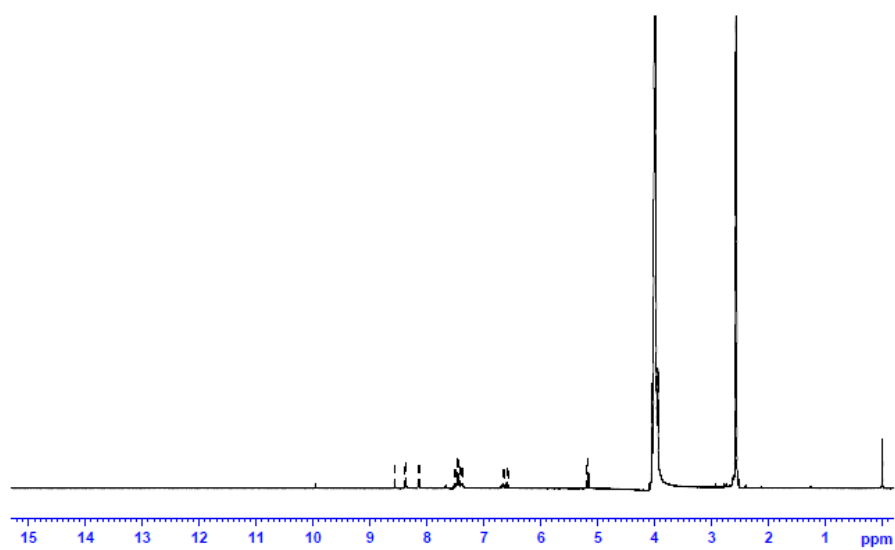


Fig. 2.11. ^1H NMR spectrum of $\text{H}_2\text{L}^1\cdot\text{C}_3\text{H}_7\text{NO}\text{-D}_2\text{O}$ exchange.

In the ^1H NMR spectrum of $\text{H}_2\text{L}^2\cdot 2\text{H}_2\text{O}\cdot\text{CH}_3\text{OH}$ the sharp singlet observed at 12.29 ppm which integrates as one hydrogen is due to the existence of the compound in the iminolic form. A singlet at 10.76 ppm in the spectrum is assigned to the phenolic proton (Fig. 2.12). These peaks are found to disappear

in the $\text{H}_2\text{L}^2 \cdot 2\text{H}_2\text{O} \cdot \text{CH}_3\text{OH} \cdot \text{D}_2\text{O}$ ^1H NMR spectrum since these protons exchange with deuterium in the D_2O (Fig. 2.13). Multiplets observed in the 7.8-9.09 ppm range are assigned to the aromatic protons. A singlet at $\delta = 3.85$ ppm corresponds to the methoxy protons.

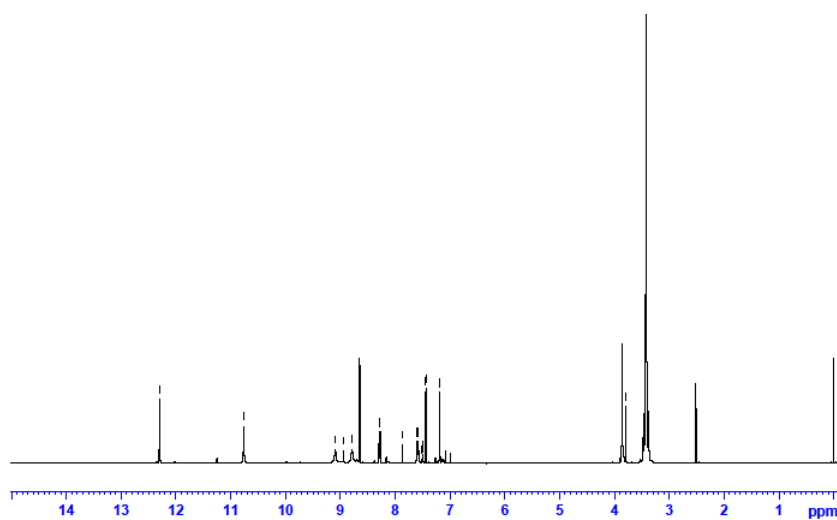


Fig. 2.12. ^1H NMR spectrum of $\text{H}_2\text{L}^2 \cdot 2\text{H}_2\text{O} \cdot \text{CH}_3\text{OH}$.

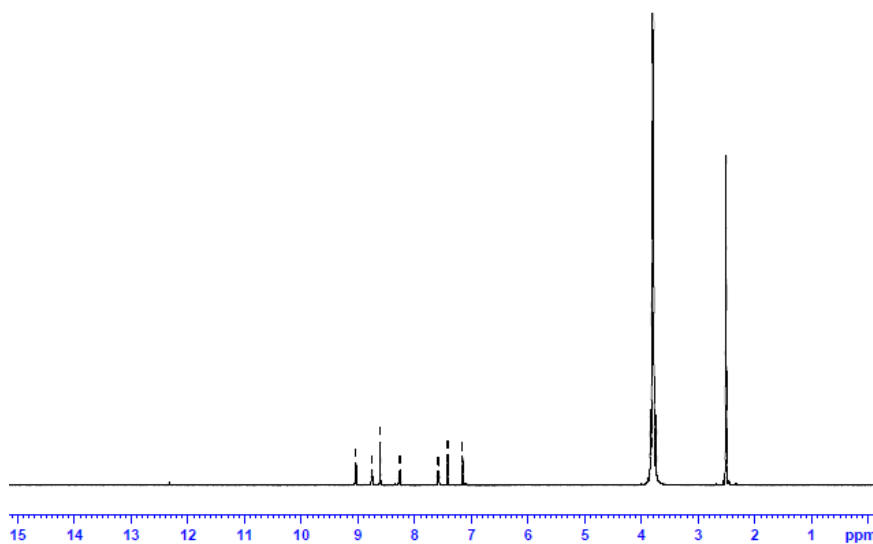


Fig. 2.13. ^1H NMR spectrum of $\text{H}_2\text{L}^2 \cdot 2\text{H}_2\text{O} \cdot \text{CH}_3\text{OH} \cdot \text{D}_2\text{O}$ exchange.

The ^1H NMR spectrum of $\text{H}_2\text{L}^3 \cdot \text{H}_2\text{O}$ is shown in Fig. 2.14. Here the singlet in the downfield region of the spectrum at δ value of 11.96 ppm is due to the iminolic proton. The phenolic proton resonates at 11.33 ppm as a singlet.

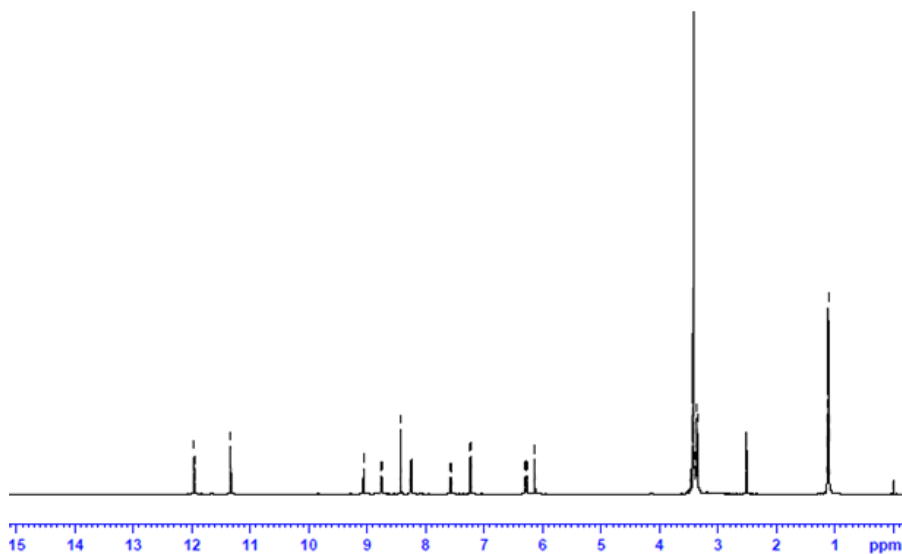


Fig. 2.14. ^1H NMR spectrum of $\text{H}_2\text{L}^3 \cdot \text{H}_2\text{O} \cdot \text{CH}_3\text{OH}$.

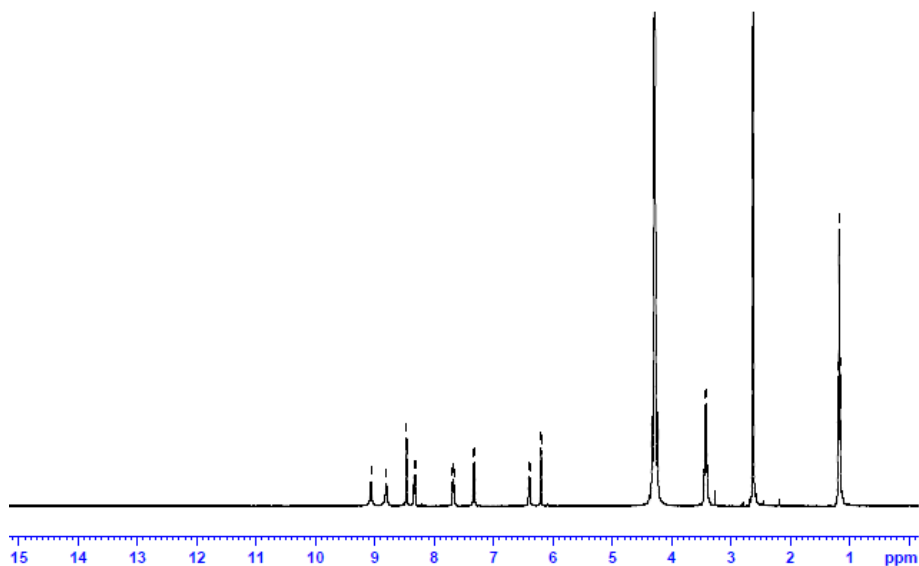


Fig. 2.15. ^1H NMR spectrum of $\text{H}_2\text{L}^3 \cdot \text{H}_2\text{O} \cdot \text{D}_2\text{O}$ exchange.

These assignments can be confirmed from the $\text{H}_2\text{L}^3 \cdot \text{H}_2\text{O} \cdot \text{D}_2\text{O}$ ^1H NMR spectrum in which these signals are absent (Fig. 2.15). Aromatic protons appear as multiplets in the 6.13-9.06 ppm range.

^1H NMR spectrum of 2-benzoylpyridine-4-nitrobenzoylhydrazone (HL^4) is given in Fig. 2.16. For HL^4 , a singlet which integrates as one hydrogen at 13.51 ppm is assigned to the iminolic NH proton. Absence of any coupling interactions by NH proton due to the lack of availability of protons on neighboring atoms renders singlet peak for it. This peak is found to disappear in the $\text{HL}^4 \cdot \text{D}_2\text{O}$ ^1H NMR spectrum since this proton exchange with deuterium in the D_2O (Fig. 2.17). Aromatic protons appear as multiplets in the 7.45-8.83 ppm range.

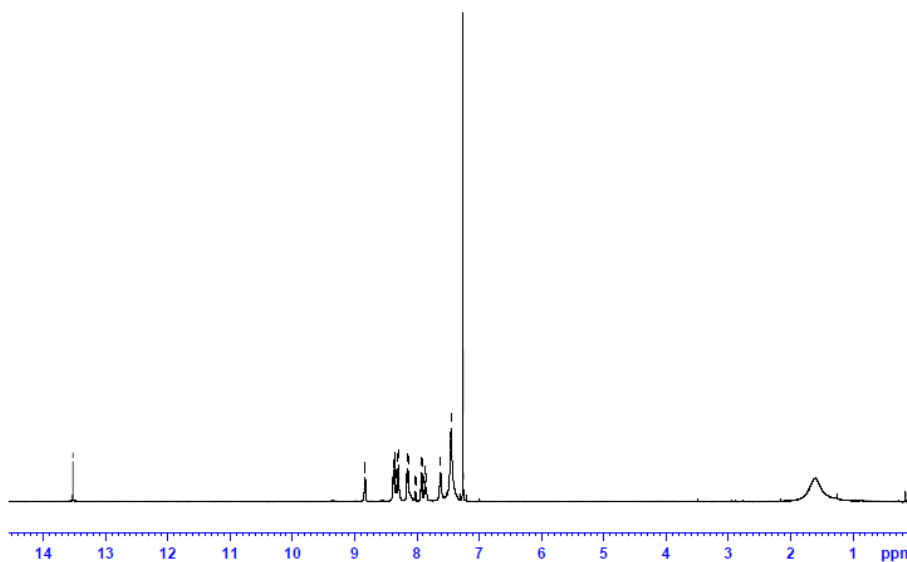


Fig. 2.16. ^1H NMR spectrum of HL^4 .

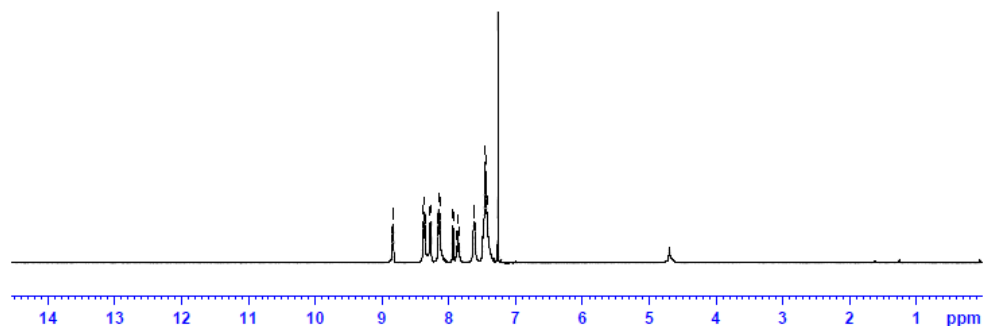


Fig. 2.17. ^1H NMR spectrum of $\text{HL}^4\text{-D}_2\text{O}$ exchange.

2.3.6. X-ray crystallography

Single crystal X-ray diffraction is an important technique in the structural determination of crystalline materials and for understanding their structure-property relationships. This powerful tool can be used to visualize the precise and detailed structural information of compounds. Single crystal X-ray diffraction studies of the aroylhydrazones were carried out using a Bruker SMART APEXII CCD diffractometer at the SAIF, Cochin University of Science and Technology, Kochi-22, Kerala, India. Bruker SMART software was used for data acquisition and Bruker SAINT software for data integration [35]. Absorption corrections were carried out using SADABS based on Laue symmetry using equivalent reflections [36]. The structure was solved by direct methods using SHELXS97 and refined by full-matrix least-squares refinement on F^2 using SHELXL97 [37]. The molecular and crystal structures were plotted using DIAMOND version 3.2g [38].

In $\text{H}_2\text{L}^1\cdot\text{C}_3\text{H}_7\text{NO}$, $\text{H}_2\text{L}^2\cdot 2\text{H}_2\text{O}\cdot\text{CH}_3\text{OH}$ and $\text{H}_2\text{L}^3\cdot\text{H}_2\text{O}$ all non-hydrogen atoms were refined anisotropically and all H atoms on C were placed in calculated positions guided by difference maps with C–H bond distances 0.93–0.97 Å. The H atoms were assigned as $U_{\text{iso}}=1.2U_{\text{eq}}$ (1.5 for Me).

N2–H2' and O2–H2'' hydrogen atoms of $\text{H}_2\text{L}^1 \cdot \text{C}_3\text{H}_7\text{NO}$ were located from difference maps and their distances were restrained using DFIX instructions. The O(2)–H(2), O(4)–H(4) and N(2)–H(2') H atoms of $\text{H}_2\text{L}^2 \cdot 2\text{H}_2\text{O} \cdot \text{CH}_3\text{OH}$ were located from difference maps and their distances were restrained using DFIX instructions. In $\text{H}_2\text{L}^3 \cdot \text{H}_2\text{O}$, N(3)–H(3), O(1)–H(1), O(1W)–H(1A) and O(1W)–H(1B) hydrogen atoms were located from difference maps and their distances were restrained using DFIX and DANG instructions. In HL^4 , all H atoms were placed in calculated positions guided by difference maps with C–H bond distance of 0.93 Å.

2.3.6.1. Crystal structure of $\text{H}_2\text{L}^1 \cdot \text{C}_3\text{H}_7\text{NO}$

The yellow block shaped crystals of $\text{H}_2\text{L}^1 \cdot \text{C}_3\text{H}_7\text{NO}$ suitable for X-ray diffraction analysis were obtained by recrystallization from a mixture of methanol and dimethylformamide (1:1 v/v). A single crystal with approximate dimensions of $0.40 \times 0.20 \times 0.20 \text{ mm}^3$ was selected for collecting the data. The molecular structure of the compound with the atom numbering scheme is given in Fig. 2.18. The crystallographic data and structure refinement parameters of the compound are given in Table 2.3, the selected bond lengths and bond angles are given in Table 2.4 and the torsion angles in Table 2.5.

Table 2.3. Crystal data and structure refinement parameters for H₂L¹·C₃H₇NO

Parameters	H ₂ L ¹ ·C ₃ H ₇ NO
Empirical formula	C ₂₄ H ₂₄ N ₄ O ₆
Formula weight	464.47
Temperature	296 K
Wavelength	0.71073 Å
Crystal system	Monoclinic
Space group	<i>P</i> 2 ₁ / <i>c</i>
Unit cell dimensions	<i>a</i> = 10.0160(8) Å <i>b</i> = 22.6610(2) Å <i>c</i> = 10.2611(11) Å <i>α</i> = 90.00° <i>β</i> = 101.39(5)° <i>γ</i> = 90.00°
Volume	2283.1(4) Å ³
<i>Z</i>	4
Density (calculated)	1.351 mg/m ³
Absorption coefficient	0.099 mm ⁻¹
<i>F</i> (000)	976
Crystal size	0.40 × 0.20 × 0.20 mm ³
θ range for data collection	1.80 to 27.00°
Limiting indices	-12 ≤ <i>h</i> ≤ 11 -28 ≤ <i>k</i> ≤ 28 -13 ≤ <i>l</i> ≤ 8
Reflections collected	16107
Unique Reflections (<i>R</i> _{int})	4979 [<i>R</i> (int) = 0.0314]
Refinement method	Full-matrix least-squares on <i>F</i> ²
Data / restraints / parameters	4910 / 2 / 318
Goodness-of-fit on <i>F</i> ²	1.035
Final <i>R</i> indices [<i>I</i> > 2σ(<i>I</i>)]	<i>R</i> ₁ = 0.0528, <i>wR</i> ₂ = 0.1367
<i>R</i> indices (all data)	<i>R</i> ₁ = 0.0987, <i>wR</i> ₂ = 0.1759
Largest diff. peak and hole	0.396 and -0.218 e Å ⁻³

$$R_1 = \sum ||F_o| - |F_c|| / \sum |F_o|$$

$$wR_2 = [\sum w(F_o^2 - F_c^2)^2 / \sum w(F_o^2)^2]^{1/2}$$

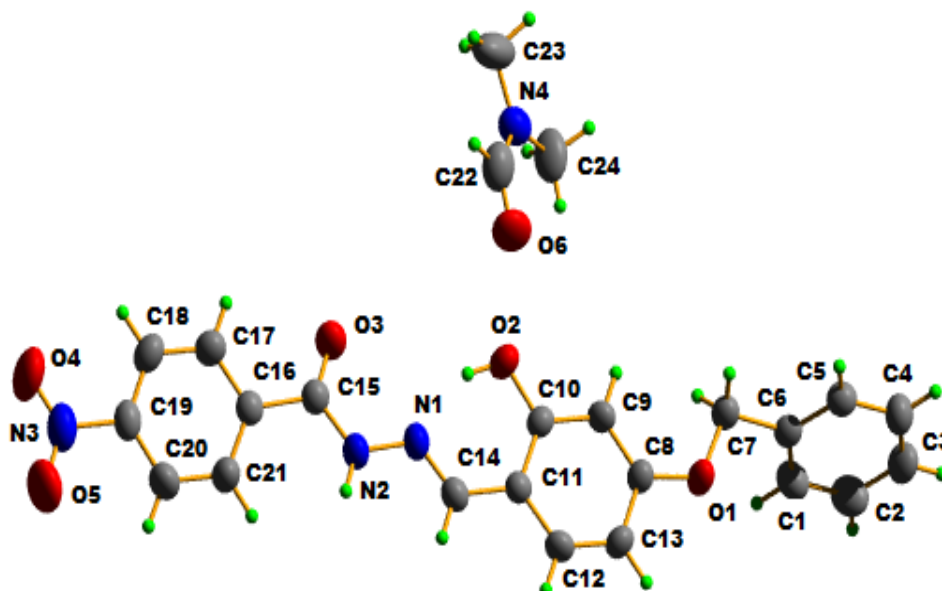


Fig. 2.18. Molecular structure of $H_2L^1 \cdot C_3H_7NO$ along with the atom numbering scheme.

Table 2.4. Selected bond lengths [\AA] and angles [$^\circ$] for $H_2L^1 \cdot C_3H_7NO$

Bond lengths		Bond angles	
N(1)–C(14)	1.271(3)	C(14)–N(1)–N(2)	118.4(2)
O(2)–C(10)	1.341(3)	N(2)–C(15)–C(16)	117.0(2)
N(1)–N(2)	1.374(2)	N(1)–C(14)–C(11)	120.1(2)
O(3)–C(15)	1.217(3)	N(2)–C(15)–O(3)	122.0(2)
N(2)–C(15)	1.337(3)	O(2)–C(10)–C(11)	122.09(18)
N(3)–C(19)	1.472(3)	C(14)–C(11)–C(10)	121.7(2)
C(11)–C(14)	1.446(3)	C(15)–N(2)–N(1)	117.33(19)

Table 2.5. Selected torsion angles [°] for H₂L¹

Torsion angles	
C(10)–C(11)–C(14)–N(1)	3.1(3)
C(11)–C(14)–N(1)–N(2)	177.93(18)
N(1)–N(2)–C(15)–C(16)	179.57(17)
N(1)–N(2)–C(15)–O(3)	0.0(3)

The compound crystallizes in monoclinic space group $P2_1/c$. The torsion angle of $177.93(18)^\circ$ perceived by C(11)–C(14)–N(1)–N(2) moiety supports the *anti* configuration with respect to C(14)–N(1) bond in the aroylhydrazone [39,40]. The compound exists in *amido* form with C(15)–O(3) bond length of $1.217(3)$ Å, which is very close to C=O bond length of previously reported hydrazones [41,42]. Also the C(14)–N(1) bond distance [$1.271(3)$ Å] is appreciably close to that of a C=N bond [1.28 Å] confirming the azomethine bond formation [43,44]. The molecule as a whole is non-planar. The maximum deviation from the least squares plane calculated for the hydrazone moiety i.e. C(14)–N(1)–N(2)–C(15)–O(3) is 0.0290 Å for the N1 atom. The aromatic rings (C8-C13) and (C16-C21) form dihedral angles $67.63(12)$ and $61.58(12)^\circ$ respectively with (C1-C6) ring of the compound. Notwithstanding the above, the N(1)–N(2) and N(2)–C(15) bond distances of $1.374(2)$ and $1.337(3)$ Å respectively indicate significant delocalization of π -electron density over the hydrazone portion of the molecule.

The compound adopts *cis* configuration with respect to C(14)–C(11) bond with torsion angle of $3.1(3)^\circ$ for C(10)–C(11)–C(14)–N(1) moiety. So the potential donors O(2) and N(1) are found to be in *syn* disposition. This arrangement enables the O(2)–H(2'') to involve in H-bonding (Fig. 2.19) with

azomethine N(1) atom of the aroylhydrazone resulting in a six membered pseudo-aromatic ring, N(1)–C(14)–C(11)–C(10)–O(2)–H(2''). Such resonance assisted hydrogen bonds seem to be the general feature of the crystal structures of Schiff bases derived from salicylaldehyde [45].

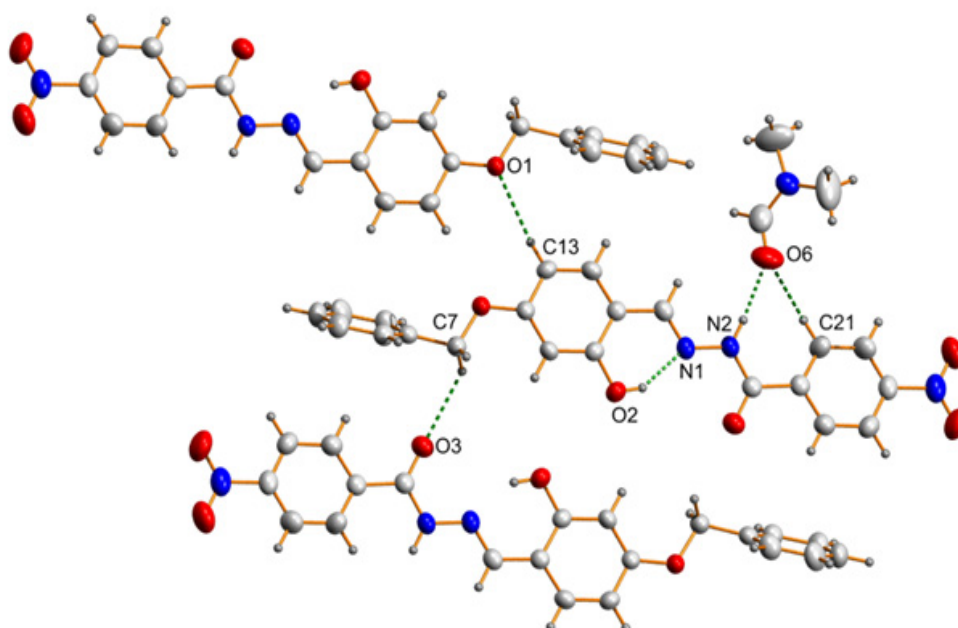


Fig. 2.19. Intra and intermolecular hydrogen bonding interactions of $H_2L^1 \cdot C_3H_7NO$.

There is one conventional N(2)–H(2'')···O(6) and three nonconventional C–H···O intermolecular hydrogen bonds present in the molecular system with D···A distances of 2.810(3), 3.167(3), 3.448(3) and 3.206(3) Å respectively (Table 2.6). The strong intramolecular conventional O–H···N hydrogen bond locks the molecular conformation and minimizes the rotational freedom about the C(11)–C(14) bond. Moreover, two C–H··· π interactions between the hydrogen attached at the C(12) and C(17) atoms and the corresponding aromatic ring C1–C6 of the neighboring molecules with H···Cg distances of

2.91 and 2.85 Å respectively, chain the molecules along c axis. This supramolecular network is augmented by a weak $\pi \cdots \pi$ interaction between the phenyl rings (C8-C13) and (C16-C21) of the molecules with a centroid-centroid distance of 3.650(13) Å by interconnecting the molecules along b axis (Fig. 2.20). Packing of molecules are predominantly favored by the hydrogen bonding and C–H \cdots π interactions. Other short ring interactions are very weak as they correspond to their centroid-centroid distances greater than 4 Å. Fig. 2.21 shows the packing diagram of the compound along c axis.

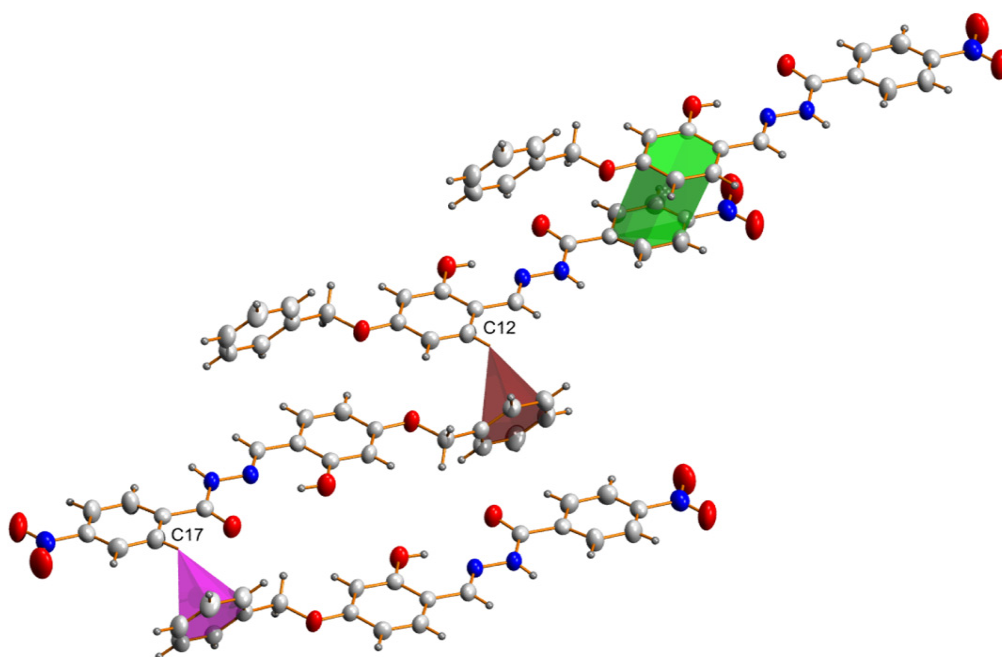


Fig. 2.20. C–H \cdots π and $\pi \cdots \pi$ interactions in H₂L¹·C₃H₇NO.

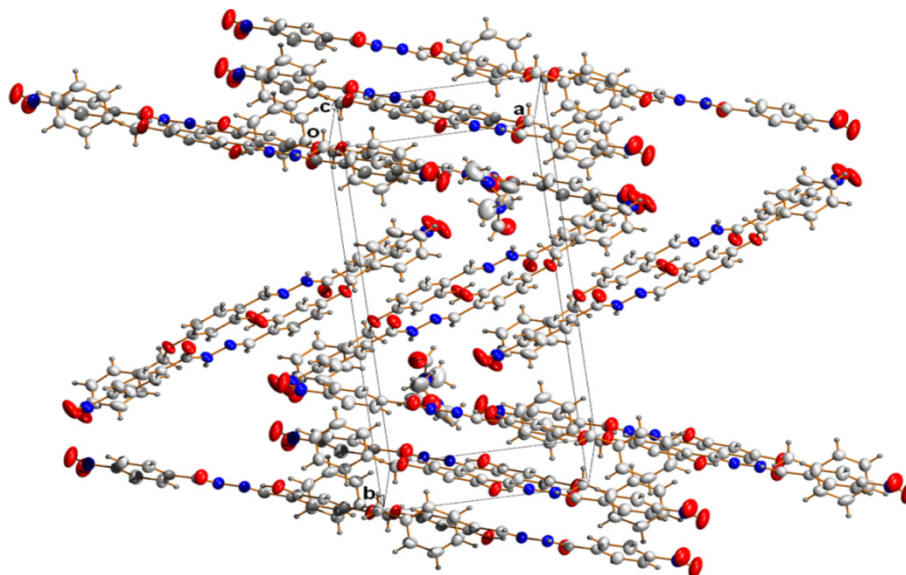

 Fig. 2.21. Packing diagram of $H_2L^1 \cdot C_3H_7NO$ viewed along c axis.

 Table 2.6. Interaction parameters of $H_2L^1 \cdot C_3H_7NO$

Hydrogen bonding interactions				
D–H···A	D–H (Å)	H···A (Å)	D···A (Å)	$\angle D-H \cdots A$ (°)
N(2)–H(2')···O(6) ^a	0.878(14)	1.950(15)	2.810(3)	166(2)
O(2)–H(2'')···N(1)	0.850(1)	1.820(3)	2.583(2)	149(3)
C(7)–H(7B)···O(3) ^b	0.970	2.490	3.167(3)	127
C(13)–H(13)···O(1) ^c	0.930	2.580	3.448(3)	156
C(21)–H(21)···O(6) ^a	0.930	2.420	3.206(3)	143
$\pi \cdots \pi$ interactions				
Cg(I)···Cg(J)	Cg···Cg (Å)	α (°)	β (°)	
Cg(2)···Cg(3) ^d	3.650(13)	6.53(11)	14.21	
C–H··· π interactions				
C–H(I)···Cg(J)	C–H (Å)	H···Cg (Å)	C···Cg (Å)	$\angle C-H \cdots Cg$ (°)
C(12)–H(12)···Cg(1) ^e	0.930	2.910	3.673(2)	140
C(17)–H(17)···Cg(1) ^f	0.930	2.850	3.630(3)	142

Equivalent position codes : a = 1-x, 1-y, -z; b = 1-x, -y, 1-z; c = -x, -y, -z; d = -1+x, 1/2-y, 1/2+z; e = -x, -y, -z; f = 1-x, -y, 1-z
 Cg(1) = C(1), C(2), C(3), C(4), C(5), C(6); Cg(2) = C(8), C(9), C(10), C(11), C(12), C(13);
 Cg(3) = C(16), C(17), C(18), C(19), C(20), C(21)
 D, Donor; A, acceptor; Cg, Centroid; α , dihedral angle between planes I & J; β , angle between Cg···Cg and Cg(J) perp.

2.3.6.2. Crystal structure of $\text{H}_2\text{L}^2 \cdot 2\text{H}_2\text{O} \cdot \text{CH}_3\text{OH}$

Colorless block shaped crystals of 5-bromo-2-hydroxy-3-methoxybenzaldehyde nicotinoylhydrazone dihydrate methanol monosolvate suitable for diffraction analyses were obtained from a solution of the compound in methanol. A single crystal with approximate dimensions of $0.35 \times 0.30 \times 0.25 \text{ mm}^3$ was selected for collecting the data. A perspective view of the molecular structure of the compound along with the atom labelling scheme is shown in Fig. 2.22 and selected geometric parameters are given in Table 2.7. The aroylhydrazone, $\text{H}_2\text{L}^2 \cdot 2\text{H}_2\text{O} \cdot \text{CH}_3\text{OH}$ is crystallized into a monoclinic space group $P2_1/c$. The two aromatic rings are twisted with dihedral angle of $17.8(4)^\circ$. The molecule as a whole has no planarity with maximum deviation of $0.386(10) \text{ \AA}$ for the atom C(14) from its least squares plane. But the central hydrazone moiety, C(7)–N(1)–N(2)–C(8)–O(3), is almost planar with maximum deviation from the least-squares plane of 0.0153 \AA for the C(7) atom.

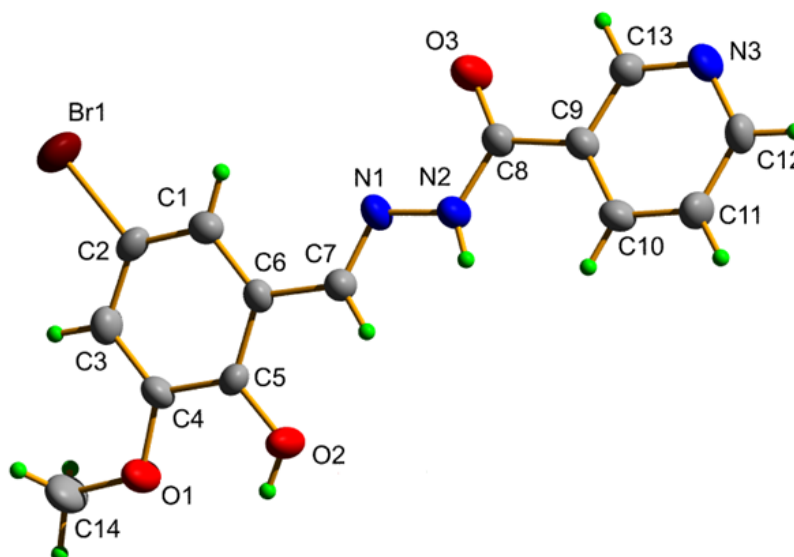


Fig. 2.22. Molecular structure of $\text{H}_2\text{L}^2 \cdot 2\text{H}_2\text{O} \cdot \text{CH}_3\text{OH}$ along with the atom numbering scheme. The solvent molecules are omitted for clarity.

Table 2.7. Crystal data and structure refinement parameters for $\text{H}_2\text{L}^2 \cdot 2\text{H}_2\text{O} \cdot \text{CH}_3\text{OH}$

Parameters	$\text{H}_2\text{L}^2 \cdot 2\text{H}_2\text{O} \cdot \text{CH}_3\text{OH}$
Empirical formula	$\text{C}_{15}\text{H}_{20}\text{BrN}_3\text{O}_6$
Formula weight	418.23
Temperature	296 K
Wavelength	0.71073 Å
Crystal system	Monoclinic
Space group	$P2_1/c$
Unit cell dimensions	$a = 7.8139(5)$ Å $b = 18.8868(13)$ Å $c = 12.8633(8)$ Å $\alpha = 90.00^\circ$ $\beta = 92.12(3)^\circ$ $\gamma = 90.00^\circ$
Volume	1897.1(2) Å ³
Z	4
Density (calculated)	1.450 mg/m ³
Absorption coefficient	2.201 mm ⁻¹
$F(000)$	840
Crystal size	0.35 × 0.30 × 0.25 mm ³
θ range for data collection	2.61 to 25.00°
Limiting indices	$-9 \leq h \leq 7$ $-22 \leq k \leq 22$ $-15 \leq l \leq 15$
Reflections collected	14251
Unique Reflections (R_{int})	3356 [$R_{\text{int}} = 0.0629$]
Refinement method	Full-matrix least-squares on F^2
Data / restraints / parameters	3351 / 3 / 248
Goodness-of-fit on F^2	1.048
Final R indices [$I > 2\sigma(I)$]	$R_1 = 0.0653$, $wR_2 = 0.1988$
R indices (all data)	$R_1 = 0.0795$, $wR_2 = 0.2099$
Largest diff. peak and hole	2.469 and -0.436 e Å ⁻³

$$R_1 = \frac{\sum ||F_o| - |F_c||}{\sum |F_o|}$$

$$wR_2 = [\frac{\sum w(F_o^2 - F_c^2)^2}{\sum w(F_o^2)^2}]^{1/2}$$

The torsion angles of $-179.7(5)^\circ$ and $-178.6(5)^\circ$ corresponding to C(6)–C(7)–N(1)–N(2) and N(1)–N(2)–C(8)–C(9) moieties respectively confirm the *E* configuration of the compound with respect to the C(7)–N(1) and N(2)–C(8) bonds [40]. The bond length of C(8)=O(3) [1.232 (6) Å] shows significant double bond character indicating that the molecule exists in the amido form in the solid state [41,42]. The N(1)–N(2) [1.385(6) Å] and N(2)–C(8) [1.339(7) Å] bond distances are intermediate between the ideal values of corresponding single [N–N: 1.45 Å and C–N: 1.47 Å] and double bonds [N=N: 1.25 Å and C=N: 1.28 Å], giving evidence for an extended π delocalization along the hydrazone moiety. The selected bond lengths and angles are given in Table 2.8 and torsion angles in Table 2.9.

Table 2.8. Selected bond lengths [Å] and angles [°] for $\text{H}_2\text{L}^2 \cdot 2\text{H}_2\text{O} \cdot \text{CH}_3\text{OH}$

Bond lengths		Bond angles	
N(1)–C(7)	1.267(6)	C(7)–N(1)–N(2)	114.2(4)
C(5)–O(2)	1.342(6)	N(2)–C(8)–C(9)	116.9(4)
N(1)–N(2)	1.385(6)	N(1)–C(7)–C(6)	121.4(5)
C(8)–O(3)	1.232(6)	N(2)–C(8)–O(3)	122.1(5)
N(2)–C(8)	1.339(7)	O(2)–C(5)–C(6)	118.4(4)
C(4)–O(1)	1.366(6)	C(7)–C(6)–C(1)	122.6(5)
C(6)–C(7)	1.460(7)	C(8)–N(2)–N(1)	118.7(4)

Table 2.9. Selected torsion angles [°] for $\text{H}_2\text{L}^2 \cdot 2\text{H}_2\text{O} \cdot \text{CH}_3\text{OH}$

Torsion angles	
C(1)–C(6)–C(7)–N(1)	-14.3(8)
C(6)–C(7)–N(1)–N(2)	-179.7(5)
N(1)–N(2)–C(8)–C(9)	-178.6(5)
N(1)–N(2)–C(8)–O(3)	1.1(8)

The strong intermolecular O–H···N hydrogen bonds propagate the 1D network with the overall motif being a wavy chain along crystallographic *b* direction (Fig. 2.23). The main structural feature that facilitate the crystal packing is the stacking of molecules along crystallographic *c* direction by means of $\pi\cdots\pi$ interaction between Cg(1) and Cg(2) of the neighboring molecules (Fig. 2.24). Fig. 2.25 shows the packing diagram of the compound along *b* axis. The assemblage of molecules in the respective manner in the unit cell is resulted by the $\pi\cdots\pi$ and hydrogen bonding interactions. The interaction parameters are shown in Table 2.10.

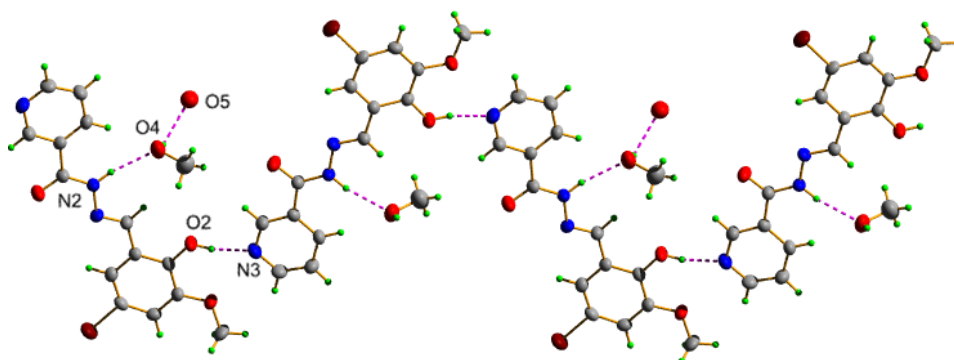


Fig. 2.23. Intra and intermolecular hydrogen bonding interactions of $\text{H}_2\text{L}^2\cdot 2\text{H}_2\text{O}\cdot\text{CH}_3\text{OH}$.

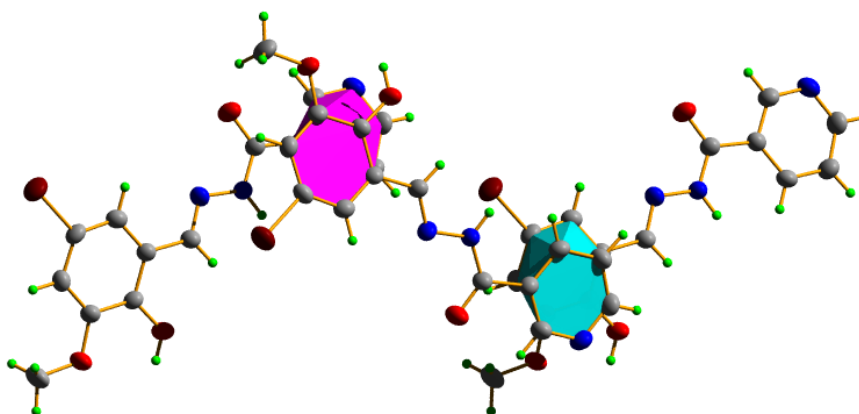
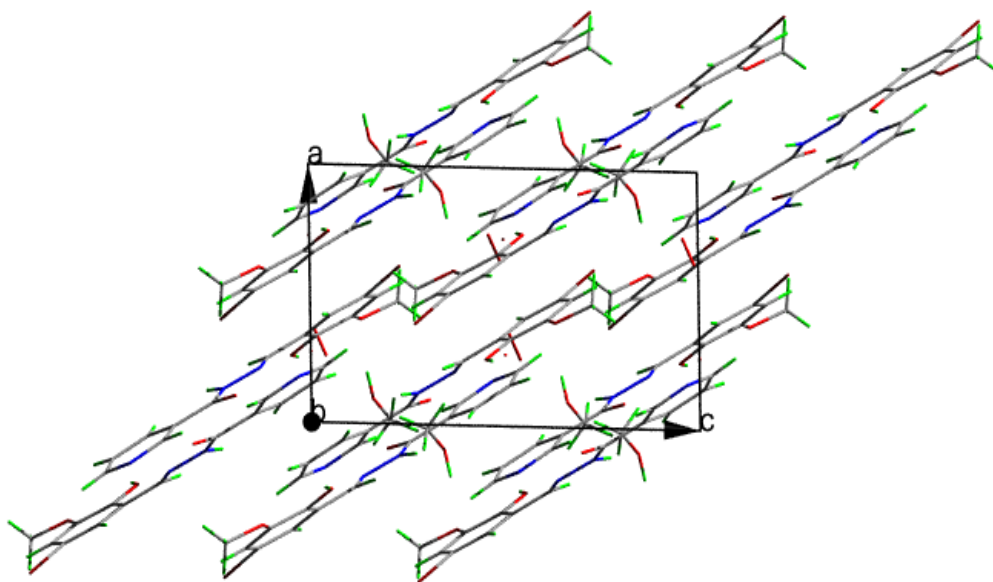


Fig. 2.24. The $\pi\cdots\pi$ interactions in $\text{H}_2\text{L}^2\cdot 2\text{H}_2\text{O}\cdot\text{CH}_3\text{OH}$.

Table 2.10. Interaction parameters of $\text{H}_2\text{L}^2 \cdot 2\text{H}_2\text{O} \cdot \text{CH}_3\text{OH}$

Hydrogen bonding interactions				
D-H...A	D-H (Å)	H...A (Å)	D...A (Å)	$\angle\text{D-H}\cdots\text{A}$ (°)
O(2)-H(2)...N(3) ^a	0.850(4)	1.89(4)	2.651(8)	149(7)
N(2)-H(2')...O(4)	0.850(1)	1.820(3)	2.583(2)	149(3)
O(4)-H(4)...O(5) ^b	0.850(9)	1.970(10)	2.781(10)	161(10)
$\pi\cdots\pi$ interactions				
Cg(I)...Cg(J)	Cg...Cg (Å)	α (°)	β (°)	
Cg(1)...Cg(2) ^c	3.725(4)	2.04	24.24	
Cg(2)...Cg(1) ^d	3.725(4)	2.04	22.79	

Equivalent position codes : a = 2-x, -1/2+y, 3/2-z; b = x, y, 1+z; c = 1+x, 1/2-y, 1/2+z; d = -1+x, 1/2-y, -1/2+z
 Cg(1) = N(3), C(9), C(10), C(11), C(12), C(13); Cg(2) = C(1), C(2), C(3), C(4), C(5), C(6)
 D, Donor; A, acceptor; Cg, Centroid; α , dihedral angle between planes I & J; β , angle between Cg...Cg and Cg(J) perp.

Fig. 2.25. Packing diagram of $\text{H}_2\text{L}^2 \cdot 2\text{H}_2\text{O} \cdot \text{CH}_3\text{OH}$ viewed along b axis.

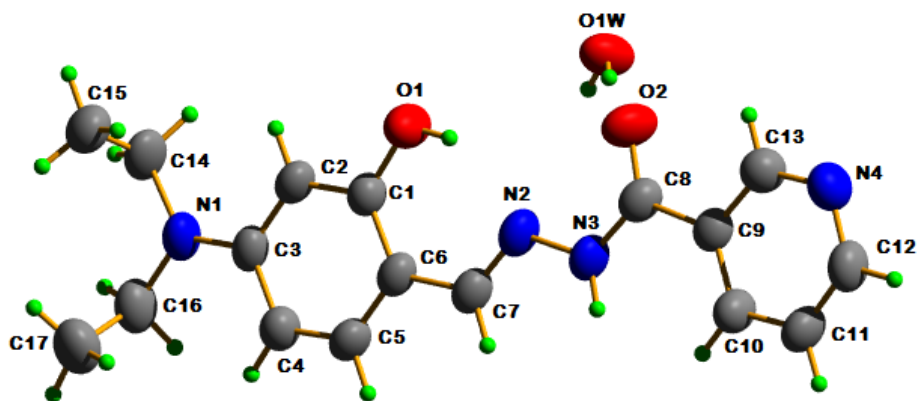
2.3.6.3. Crystal structure of $\text{H}_2\text{L}^3 \cdot \text{H}_2\text{O}$ 

Fig. 2.26. Molecular structure of $\text{H}_2\text{L}^3 \cdot \text{H}_2\text{O}$ along with the atom numbering scheme.

Yellow block shaped crystals of $\text{H}_2\text{L}^3 \cdot \text{H}_2\text{O}$ suitable for single crystal X-ray diffraction analyses were obtained by slow evaporation of its methanolic solution. The compound crystallizes in triclinic space group $P\bar{1}$. Its approximate dimensions are $0.40 \times 0.30 \times 0.25 \text{ mm}^3$. The crystallographic data along with structure refinement parameters are given in Table 2.11. A perspective view of the molecular structure of the compound along with the atom labelling is shown in Fig. 2.26.

The bond length of $\text{C}(8)=\text{O}(2)$ [$1.231(2) \text{ \AA}$] is closer to that expected for $\text{C}=\text{O}$ bond indicating that the molecule exists in amido form in the solid state [41,42]. Also the $\text{C}(7)-\text{N}(2)$ bond distance [$1.275(3) \text{ \AA}$] is appreciably close to that of a $\text{C}=\text{N}$ bond [1.28 \AA], indicating the azomethine bond formation [43,44]. The selected bond lengths and bond angles are given in Table 2.12 and torsion angles in Table 2.13. The bond distances and angles agree with the corresponding bond distances and angles reported in closely related compounds [45,46].

Table 2.11. Crystal data and structure refinement parameters for H₂L³·H₂O

Parameters	H ₂ L ³ ·H ₂ O
Empirical formula	C ₁₇ H ₂₂ N ₄ O ₃
Formula weight	330.39
Temperature	296 K
Wavelength	0.71073 Å
Crystal system	Triclinic
Space group	$P\bar{1}$
Unit cell dimensions	$a = 6.6773(8)$ Å $b = 7.9344(8)$ Å $c = 16.700(2)$ Å $\alpha = 86.243(6)^\circ$ $\beta = 78.516(6)^\circ$ $\gamma = 74.152(6)^\circ$
Volume	834.05(17) Å ³
Z	2
Density (calculated)	1.316 mg/m ³
Absorption coefficient	0.092 mm ⁻¹
$F(000)$	352.0
Crystal size	0.40 × 0.30 × 0.25 mm ³
θ range for data collection	1.24 to 28.37°
Limiting indices	-8 ≤ h ≤ 8 -10 ≤ k ≤ 10 -22 ≤ l ≤ 22
Reflections collected	15107
Unique Reflections (R_{int})	4138 [$R_{int} = 0.0905$]
Refinement method	Full-matrix least-squares on F^2
Data / restraints / parameters	4138 / 5 / 236
Goodness-of-fit on F^2	0.961
Final R indices [$I > 2\sigma(I)$]	$R_1 = 0.0632$, $wR_2 = 0.1649$
R indices (all data)	$R_1 = 0.1251$, $wR_2 = 0.2210$
Largest diff. peak and hole	0.241 and -0.202 e Å ⁻³

$$R_1 = \frac{\sum ||F_o| - |F_c||}{\sum |F_o|}$$

$$wR_2 = [\sum w(F_o^2 - F_c^2)^2 / \sum w(F_o^2)^2]^{1/2}$$

Table 2.12. Selected bond lengths [Å] and angles [°] for H₂L³·H₂O

Bond lengths		Bond angles	
N(2)–C(7)	1.275(3)	C(7)–N(2)–N(3)	115.98(18)
O(1)–C(1)	1.356(3)	N(3)–C(8)–C(9)	117.08(19)
N(2)–N(3)	1.381(2)	N(2)–C(7)–C(6)	122.2(2)
O(2)–C(8)	1.231(2)	N(3)–C(8)–O(2)	122.43(19)
N(3)–C(8)	1.334(3)	O(1)–C(1)–C(6)	121.34(18)
N(1)–C(3)	1.369(2)	C(7)–C(6)–C(5)	120.13(19)
C(6)–C(7)	1.430(3)	C(8)–N(3)–N(2)	119.06(18)

Table 2.13. Selected torsion angles [°] for H₂L³·H₂O

Torsion angles	
C(5)–C(6)–C(7)–N(2)	176.14(19)
C(6)–C(7)–N(2)–N(3)	179.27(16)
N(2)–N(3)–C(8)–C(9)	176.96(15)
N(2)–N(3)–C(8)–O(2)	-3.6(3)
N(2)–C(7)–C(6)–C(1)	-1.5(3)

The molecule is almost planar with a dihedral angle of 1.92(11)° between the aromatic rings. The maximum deviation from the least-squares plane calculated for the hydrazone moiety, C(7)–N(2)–N(3)–C(8)–O(2) is 0.0167 Å for the C(8) atom. The torsion angle value 179.27(16)° corresponding to C(6)–C(7)–N(2)–N(3) moiety confirms the *E* configuration of the compound with respect to the C(7)–N(2) bond. Atom N(2) lies *cis* to O(1) with torsion angle of -1.5(3)° for N(2)–C(7)–C(6)–C(1) moiety. This arrangement enables the O(1)–H(1) to involve in hydrogen bonding with azomethine N(2) atom of the aroylhydrazone resulting in a six membered pseudo-aromatic ring, N(2)–C(7)–C(6)–C(1)–O(1)–H(1) (Fig. 2.27). Such resonance assisted hydrogen

bonds seem to be the general feature of the crystal structures of hydrazones derived from salicylaldehyde [45].

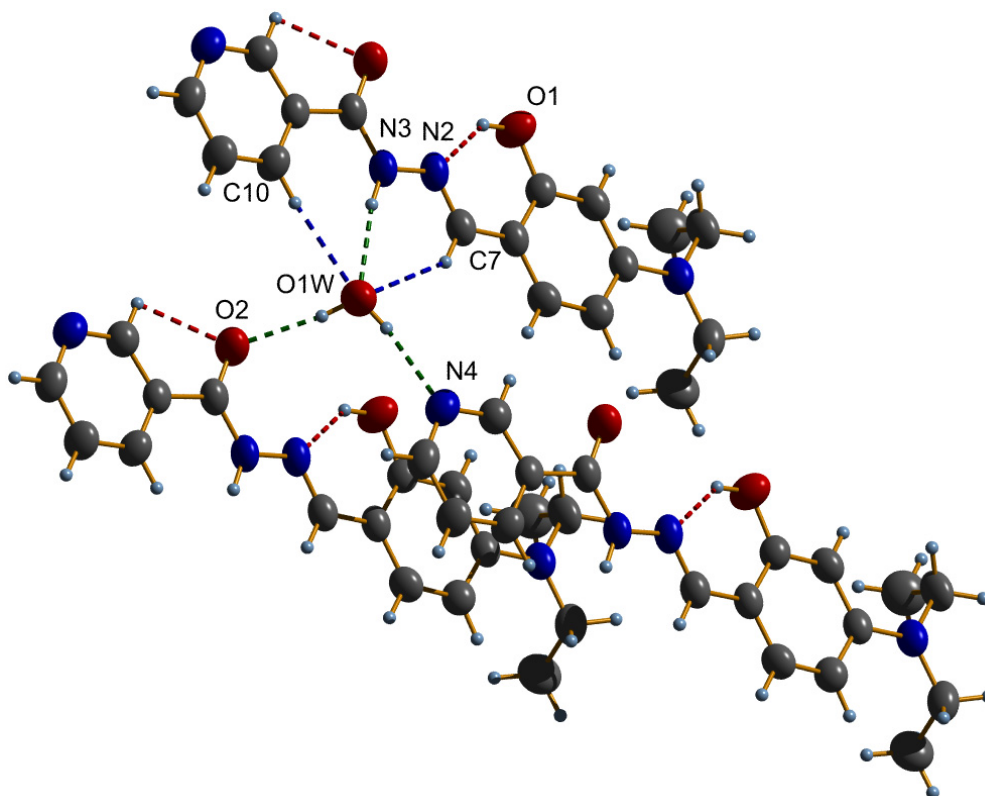


Fig. 2.27. Intra and intermolecular hydrogen bonding interactions of $H_2L^3 \cdot H_2O$.

Fig. 2.28 shows the packing diagram of the compound. The lattice water molecule plays an essential role in packing of the molecules forming conventional and nonconventional hydrogen bonds between the hydrazone and water molecule (Fig. 2.27). Three types of $\pi \cdots \pi$ interactions are also observed in the crystal structure with a shortest centroid-centroid distance of 3.7137(13) Å (Fig. 2.29). The interaction parameters are shown in Table 2.14. The conventional and nonconventional intramolecular hydrogen bonds (O–H \cdots N,

O–H···O and C–H···O) present in the molecule increase the rigidity of the molecule whereas the intermolecular hydrogen bonding interactions (O–H···N, N–H···O and C–H···O) supported with $\pi\cdots\pi$ and C–H··· π interactions establish a supramolecular linkage among the molecules in the crystal system.

Table 2.14. Interaction parameters of $H_2L^3 \cdot H_2O$

Hydrogen bonding interactions				
D–H···A	D–H (Å)	H···A (Å)	D···A (Å)	\angle D–H···A (°)
N(3)–H(3)···O(1W) ^a	0.850(14)	2.131(15)	2.970(3)	169(3)
O(1W)–H(1A)···N(4) ^b	0.851(16)	2.138(19)	2.975(2)	168(2)
O(1W)–H(1B)···O(2)	0.85(2)	1.94(2)	2.789(2)	172(3)
O(1)–H(1)···N(2)	0.85(2)	1.96(3)	2.667(3)	141(2)
C(7)–H(7)···O(1W) ^a	0.93	2.58	3.385(3)	145
C(10)–H(10)···O(1W) ^a	0.93	2.42	3.339(3)	167
C(13)–H(13)···O(2)	0.93	2.40	2.752(3)	102
$\pi\cdots\pi$ interactions				
Cg(I)···Cg(J)	Cg···Cg (Å)	α (°)	β (°)	
Cg(1)···Cg(1) ^c	3.7934(13)	0	19.72	
Cg(1)···Cg(2) ^d	3.7137(13)	1.93(10)	23.33	
Cg(2)···Cg(1) ^e	3.7137(13)	1.93(10)	21.52	

Equivalent position codes : a = 1+x, y, z; b = x, -1+y, z; c = 1-x, 2-y, -z; d = x, 1+y, z; e = x, -1+y, z
 Cg(1) = N(4), C(9), C(10), C(11), C(12), C(13); Cg(2) = C(1), C(2), C(3), C(4), C(5), C(6)
 D, Donor; A, acceptor; Cg, Centroid; α , dihedral angle between planes I & J; β , angle between Cg···Cg and Cg(J) perp.

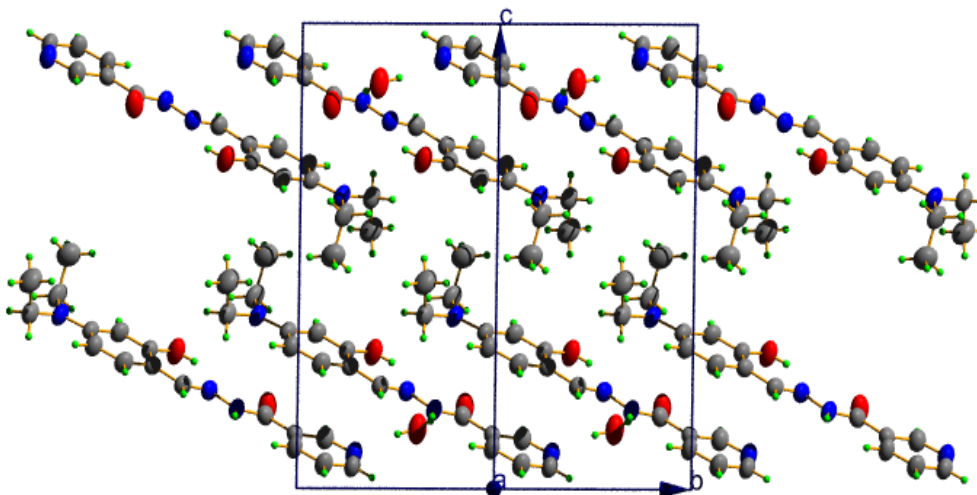


Fig. 2.28. Packing diagram of $\text{H}_2\text{L}^3 \cdot \text{H}_2\text{O}$ viewed along a axis.

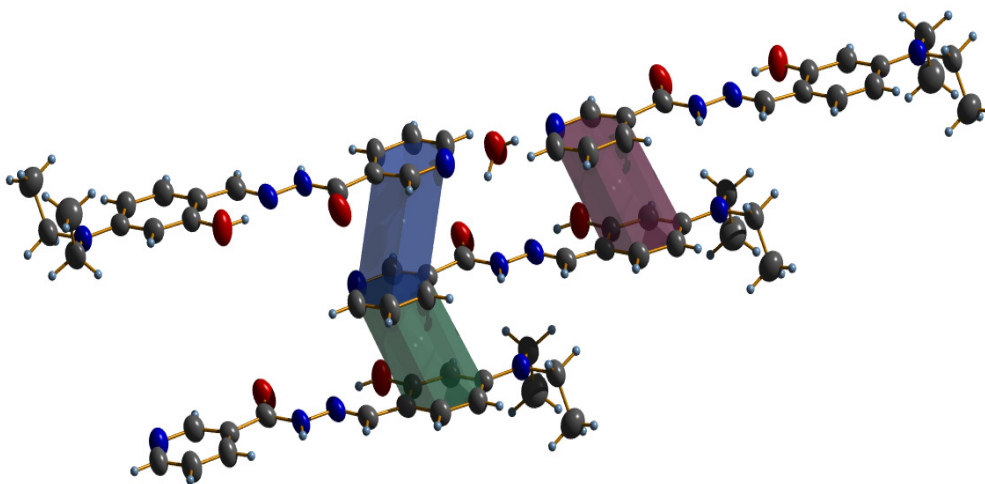


Fig. 2.29. The $\pi \cdots \pi$ interactions in $\text{H}_2\text{L}^3 \cdot \text{H}_2\text{O}$.

2.3.6.4. Crystal structure of HL⁴

Colorless block shaped crystals of 2-benzoylpyridine-4-nitrobenzoyl hydrazone suitable for single crystal X-ray diffraction analysis were obtained by slow evaporation of its solution in methanol over 4 days. A single crystal

with approximate dimensions of $0.30 \times 0.20 \times 0.15 \text{ mm}^3$ was selected for collecting the data. The molecular structure of HL⁴ along with the atom numbering scheme is given in Fig. 2.30. The crystallographic data and structure refinement parameters of the compound are given in Table 2.15, the selected bond lengths and bond angles are given in Table 2.16 and the torsion angles in Table 2.17.

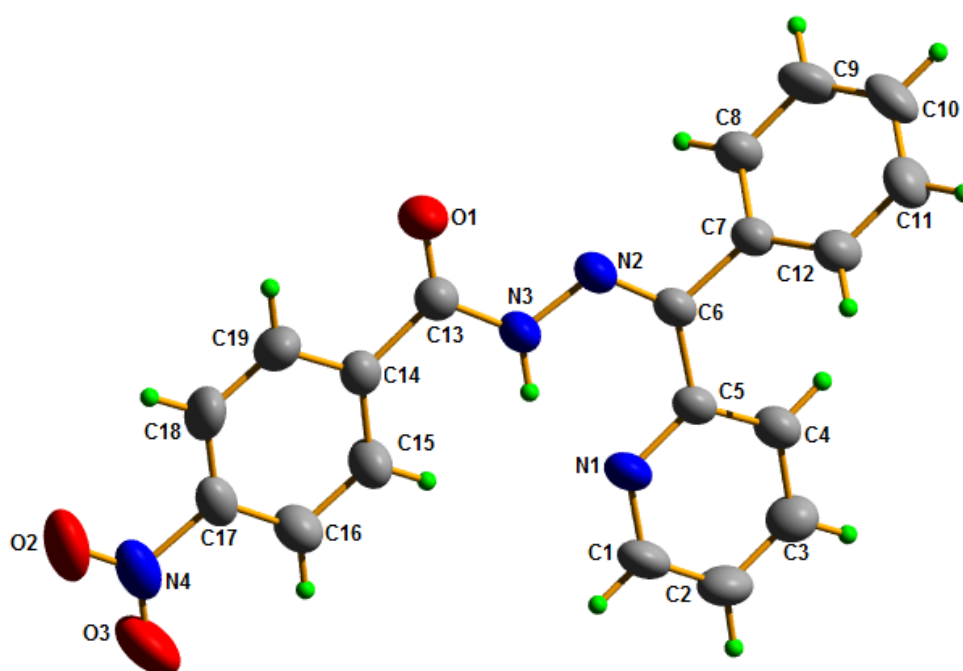


Fig. 2.30. Molecular structure of HL⁴ along with the atom numbering scheme.

Table 2.15. Crystal data and structure refinement parameters for HL⁴

Parameters	HL ⁴
Empirical formula	C ₁₉ H ₁₄ N ₄ O ₃
Formula weight	346.34
Temperature	296 K
Wavelength	0.71073 Å
Crystal system	Monoclinic
Space group	<i>P</i> 2 ₁ / <i>c</i>
Unit cell dimensions	<i>a</i> = 15.6546(9) Å <i>b</i> = 7.4060(5) Å <i>c</i> = 13.9690(8) Å <i>α</i> = 90.000° <i>β</i> = 92.645(3)° <i>γ</i> = 90.000°
Volume	1617.81(17) Å ³
<i>Z</i>	4
Density (calculated)	1.422 mg/m ³
Absorption coefficient	0.100 mm ⁻¹
<i>F</i> (000)	720
Crystal size	0.30 × 0.20 × 0.15 mm ³
θ range for data collection	2.92 to 27.50°
Limiting indices	-20 ≤ <i>h</i> ≤ 19 -9 ≤ <i>k</i> ≤ 8 -18 ≤ <i>l</i> ≤ 17
Reflections collected	12811
Unique Reflections (<i>R</i> _{int})	3684 [<i>R</i> (int) = 0.0204]
Refinement method	Full-matrix least-squares on <i>F</i> ²
Data / restraints / parameters	3684 / 0 / 239
Goodness-of-fit on <i>F</i> ²	1.025
Final <i>R</i> indices [<i>I</i> > 2σ(<i>I</i>)]	<i>R</i> ₁ = 0.0465, <i>wR</i> ₂ = 0.1237
<i>R</i> indices (all data)	<i>R</i> ₁ = 0.0751, <i>wR</i> ₂ = 0.1467
Largest diff. peak and hole	0.170 and -0.202e Å ⁻³

$$R_1 = \frac{\sum ||F_o| - |F_c||}{\sum |F_o|}$$

$$wR_2 = [\sum w(F_o^2 - F_c^2)^2 / \sum w(F_o^2)^2]^{1/2}$$

Table 2.16. Selected bond lengths [Å] and angles [°] for HL⁴

Bond lengths		Bond angles	
N(2)–C(6)	1.296(19)	C(6)–N(2)–N(3)	117.92(13)
N(2)–N(3)	1.366(17)	N(3)–C(13)–C(14)	113.53(14)
C(13)–O(1)	1.209(19)	N(2)–C(6)–C(7)	113.16(13)
N(3)–C(13)	1.357(2)	N(2)–C(6)–C(5)	127.93(13)
N(4)–C(17)	1.477(2)	C(7)–C(6)–C(5)	118.89(13)
C(6)–C(7)	1.487(2)	C(13)–N(3)–N(2)	119.50(14)

Table 2.17. Selected torsion angles [°] for HL⁴

Torsion angles	
C(8)–C(7)–C(6)–N(2)	-51.8(2)
C(7)–C(6)–N(2)–N(3)	-179.42(14)
N(2)–N(3)–C(13)–C(14)	177.84(14)
N(2)–N(3)–C(13)–O(1)	1.8(3)
C(5)–C(6)–N(2)–N(3)	2.2(3)
N(3)–C(13)–C(14)–C(19)	171.50(17)

The compound crystallizes into a monoclinic space group $P2_1/c$. The C(13)–O(1) bond [1.209(19) Å] has a double bond character [41,42] which shows that the molecule exists in amido form in the solid state. The N(2)–C(6) bond length 1.296(19) Å with significant double bond character is comparable to those previously reported analogous of hydrazone structures [43,47]. The torsion angle of 2.2(3)° perceived by C(5)–C(6)–N(2)–N(3) moiety supports the *cis* configuration with respect to C(6)=N(2) bond in the aroylhydrazone. The molecule also exists in *cis* configuration with respect to N(3)–C(13) bond with N(2)–N(3)–C(13)–O(1) torsion angle of 1.8(3)°. The central part of the molecule is essentially planar due to the presence of an intramolecular

N–H \cdots N_{pyridine} hydrogen bonding (Fig. 2.31). The N(2)–N(3) and N(3)–C(13) bond distances of 1.366(17) and 1.357(2) Å respectively indicate significant delocalization of π -electron density over the hydrazone moiety. The planarity of hydrazone moiety allows delocalization of the π electrons throughout the molecule. The maximum deviation from the least-squares plane calculated for the hydrazone moiety, C(6)–N(2)–N(3)–C(13)–O(1), is 0.0123 Å for the C(13) atom. The terminal aromatic rings (C14–C19) and (C7–C12) are twisted out of this plane as seen in the values of the N(2)–C(6)–C(7)–C(8) and N(3)–C(13)–C(14)–C(19) torsion angles of $-51.8(2)$ and $171.50(17)^\circ$ respectively. The dihedral angle formed between the terminal rings (C14–C19) & (C7–C12) is $61.99(12)^\circ$ and that between (C14–C19) & (C1–N1) rings is 6.00° . The above observations indicate nonplanarity of the aroylhydrazone, HL⁴ although the hydrazone part itself is planar.

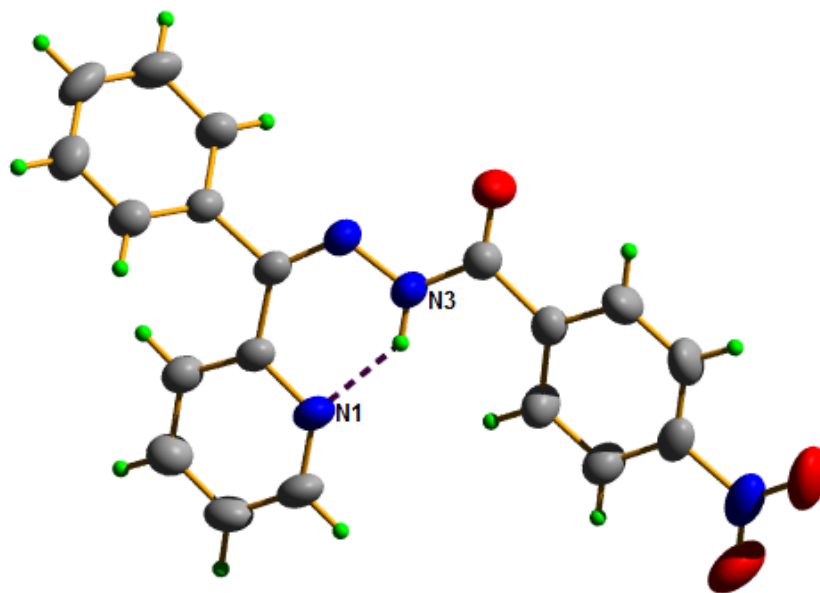


Fig. 2.31. Hydrogen bonding interaction shown as dotted line.

The packing diagram of the compound viewed along *c* axis is shown in Fig. 2.32. Rings Cg(1) and Cg(2) of neighboring molecules are involved in $\pi \cdots \pi$ stacking with a distance of 3.8393(11) Å (Fig. 2.33). A prominent C–H $\cdots\pi$ interaction is also observed between the H atom attached at the C(11) and Cg(2) ring at a distance of 2.880 Å (Fig. 2.34). The packing of crystal structure is also stabilized by weak N–O $\cdots\pi$ interactions (Fig. 2.34). The interaction parameters are shown in Table 2.18.

Table 2.18. Interaction parameters of HL⁴

Hydrogen bonding interactions				
D–H \cdots A	D–H (Å)	H \cdots A (Å)	D \cdots A (Å)	\angle D–H \cdots A (°)
N2–H3' \cdots N1	0.877(19)	1.887(19)	2.610 (2)	138.6(16)
$\pi \cdots \pi$ interactions				
Cg(I) \cdots Cg(J)	Cg \cdots Cg (Å)	α (°)	β (°)	
Cg(1) \cdots Cg(2) ^a	3.8393(11)	10.13(9)	27.11	
Cg(2) \cdots Cg(1) ^b	3.8393(11)	10.13(9)	18.98	
Y–X$\cdots\pi$ interactions				
Y–X(I) \cdots Cg(J)	Y–X (Å)	X \cdots Cg (Å)	Y \cdots Cg (Å)	\angle Y–X \cdots Cg (°)
C(11)–H(11) \cdots Cg(2) ^c	0.930	2.880	3.591(2)	134
N(4)–O(2) \cdots Cg(1) ^d	1.223(2)	3.800	3.707)	76.35
Equivalent position codes : a = x, 1/2-y, -1/2+z; b = x, 1/2-y, 1/2+z; c = -x, -y, -z; d = -1+x, 1/2-y, 1/2+z				
Cg(1) = N(1), C(1), C(2), C(3), C(4), C(5); Cg(2) = C(7), C(8), C(9), C(10), C(11), C(12)				
D, Donor; A, acceptor; Cg, Centroid; α , dihedral angle between planes I & J; β , angle between Cg \cdots Cg and Cg(J) perp.				

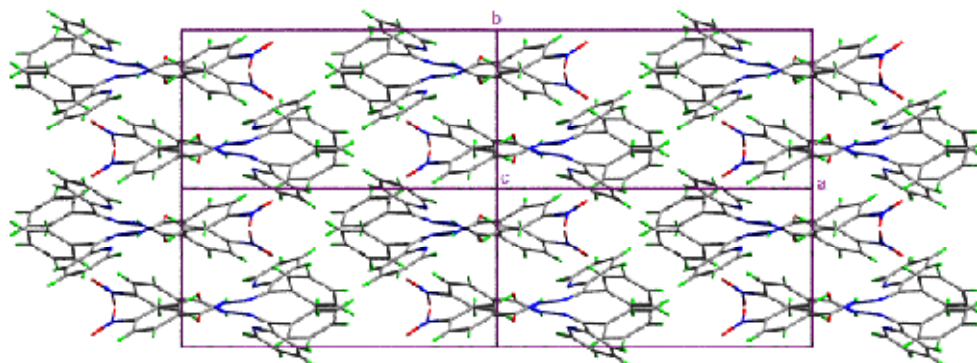


Fig. 2.32. Packing diagram of HL⁴ viewed along *c* axis.

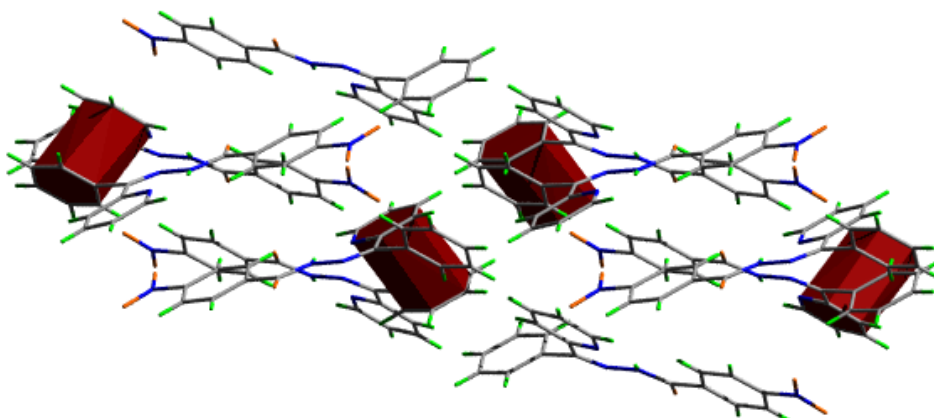


Fig. 2.33. The $\pi \cdots \pi$ interactions in HL⁴.

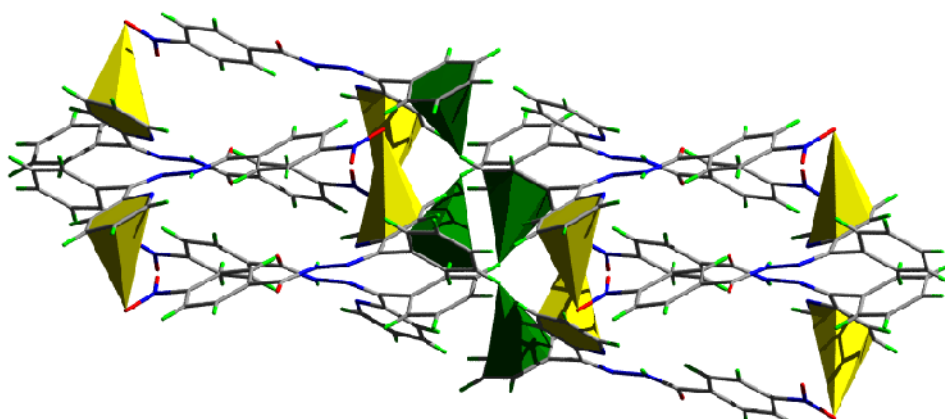


Fig. 2.34. C-H $\cdots\pi$ and N-O $\cdots\pi$ interactions in HL⁴.

References

- [1] H.H. Monfared, R. Bikas, P.M. Anarjan, A.J. Blake, V. Lippolis, N.B. Arslan, C. Kazak, *Polyhedron* 69 (2014) 90.
- [2] N.A. Mangalam, S. Sivakumar, M.R.P. Kurup, E. Suresh, *Spectrochim. Acta A* 75 (2010) 686.
- [3] M. Alagesan, N.S.P. Bhuvanesh, N. Dharmaraj, *Dalton Trans.* 42 (2013) 7210.
- [4] V.P. Singh, S. Singh, D. Singh, P. Singh, K. Tiwari, M. Mishra, R. Butcher, *Polyhedron* 56 (2013) 71.
- [5] M. Sutradhar, M.V. Kirillova, M.F.C.G. da Silva, C.M. Liu, A.J.L. Pombeiro, *Dalton Trans.* 42 (2013) 16578.
- [6] H. Shi, Y. Yin, *Inorg. Chim. Acta* 421 (2014) 446.
- [7] S. Mukherjee, P. Mal, H.S. Evans, *Polyhedron* 73 (2014) 87.
- [8] M.A.A. El-Sayed, N.I. Abdel-Aziz, A.A.M. Abdel-Aziz, A.S. El-Azab, Y.A. Asiri, K.E.H. El-Tahir, *Bioorg. Med. Chem.* 19 (2011) 3416.
- [9] G. Tamasi, L. Chiasserini, L. Savini, A. Sega, R. Cini, *J. Inorg. Biochem.* 99 (2005) 1347.
- [10] S. Lee, K.Y. Jung, J. Park, J.H. Cho, Y.C. Kim, S. Chang, *Bioorg. Med. Chem. Lett.* 20 (2010) 4858.
- [11] G.L. Parrilha, R.P. Vieira, A.P. Rebolledo, I.C. Mendes, L.M. Lima, E.J. Barreiro, O.E. Piro, E.E. Castellano, H. Beraldo, *Polyhedron* 30 (2011) 1891.
- [12] J.R. Dimmock, S.C. Vashishtha, J.P. Stables, *Eur. J. Med. Chem.* 35 (2000) 241.
- [13] P. Dandawate, K. Vemuri, E.M. Khan, M. Sritharan, S. Padhye, *Carbohydr. Polym.* 108 (2014) 135.

- [14] R.S. Nair, M. Kuriakose, V. Somasundaram, V. Shenoi, M.R.P. Kurup, P. Srinivas, *Life Sci.* 116 (2014) 90.
- [15] E.B. Lindgren, M.A. Brito, T.R.A. Vasconcelos, M.O. Moraes, R.C. Montenegro, J.D. Yoneda, K.Z. Leal, *Eur. J. Med. Chem.* 86 (2014) 12.
- [16] P. Vicini, M. Incerti, P.L. Colla, R. Loddo, *Eur. J. Med. Chem.* 44 (2009) 1801.
- [17] B. Hollo, J. Magyari, V.Z. Radovanovic, G. Vuckovic, Z.D. Tomic, I.M. Szilagy, G. Pokol, K.M. Szecsenyi, *Polyhedron* 80 (2014) 142.
- [18] E.N. Nfor, A. Husian, F. Majoumo-Mbe, I.N. Njah, O.E. Offiong, S.A. Bourne, *Polyhedron* 63 (2013) 207.
- [19] D. Sadhukhan, M. Maiti, E. Zangrando, S. Pathan, S. Mitra, A. Patel, *Polyhedron* 69 (2014) 1.
- [20] X. Deng, N.S. Mani, *Org. Lett.* 8 (2006) 3505.
- [21] X. Su, I. Aprahamian, *Chem. Soc. Rev.* 43 (2014) 1963.
- [22] K.H. Reddy, K.B. Chandrasekhar, *Indian J. Chem.* 40 (2001) 727.
- [23] S.Y. Ebrahimipour, I. Sheikhshoae, A. Crochet, M. Khaleghi, K.M. Fromm, *J. Mol. Struct.* 1072 (2014) 267.
- [24] A.H. Reshak, H. Kamarudin, S. Auluck, *J. Phys. Chem.* 116 (2012) 4677.
- [25] K. Naseema, K.V. Sujith, K.B. Manjunatha, B. Kalluraya, G. Umesh, V. Rao, *Optic. Laser Tech.* 42 (2010) 741.
- [26] S.R. Sheeja, N.A. Mangalam, M.R.P. Kurup, Y.S. Mary, K. Raju, H.T. Varghese, C.Y. Panicker, *J. Mol. Struct.* 973 (2010) 36.
- [27] A.A.R. Despaigne, J.G. Da Silva, A.C.M. Carmo, O.E. Piro, E.E. Castellano, H. Beraldo, *Inorg. Chim. Acta* 362 (2009) 2117.
- [28] A. Yasuhara, Y. Tanaka, M. Makishima, S. Suzuki, T. Shibamoto, *J. Chromatograph. Separat. Techniq.* 2 (2011) 1.

- [29] D. Strazic, T. Benkovic, D. Gembarovski, D. Kontrec, N. Galic, *Int. J. Mass Spectrom.* 371 (2014) 54.
- [30] M.M.A. Neaimi, M.M.A. Khuder, *Spectrochim. Acta A* 105 (2013) 365.
- [31] N.K. Ngan, K.M. Lo, C.S.R. Wong, *Polyhedron* 33 (2012) 235.
- [32] M.K. Prasanna, K. Pradeepkumar, *Int. J. Pharm. Biomed. Sci.* 4 (2013) 24.
- [33] O.S. Devi, A.M. Singh, *J. Chem. Pharm. Res.* 3 (2011) 1055.
- [34] P. Krishnamoorthy, P. Sathyadevi, R.R. Butorac, A.H. Cowley, N.S.P. Bhuvanesh, N. Dharmaraj, *Dalton Trans.* 41 (2012) 6842.
- [35] SMART and SAINT, Area Detector Software Package and SAX Area Detector Integration Program, Bruker Analytical X-ray; Madison, WI, USA, 1997.
- [36] Bruker, SADABS, APEX2, XPREP and SAINT, Bruker AXS Inc., Madison, Wisconsin, USA, 2004.
- [37] G.M. Sheldrick, *Acta Cryst. Sect. A* 64 (2008) 112.
- [38] K. Brandenburg, Diamond Version 3.2g, Crystal Impact GbR, Bonn, Germany, 2010.
- [39] B. Ghosh, S. Naskar, A. Espinosa, S.C.K. Hau, T.C.W. Mak, R. Sekiya, R. Kuroda, S.K. Chattopadhyay, *Polyhedron* 72 (2014) 115.
- [40] M.K. Prasanna, M. Sithambaresan, K. Pradeepkumar, M.R.P. Kurup, *Acta Cryst. E* 69 (2013) o1342.
- [41] A.A.R. Despaigne, J.G. Da Silva, A.C.M. Do Carmo, O.E. Piro, E.E. Castellano, H. Berado, *J. Mol. Struct.* 920 (2009) 97.
- [42] M. Bakir, O. Brown, *J. Mol. Struct.* 609 (2002) 129.
- [43] B.N.B. Raj, M.R.P. Kurup, E. Suresh, *Spectrochim. Acta A* 71 (2008) 1253.

- [44] P. Singh, D.P. Singh, V.P. Singh, *Polyhedron* 81 (2014) 56.
- [45] R.G. Baughman, K.L. Martin, R.K. Singh, J.O. Stoffer, *Acta Cryst. C* 60 (2004) o103.
- [46] X.W. Zhu, Y.J. Zhang, C.X. Zhang, H.Y. Qian, Z. *Kristallogr.* 226 (2011) 375.
- [47] A.A.R. Despaigne, G.L. Parrilha, J.B. Izidoro, P.R. da Costa, R.G. dos Santos, O.E. Piro, E.E. Castellano, W.R. Rocha, H. Berado, *Eur. J. Med. Chem.* 50 (2012) 163.

..........

**SYNTHESES AND SPECTRAL CHARACTERIZATION OF
OXIDOVANADIUM(IV) CHELATES OF TRIDENTATE
AROYLHYDRAZONES**

3.1 Introduction
3.2 Experimental
3.3 Results and discussion
References

3.1. Introduction

Vanadium is widely distributed in the biosphere and its essential role has been recognized in both plants and animals. It is a greyish silvery metal and is soft and ductile. It has good corrosion resistance due to a protective film of oxide on the surface. Vanadium was discovered by Andres Manuel del Rio in 1801 by analyzing a new lead-bearing mineral called 'brown lead' and named the new element *erythronium* (Greek for 'red') as most of its salts turned red upon heating. The element was rediscovered in 1831 by Nils Gabriel Sefstrom, who named it vanadium after the Scandinavian goddess of beauty and fertility, Vanadis. Vanadium is found naturally in soil and sea water as trace metal. The coordination chemistry of vanadium has great interest since the discovery of vanadium in organisms such as certain ascidians and amanita mushrooms and as a constituent of the cofactors in vanadate dependent

haloperoxidases and vanadium nitrogenases [1,2]. Vanadium is probably a micronutrient in mammals including human but its precise role in this regard is unknown. It is mainly used to produce specialty steel alloys such as high speed tool steels. The metal oxidizes readily above 660 °C to form vanadium pentoxide, the most important industrial vanadium compound, which is used as a catalyst for the production of sulfuric acid.

Vanadium has multiple biological roles when present in traces, therapeutic effects in small doses and toxicity in excess. Vanadium compounds with oxidation states IV and V exist in the biological systems. The oral administration of vanadate is reported to reduce hyperglycemia in diabetic rats. The insulin-like effect of vanadium coordination compounds is one of the intriguing and promising features that has further stimulated interest in vanadium chemistry. Vanadate(+5) and vanadyl(+4) complexes have been shown to exert insulin-mimetic behavior. The complexes of vanadium with organic ligands seemed to be safer and more effective antidiabetic agents than inorganic vanadium salts. In recent years, a number of oxidovanadium complexes with hydrazone ligands have been reported for their insulin mimetic properties [3-6]. Besides the antidiabetic effects for which it is now well known, vanadium compounds have potential applications as antitumor [7], antitubercular [8], antifungal and antibacterial [9] agents.

Another important impetus to the coordination chemistry of vanadium is in the context of catalytic oxidation reactions. Vanadium compounds have been utilized in various homogeneous and heterogeneous catalytic processes where they exhibited good synthetic potential. Oxidovanadium complexes are active catalysts in oxidation reactions and some of them have also been used

for enantioselective oxidation of prochiral substrates. They are active precatalysts for olefin epoxidation and sulfide oxidation when combined with peroxide co-oxidants [10-14].

Vanadium is a versatile transition element because it possesses a large number of stable and accessible oxidation states as well as coordination numbers. The formal oxidation state of vanadium ranges from +5 to -1. As the oxidation state increases the oxophilicity of vanadium also increases. Simple vanadium compounds having +3 or lower oxidation states are quite susceptible to oxidation to the +4 and +5 oxidation states [15]. The oxidovanadium(IV) ion, VO^{2+} is considered to be the most stable oxidation of the first row transition metal ions. It forms stable anionic, cationic and neutral complexes with various types of ligands. In these complexes V(IV) could exist in a five or six coordinated state. A square pyramidal or distorted trigonal bipyramidal structure is observed for five coordinated complexes while distorted octahedral geometry is reported for the six coordinated ones [16-18]. The structural investigation of oxidovanadium(IV) complexes is more interesting because of their importance in biological systems and their ability to coordinate with four or five donor atoms to form stable complexes. Moreover vanadyl ion is less toxic than vanadate ion. The coordination chemistry of oxidovanadium(IV) with multidentate ligands is inviting attention of researchers because of its growing applications in therapeutics and catalytic roles in many biological systems and industrial processes. Hydrazone based ligands are N, O donor systems and are good candidates for catalytic oxidation studies because of their resistance to oxidation in oxo transfer reactions. The hard acidic nature of the VO^{2+} is probably the main reason for its rich chemistry with O, N donor ligands [19]. Several generalizations regarding the stereochemistry, spin state and other

characteristics such as monomeric, dimeric and polymeric nature of the vanadyl complexes can be made on the basis of spectral and magnetic studies. Keeping all these facts in mind we have synthesized and characterized seven VO(IV) complexes of ONO donor aroylhydrazones.

3.2. Experimental

3.2.1. Materials

4-Benzyloxy-2-hydroxybenzaldehyde (Sigma-Aldrich), 5-bromo-2-hydroxy-3-methoxybenzaldehyde (Sigma-Aldrich), 4-diethylamino-2-hydroxybenzaldehyde (Sigma-Aldrich), nicotinic hydrazide (Sigma-Aldrich), 4-nitrobenzoic hydrazide (Sigma-Aldrich), vanadyl sulfate (Sigma-Aldrich), 1,10-phenanthroline (Rankem), 2,2'-bipyridine (Qualigens), pyridine (S.D. Fine) and 3-picoline (Sigma-Aldrich) were of Analar grade and were used as received. Solvents used were methanol and dimethylformamide.

3.2.2. Syntheses of hydrazones

The syntheses of hydrazones 4-benzyloxy-2-hydroxybenzaldehyde-4-nitrobenzoylhydrazone dimethylformamide monosolvate ($H_2L^1 \cdot C_3H_7NO$), 5-bromo-2-hydroxy-3-methoxybenzaldehyde nicotinoylhydrazone dihydrate methanol monosolvate ($H_2L^2 \cdot 2H_2O \cdot CH_3OH$) and 4-diethylamino-2-hydroxybenzaldehyde nicotinoylhydrazone monohydrate ($H_2L^3 \cdot H_2O$) have already discussed in Chapter 2.

3.2.3. Syntheses of VO(IV) complexes

3.2.3.1. $[(VOL^1)_2]$ (1)

The complex, $[(VOL^1)_2]$ (1) was prepared by refluxing a solution of $H_2L^1 \cdot C_3H_7NO$ (0.464 g, 1 mmol) in 1:1 (v/v) mixture of DMF and methanol

with an aqueous solution of vanadyl sulfate (0.163 g, 1 mmol) for 4 h. The resulting solution was allowed to evaporate at room temperature and the yellow colored product formed was filtered, washed with methanol followed by ether and dried over P_4O_{10} *in vacuo*.

$[(VOL^1)_2]$ (1): Yield: 69%, μ_{eff} (B.M.): 1.27, Elemental Anal. Found (Calcd.) (%): C: 55.81 (55.28); H: 3.84 (3.31); N: 9.00 (9.21).

3.2.3.2. $[VOL^1\text{pic}]$ (2)

To a stirred mixture of $H_2L^1 \cdot C_3H_7NO$ (0.464 g, 1 mmol) in DMF and 3-picoline (0.093 g, 1 mmol), an aqueous solution of vanadyl sulfate (0.163 g, 1 mmol) was added. The resulting solution was refluxed for 4 h. and the yellow colored product formed was filtered, washed with methanol followed by ether and dried over P_4O_{10} *in vacuo*.

$[VOL^1\text{pic}]$ (2): Yield: 72%, λ_m (DMF): $8 \text{ ohm}^{-1} \text{ cm}^2 \text{ mol}^{-1}$, μ_{eff} (B.M.): 1.70, Elemental Anal. Found (Calcd.) (%): C: 59.60 (59.02); H: 3.84 (4.04); N: 10.03 (10.20).

3.2.3.3. $[VOL^1\text{py}]$ (3)

Aqueous solution of vanadyl sulfate (0.163 g, 1 mmol) was added to a stirred mixture of $H_2L^1 \cdot C_3H_7NO$ (0.464 g, 1 mmol) in DMF and pyridine (0.079 g, 1 mmol). The resulting solution was refluxed for 4 h. The yellow product obtained was filtered, washed with methanol followed by ether and dried over P_4O_{10} *in vacuo*.

$[VOL^1\text{py}]$ (3): Yield: 62%, λ_m (DMF): $8 \text{ ohm}^{-1} \text{ cm}^2 \text{ mol}^{-1}$, μ_{eff} (B.M.): 1.75, Elemental Anal. Found (Calcd.) (%): C: 58.73 (58.33); H: 3.66 (3.77); N: 10.10 (10.46).

3.2.3.4. [(VOL²)₂] (4)

This complex was synthesized by refluxing a methanolic solution of H₂L²·2H₂O·CH₃OH, (0.418 g, 1 mmol) and an aqueous solution of vanadyl sulfate (0.163 g, 1 mmol) for 4 h. The green colored complex formed was filtered, washed with methanol followed by ether and dried over P₄O₁₀ *in vacuo*.

[(VOL²)₂] (4): Yield: 69%, μ_{eff} (B.M.): 1.24, Elemental Anal. Found (Calcd.) (%): C: 40.22 (40.51); H: 2.66 (2.43); N: 10.37 (10.12).

3.2.3.5. [VOL²phen] (5)

To a methanolic solution of H₂L²·2H₂O·CH₃OH (0.418 g, 1 mmol), an aqueous solution of vanadyl sulfate (0.163 g, 1 mmol) was added. 1,10-phenanthroline (0.198 g, 1 mmol) was also added to it. The resulting mixture was refluxed for 4 h. The complex formed was brown in color. It was filtered, washed with methanol followed by ether and dried over P₄O₁₀ *in vacuo*.

[VOL²phen] (5) : Yield: 63%, λ_{m} (DMF): 5 ohm⁻¹ cm² mol⁻¹, μ_{eff} (B.M.): 1.75, Elemental Anal. Found (Calcd.) (%): C: 52.85 (52.46); H: 2.91 (3.05); N: 11.21 (11.76).

3.2.3.6. [VOL²bipy] (6)

Methanolic solutions of H₂L²·2H₂O·CH₃OH (0.418 g, 1 mmol) and 2,2'-bipyridine (0.156 g, 1 mmol) and vanadyl sulfate (0.163 g, 1 mmol) were mixed and the resulting mixture was refluxed for 4 h. The brown colored complex separated out was filtered, washed with methanol followed by ether and dried over P₄O₁₀ *in vacuo*.

[VOL²bipy] (**6**): Yield: 70%, λ_m (DMF): 13 ohm⁻¹ cm² mol⁻¹, μ_{eff} (B.M.): 1.74, Elemental Anal. Found (Calcd.) (%): C: 50.12 (50.46); H: 3.54 (3.18); N: 11.93 (12.26).

3.2.3.7. [(VOL³)₂] (**7**)

The complex **7** was prepared by refluxing a methanolic solution of H₂L³·H₂O (0.330 g, 1 mmol) and vanadyl sulfate (0.163 g, 1 mmol) for 6 h. The resulting solution was allowed to evaporate at room temperature and the yellow colored product formed was filtered, washed with methanol followed by ether and dried over P₄O₁₀ *in vacuo*.

[(VOL³)₂] (**7**): Yield: 56%, λ_m (DMF): 14 ohm⁻¹ cm² mol⁻¹, μ_{eff} (B.M.): 1.20, Elemental Anal. Found (Calcd.) (%): C: 54.43 (54.12); H: 4.66 (4.81); N: 14.30 (14.85).

3.3. Results and discussion

Seven oxidovanadium(IV) complexes were synthesized. The oxidovanadium(IV) complexes **1**, **4** and **7** were synthesized by refluxing vanadyl sulfate and the respective hydrazones in 1:1 ratio. Complexes **2**, **3**, **5** and **6** were synthesized by the reaction of equimolar mixture of the appropriate hydrazone, heterocyclic base and vanadyl sulfate in 1:1:1 ratio. In all the complexes, hydrazones exist in the iminolate form and act as dideprotonated tridentate ligands, coordinating through phenolate oxygen, iminolate oxygen and azomethine nitrogen. Complexes **2**, **3**, **5**, **6** and **7** are soluble in solvents like DMSO and DMF while **1** and **4** are sparingly soluble in DMSO and DMF. Complexes **1**, **4** and **7** are dimeric in nature, while others are monomeric mixed ligand metal chelates. They are characterized by the following physico-chemical methods.

3.3.1. Elemental analyses

Elemental (C, H, N) analyses of all the samples were carried out using a Vario EL III CHN analyzer at the SAIF, Kochi, India and the values are given in Section 3.2.3. The analytical data indicate that all the complexes are analytically pure. The elemental analyses data are consistent with the general formula [(VOL)₂] for complexes **1**, **4** and **7** and [VOLB] for complexes **2**, **3**, **5** and **6**, where L is the dideprotonated hydrazone and B is the heterocyclic base.

3.3.2. Molar conductivity and magnetic susceptibility measurements

The molar conductivity values of 10⁻³ M DMF solutions of soluble complexes lie in the 5-14 ohm⁻¹ cm² mol⁻¹ range, which are much less than the value obtained for uni-univalent electrolytes in the same solvent (65-90 ohm⁻¹ cm² mol⁻¹) indicate the non-electrolytic nature of the complexes [20]. Magnetic susceptibility measurements revealed that all complexes are paramagnetic. The room temperature magnetic moments of the mononuclear oxidovanadium(IV) complexes lie in the 1.70-1.75 B.M. range which are very close to the spin only value of 1.73 B.M. for *d*¹ system [21]. Complexes **1**, **4** and **7** show μ_{eff} values of 1.27, 1.24 and 1.20 B.M. respectively and these subnormal magnetic moments may be due to the considerable antiferromagnetic interaction between metal centers suggesting dimeric nature to these complexes [22].

3.3.3. Infrared spectra

The bonding sites of the hydrazones involved in coordination with the metal ions have been examined by the comparison of the infrared spectra of hydrazones and their complexes. The prominent infrared spectral data of the hydrazones and oxidovanadium complexes are given in Table 3.1. The IR spectra of the proligands exhibit bands in the 3377-3505, 3067-3186 and

1632-1669 cm^{-1} regions due to the $\nu(\text{O-H})$, $\nu(\text{N-H})$ and $\nu(\text{C=O})$ vibrations respectively. The absence of these bands in the spectra of all the complexes is consistent with the iminolization of the amide functionality and subsequent deprotonation of phenolic and iminolic groups and coordination of ligand to central metal ion through phenolate and iminolate oxygen atoms.

Table 3.1. The important IR frequencies (cm^{-1}) of hydrazones and their VO(IV) complexes

Compound	$\nu(\text{C=N})$	$\nu(\text{C=N})^a$	$\nu(\text{C=O})/$ $\nu(\text{C-O})$	$\nu(\text{N-H})$	$\nu(\text{V=O})$	$\nu(\text{V-O})$	$\nu(\text{V-N})$
$\text{H}_2\text{L}^1 \cdot \text{C}_3\text{H}_7\text{NO}$	1604	----	1661	3186	----	----	----
$[(\text{VOL}^1)_2]$ (1)	1601	1530	1338	----	961	562	454
$[\text{VOL}^1\text{pic}]$ (2)	1596	1525	1341	----	984	512	425
$[\text{VOL}^1\text{py}]$ (3)	1600	1524	1343	----	985	509	472
$\text{H}_2\text{L}^2 \cdot 2\text{H}_2\text{O} \cdot \text{CH}_3\text{OH}$	1609	----	1669	3067	----	----	----
$[(\text{VOL}^2)_2]$ (4)	1604	1540	1365	----	967	530	489
$[\text{VOL}^2\text{phen}]$ (5)	1604	1540	1356	----	957	568	454
$[\text{VOL}^2\text{bipy}]$ (6)	1600	1540	1358	----	954	569	456
$\text{H}_2\text{L}^3 \cdot \text{H}_2\text{O}$	1603	----	1632	3075	----	----	----
$[(\text{VOL}^3)_2]$ (7)	1598	1542	1350	----	937	571	442

^aNewly formed C=N

The bands appearing at about 1340 cm^{-1} are assigned to the $\nu(\text{C-O})$ (iminolic) mode. The $\nu(\text{C=N})$ (azomethine) bands of the proligands (1603-1609 cm^{-1}) undergo shift to the lower wavenumbers (1596-1604 cm^{-1}) upon complexation which suggest the coordination of the azomethine nitrogen to vanadium. IR spectra of complexes show bands in the 1524-1542 cm^{-1} region, assigned to newly formed C=N due to iminolization of the ligands during complexation. The bands corresponding to heterocyclic breathing are observed

in the 740-1450 cm^{-1} region for complexes **2**, **3**, **5** and **6** [23,24]. The bands observed in the 937-985 cm^{-1} region are assigned to the V=O stretching and this is close to the usual range ($960 \pm 50 \text{ cm}^{-1}$) observed for majority of oxidovanadium(IV) complexes [25]. The bands in the 509-571 and 425-489 cm^{-1} regions can be assigned to the stretching modes of the ligand to metal bonds, $\nu(\text{V-O})$ and $\nu(\text{V-N})$ respectively [26]. In addition to this, a prominent band is observed in the 830-850 cm^{-1} region for binuclear complexes **1**, **4**, and **7** due to V-O-V bridging vibrations [27]. Thus it is observed that hydrazones act as a dianionic tridentate chelating agents in all the complexes. Figs. 3.1-3.3 depict the infrared spectra of some of the oxidovanadium complexes.

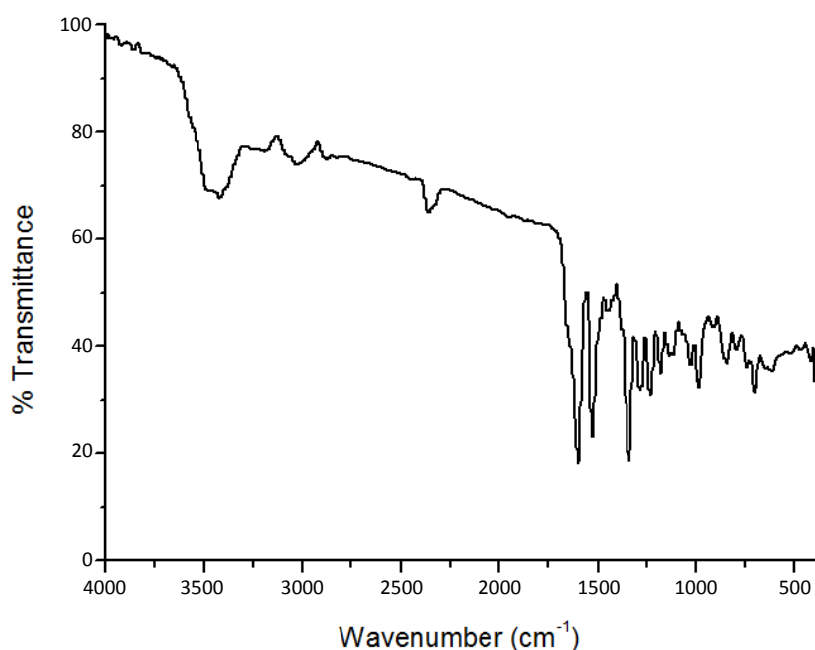


Fig. 3.1. IR spectrum of [VOL¹pic] (**2**).

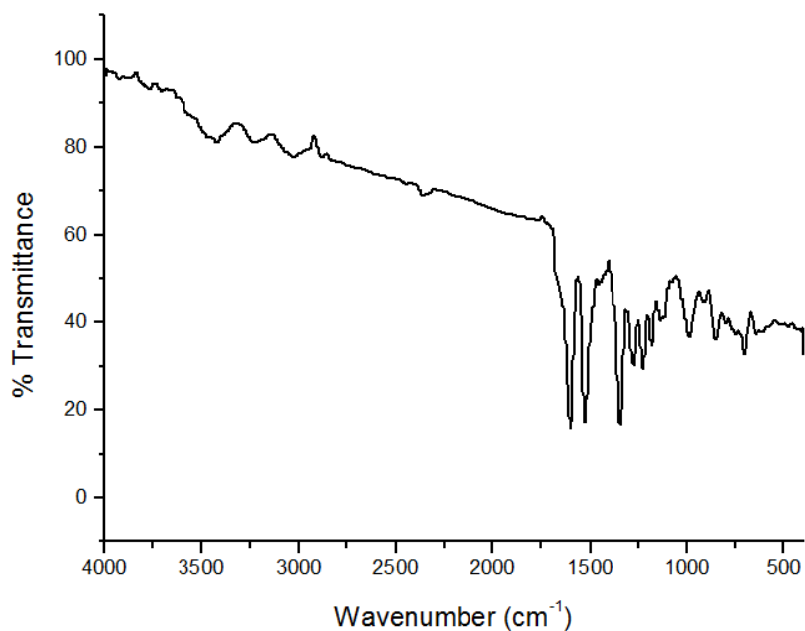


Fig. 3.2. IR spectrum of [VOL¹py] (3).

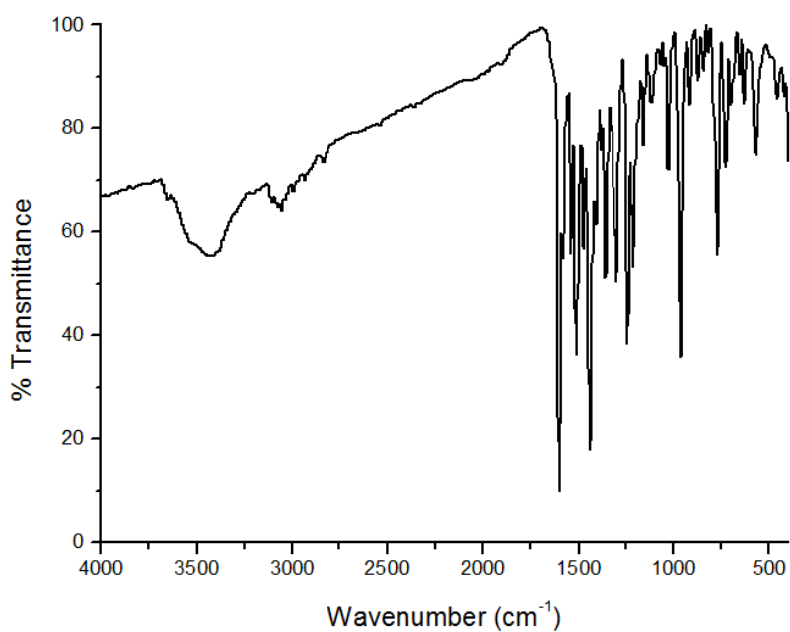


Fig. 3.3. IR spectrum of [VOL²bipy] (6).

3.3.4. Electronic spectra

The UV-Vis spectra give much insight into the coordination geometry around VO(IV) ion. The electronic spectra of all the complexes were taken in DMF. The significant electronic absorption bands in the spectra of hydrazones and the oxidovanadium complexes are given in Table 3.2. The bands in the 27020-36990 cm^{-1} range attributed to the $n \rightarrow \pi^*$ and $\pi \rightarrow \pi^*$ transitions for hydrazones suffered a marginal shift upon complexation and they are observed in the 36280-28950 cm^{-1} range.

In the complexes, the absorption bands observed in the 22610-23960 cm^{-1} region are assigned to ligand to metal charge transfer transitions arising from the phenolate oxygen to an empty d orbital of the vanadium(IV) center [28,29]. Figs. 3.4 and 3.5 represent the electronic spectra of some of the complexes.

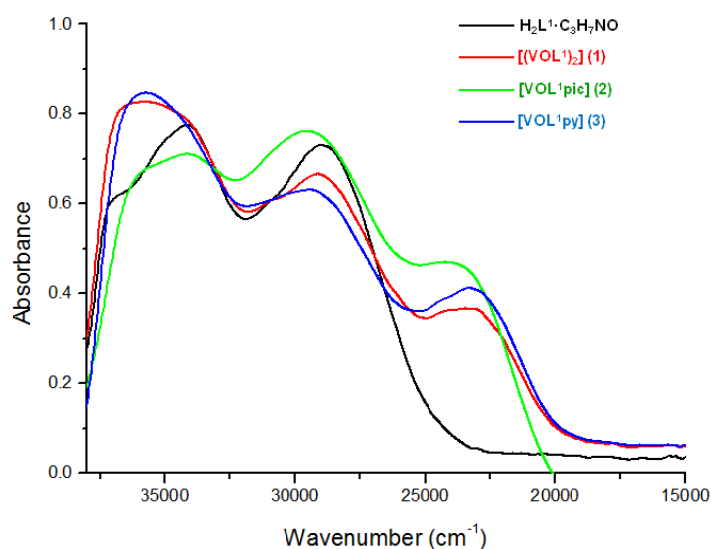


Fig. 3.4. UV spectra of H₂L¹·C₃H₇NO and its oxidovanadium(IV) complexes.

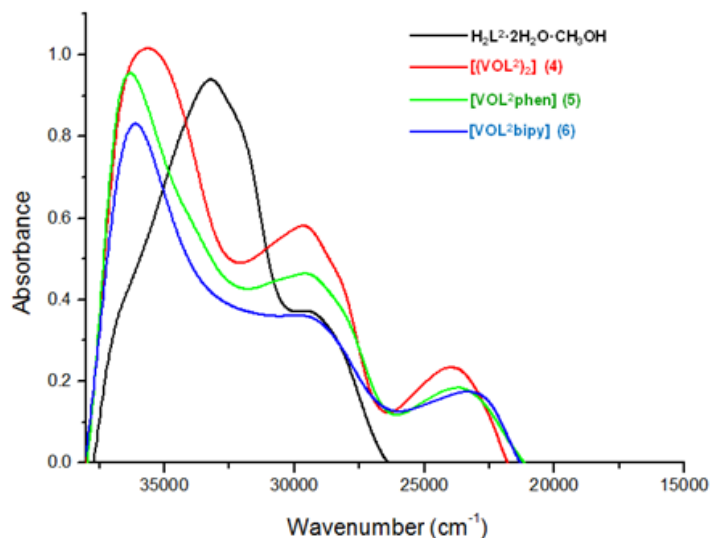


Fig. 3.5. UV spectra of $H_2L^2 \cdot 2H_2O \cdot CH_3OH$ and its oxidovanadium(IV) complexes.

Table 3.2. Electronic spectral assignments (cm^{-1}) of hydrazones and their VO(IV) complexes

Compound	$n \rightarrow \pi^* / \pi \rightarrow \pi^*$	LMCT	$d-d$
$H_2L^1 \cdot C_3H_7NO$	36990, 34130, 28970	----	----
$[(VOL^1)_2]$ (1)	36070, 29050	23220	21900, 19840, 14080
$[VOL^1pic]$ (2)	34210, 29490	23890	14090
$[VOL^1py]$ (3)	35810, 29310	23340	14080
$H_2L^2 \cdot 2H_2O \cdot CH_3OH$	33240, 29350	----	----
$[(VOL^2)_2]$ (4)	35770, 29560	23960	20600, 14420
$[VOL^2phen]$ (5)	36280, 29430	23640	19810
$[VOL^2bipy]$ (6)	36150, 28950	23220	----
$H_2L^3 \cdot H_2O$	36780, 27020	----	----
$[(VO_2L^3)_2]$ (7)	36150	22610	19730, 14040

Several methods are available to interpret the electronic spectra of vanadyl complexes of distorted square pyramidal or octahedral geometry. Ballhausen and Gray [30] delineated an energy level scheme for vanadyl complexes as; $d_{xy} < d_{xz}, d_{yz} < d_{x^2-y^2} < d_z^2$, a similar scheme was proposed by Selbin *et al.* [31] to explain the electronic spectra of lower symmetry complexes and those recorded at low temperature.

According to Ballhausen and Gray, three absorptions are observed in the visible spectra of most of the oxidovanadium complexes, arising from the tetragonal compression caused by V=O bond, which results in further splitting of *d* orbitals and gives rise to three spin allowed transitions assigned to ${}^2E \leftarrow {}^2B_2$ (ν_1) ($d_{xy} \rightarrow d_{xz}, d_{yz}$), ${}^2B_1 \leftarrow {}^2B_2$ (ν_2) ($d_{xy} \rightarrow d_{x^2-y^2}$), ${}^2A_1 \leftarrow {}^2B_2$ (ν_3) ($d_{xy} \rightarrow d_z^2$). Since the 2E and 2B_1 levels are very close in energy, they may cross and result in a weak broad band. In complex **1**, three absorption bands are observed due to ν_1 , ν_2 and ν_3 while in complexes **4** and **7** two weak *d-d* bands are observed. The third band is not observed and is thought to be buried beneath the low energy tail of the much more intense charge transfer bands. We could locate only one band for complexes **2**, **3** and **5** due to the masking by high intensity charge transfer bands. In complex **6**, the expected *d-d* bands are not observed and are probably obscured by the intense LMCT absorptions. The observed visible spectra of the complexes are presented in Fig. 3.6.

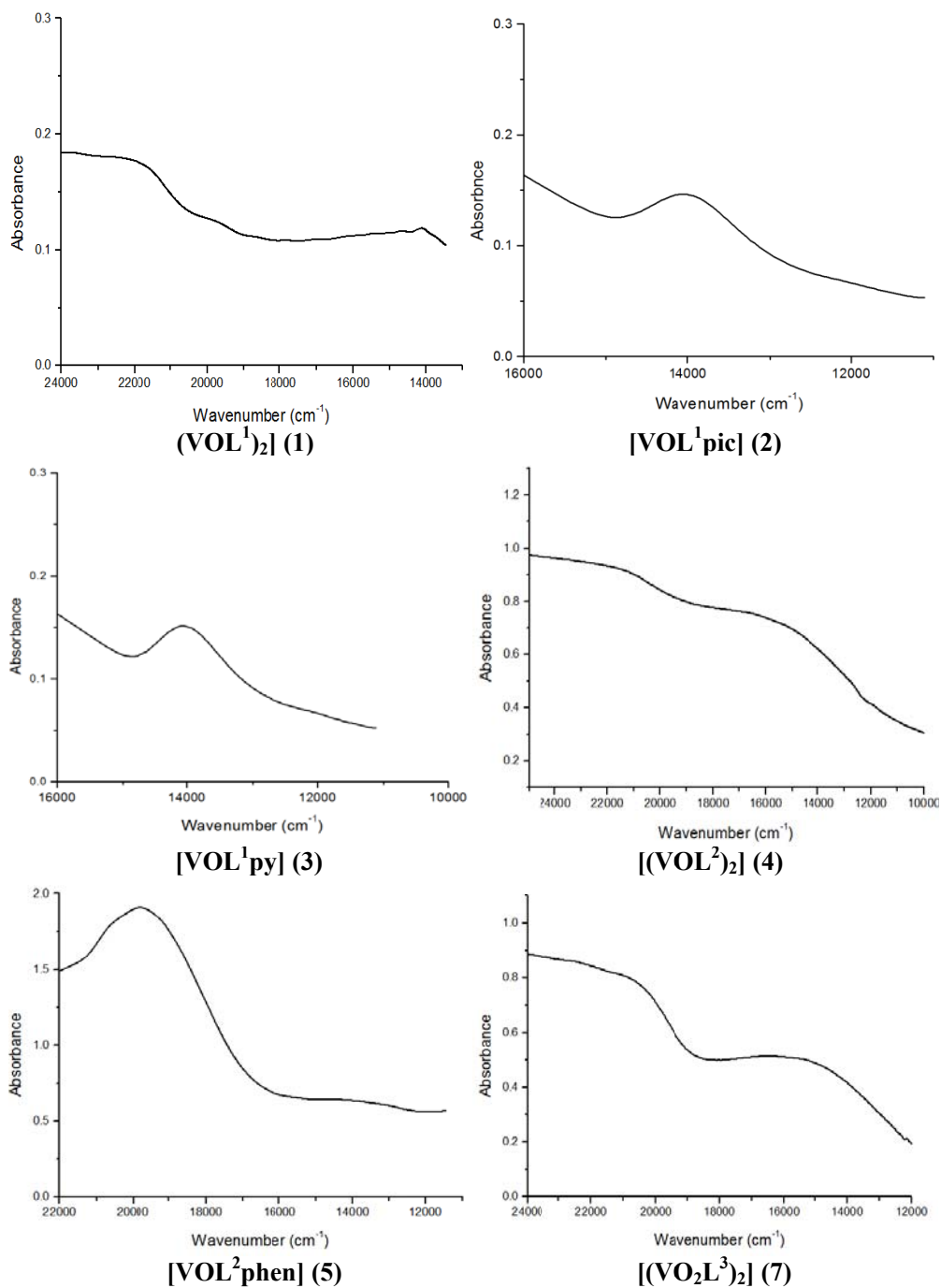


Fig. 3.6. Visible spectra of VO(IV) complexes.

3.3.5. Electron paramagnetic resonance spectra

The basic objectives of EPR studies in transition metal complexes is to obtain as much information as possible about the ligand to metal bond, the unpaired electron distribution and spatial arrangements of the ligands around the central metal ion. In vanadyl complexes containing the VO^{2+} unit, vanadium is in +4 oxidation state with d^1 configuration and they are EPR active. Since the orbital angular momentum is quenched by the crystalline fields, the paramagnetism of the vanadyl(IV) ion in its complexes arises from the single unpaired electron. For V(IV) complexes, value of g is below the free electron value of 2.0023. All the seven complexes synthesized are EPR active and contain VO^{2+} unit. In the case of vanadium(IV) ($I = 7/2$), eight and fifteen hyperfine lines are expected for mononuclear and binuclear complexes respectively separated by the hyperfine coupling constant A . Under the influence of magnetic field, the electronic ground state ($S = 1/2$) is split into two ($m_s = +1/2$ and $-1/2$) and additional splitting occurs through the different magnetic orientations of the nuclear spin (m_I).

EPR spectra of all the oxidovanadium complexes were recorded in polycrystalline state at 298 K and in DMF at 77 K using TCNE as the standard with 100 kHz modulation frequency, 1 G modulation amplitude and 9.4 GHz microwave frequency. The EPR spectra of complexes **1**, **2**, **3**, **5** and **6** in the solid state at 298 K are isotropic in nature and hence only one g value, arising due to dipolar interactions and enhanced spin-lattice relaxation. Complexes **4** and **7** give axial spectra in the polycrystalline state in which that of **7** is poorly resolved and difficult to interpret. In DMF at 77 K, all the complexes display well resolved axial anisotropy with two sets of eight

line pattern with $g_{\parallel} < g_{\perp}$ and $A_{\parallel} > A_{\perp}$ relationships characteristic of an axially compressed d_{xy}^1 configuration [32].

The spectrum of $[(VOL^1)_2]$ (**1**) in polycrystalline state at 298 K is isotropic in nature with $g_{iso} = 1.997$ (Fig. 3.7). The anisotropy is not observed and only one g value is obtained due to dipolar interactions and enhanced spin-lattice relaxation.

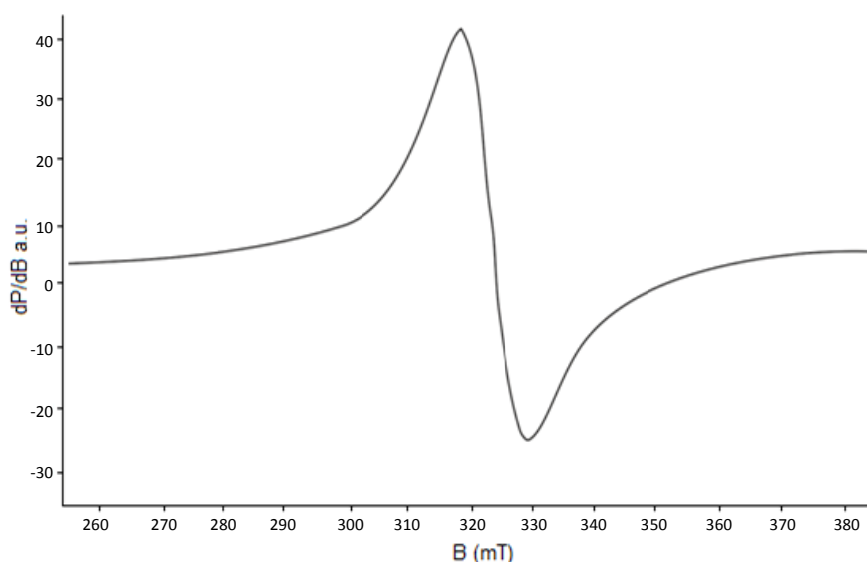


Fig. 3.7. EPR spectrum of $[(VOL^1)_2]$ (**1**) in polycrystalline state at 298 K.

In DMF at 77 K, $[(VOL^1)_2]$ (**1**) exhibits well resolved axial anisotropy with two sets of eight line pattern, characteristic of an unpaired electron being coupled to the vanadium nuclear spin (^{51}V , $I = 7/2$) with anisotropic hyperfine parameters $g_{\parallel} = 1.945$, $g_{\perp} = 1.979$, $A_{\parallel} = 174 \times 10^{-4} \text{ cm}^{-1}$ and $A_{\perp} = 56 \times 10^{-4} \text{ cm}^{-1}$ (Fig. 3.8). The $g_{\parallel} < g_{\perp}$ and $A_{\parallel} > A_{\perp}$ relationships are characteristic of square pyramidal VO(IV) complexes with axially compressed d_{xy}^1 configuration. The half field signal due to forbidden $\Delta m_s = \pm 2$ transition is not observed for

this complex. Here the spin-spin interaction is not so significant such that unpaired electron virtually interact with only one vanadium centre [33].

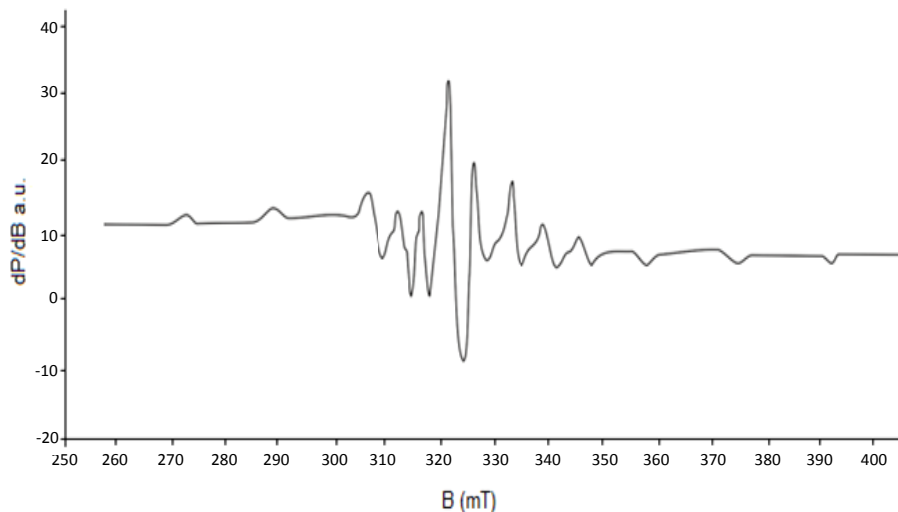


Fig. 3.8. The EPR spectrum of $[(VOL^1)_2]$ (1) in DMF at 77 K.

EPR spectrum of the complex $[VOL^1pic]$ (2) in polycrystalline state at 298 K is found to be isotropic with $g_{iso} = 1.996$ (Fig. 3.9).

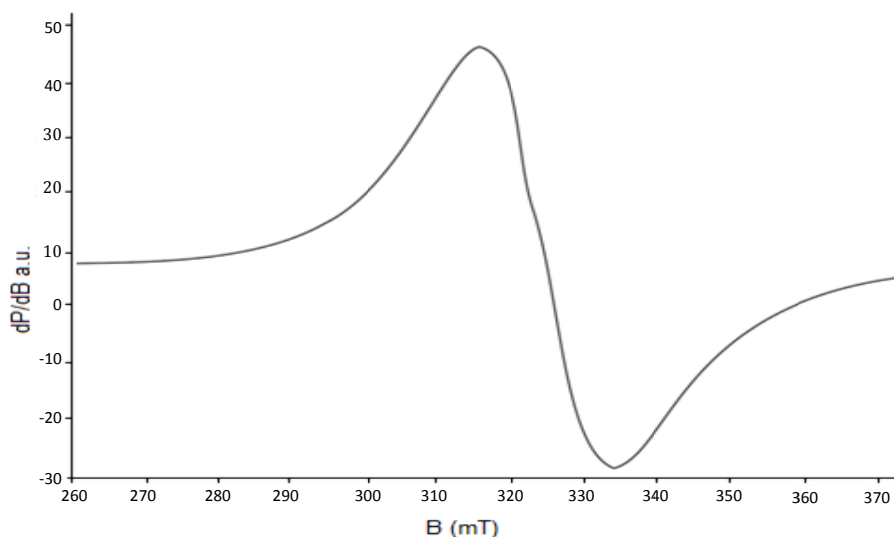


Fig. 3.9. EPR spectrum of $[VOL^1pic]$ (2) in polycrystalline state at 298 K.

The spectrum of [VOL¹pic] (**2**) in frozen DMF at 77 K is depicted in Fig. 3.10. The spectrum shows well resolved axial anisotropy with two sets of eight line pattern with $g_{\parallel} = 1.946$ and $g_{\perp} = 1.979$, $A_{\parallel} = 179 \times 10^{-4} \text{ cm}^{-1}$ and $A_{\perp} = 62 \times 10^{-4} \text{ cm}^{-1}$. In a square pyramidal VO(IV) complex, the $g_{\parallel} < g_{\perp}$ and $A_{\parallel} > A_{\perp}$ relationship is characteristic of an axially compressed d_{xy}^1 configuration.

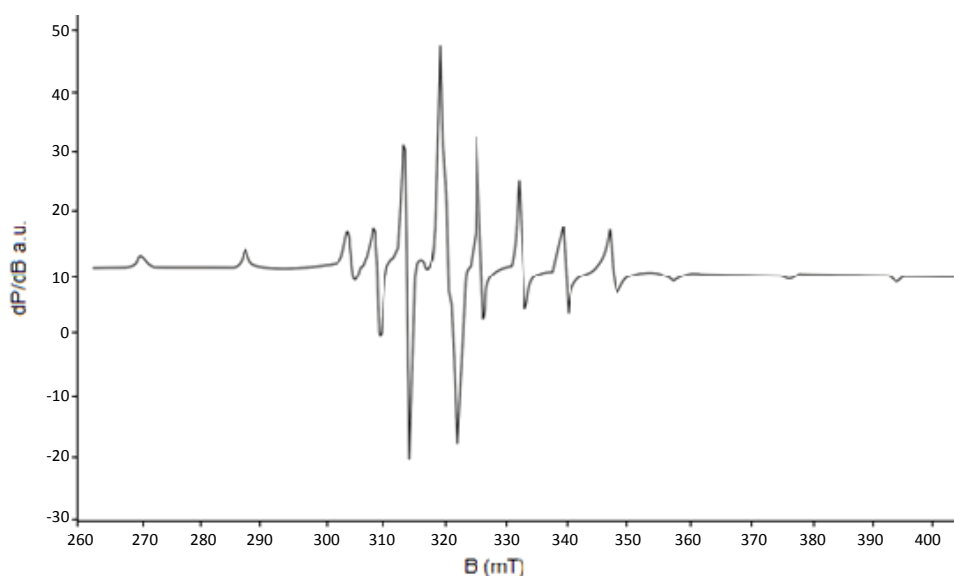


Fig. 3.10. The EPR spectrum of [VOL¹pic] (**2**) in DMF at 77 K.

Complex [VOL¹py] (**3**) exhibits an isotropic spectrum with $g_{\text{iso}} = 1.993$ (Fig. 3.11) in polycrystalline state at 298 K. The anisotropic EPR spectrum obtained for this complex in frozen DMF is shown in Fig. 3.12. The observed order of anisotropic parameters ($g_{\parallel} = 1.949 < g_{\perp} = 1.979$ and $A_{\parallel} = 178 \times 10^{-4} \text{ cm}^{-1} > A_{\perp} = 62 \times 10^{-4} \text{ cm}^{-1}$) indicate that the unpaired electron is present in the d_{xy} orbital with square pyramidal geometry for the VO(IV) chelate.

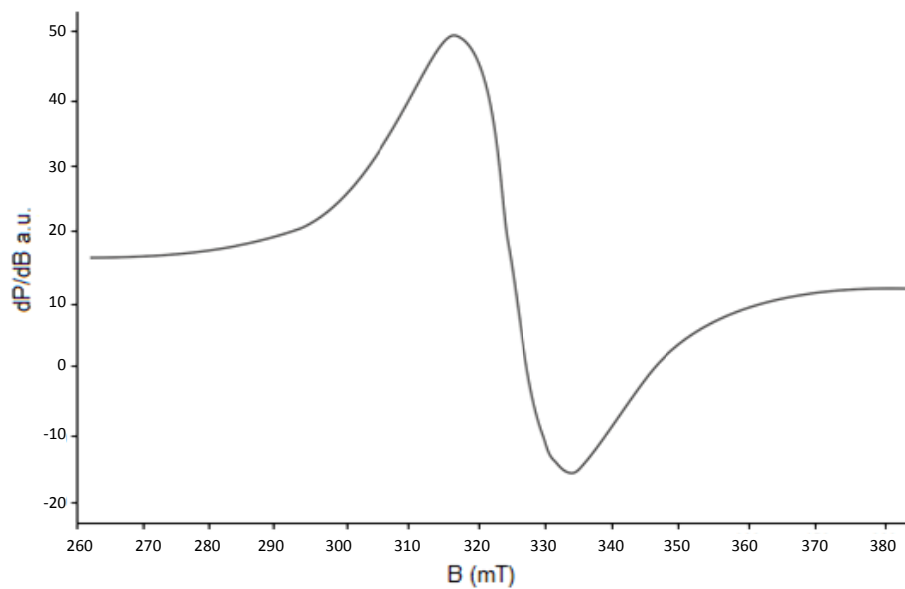


Fig. 3.11. EPR spectrum of [VOL¹py] (3) in polycrystalline state at 298 K.

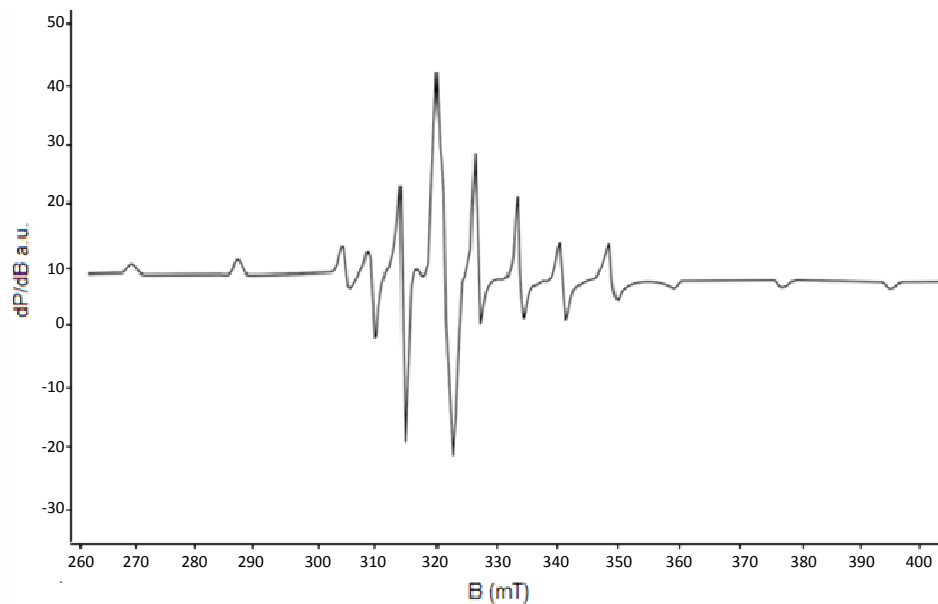


Fig. 3.12. The EPR spectrum of [VOL¹py] (3) in DMF at 77 K.

In polycrystalline state at 298 K, EPR spectrum of $[(VOL^2)_2]$ (**4**) is axial with two sets of eight line pattern with $g_{\parallel} = 1.974$ and $g_{\perp} = 1.989$ (Fig. 3.13). In frozen DMF, the complex **4** displays a well resolved axial anisotropy characterized by two sets of eight lines with $g_{\parallel} = 1.952$ and $g_{\perp} = 1.981$, $A_{\parallel} = 177 \times 10^{-4} \text{ cm}^{-1}$ and $A_{\perp} = 62 \times 10^{-4} \text{ cm}^{-1}$ (Fig. 3.14). In a square pyramidal vanadyl complex, the $g_{\parallel} < g_{\perp}$ and $A_{\parallel} > A_{\perp}$ relationships are characteristic of an axially compressed d_{xy}^1 configuration. Here a half field signal is obtained due to $\Delta m_s = \pm 2$ transitions indicating dimeric nature of the complex. In the X-band spectra, transitions due to $\Delta m_s = \pm 1$ are associated with magnetic fields of *ca.* 300 mT, while transitions due to $\Delta m_s = \pm 2$ generate an absorption at half of this field i.e. *ca.* 150 mT.

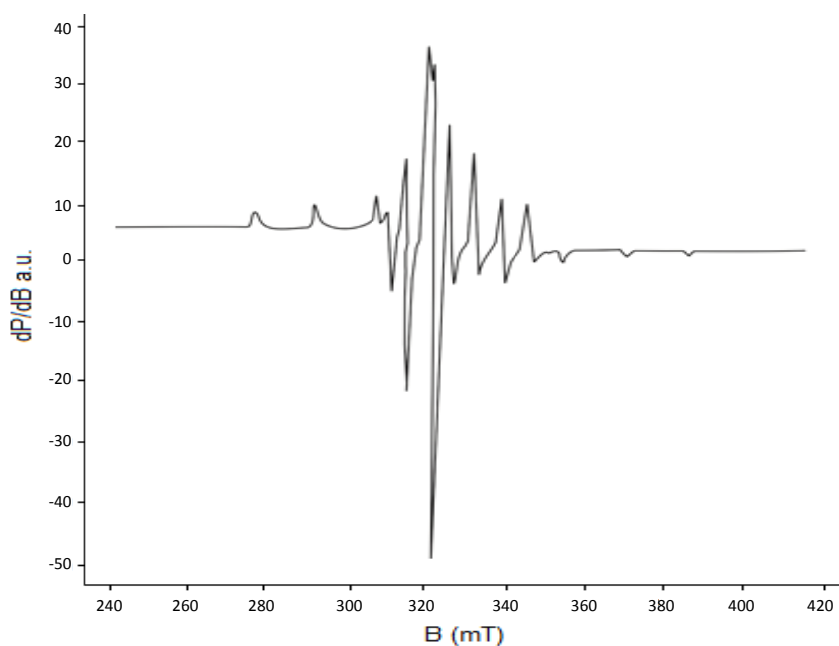


Fig. 3.13. EPR spectrum of $[(VOL^2)_2]$ (**4**) in polycrystalline state at 298 K.

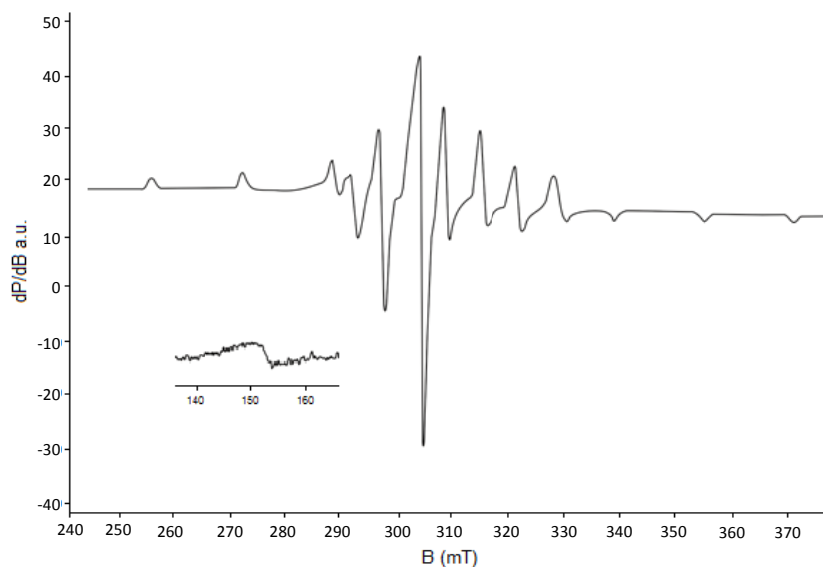


Fig. 3.14. EPR spectrum of $[(VOL^2)_2]$ (4) in DMF at 77 K.

The anisotropy is not observed for the complex $[VOL^2phen]$ (5) in polycrystalline state at room temperature. The g_{iso} value obtained for the complex is 1.991 (Fig. 3.15).

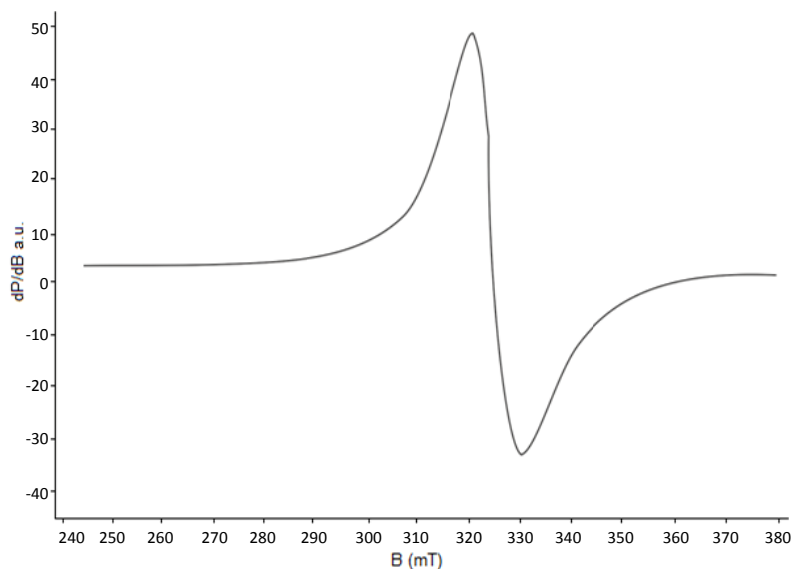


Fig. 3.15. EPR spectrum of $[VOL^2phen]$ (5) in polycrystalline state at 298 K.

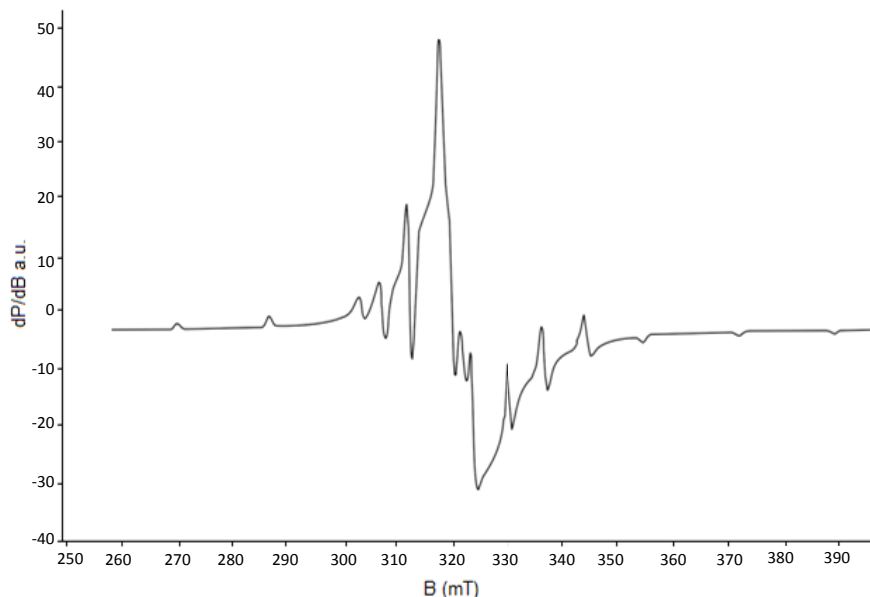


Fig. 3.16. The EPR spectrum of [VOL²phen] (**5**) in DMF at 77 K.

The anisotropy is visible in the spectrum taken in frozen DMF at 77 K. The spectrum shows two sets of eight line pattern with $g_{\parallel} = 1.948$, $g_{\perp} = 1.982$, $A_{\parallel} = 174 \times 10^{-4} \text{ cm}^{-1}$ and $A_{\perp} = 60 \times 10^{-4} \text{ cm}^{-1}$ (Fig. 3.16). In an octahedral vanadyl complex the $g_{\parallel} < g_{\perp}$ and $A_{\parallel} > A_{\perp}$ relationships are characteristic of axially compressed d_{xy}^1 configuration.

The EPR spectrum of the complex [VOL²bipy] (**6**) in polycrystalline state at 298 K exhibits an isotropic spectrum with $g_{\text{iso}} = 1.983$ (Fig. 3.17). In frozen DMF at 77 K, the complex **6** gives an axial spectrum with $g_{\parallel} = 1.947$, $g_{\perp} = 1.978$, $A_{\parallel} = 173 \times 10^{-4} \text{ cm}^{-1}$ and $A_{\perp} = 60 \times 10^{-4} \text{ cm}^{-1}$ (Fig. 3.18). The $g_{\parallel} < g_{\perp}$ and $A_{\parallel} > A_{\perp}$ relationships are consistent with an axially compressed octahedral geometry around the vanadium(IV) centre with the unpaired electron in the d_{xy} orbital.

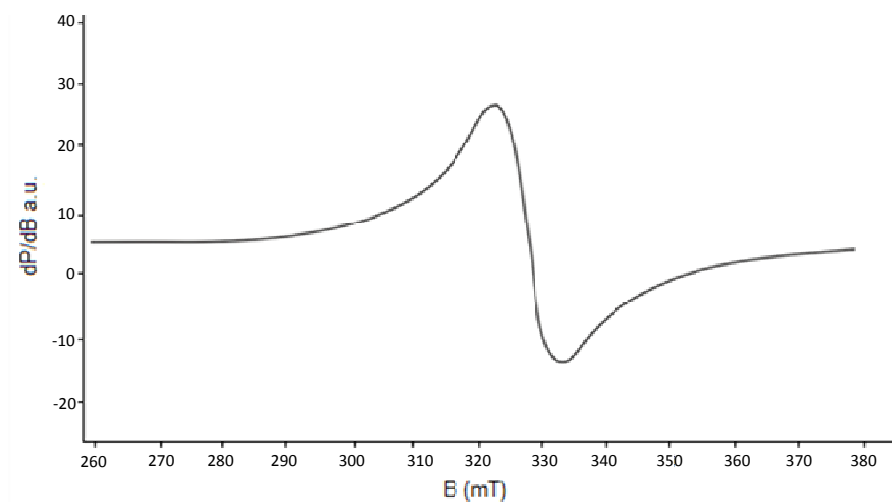


Fig. 3.17. EPR spectrum of [VOL²bipy] (6) in polycrystalline state at 298 K.

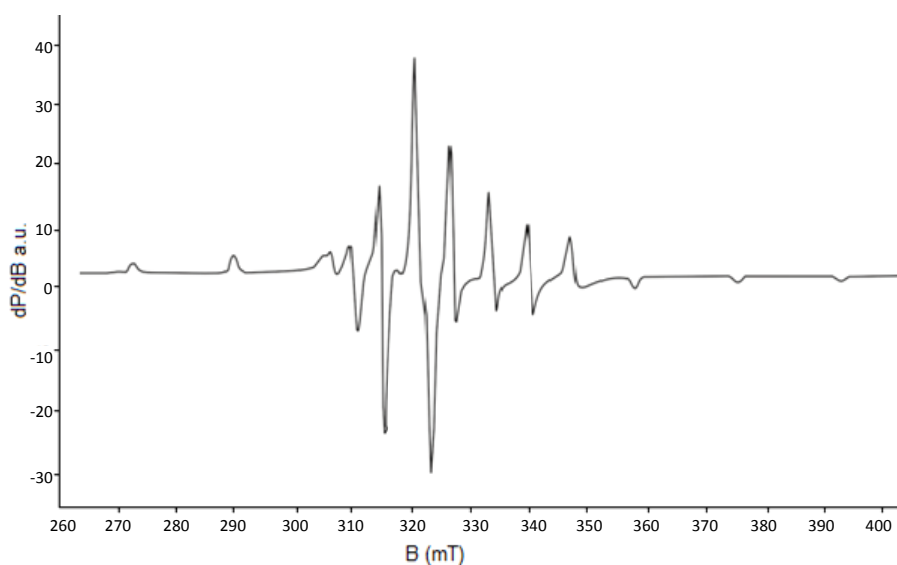


Fig. 3.18. The EPR spectrum of [VOL²bipy] (6) in DMF at 77 K.

The EPR spectrum of [(VOL³)₂] (7) in polycrystalline state is poorly resolved and is difficult to interpret. In frozen DMF at 77 K, EPR spectrum of complex 7 exhibits well resolved axial anisotropy (Fig. 3.19) with two sets of eight lines ($g_{\parallel} = 1.950$ and $g_{\perp} = 1.978$, $A_{\parallel} = 179 \times 10^{-4} \text{ cm}^{-1}$ and $A_{\perp} = 62 \times 10^{-4} \text{ cm}^{-1}$).

The $g_{\parallel} < g_{\perp}$ and $A_{\parallel} > A_{\perp}$ relationships are characteristic of an axially compressed square pyramidal geometry around the vanadium(IV) centre with the unpaired electron in d_{xy} orbital. The expected half field signal due to forbidden $\Delta m_s = \pm 2$ transition is absent in this dimeric complex which indicates that spin-spin interaction is not much significant.

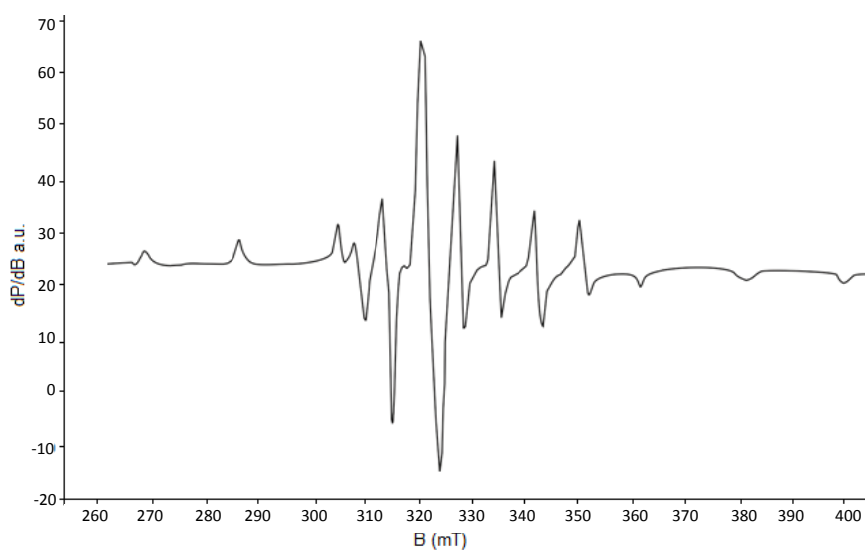


Fig. 3.19. The EPR spectrum of $[(VOL^3)_2]$ (7) in DMF at 77 K.

The absence of any superhyperfine lines in the spectrum of all the complexes and the trend of g values calculated from the frozen spectrum ($g_{\parallel} < g_{\perp} < 2.0023$) indicates that the unpaired electron residing in the d_{xy} orbital (2B_2 ground state) is localized on metal, thus excluding the possibility of its direct interaction with the azomethine nitrogen of the hydrazone [34]. Further, g values are very close to the spin-only value of 2.0023, a slight variation may be accounted due to spin-orbit coupling [35].

In all these complexes, the anisotropic parameters are related with isotropic parameters by the equations, $A_{av} = \frac{1}{3}(A_{\parallel} + 2A_{\perp})$ and $g_{av} = \frac{1}{3}(g_{\parallel} + 2g_{\perp})$

[36]. The calculated g_{av} values are in good agreement with the g_{iso} values obtained from the polycrystalline state spectra suggest that the molecules retain their structural identity in solution.

Table 3.3. EPR spectral data for VO(IV) complexes

Compound	Polycrystalline State (298 K)			DMF (77 K)					
	$g_{iso}/g_{ }, g_{\perp}$	$g_{ }$	g_{\perp}	g_{av}	$A_{ }^a$	A_{\perp}^a	A_{av}	α^2	β^2
[(VOL ¹) ₂] (1)	1.997	1.945	1.979	1.967	174	56	95	0.659	1.13
[VOL ¹ pic] (2)	1.996	1.946	1.979	1.968	179	62	101	0.655	1.12
[VOL ¹ py] (3)	1.993	1.949	1.979	1.969	178	62	100	0.625	1.10
[(VOL ²) ₂] (4)	1.974, 1.989	1.952	1.981	1.971	177	62	100	0.612	1.09
[VOL ² phen] (5)	1.991	1.948	1.982	1.970	174	60	98	0.910	1.09
[VOL ² bipy] (6)	1.983	1.947	1.978	1.967	173	60	97	----	1.08
[(VOL ³) ₂] (7)	----	1.950	1.978	1.968	179	62	101	0.608	1.11

^a Expressed in units of cm^{-1} multiplied by a factor of 10^4

The molecular orbital coefficients α^2 and β^2 for the complexes were also calculated by using the following equations:

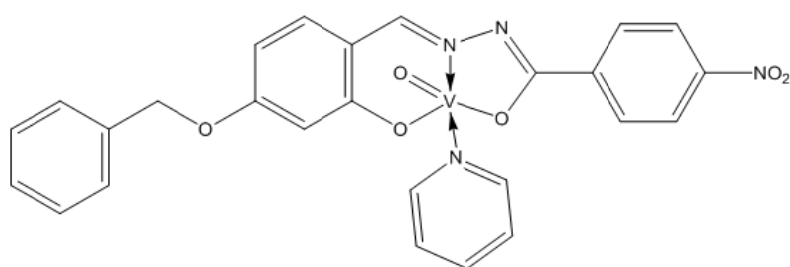
$$\alpha^2 = \frac{(2.0023 - g_{||})E_{d-d}}{8\lambda\beta^2}$$

$$\beta^2 = \frac{7}{6} \left[\left(\frac{-A_{||}}{P} \right) + \left(\frac{A_{\perp}}{P} \right) + \left(g_{||} - \frac{5}{14}g_{\perp} \right) - \frac{9}{14}g_e \right]$$

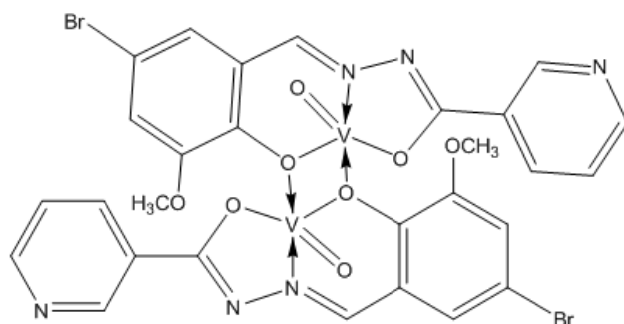
where $P = 128 \times 10^4 \text{ cm}^{-1}$, $\lambda = 135 \text{ cm}^{-1}$ and E_{d-d} is the energy of $d-d$ transition

The value of α^2 is less than unity which is an indication of increasing covalency while that of β^2 does not found to vary significantly from the most often observed value of 1.0 for most of the complexes. The lower values for α^2 compared to β^2 indicates that in-plane σ bonding is more covalent than in-plane π bonding [37]. EPR spectral data for VO(IV) complexes are presented in Table 3.3.

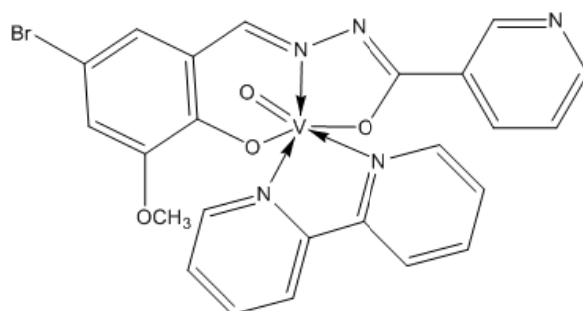
Based on the above physico-chemical methods, tentative structures (Fig. 3.20) for some complexes are given below. Out of the seven oxidovanadium complexes prepared, three are dimers and the remaining four are mixed ligand metal chelates incorporating heterocyclic bases. In all the complexes the tridentate hydrazones coordinate in the iminolate form and act as dideprotonated ONO donor ligands.



[VOL¹py] (3)



[(VOL²)₂] (4)



[VOL²bipy] (6)

Fig. 3.20. Tentative structures of some of the VO(IV) complexes.

References

- [1] D. Rehder, *Inorg. Chem. Commun.* 6 (2003) 604.
- [2] G. Wilkinson, *Comprehensive Coordination Chemistry*, Ed., Pergamon Press, Oxford, UK, 6 (1987).
- [3] S. Sheela, S.M. Roopan, R. Vijayaraghavan, *Eur. J. Med. Chem.* 43 (2008) 2206.
- [4] M.N. Islam, A.A. Kumbhar, A.S. Kumbhar, M. Zeller, R.J. Butcher, M.B. Dusane, B.N. Joshi, *Inorg. Chem.* 49 (2010) 8237.
- [5] T. Scior, J.A.G. Garcia, F.J. Melendez, H.H. Abdallah, Q.T. Do, P. Bernard, *Drug Des. Devel. Ther.* 4 (2010) 231.
- [6] Z.X. Hang, X.W. Wang, B. Dong, *Synth. React. Inorg. Met-Org. Nano-Met. Chem.* 42 (2012) 1351.
- [7] X. Liao, J. Lu, P. Ying, P. Zhao, Y. Bai, W. Li, M. Liu, *J. Biol. Inorg. Chem.* 18 (2013) 975.
- [8] F. R. Pavan, P.S. Maia, S.R.A. Leite, V.M. Deflon, A.A. Batista, D.N. Sato, S.G. Franzblau, C.Q.F. Leite, *Eur. J. Med. Chem.* 45 (2010) 1898.
- [9] M.N. Vinyak, G.T. Kuchinad, S.K. Patil, N.B. Mallur, *Der Pharma Chemica* 5 (2013) 43.
- [10] N. Wang, J.Y. Guo, J.Y. Hu, *Russ. J. Coord. Chem.* 39 (2013) 891.
- [11] Y. Wang, M. Wang, X. Wang, L. Wang, L. Sun, *J. Catal.* 273 (2010) 177.
- [12] H.H. Monfared, R. Bikas, P.M. Anarjan, A.J. Blake, V. Lippolis, N.B. Arslan, C. Kazak, *Polyhedron* 69 (2014) 90.
- [13] A.T. Radosevich, C. Musich, F.D. Toste, *J. Am. Chem. Soc.* 127 (2005) 1090.
- [14] A.G.J. Ligtenbarg, R. Hage, B.L. Feringa, *Coord. Chem. Rev.* 237 (2003) 89.

- [15] M. Chatterjee, S. Ghosh, A.K. Nandi, *Polyhedron* 16 (1997) 2917.
- [16] J. Devi, N. Batra, *Der Pharma Chemica* 5 (2013) 167.
- [17] S.K. Patil, V.M. Naik, N.B. Mallur, *J. Chem. Pharm. Res.* 4 (2012) 2029.
- [18] E.B. Seena, N. Mathew, M. Kuriakose, M.R.P. Kurup, *Polyhedron* 27 (2008) 1455.
- [19] T. Ghosh, B. Mondal, *Indian J. Chem.* 47 (2008) 361.
- [20] W.J. Geary, *Coord. Chem. Rev.* 7 (1971) 81.
- [21] A.P. Mishra, L.R. Pandey, *Indian J. Chem.* 44 (2005) 94.
- [22] S.N. Rao, D.D. Mishra, R.C. Maurya, N.N. Rao, *Polyhedron* 16 (1997) 1825.
- [23] M.R.P. Kurup, E.B. Seena, M. Kuriakose, *Struct. Chem.* 21 (2010) 599.
- [24] B.N. Raj, M.R.P. Kurup, E. Suresh, *Struct. Chem.* 17 (2006) 201.
- [25] N.A. Mangalam, S. Sivakumar, S.R. Sheeja, M.R.P. Kurup, E.R.T. Tiekink, *Inorg. Chim. Acta* 362 (2009) 4191.
- [26] E.J. Baran, *J. Coord. Chem.* 54 (2001) 215.
- [27] S.K. Dutta, S.B. Kumar, S. Bhattacharyya, E.R.T. Tiekink, M. Chaudhury, *Inorg. Chem.* 36 (1997) 4954.
- [28] F.A. Walker, R.L. Carlin, P.H. Rieger, *J. Chem. Phys.* 45 (1966) 4181.
- [29] M. Kuriakose, M.R.P. Kurup, E. Suresh, *Polyhedron* 26 (2007) 2713.
- [30] C.J. Ballhausen, H.B. Grey, *Inorg. Chem.* 1 (1962) 111.
- [31] J. Selbin, *Chem. Rev.* 65 (1965) 153.
- [32] T. Ghosh, S. Bhattacharya, A. Das, G. Mukherjee, M.G.B. Drew, *Inorg. Chim. Acta* 358 (2005) 989.

- [33] S.K. Dutta, E.R.T. Tiekink, M. Chaudhury, *Polyhedron* 16 (1997) 1863.
- [34] N. Raman, J.D. Raja, A. Sakthivel, *J. Chem. Sci.* 119 (2007) 303.
- [35] S.S. Dodwad, R.S. Dhamnaskar, P.S. Prabhu, *Polyhedron* 8 (1989) 1748.
- [36] D. Rehder, *Bioinorganic Vanadium Chemistry*, Wiley, Chichester (2008).
- [37] P.B. Sreeja, M.R.P. Kurup, *Spectrochim. Acta A* 61 (2005) 331.

.....❧.....

**SYNTHESES AND SPECTRAL CHARACTERIZATION OF
COBALT(II) CHELATES OF TRIDENTATE AROYLHYDRAZONES**

4.1 Introduction
4.2 Experimental
4.3 Results and discussion
References

4.1. Introduction

Coordination chemistry emerged from the work of Alfred Werner, a Swiss chemist who examined different compounds composed of cobalt(III) chloride and ammonia. Cobalt forms numerous coordination compounds. In its compounds cobalt always exhibits +2 or +3 oxidation state although states of +4, +1, 0 and -1 are known. Cobalt is a hard, lustrous, silver-grey ductile transition metal. It constitutes about 0.002 percent of the earth's crust. It has been used by human for thousands of years as blue coloring in pottery, glass and ceramics, but in recent years demand has surged mainly due to its use in hybrid electric vehicle (HEV) rechargeable batteries. Cobalt is used in many alloys, in magnets and magnetic recording media, as catalysts for petroleum and chemical industries and as drying agents for paints and inks. The radioactive isotope, cobalt-60, is used in medical treatment and also to irradiate food in order to preserve the food and protect the consumer. Cobalt

is a ferromagnetic metal at room temperature. The metal is used in electroplating because of its appearance, hardness and resistance to oxidation.

Co is present in the active center of coenzymes called cobalamines, the most common example of which is vitamin B₁₂, which regulates indirectly the synthesis of DNA. Cobalt is a trace mineral in the human body. Cobalt is a necessary cofactor for making the thyroid hormone thyroxine. In the marine environment cobalt is needed by blue-green algae (cyanobacteria) and other nitrogen fixing organisms. Cobalt is not found as a free metal and is generally found in the form of ores. Cobalt possesses a diverse array of properties that can be manipulated to yield promising drug candidates. Investigations into the mechanism of cobalt therapeutic agents can provide valuable insight into the physico-chemical properties that can be harnessed for drug development. Many cobalt containing compounds have been proved to show antitumor, antiproliferative, antimicrobial and antifungal activities [1-6]. Like any other element, a high concentration of cobalt is harmful to the human body. Some Schiff base cobalt complexes are well known for their catalytic activities in the oxidation as well as reduction of organic substrates and for the synthesis of fine chemicals [7,8]. In addition, cobalt complexes display efficient second order nonlinear optical (NLO) responses. W.Y. Wang *et al.* have recently investigated the second order nonlinear optical (NLO) properties of cyclopentadienyl cobalt phenylene complexes and found that the cobalt (Co) atom acts as a donor in the complexes and the $d \rightarrow \pi^*$ and $\pi \rightarrow \pi^*$ charge transfer (CT) transitions contribute to the enhancement of second order NLO response [9].

Hydrazones are interesting ligands with multiple functional groups which display variable coordination modes under different chemical environment. Cobalt(II) complexes of hydrazones have also extended their role in the development of coordination chemistry. The chemical properties of cobalt complexes of hydrazones have been widely investigated due to their chelating capability, pharmacological activity and analytical applications [10,11]. This chapter is focused on the characterization of cobalt(II) complexes of three ONO donor arylhydrazones including two mixed ligand metal chelates incorporating heterocyclic bases pyridine and 3-picoline as coligands.

4.2. Experimental

4.2.1. Materials

4-Benzyloxy-2-hydroxybenzaldehyde (Sigma-Aldrich), 5-bromo-2-hydroxy-3-methoxybenzaldehyde (Sigma-Aldrich), 4-diethylamino-2-hydroxybenzaldehyde (Sigma-Aldrich), nicotinic hydrazide (Sigma-Aldrich), 4-nitrobenzoic hydrazide (Sigma-Aldrich), cobalt(II) acetate tetrahydrate (Sigma-Aldrich), pyridine (S.D.Fine) and 3-picoline (Sigma-Aldrich) were of Analar grade and were used as received. Solvents used were methanol and DMF.

4.2.2. Syntheses of hydrazones

The syntheses of hydrazones 4-benzyloxy-2-hydroxybenzaldehyde-4-nitrobenzoylhydrazone dimethylformamide monosolvate ($H_2L^1 \cdot C_3H_7NO$), 5-bromo-2-hydroxy-3-methoxybenzaldehyde nicotinoylhydrazone dihydrate methanol monosolvate ($H_2L^2 \cdot 2H_2O \cdot CH_3OH$) and 4-diethylamino-2-hydroxybenzaldehyde nicotinoylhydrazone monohydrate ($H_2L^3 \cdot H_2O$) have already discussed in Chapter 2.

4.2.3. Syntheses of Co(II) complexes

4.2.3.1. [(CoL¹)₂] (8)

A hot methanolic solution of H₂L¹·C₃H₇NO (0.464 g, 1 mmol) was treated with a methanolic solution of cobalt(II) acetate tetrahydrate (0.249 g, 1 mmol) and 1 mL of DMF and the mixture was heated under reflux for 4 h. and cooled. The brown colored complex separated was filtered, washed thoroughly with methanol followed by ether and dried over P₄O₁₀ *in vacuo*.

[(CoL¹)₂] (8): Yield: 77%, λ_m (DMF): 4 ohm⁻¹ cm² mol⁻¹, μ_{eff} (B.M.): 3.84, Elemental Anal. Found (Calcd.) (%): C: 56.75 (56.26); H: 2.93 (3.37); N: 9.65 (9.37).

4.2.3.2. [CoL¹pic] (9)

A hot methanolic solution of H₂L¹·C₃H₇NO (0.464 g, 1 mmol) was treated with a methanolic solution of cobalt(II) acetate tetrahydrate (0.249 g, 1 mmol), 3-picoline (0.093 g, 1 mmol) and 1 mL of DMF and the resulting solution was refluxed for 4 h., cooled to room temperature and then poured into 40 mL of water containing crushed ice. The red colored product formed was filtered, washed with methanol followed by ether and dried over P₄O₁₀ *in vacuo*.

[CoL¹pic] (9): Yield: 78%, λ_m (DMF): 9 ohm⁻¹ cm² mol⁻¹, μ_{eff} (B.M.): 4.58, Elemental Anal. Found (Calcd.) (%): C: 54.82 (54.51); H: 4.03 (3.73); N: 9.67 (9.42).

4.2.3.3. [CoL¹py]·2H₂O (10)

A hot solution of H₂L¹·C₃H₇NO (0.464 g, 1 mmol) in methanol was mixed with methanolic solution of cobalt(II) acetate tetrahydrate (0.249 g, 1 mmol)

and pyridine (0.079 g, 1 mmol). The resulting mixture was refluxed for 4 h., cooled to room temperature and then poured into 40 mL of water containing crushed ice. The red colored product formed was filtered, washed with methanol followed by ether and dried over P_4O_{10} *in vacuo*.

$[CoL^1py] \cdot 2H_2O$ (**10**): Yield: 75%, λ_m (DMF): $12 \text{ ohm}^{-1} \text{ cm}^2 \text{ mol}^{-1}$, μ_{eff} (B.M.): 4.65, Elemental Anal. Found (Calcd.) (%): C: 56.01 (55.43); H: 4.33 (4.29); N: 10.01 (9.94).

4.2.3.4. $[(CoL^2)_2] \cdot 2H_2O$ (**11**)

This complex was prepared by refluxing a mixture of methanolic solutions of the ligand $H_2L^2 \cdot 2H_2O \cdot CH_3OH$ (0.418 g, 1 mmol) and cobalt(II) acetate tetrahydrate (0.249 g, 1 mmol) for 4 h. and cooled. The brown colored complex separated was filtered, washed with methanol followed by ether and dried over P_4O_{10} *in vacuo*.

$[(CoL^2)_2] \cdot 2H_2O$ (**11**): Yield: 65%, λ_m (DMF): $10 \text{ ohm}^{-1} \text{ cm}^2 \text{ mol}^{-1}$, μ_{eff} (B.M.): 3.79, Elemental Anal. Found (Calcd.) (%): C: 39.85 (39.56); H: 2.25 (2.85); N: 10.45 (9.88).

4.2.3.5. $[(CoL^3)_2] \cdot 4H_2O$ (**12**)

A solution of $H_2L^3 \cdot H_2O$ (0.330 g, 1 mmol) in methanol was treated with a methanolic solution of cobalt(II) acetate tetrahydrate (0.249 g, 1 mmol). The solution was heated under reflux for 4 h. The resulting solution was allowed to stand at room temperature and after slow evaporation brown colored complex separated out was filtered, washed with methanol followed by ether and dried over P_4O_{10} *in vacuo*.

$[(\text{CoL}^3)_2] \cdot 4\text{H}_2\text{O}$ (**12**): Yield: 70%, λ_m (DMF): $5 \text{ ohm}^{-1} \text{ cm}^2 \text{ mol}^{-1}$, μ_{eff} (B.M.): 3.83, Elemental Anal. Found (Calcd.) (%): C: 50.07 (50.38); H: 5.55 (5.47); N: 13.53 (13.82).

4.3. Results and discussion

Five cobalt complexes were synthesized. The complexes **8**, **11** and **12** were prepared by the reaction of the appropriate hydrazone with cobalt(II) acetate tetrahydrate in 1:1 ratio. Complexes **9** and **10** were synthesized by refluxing the metal salt, corresponding hydrazones and heterocyclic bases in 1:1:1 ratio. In all the complexes hydrazones coordinate in the iminolate form and act as dideprotonated tridentate ligands, coordinating through phenolate oxygen, iminolate oxygen and azomethine nitrogen. All complexes are soluble in solvents like DMSO, DMF and CH_3CN . Complexes **8**, **11** and **12** are dimeric in nature, while others are monomeric mixed ligand metal chelates. They are characterized by the following physico-chemical methods.

4.3.1. Elemental analyses

The analytical data indicate that all the complexes are analytically pure and supported the suggested formula given in Section 4.2.3. Carbon, hydrogen and nitrogen analyses data of all the five samples are given in Section 4.2.3.

4.3.2. Molar conductivity and magnetic susceptibility measurements

The molar conductivity values of the complexes **8-12** in DMF are in the $4-12 \text{ ohm}^{-1} \text{ cm}^2 \text{ mol}^{-1}$ range, which are well below the range ($65-90 \text{ ohm}^{-1} \text{ cm}^2 \text{ mol}^{-1}$) observed for uni-univalent electrolytes in the same solvent, confirming the non-electrolytic nature of the complexes [12].

According to the theory of magnetic susceptibility of Co(II) ion given by Schlapp and Penny, the observed values of magnetic moment for Co(II) complexes are generally diagnostic of the coordination geometry about the metal ion [13]. The magnetic moments of Co(II) complexes with an orbitally non-degenerate ground term is increased above the spin only value *via* orbital contribution. Magnetic moments of tetrahedral, octahedral and square planar complexes differ significantly and therefore topology can be easily identified using this data. Tetrahedral and octahedral Co(II) complexes can be distinguished from one another by the magnitude of deviation of μ_{eff} from the spin only value even if they possess same number of unpaired electrons. The tetrahedral Co(II) complexes have magnetic moments in the 4.2-4.7 B.M. range while octahedral Co(II) complexes exhibit μ_{eff} in the 4.8-5.6 B.M. range due to large contribution from its 4T_g ground term [14]. The low spin square planar Co(II) complexes have magnetic moments in the 2.1-2.9 B.M. range at room temperature due to spin and orbital contribution. The observed magnetic moment values in the 3.79-4.65 B.M. range (Section 4.2.3), exclude the possibility of octahedral and square planar geometry for the Co(II) complexes. From this we conclude that all the Co(II) complexes reported herein are of tetrahedral geometry. The low magnetic moment values for complexes **8**, **11** and **12** may be due to the antiferromagnetic interaction between metal centers suggesting dimeric nature to these complexes [15].

4.3.3. Infrared spectra

The characteristic IR bands of the complexes differ from their hydrazones and provide significant indications regarding the bonding sites of hydrazones. The selected IR frequencies with tentative assignments of the Co(II) complexes are presented in Table 4.1. The IR spectra of hydrazones

show strong bands in the 3067-3186 cm^{-1} and 1632-1669 cm^{-1} regions which are assigned to $\nu(\text{N-H})$ and $\nu(\text{C=O})$ vibrations respectively indicating that the hydrazones exist in the amido form in the solid state. These bands are absent in the spectra of all the complexes suggesting that hydrazones have undergone deprotonation and coordinated in the iminolate form. Coordination of iminolate oxygen is consistent with the presence of new bands in the 1335-1348 cm^{-1} region, assignable to $\nu(\text{C-O})$ stretching vibration for these complexes. This is further confirmed by the appearance of new bands in the 488-559 cm^{-1} region assigned to $\nu(\text{Co-O})$. The bands corresponding to the stretching vibration of the azomethine group of the free hydrazones which appeared in the 1603-1609 cm^{-1} region have been shifted to 1592-1603 cm^{-1} region in the spectra of the complexes indicating the coordination of the azomethine nitrogen to the central metal ion. This is further corroborated with the appearance of new bands in the 1519-1523 cm^{-1} region due to the newly formed C=N moiety. Bonding through the N of the azomethine group has been further confirmed by the observation of $\nu(\text{Co-N})$ bands in the 422-456 cm^{-1} region. The bands due to heterocyclic bases are observed at *ca.* 724-1426 cm^{-1} for complexes **9** and **10**. The broad bands in the 3337-3433 cm^{-1} region in the spectra of complexes **10**, **11** and **12** are due to the presence of lattice water molecules which is also evident from the thermogravimetric analyses [16-18]. IR spectra of some of the complexes are shown in Figs. 4.1-4.3.

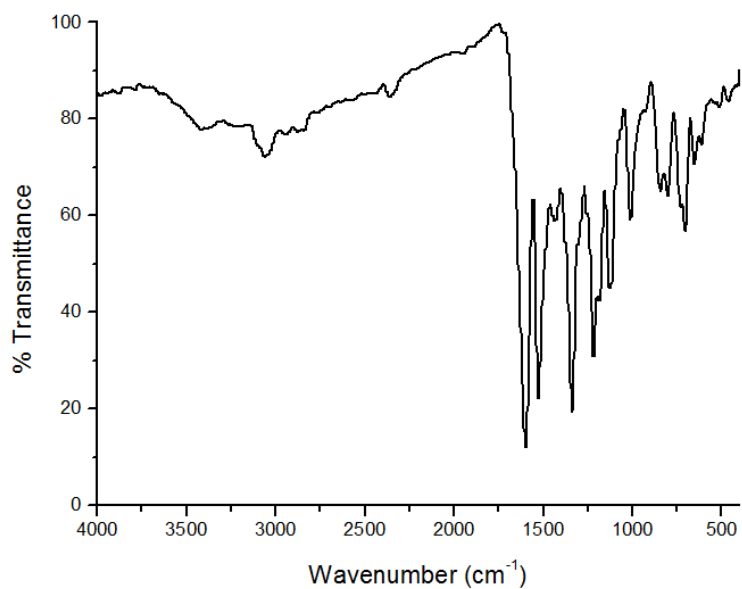


Fig. 4.1. IR spectrum of [CoL¹pic] (9).

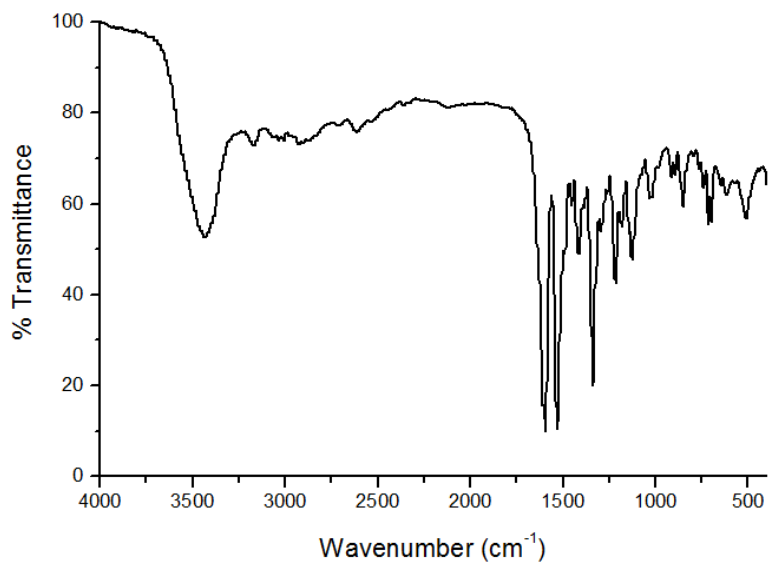


Fig. 4.2. IR spectrum of [CoL¹py]·2H₂O (10).

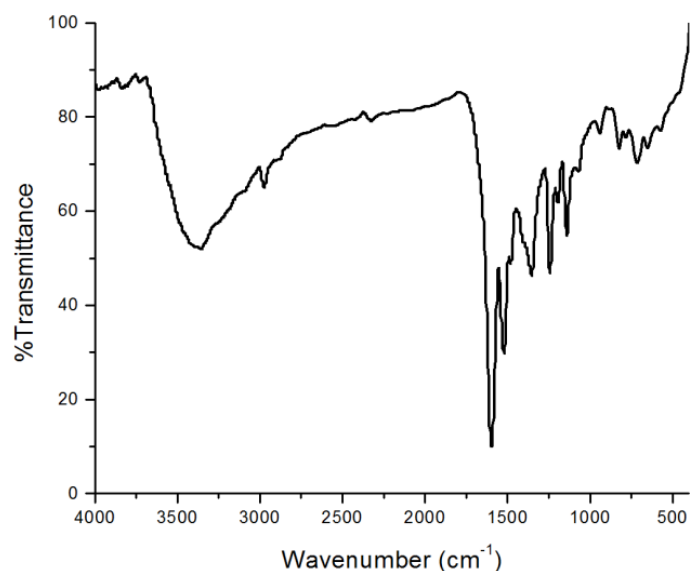


Fig. 4.3. IR spectrum of $[(\text{CoL}^3)_2] \cdot 4\text{H}_2\text{O}$ (**12**).

Table 4.1. The important IR frequencies (cm^{-1}) of hydrazones and their Co(II) complexes

Compound	$\nu(\text{C}=\text{N})$	$\nu(\text{C}=\text{N})^a$	$\nu(\text{C}=\text{O})/\nu(\text{C}-\text{O})$	$\nu(\text{N}-\text{H})$	$\nu(\text{Co}-\text{O})$	$\nu(\text{Co}-\text{N})$
$\text{H}_2\text{L}^1 \cdot \text{C}_3\text{H}_7\text{NO}$	1604	----	1661	3186	----	----
$[(\text{CoL}^1)_2]$ (8)	1593	1523	1335	----	526	456
$[\text{CoL}^1\text{pic}]$ (9)	1592	1522	1342	----	528	451
$[\text{CoL}^1\text{py}] \cdot 2\text{H}_2\text{O}$ (10)	1600	1520	1342	----	509	422
$\text{H}_2\text{L}^2 \cdot 2\text{H}_2\text{O} \cdot \text{CH}_3\text{OH}$	1609	----	1669	3067	----	----
$[(\text{CoL}^2)_2] \cdot 2\text{H}_2\text{O}$ (11)	1603	1519	1348	----	488	429
$\text{H}_2\text{L}^3 \cdot \text{H}_2\text{O}$	1603	----	1632	3075	----	----
$[(\text{CoL}^3)_2] \cdot 4\text{H}_2\text{O}$ (12)	1593	1522	1345	----	559	445

^aNewly formed C=N

4.3.4. Electronic spectra

The electronic absorption spectra of all the complexes were recorded in DMF and the spectral assignments are presented in Table 4.2. The bands in the $27020\text{-}36990\text{ cm}^{-1}$ region attributed to the $n \rightarrow \pi^*$ and $\pi \rightarrow \pi^*$ transitions of hydrazones are slightly shifted upon complexation and they are observed in

the 27190-36860 cm^{-1} region. The bands in the 23160-24060 cm^{-1} region correspond to ligand to metal charge transfer (LMCT) transitions. The broadness is explained as the combination of $\text{O} \rightarrow \text{Co}$ and $\text{N} \rightarrow \text{Co}$ charge transfer bands. Figs. 4.4-4.5 represent the electronic spectra of some of the Co(II) complexes.

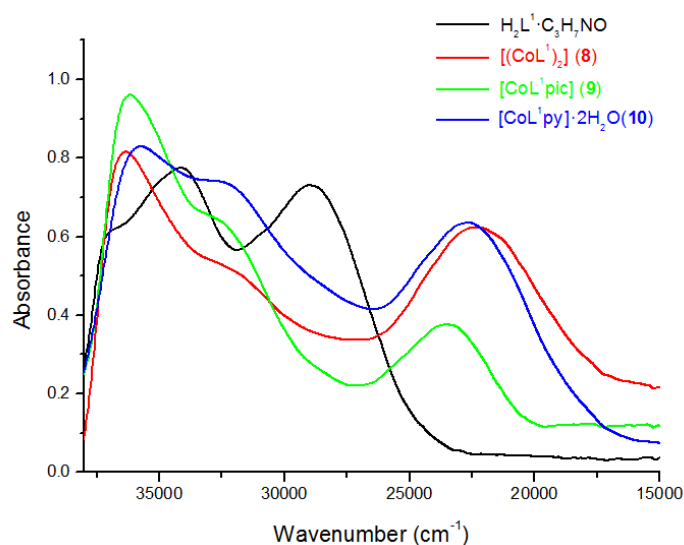


Fig. 4.4. UV spectra of $\text{H}_2\text{L}^1 \cdot \text{C}_3\text{H}_7\text{NO}$ and its Co(II) complexes.

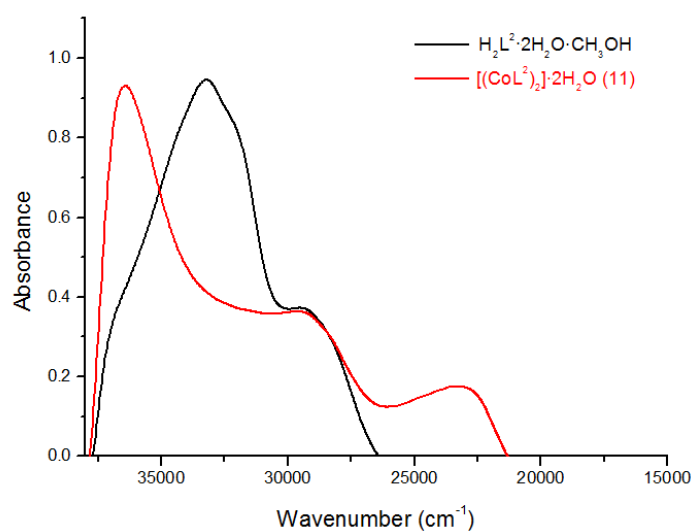


Fig. 4.5. UV spectra of $\text{H}_2\text{L}^2 \cdot 2\text{H}_2\text{O} \cdot \text{CH}_3\text{OH}$ and its Co(II) complex.

The ground state of Co(II) in tetrahedral complex is 4A_2 and three spin allowed transitions are expected: ${}^4T_2(F) \leftarrow {}^4A_2(F)$ (ν_1), ${}^4T_1(F) \leftarrow {}^4A_2(F)$ (ν_2) and ${}^4T_1(P) \leftarrow {}^4A_2(F)$ (ν_3); but we could observe only a weak broad band for complexes **11** and **12** due to masking by high intensity charge transfer bands [19-20] (Figs. 4.6-4.7).

Table 4.2. Electronic spectral assignments (cm^{-1}) of hydrazones and their Co(II) complexes

Compound	$n \rightarrow \pi^*/\pi \rightarrow \pi^*$	LMCT	$d-d$
$\text{H}_2\text{L}^1 \cdot \text{C}_3\text{H}_7\text{NO}$	36990, 34130, 28970	----	----
$[(\text{CoL}^1)_2]$ (8)	36860, 32720	23160	----
$[\text{CoL}^1\text{pic}]$ (9)	36300, 32670	23450	----
$[\text{CoL}^1\text{py}] \cdot 2\text{H}_2\text{O}$ (10)	36080, 32570	23490	----
$\text{H}_2\text{L}^2 \cdot 2\text{H}_2\text{O} \cdot \text{CH}_3\text{OH}$	33240, 29350	----	----
$[(\text{CoL}^2)_2] \cdot 2\text{H}_2\text{O}$ (11)	36280, 27190	23760	18250
$\text{H}_2\text{L}^3 \cdot \text{H}_2\text{O}$	36780, 27020	----	----
$[(\text{CoL}^3)_2] \cdot 4\text{H}_2\text{O}$ (12)	36280, 31670	24060	19840

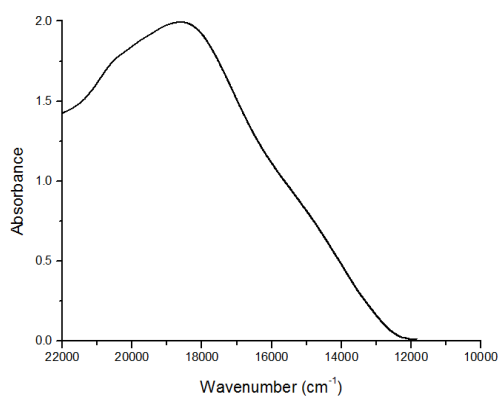


Fig. 4.6. Visible spectrum of $[(\text{CoL}^2)_2] \cdot 2\text{H}_2\text{O}$ (11**).**

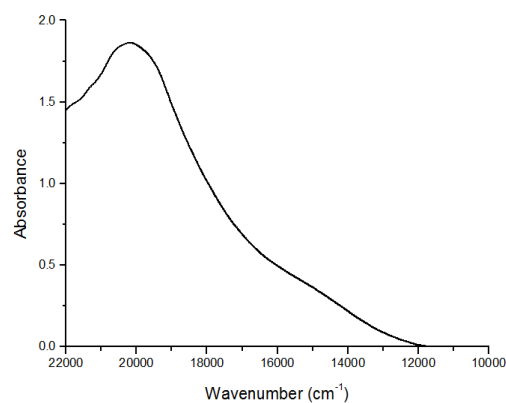


Fig. 4.7. Visible spectrum of $[(\text{CoL}^3)_2] \cdot 4\text{H}_2\text{O}$ (12**).**

4.3.5. Thermogravimetric analyses

Thermogravimetry is a powerful method for determining complex stoichiometries. Thermal analyses provide valuable information regarding the thermal stability and nature of water molecules in complexes [21,22]. Thermogravimetric analyses of the complexes were done in the temperature range of 50-700 °C in nitrogen atmosphere at a heating rate of 10 °C/min. The TG-DTG curves of the metal(II) complexes are presented in Figs. 4.8-4.10.

The thermogram of $[\text{CoL}^1\text{py}] \cdot 2\text{H}_2\text{O}$ (**10**) in the 130-188 °C range is accompanied by a weight loss of 6.26% (calcd. 6.39%). This may be due to loss of two lattice water molecules. On increasing the temperature further, the residue decomposes resulting in a weight loss of 16.37% (calcd. 15.00%) in the 398-428 °C range corresponding to the loss of pyridine ring moiety and above 450 °C degradation of the ligand takes place.

In complex $[(\text{CoL}^2)_2] \cdot 2\text{H}_2\text{O}$ (**11**), the first stage of decomposition is observed in the 52-83 °C range, which is due to the loss of two molecules of lattice water with a weight loss of 4.43% (calcd. 4.23%). The second weight loss of 43.70% (calcd. 42.75%) in the 276-322 °C range is due to the decomposition of one of the hydrazone ligands. After this temperature a gradual weight loss occurs due to the thermal degradation of the second ligand moiety.

The TGA curve for the complex $[(\text{CoL}^3)_2] \cdot 4\text{H}_2\text{O}$ (**12**) displays the first weight loss in the temperature range of 46-84 °C, which is due to the loss of four molecules of water with 8.4% of the total weight of the complex (calcd. 8.8%). This suggests that water molecules are present outside the coordination sphere. Above this temperature a gradual weight loss occurs due to the thermal degradation of the ligand.

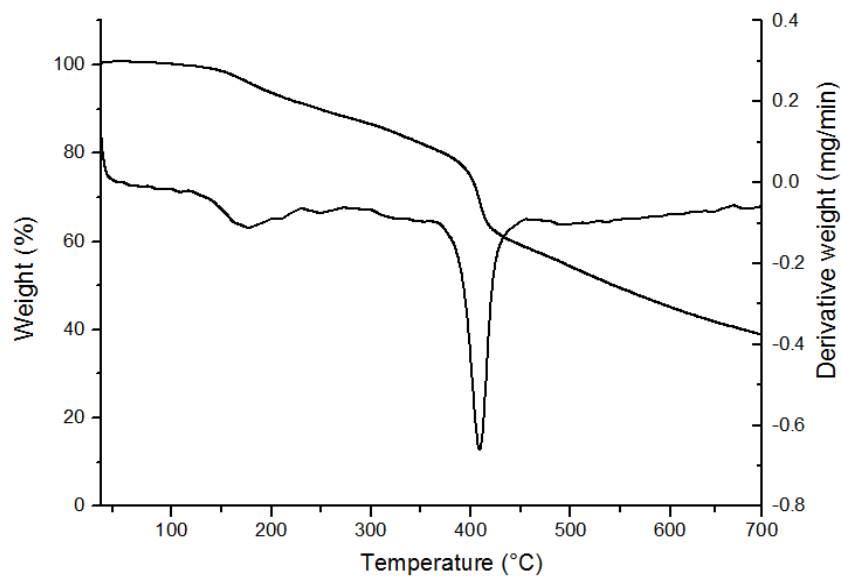


Fig. 4.8. Thermogram of $[\text{CoL}^1\text{py}] \cdot 2\text{H}_2\text{O}$ (10).

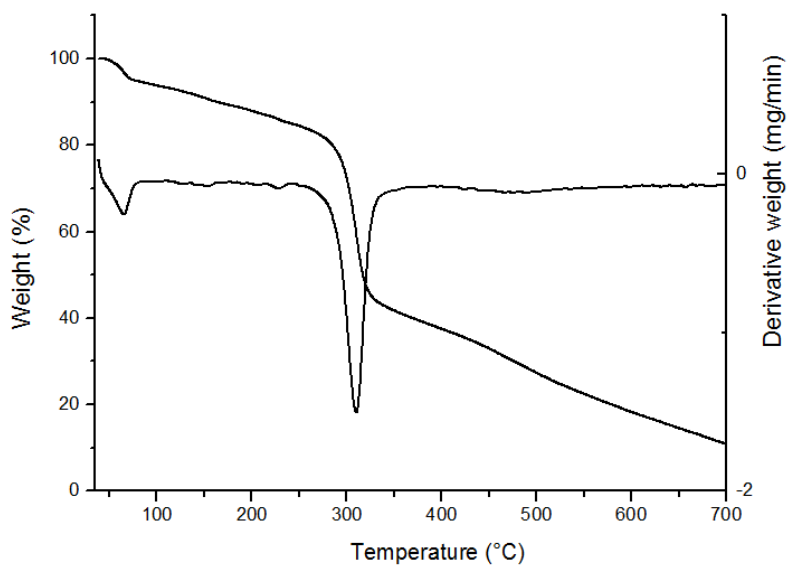


Fig. 4.9. Thermogram of $[(\text{CoL}^2)_2] \cdot 2\text{H}_2\text{O}$ (11).

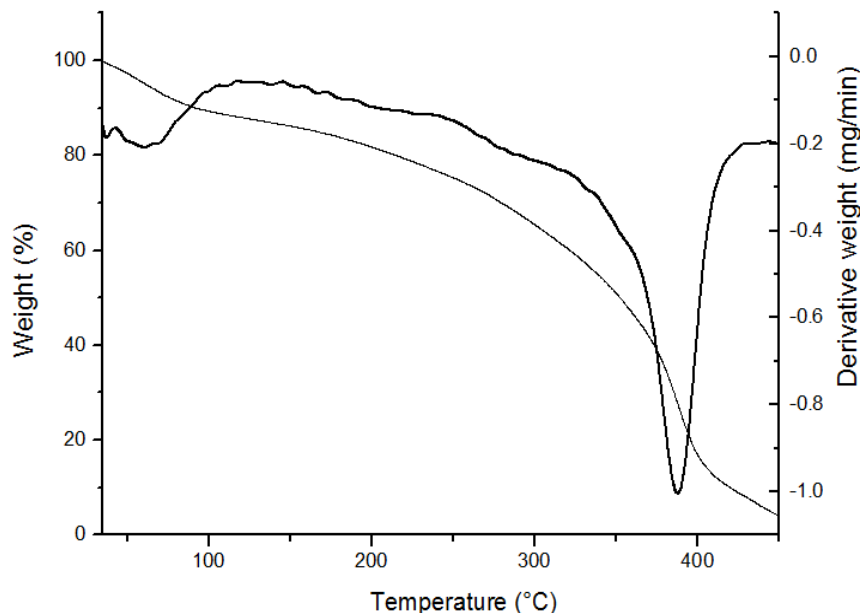
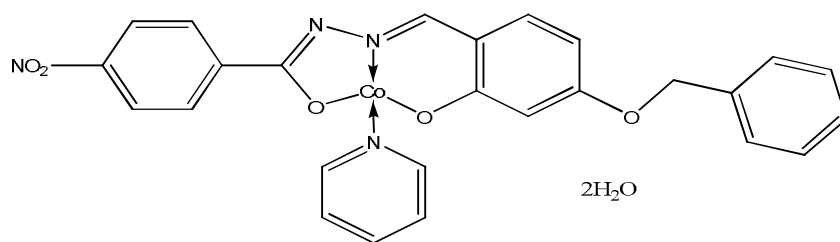
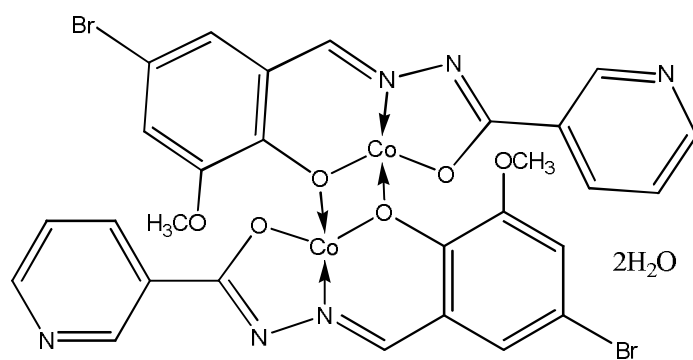


Fig. 4.10. Thermogram of $[(CoL^3)_2] \cdot 4H_2O$ (12).

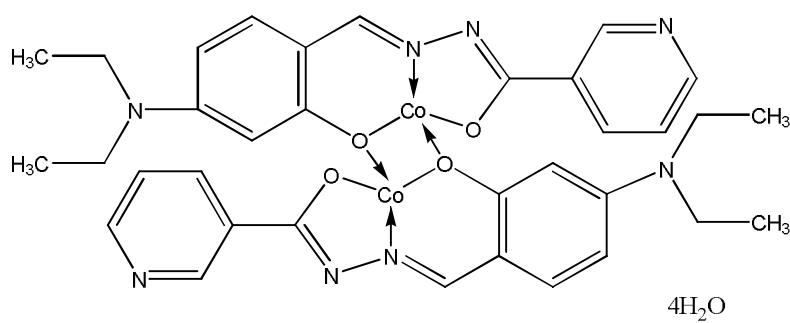
On the basis of the physico-chemical characterizations discussed above, the tentative structures proposed for some Co(II) complexes are presented below. Complexes **8**, **11** and **12** are binuclear and the remaining two (**9** and **10**) are mononuclear mixed ligand metal chelates. The Co(II) complexes synthesized have got tetrahedral geometry and in all the complexes the hydrazones exist in the iminolate form.



[CoL¹py]·2H₂O (10)



[(CoL²)₂]·2H₂O (11)



[(CoL³)₂]·4H₂O (12)

Fig. 4.11. Tentative structures of some of the Co(II) complexes.

References

- [1] M.D. Hall, T.W. Failes, N. Yamamoto, T.W. Hambley, Dalton Trans., (2007) 3983.
- [2] H.L. Sandoval, M.E.L. Lemos, R.G. Velasco, I.P. Melendez, P.G. Macias, I.G. Mora, N.B. Behrens, J. Inorg. Biochem. 102 (2008) 1267.
- [3] I. Ott, A. Abraham, P. Schumacher, H. Shorafa, G. Gastl, R. Gust, B. Kircher, J. Inorg. Biochem. 100 (2006) 1903.
- [4] L.S. Kumar, K.S. Prasad, H.D. Revanasiddappa, Eur. J. Chem. 2 (2011) 394.
- [5] D.U. Miodragovic, G.A. Bogdanovic, Z.M. Miodragovic, M.D. Radulovic, S.B. Novakovic, G.N. Kaluderovic, H. Kozlowski, J. Inorg. Biochem. 100 (2006) 1568.
- [6] J. Lv, T. Liu, S. Cai, X. Wang, L. Liu, Y. Wang, J. Inorg. Biochem. 100 (2006) 1888.
- [7] A. Banerjee, A. Guha, J. Adhikary, A. Khan, K. Manna, S. Dey, E. Zangrando, D. Das, Polyhedron 60 (2013) 102.
- [8] Z. Li, S. Wu, H. Ding, D. Zheng, J. Hu, X. Wang, Q. Huo, J. Guan, Q. Kan, New J. Chem. 37 (2013) 1561.
- [9] W.Y. Wang, X.F. Du, N.N. Ma, S.L. Sun, Y.Q. Qiu, J. Mol. Model 19 (2013) 1779.
- [10] O.S. Devi, A.M. Singh, J. Chem. Pharm. Res. 3 (2011) 1055.
- [11] L.N. Suvarapu, Y.K. Seo, S.O. Baek, V.R. Ammireddy, E-Journal of Chemistry 9 (2012) 1288.
- [12] M.S. Rao, K.H. Reddy, Indian J. Chem. 38 (1999) 262.
- [13] R. Schlapp, W.G. Penny, Phys. Rev. 42 (1932) 666.
- [14] S.M. Devi, A.M. Singh, Int. J. Res. Chem. Environ. 2 (2012) 290.

- [15] B. Lakshmi, K.N. Shivananda, G.A. Prakash, A.M. Isloor, K.N. Mahendra, Bull. Korean Chem. Soc. 33 (2012) 473.
- [16] M.V. Angelusiu, S.F. Barbuceanu, C. Draghici, G.L. Almajan, Eur. J. Med. Chem. 45 (2010) 2055.
- [17] H.S. Seleem, M. Mostafa, S.L. Stefan, E.A. Aziz, Res. J. Chem. Sci. 1 (2011) 67.
- [18] B. Jain, M. Verma, S. Malik, Int. J. Pharm. Res. Sci. 02 (2014) 155.
- [19] N. Nawar, N.M. Hosny, Transit. Met. Chem. 25 (2000) 1.
- [20] A.B.P. Lever, Inorganic Electronic Spectroscopy, 2nd edition, Elsevier, Amsterdam, 1984.
- [21] P.K. Singh, D.N. Kumar, Spectrochim. Acta A 64 (2006) 853.
- [22] O.M.I. Adly, Spectrochim. Acta A 79 (2011) 1295.



**SYNTHESES, SPECTRAL CHARACTERIZATION AND CRYSTAL
STRUCTURE OF NICKEL(II) CHELATES OF TRIDENTATE
AROYLHYDRAZONES**

Contents	5.1 Introduction
	5.2 Experimental
	5.3 Results and discussion
	References

5.1. Introduction

Nickel is a strong, lustrous, silvery-white metal that was not isolated by scientists until the mid-18th century, but is now a staple of our daily lives and can be found in everything from the batteries that power our television remotes to the stainless steel that is used to make our kitchen sinks. Nickel is one of the most corrosion-resistant metals in the world and there is evidence of it being mined and used more than five and a half thousand years ago. Nickel was discovered by the Swedish chemist Axel Fredrik Cronstedt in the mineral niccolite (NiAs) in 1751. Today, most nickel is obtained from minerals garnierite and pentlandite. The metal holds its strength through wide temperature ranges. Nickel is an incredibly versatile element and can be used to alloy with many other metals, each with its own benefits. As well as being so corrosion-resistant, alloys containing nickel are usually both very tough and

extremely ductile. Between eight to twelve percent of stainless steel is nickel and this is one of more than three thousand such alloys which are in everyday use around the world. This usage is growing at about 4% every year and about 90% of all new nickel mined is used for the production of alloys. It is alloyed with copper to make pipes that are used in desalination plants. Of the various transition metal oxides, Ni/NiO nanoparticles have shown exceptional nonlinear optical and magnetic properties indicating great potential in applications such as sensors, electronic components and magnetic data storage [1]. In certain combinations it also exhibits useful magnetic and electronic properties. Nickel is one of the four elements that are ferromagnetic around room temperature. Very powerful permanent magnets known as alnico magnets, can be made from an alloy of aluminium, nickel, cobalt and iron. It can be electroplated onto other metals to form a protective coating. Finely divided nickel is used as a catalyst for the hydrogenation of vegetable oils to produce vanaspati and is a good methanation catalyst for the production of methane from carbon monoxide and hydrogen. Adding nickel to glass gives it a green color. It resists corrosion even at high temperatures and for this reason it is used in gas turbines and rocket engines.

Nickel is abundant in lithosphere and biosphere so that natural deficiency does not occur. It is an important metal in the chemistry of life. Enzymes of some microorganisms and plants contain nickel in their active sites, which make the metal an essential nutrient for them. One of the most investigated metalloenzymes is nickel hydrogenase [2,3]. The enzyme urease (an enzyme which assists in the hydrolysis of urea) contains nickel. A nickel-tetrapyrrole coenzyme, F430, is present in the methyl coenzyme-M reductase which powers methanogenic archaea. Other nickel containing enzymes

include a class of super oxide dismutase and a glyoxalase [4]. For animals nickel is an essential foodstuff in small amounts. But nickel is not only favorable as an essential element; it can also be dangerous when the maximum tolerable amounts are exceeded. This can cause various kinds of cancer on different sites within the bodies of animals, mainly of those that live near refineries. In small quantities nickel is essential; but when the uptake is too high it can be a danger to human health.

In its familiar compounds nickel is bivalent, although it assumes other valencies. It also forms a number of coordination compounds with a wide variety of coordination number which complicates its coordination chemistry. The bioinorganic chemistry of nickel has been rapidly expanded due to the increasing interest in nickel complexes that have shown antibacterial, antifungal and anticancer activities [5-10]. In addition, they find increasing application in nonlinear optics. The second order NLO properties of asymmetric push-pull Ni(II) complexes have been extensively studied in the last decades and several of them show high values of the first molecular hyperpolarizability (β) [11-13].

The Ni(II) complexes of hydrazone derivatives are known for their versatile coordination. These complexes have tendency to yield stereochemistries of higher coordination number, to behave as neutral or deprotonated ligand and have the flexibility in assuming different conformation [14]. The synthesis and structural investigation of hydrazones and their nickel complexes have attracted great and growing interest due to their coordinative properties, biological significance, industrial importance and structural variety. Hydrazone ligands create an environment similar to the one present in biological systems usually by

making coordination through oxygen and nitrogen atoms. In view of coordinative capability and importance of Ni(II) complexes of hydrazones, we have synthesized five Ni(II) complexes of ONO donor hydrazones.

5.2. Experimental

5.2.1. Materials

4-Benzyloxy-2-hydroxybenzaldehyde (Sigma-Aldrich), 5-bromo-2-hydroxy-3-methoxybenzaldehyde (Sigma-Aldrich), 4-diethylamino-2-hydroxybenzaldehyde (Sigma-Aldrich), nicotinic hydrazide (Sigma-Aldrich), 4-nitrobenzoic hydrazide (Sigma-Aldrich), nickel(II) acetate tetrahydrate (Sigma-Aldrich), pyridine (S.D.Fine) and 3-picoline (Sigma-Aldrich) were of Analar grade and were used as received. Solvents used were methanol and DMF.

5.2.2. Syntheses of hydrazones

The syntheses of hydrazones 4-benzyloxy-2-hydroxybenzaldehyde-4-nitrobenzoylhydrazide dimethylformamide monosolvate ($H_2L^1 \cdot C_3H_7NO$), 5-bromo-2-hydroxy-3-methoxybenzaldehyde nicotinoylhydrazide dihydrate methanol monosolvate ($H_2L^2 \cdot 2H_2O \cdot CH_3OH$) and 4-diethylamino-2-hydroxybenzaldehyde nicotinoylhydrazide monohydrate ($H_2L^3 \cdot H_2O$) have already discussed in Chapter 2.

5.2.3. Syntheses of Ni(II) complexes

5.2.3.1. $[NiL^1(H_2O)_2]_2 \cdot 4C_3H_7NO$ (13)

This complex was prepared by refluxing hot methanolic solutions of $H_2L^1 \cdot C_3H_7NO$ (0.464 g, 1 mmol) and $Ni(OAc)_2 \cdot 4H_2O$ (0.248 g, 1 mmol) for 4 h. On cooling, the brown colored product formed were collected, washed with few drops of methanol followed by ether and dried over P_4O_{10} *in vacuo*.

Single crystals of the complex suitable for X-ray analysis were obtained by recrystallization from a mixture of methanol and dimethylformamide (1:1 v/v).

$[\text{NiL}^1(\text{H}_2\text{O})_2]_2 \cdot 4\text{C}_3\text{H}_7\text{NO}$ (**13**): Yield: 65%, λ_m (DMF): $12 \text{ ohm}^{-1} \text{ cm}^2 \text{ mol}^{-1}$, μ_{eff} (B.M.): 2.77, Elemental Anal. Found (Calcd.) (%): C: 51.73 (51.45); H: 5.61 (5.28); N: 10.90 (11.11).

5.2.3.2. $[\text{NiL}^1\text{pic}]$ (**14**)

To a solution of $\text{H}_2\text{L}^1 \cdot \text{C}_3\text{H}_7\text{NO}$ (0.464 g, 1 mmol) in DMF, a methanolic solution of $\text{Ni}(\text{OAc})_2 \cdot 4\text{H}_2\text{O}$ (0.248 g, 1 mmol) was added followed by 3-picoline (0.093 g, 1 mmol). The resulting solution was refluxed for 4 h. The brown colored complex separated out was filtered, washed with methanol followed by ether and dried over P_4O_{10} *in vacuo*.

$[\text{NiL}^1\text{pic}]$ (**14**): Yield: 67%, λ_m (DMF): $9 \text{ ohm}^{-1} \text{ cm}^2 \text{ mol}^{-1}$, μ_{eff} (B.M.): 3.55, Elemental Anal. Found (Calcd.) (%): C: 59.85 (59.92); H: 4.23 (4.10); N: 10.45 (10.35).

5.2.3.3. $[\text{NiL}^1\text{py}]$ (**15**)

To a solution of $\text{H}_2\text{L}^1 \cdot \text{C}_3\text{H}_7\text{NO}$ (0.464 g, 1 mmol) in DMF, a methanolic solution of $\text{Ni}(\text{OAc})_2 \cdot 4\text{H}_2\text{O}$ (0.248 g, 1 mmol) was added followed by pyridine (0.079 g, 1 mmol) and the resulting mixture was refluxed for 4 h. The brown colored product formed was filtered, washed with methanol followed by ether and dried over P_4O_{10} *in vacuo*.

$[\text{NiL}^1\text{py}]$ (**15**): Yield: 68%, λ_m (DMF): $9 \text{ ohm}^{-1} \text{ cm}^2 \text{ mol}^{-1}$, μ_{eff} (B.M.): 3.51, Elemental Anal. Found (Calcd.) (%): C: 59.09 (59.24); H: 3.96 (3.82); N: 10.56 (10.63).

5.2.3.4. $[(NiL^2)_2] \cdot H_2O$ (**16**)

This complex was synthesized by refluxing a solution of $H_2L^2 \cdot 2H_2O \cdot CH_3OH$ (0.418 g, 1 mmol) in methanol with a methanolic solution of $Ni(OAc)_2 \cdot 4H_2O$ (0.248 g, 1 mmol) for 4 h. The brown colored complex formed was filtered, washed with methanol followed by ether and dried over P_4O_{10} *in vacuo*.

$[(NiL^2)_2] \cdot H_2O$ (**16**): Yield: 72%, μ_{eff} (B.M.): 3.26, Elemental Anal. Found (Calcd.) (%): C: 41.01 (40.43); H: 2.32 (2.67); N: 10.59 (10.10).

5.2.3.5. $[(NiL^3)_2]$ (**17**)

This complex was synthesized by refluxing a methanolic solution of $H_2L^3 \cdot H_2O$ (0.330 g, 1 mmol) with a methanolic solution of $Ni(OAc)_2 \cdot 4H_2O$ (0.248 g, 1 mmol) for 4 h. The brown colored complex formed was filtered, washed with methanol followed by ether and dried over P_4O_{10} *in vacuo*.

$[(NiL^3)_2]$ (**17**): Yield: 70%, μ_{eff} (B.M.): 3.21, Elemental Anal. Found (Calcd.) (%): C: 55.45 (55.33); H: 5.49 (4.92); N: 14.80 (15.18).

5.3. Results and discussion

Five nickel(II) complexes of the hydrazones were synthesized. The complexes **13**, **16** and **17** were prepared by the reaction of equimolar mixture of the appropriate hydrazone and nickel acetate tetrahydrate. Complexes **14** and **15** were synthesized by refluxing metal salt, corresponding heterocyclic base and the hydrazone in 1:1:1 ratio. Complexes **13**, **14** and **15** are soluble in solvents like DMSO and DMF while **16** and **17** are partially soluble in DMSO and DMF. Single crystals of $[NiL^1(H_2O)_2]_2 \cdot 4C_3H_7NO$ (**13**) could be isolated and the structure was established by single crystal XRD studies. In all the complexes, hydrazones coordinate to the central metal ion in the iminolate

form. The complexes were characterized by the following physico-chemical methods.

5.3.1. Elemental analyses

Elemental analyses data of the complexes are given in Section 5.2.3. The observed C, H, N values show that all the complexes are analytically pure and are consistent with the stoichiometry of the formula given in Section 5.2.3.

5.3.2. Molar conductivity and magnetic susceptibility measurements

The molar conductivity values for the complexes **13-15** in DMF are found to be less than $13 \text{ ohm}^{-1} \text{ cm}^2 \text{ mol}^{-1}$ which is well below the range ($65\text{-}90 \text{ ohm}^{-1} \text{ cm}^2 \text{ mol}^{-1}$) for uni-univalent electrolytes in the same solvent, indicating the non-electrolytic nature of the complexes [15]. The complexes **16** and **17** are slightly soluble in most of the common solvents like DMSO, DMF, ethanol, methanol, benzene etc. and therefore, conductance measurements were not carried out. The magnetic properties of the complexes provide valuable information for distinguishing their stereochemistry. The magnetic moments of the complexes were calculated from the magnetic susceptibility measurements at room temperature. Out of the five complexes synthesized, $[\text{NiL}^1(\text{H}_2\text{O})_2]_2 \cdot 4\text{C}_3\text{H}_7\text{NO}$ (**13**) is hexacoordinate and the remaining four are tetracoordinate. All the complexes are found to be paramagnetic which excludes the possibility of a square planar geometry. For complex **13**, magnetic moment is found to be 2.77 B.M. corresponding to two unpaired electrons in an octahedral geometry. Complexes **14-17** have magnetic moments in the 3.21-3.55 B.M. range which are slightly greater than the spin only value which may be due to orbital contribution. This suggests a tetrahedral geometry for complexes **14-17** which are similar to that reported in other tetrahedral Ni(II) complexes [16-18].

5.3.3. Infrared spectra

IR spectra give enough information regarding the coordination modes of the hydrazones. The prominent infrared spectral data of hydrazones and their Ni(II) complexes are presented in Table 5.1. The bands due to $\nu(\text{N-H})$ and $\nu(\text{C=O})$ which appeared in the $3067\text{-}3186\text{ cm}^{-1}$ and $1632\text{-}1669\text{ cm}^{-1}$ regions respectively in the IR spectra of the free hydrazones disappeared completely in the spectra of the complexes **13-17** indicating the iminolization followed by deprotonation prior to coordination of the ligands. This is further confirmed by the appearance of new bands in the $1210\text{-}1293\text{ cm}^{-1}$ range assigned to $\nu(\text{C-O})$. The azomethine stretching frequencies of the free hydrazones which appeared in the $1603\text{-}1609\text{ cm}^{-1}$ region have been shifted to $1599\text{-}1603\text{ cm}^{-1}$ region in the spectra of the complexes in accordance with the coordination of the azomethine nitrogen. Further proof for the coordination of azomethine nitrogen to nickel is the appearance of new bands in the $1513\text{-}1537\text{ cm}^{-1}$ range due to $>\text{C}=\text{N}-\text{N}=\text{C}<$ moiety of the complexes. The $\nu(\text{O-H})$ bands in the $3377\text{-}3505\text{ cm}^{-1}$ region due to phenolic $-\text{OH}$ group of the hydrazones have disappeared in the spectra of complexes, giving evidence for deprotonation of phenolic $-\text{OH}$ group and its coordination to the central metal ion. For complexes **14** and **15**, bands due to heterocyclic breathing are observed in the $740\text{-}1450\text{ cm}^{-1}$ region. The bands in the $508\text{-}570$ and $435\text{-}477\text{ cm}^{-1}$ regions can be assigned to the stretching modes of the metal to ligand bonds, $\nu(\text{Ni-O})$ and $\nu(\text{Ni-N})$ respectively. The broad bands observed around 3400 cm^{-1} in complexes **13** and **16** indicate the presence of water in these structures [19-21]. These spectral data show that the hydrazones behave as tridentate dianionic ligands in all the five complexes. Figs. 5.1-5.4 represent the infrared spectra of some of the Ni(II) complexes of hydrazones.

Table 5.1. The important IR frequencies (cm⁻¹) of hydrazones and their Ni(II) complexes

Compound	$\nu(\text{C}=\text{N})$	$\nu(\text{C}=\text{N})^{\text{a}}$	$\nu(\text{C}=\text{O})/$ $\nu(\text{C}-\text{O})$	$\nu(\text{N}-\text{H})$	$\nu(\text{Ni}-\text{O})$	$\nu(\text{Ni}-\text{N})$
H ₂ L ¹ ·C ₃ H ₇ NO	1604	----	1661	3186	----	----
[NiL ¹ (H ₂ O) ₂] ₂ ·4C ₃ H ₇ NO (13)	1602	1531	1215	----	508	466
[NiL ¹ pic] (14)	1599	1535	1216	----	539	435
[NiL ¹ py] (15)	1603	1513	1210	----	549	449
H ₂ L ² ·2H ₂ O·CH ₃ OH	1609	----	1669	3067	----	----
[(NiL ²) ₂]·H ₂ O (16)	1602	1537	1293	----	570	477
H ₂ L ³ ·H ₂ O	1603	----	1632	3075	----	----
[(NiL ³) ₂] (17)	1600	1514	1238	----	564	442

^aNewly formed C=N

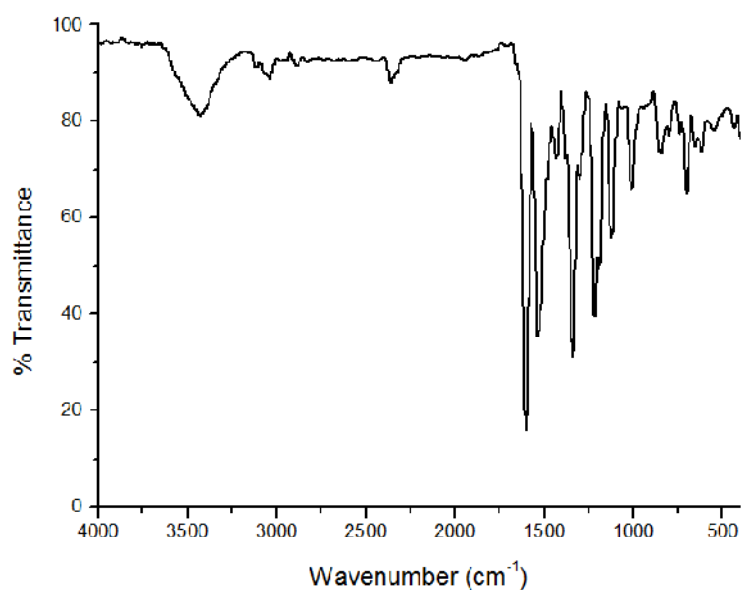


Fig. 5.1. IR spectrum of [NiL¹pic] (14**).**

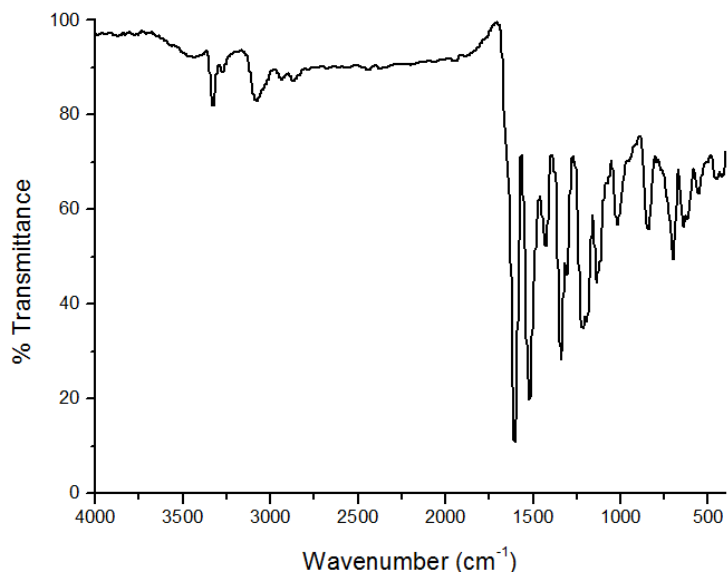


Fig. 5.2. IR spectrum of [NiL¹py] (15).

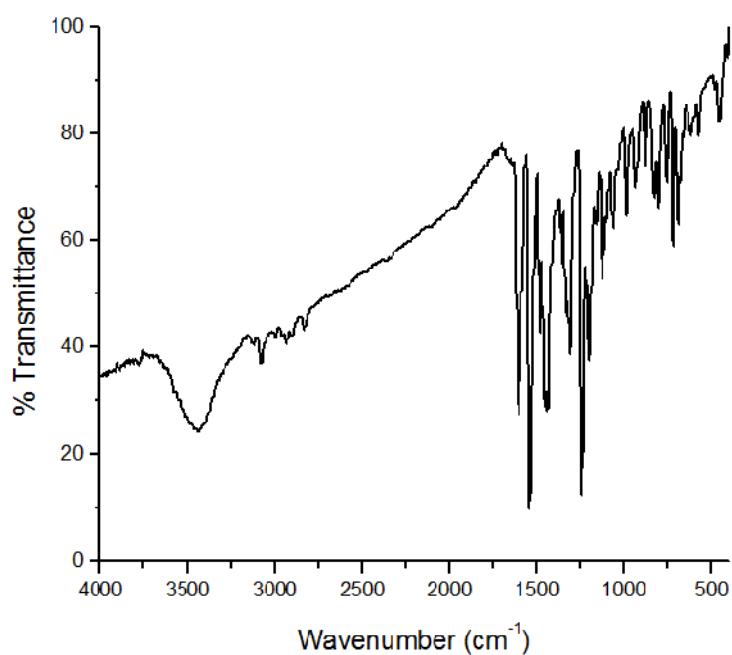


Fig. 5.3. IR spectrum of [(NiL²)₂]·H₂O (16).

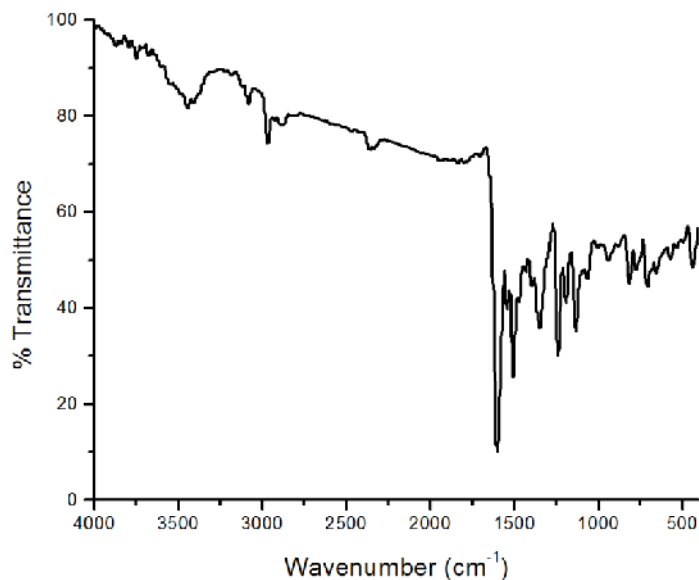


Fig. 5.4. IR spectrum of $[(NiL^3)_2]$ (**17**).

5.3.4. Electronic spectra

The UV-Vis spectra give much insight into the coordination geometry around the Ni(II) ion. The absorption bands of the complexes were recorded in DMF and the spectral data are given in Table 5.2. The electronic transitions of hydrazones suffered considerable shift on complexation. In the complexes the bands in the 27190-36860 cm^{-1} region can be assigned to the shifted intraligand transitions and the bands appeared in the 23160-24060 cm^{-1} region are ascribed to ligand to metal charge transfer transitions. Figs. 5.5-5.6 depict the electronic spectra of some of the complexes.

All the complexes synthesized except **13** have tetrahedral geometry as evidenced from their magnetic moments. The ground state of Ni(II) in tetrahedral complex is $^3T_1(F)$ and three spin allowed transitions are expected i.e. $^3T_2(F) \leftarrow ^3T_1(F)$, $^3A_2(F) \leftarrow ^3T_1(F)$, $^3T_1(P) \leftarrow ^3T_1(F)$; but unfortunately these *d-d* bands are masked by the stronger CT absorption bands in these

complexes. In nickel(II) complexes with octahedral geometry also, we expect three transitions; ${}^3T_{2g}(F) \leftarrow {}^3A_{2g}(F)$ (ν_1), ${}^3T_{1g}(F) \leftarrow {}^3A_{2g}(F)$ (ν_2) and ${}^3T_{1g}(P) \leftarrow {}^3A_{2g}(F)$ (ν_3) [22,23]. But we could locate only one band for $[\text{NiL}^1(\text{H}_2\text{O})_2]_2 \cdot 4\text{C}_3\text{H}_7\text{NO}$ (**13**) due to masking by high intensity charge transfer bands (Fig. 5.7).

Table 5.2. Electronic spectral assignments (cm^{-1}) of hydrazones and their Ni(II) complexes

Compound	$n \rightarrow \pi^*/\pi \rightarrow \pi^*$	LMCT	$d-d$
$\text{H}_2\text{L}^1 \cdot \text{C}_3\text{H}_7\text{NO}$	36990, 34130, 28970	----	----
$[\text{NiL}^1(\text{H}_2\text{O})_2]_2 \cdot 4\text{C}_3\text{H}_7\text{NO}$ (13)	36860, 32720	23160	19290
$[\text{NiL}^1\text{pic}]$ (14)	36300, 32670	23450	----
$[\text{NiL}^1\text{py}]$ (15)	36080, 32570	23490	----
$\text{H}_2\text{L}^2 \cdot 2\text{H}_2\text{O} \cdot \text{CH}_3\text{OH}$	33240, 29350	----	----
$[(\text{NiL}^2)_2] \cdot \text{H}_2\text{O}$ (16)	36280, 27190	23760	----
$\text{H}_2\text{L}^3 \cdot \text{H}_2\text{O}$	36780, 27020	----	----
$[(\text{NiL}^3)_2]$ (17)	36280, 31670	24060	----

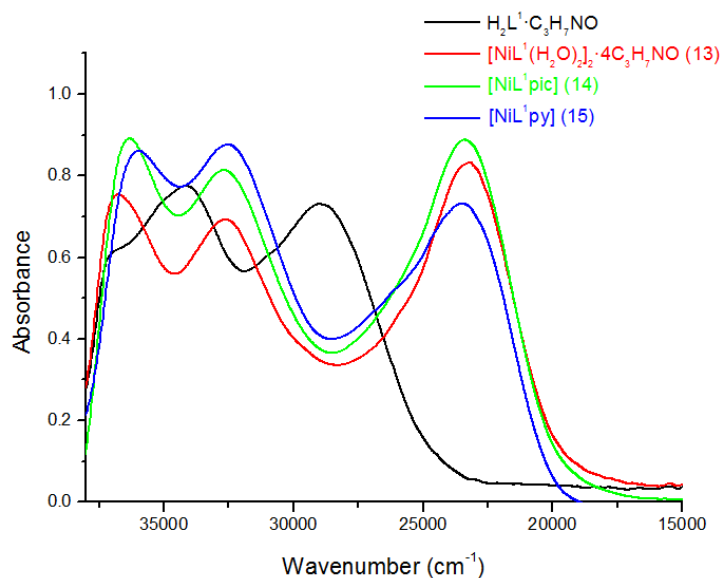


Fig. 5.5. UV spectra of $\text{H}_2\text{L}^1 \cdot \text{C}_3\text{H}_7\text{NO}$ and its Ni(II) complexes.

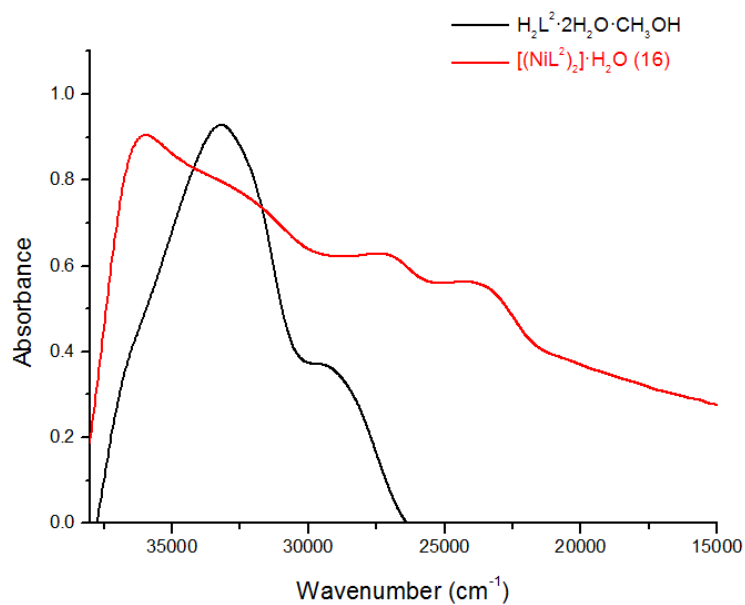


Fig. 5.6. UV spectra of H₂L²·2H₂O·CH₃OH and its Ni(II) complex.

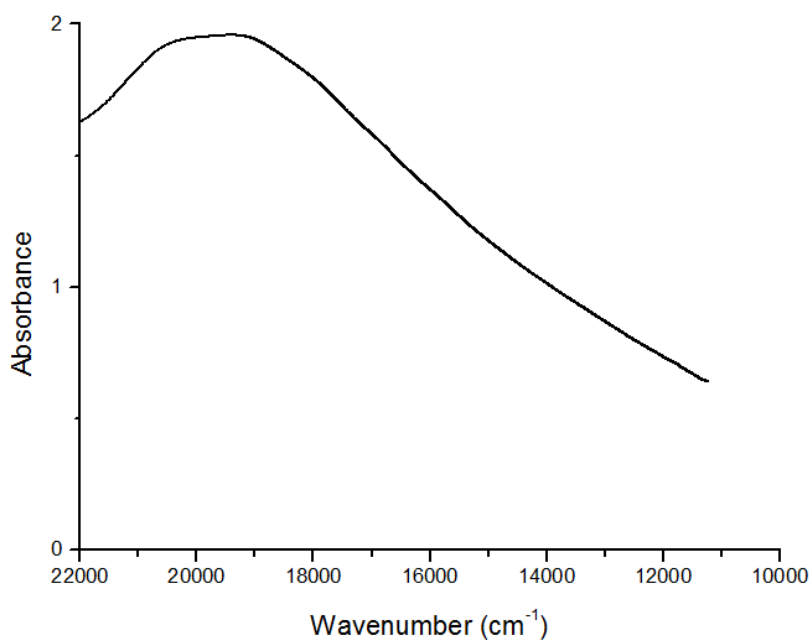


Fig. 5.7. Visible spectrum of [NiL¹(H₂O)₂]₂·4C₃H₇NO (13).

5.3.5. X-ray crystallography

Single crystals of the complex $[\text{NiL}^1(\text{H}_2\text{O})_2]_2 \cdot 4\text{C}_3\text{H}_7\text{NO}$ (**13**) suitable for X-ray analysis were obtained by recrystallization from a mixture of methanol and dimethylformamide (1:1 v/v). A brown colored block shaped crystal with approximate dimensions of $0.40 \times 0.25 \times 0.20 \text{ mm}^3$ was selected and mounted on a Bruker SMART APEXII CCD diffractometer equipped with a graphite crystal, incident-beam monochromator and a fine focus sealed tube with Mo K α ($\lambda = 0.71073 \text{ \AA}$) radiation as the X-ray source. The crystal data and structure refinement details of the complex are summarized in Table 5.3. The unit cell dimensions were measured and the data collections were performed at 293 K. Bruker SMART software was used for data acquisition and Bruker SAINT software for data integration [24]. Absorption corrections were carried out using SADABS based on Laue symmetry using equivalent reflections [25]. The structure was solved by direct methods and refined by full matrix least-squares calculations with the SHELXL97 software package [26]. All non-hydrogen atoms were refined anisotropically and all H atoms on C were placed in calculated positions, guided by difference maps with C–H bond distances 0.93–0.96 \AA . H atoms were assigned as $U_{\text{iso}}=1.2U_{\text{eq}}$ (1.5 for Me). The graphics tools used were ORTEP-3 and DIAMOND version 3.2g. A perspective view of the molecular structure of the binuclear centrosymmetric Ni(II) complex with the atom numbering scheme is given in Fig. 5.8. The asymmetric unit consists of one half of the molecule and two DMF molecules and the other half is related by a center of inversion in the Ni(1)–O(2)–Ni(1A)–O(2A) ring (Fig. 5.9).

Table 5.3. Crystal data and structure refinement parameters for [NiL^I(H₂O)₂]₂·4C₃H₇NO (13)

Parameters	[NiL ^I (H ₂ O) ₂] ₂ ·4C ₃ H ₇ NO (13)
Empirical formula	C ₅₄ H ₆₆ N ₁₀ Ni ₂ O ₁₈
Formula weight	1260.55
Temperature	293 K
Wavelength	0.71073 Å
Crystal system	Triclinic
Space group	<i>P</i> $\bar{1}$
Unit cell dimensions	<i>a</i> = 8.4939(3) Å <i>b</i> = 12.5451(6) Å <i>c</i> = 14.6717(6) Å α = 81.662(2)° β = 75.613(10) (3)° γ = 79.4420(10)°
Volume	1480.56(11) Å ³
Z	1
Density (calculated)	1.414 mg/m ³
Absorption coefficient	0.715 mm ⁻¹
<i>F</i> (000)	660
Crystal size	0.40 × 0.25 × 0.20 mm ³
θ range for data collection	2.59 to 27.50°
Limiting indices	-11 ≤ <i>h</i> ≤ 6 -16 ≤ <i>k</i> ≤ 16 -19 ≤ <i>l</i> ≤ 16
Reflections collected	11081
Unique Reflections (<i>R</i> _{int})	6785 [<i>R</i> (int) = 0.0253]
Refinement method	Full-matrix least-squares on <i>F</i> ²
Data / restraints / parameters	6571 / 0 / 383
Goodness-of-fit on <i>F</i> ²	1.019
Final <i>R</i> indices [<i>I</i> > 2σ(<i>I</i>)]	<i>R</i> ₁ = 0.0480, <i>wR</i> ₂ = 0.1192
<i>R</i> indices (all data)	<i>R</i> ₁ = 0.0748, <i>wR</i> ₂ = 0.1374
Largest diff. peak and hole	0.443 and -0.420 e Å ⁻³

$$R_1 = \frac{\sum ||F_o| - |F_c||}{\sum |F_o|}$$

$$wR_2 = \left[\frac{\sum w(F_o^2 - F_c^2)^2}{\sum w(F_o^2)^2} \right]^{1/2}$$

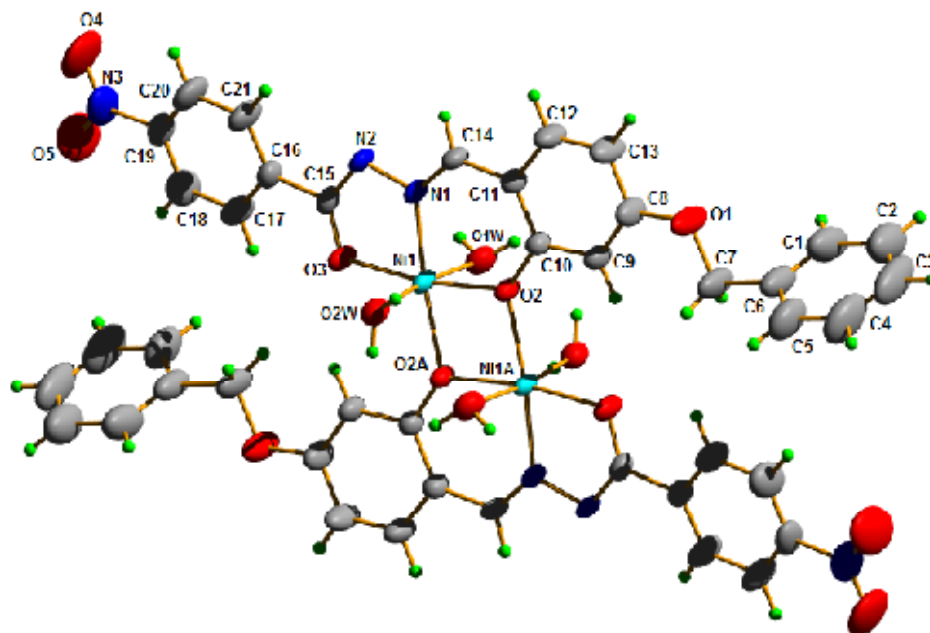


Fig. 5.8. Molecular structure of $[\text{NiL}^1(\text{H}_2\text{O})_2]_2 \cdot 4\text{C}_3\text{H}_7\text{NO}$ (13) along with the atom numbering scheme. The solvent molecules are omitted for clarity.

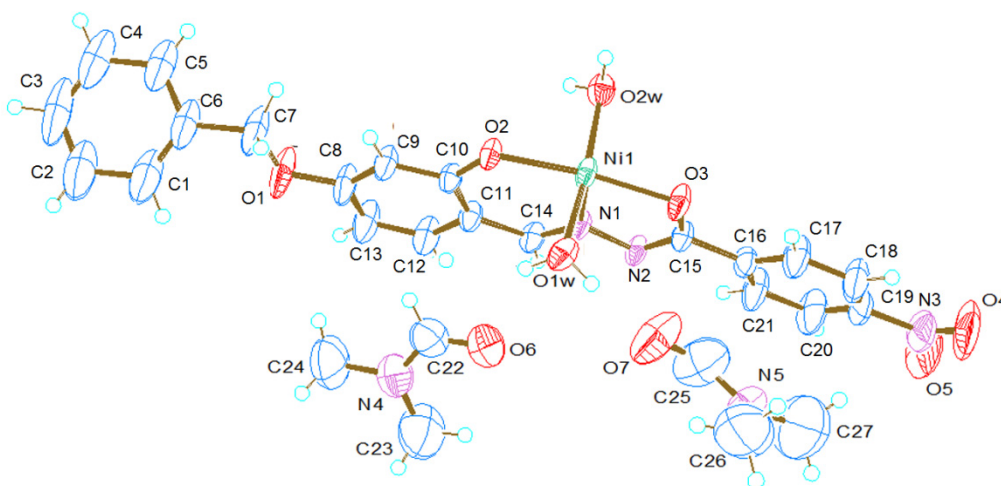


Fig. 5.9. Asymmetric unit of $[\text{NiL}^1(\text{H}_2\text{O})_2]_2 \cdot 4\text{C}_3\text{H}_7\text{NO}$ (13).

The complex crystallizes into a triclinic $P\bar{1}$ space group and has a dimeric structure with the two Ni(II) atoms bridged by phenolate oxygen atoms. The X-ray structural investigation of the complex **13** confirms that the principal ligand, 4-benzyloxy-2-hydroxybenzaldehyde-4-nitrobenzoylhydrazone (H_2L^1) behaves as a tridentate coordinating agent *via* the azomethine nitrogen, iminolate oxygen and phenolate oxygen atoms, forming five and six membered chelate rings surrounding each nickel atom, with a dihedral angle of 2.21° between them. The ligand is coordinated to each Ni atom *via* iminolate form without changing its configuration since the hydrazone and the complex adopts an *E* configuration with respect to C(14)=N(1) bond. The C(14)=N(1) [1.272(3) Å] and C(15)–O(3) [1.282(3) Å] bond distances are very close to the formal C=N and C–O bond lengths respectively confirming the azomethine bond formation and the coordination *via* iminolate form. The dihedral angle between the phenyl ring of hydrazide part C(16)–C(21) and the phenyl ring of aldehyde part C(8)–C(13) is 12.56° . The bond lengths Ni(1)–O(3), Ni(1)–N(1) and C(14)–N(1) are very close to other reported nickel complexes of hydrazones [27,28]. Table 5.4 shows the selected bond lengths and angles for the complex **13**.

Table 5.4. Selected bond lengths and angles for complex $[\text{NiL}^1(\text{H}_2\text{O})_2]_2 \cdot 4\text{C}_3\text{H}_7\text{NO}$ (13)

Bond lengths (Å)		Bond angles (°)	
Ni(1)–N(1)	1.974(2)	N(1)–Ni(1)–O(2)	91.70(8)
Ni(1)–O(2)	2.023(16)	N(1)–Ni(1)–O(3)	79.10(8)
Ni(1)–O(3)	2.033(17)	O(2)–Ni(1)–O(2A)	80.54(7)
Ni(1)–O(2A)	2.045(16)	O(3)–Ni(1)–O(2A)	108.71(7)
Ni(1)–O(2W)	2.136(2)	N(1)–Ni(1)–O(2W)	91.81(9)
Ni(1)–O(1W)	2.147(2)	O(2)–Ni(1)–O(2W)	88.30(7)
C(10)–O(2)	1.323(2)	O(3)–Ni(1)–O(2W)	93.28(8)
C(14)–N(1)	1.272(3)	O(2A)–Ni(1)–O(2W)	85.99(7)
N(1)–N(2)	1.399(3)	N(1)–Ni(1)–O(1W)	92.89(9)
C(15)–O(3)	1.282(3)	O(2)–Ni(1)–O(1W)	87.03(8)
N(2)–C(15)	1.311(3)	O(3)–Ni(1)–O(1W)	92.07(8)
O(1)–C(7)	1.434(4)	O(2A)–Ni(1)–O(1W)	88.74(7)
O(1)–C(8)	1.372(3)	O(2)–Ni(1)–O(3)	170.70(7)
N(3)–C(19)	1.474(4)	N(1)–Ni(1)–O(2A)	171.98(7)
Ni(1)···Ni(1A)	2.351(2)	O(2W)–Ni(1)–O(1W)	173.47(7)

Both the Ni centers being hexacoordinated, the coordination around the Ni(II) ion can be best described as a distorted octahedron with NiO_5N_1 chromophore. For each Ni(II) center of the octahedral dimeric complex, the water molecules complete the coordination sphere. The coordination sites of the basal square plane are occupied by azomethine nitrogen N(1), iminolate oxygen O(3) and two phenolate oxygen atoms O(2) and O(2A) of the hydrazone ligands and the axial positions by two coordinated water molecules. This is further confirmed from the respective bond lengths and bond angles.

The equatorial bond lengths are shorter than the axial bond lengths. The atoms N(1), O(2), O(2A) and O(3) in the complex define a plane showing high degree of planarity, the Ni atoms are displaced by 0.0016 Å from this plane. There is slight deviation for the equatorial bond angles from the expected value of 90° which indicates a distortion of the basal plane from a square geometry. The two trans oxygen atoms are not exactly linear since O(2W)–Ni(1)–O(1W) bond angle is 173.47(7)°. The coordination polyhedra present in a unit cell is shown in Fig. 5.10.

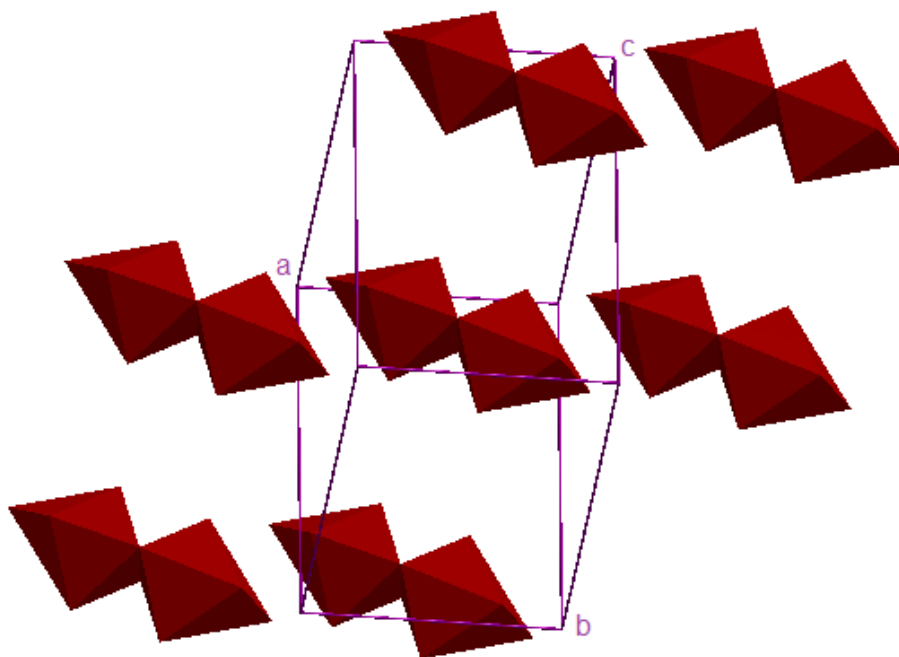


Fig. 5.10. Coordination polyhedra in a unit cell.

The O–H···O and C–H···O (conventional and nonconventional) hydrogen bonding interactions interconnect the neighboring complex and the solvent DMF molecules which make the crystal structure more stable (Table 5.5). The π ··· π interaction between Cg(5) [C(8), C(9), C(10), C(11), C(12), C(13)]

and Cg(6) [C(16), C(17), C(18), C(19), C(20), C(21)] of neighboring molecules occur at a Cg...Cg distance of 3.681(2) Å. C–H... π interactions also play an important role in the stabilization of the unit cell. Two C–H... π interactions progressing along *c* axis and a π ... π interaction (Fig. 5.11) progressing along *b* axis also support the dominant intermolecular hydrogen bonding interactions to establish a supramolecular three-dimensional network in the crystal system (Fig. 5.12). Fig. 5.13 shows the packing diagram of the complex along *b* axis.

Table 5.5. Interaction parameters of [NiL¹(H₂O)₂]₂·4C₃H₇NO (13)

Hydrogen bonding interactions				
D–H...A	D–H (Å)	H...A (Å)	D...A (Å)	D–H...A (°)
O(1W)–H(1A)...O(7) ^a	0.84	1.98	2.674(4)	139
O(1W)–H(1B)...O(6)	0.84	2.00	2.702(4)	140
C(9)–H(9)...O(3) ^b	0.93	2.36	3.217(3)	153
C(18)–H(18)...O(7) ^c	0.93	2.43	3.257(6)	147
C(26)–H(26B)...O(5) ^d	0.96	2.56	3.320(8)	136
π...π interaction				
Cg(I)...Cg(J)	Cg...Cg (Å)	α (°)	β (°)	
Cg(5)...Cg(6) ^e	3.681(2)	12.54(18)	9.12	
C–H...π interactions				
C–H(I)...Cg(J)	H...Cg (Å)	C–H...Cg (°)	C...Cg (Å)	
C(23)–H(23B)...Cg(4) ^f	2.94	172	3.89(8)	
C(22)–H(22A)...Cg(5)	2.95	115	3.440(5)	

Equivalent position codes : a = x, 1+y, z; b = 1-x, 1-y, 1-z; c = x-1, y, z; d = x+1, y, z; e = -x, 1-y, 1-z; f = -x+1, y+1, -z

Cg(4) = C(1), C(2), C(3), C(4), C(5), C(6); Cg(5) = C(8), C(9), C(10), C(11), C(12), C(13);
Cg(6) = C(16), C(17), C(18), C(19), C(20), C(21)

D, Donor; A, acceptor; Cg, Centroid; α , dihedral angle between planes I & J; β , angle between Cg...Cg and Cg(J) perp.

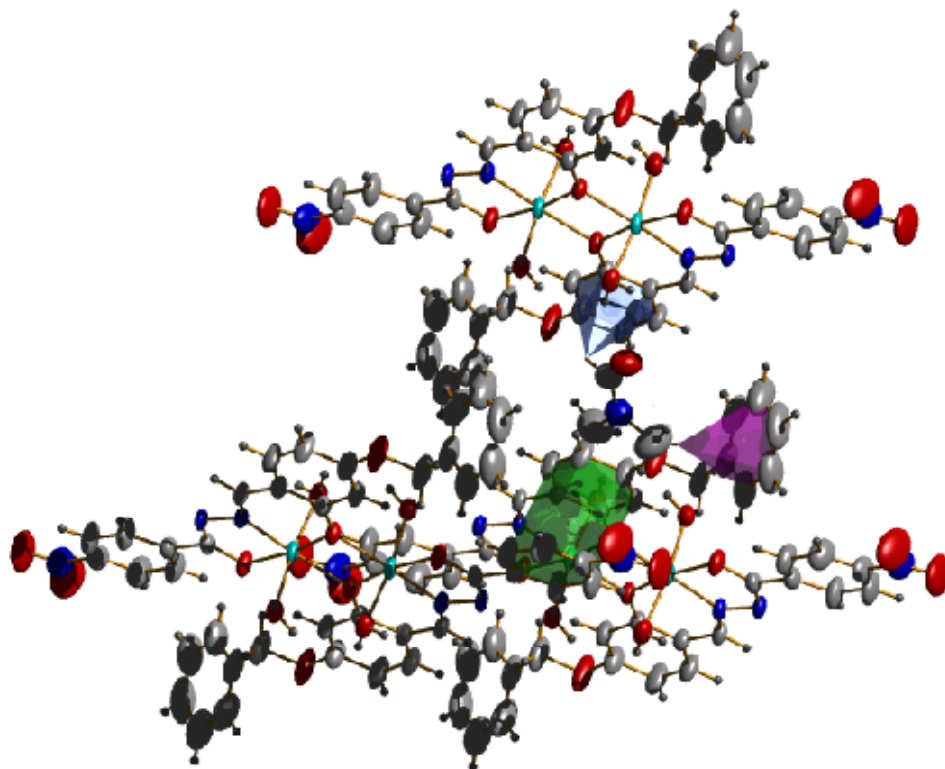


Fig. 5.11. C–H··· π and π ··· π interactions present in $[\text{NiL}^1(\text{H}_2\text{O})_2]_2 \cdot 4\text{C}_3\text{H}_7\text{NO}$ (13).

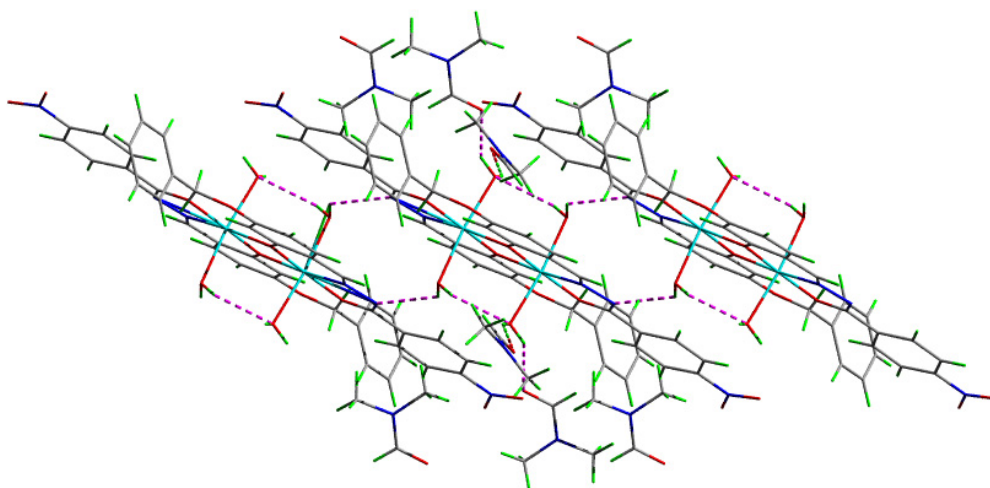


Fig. 5.12. Supramolecular chain mediated by hydrogen bonding interactions.

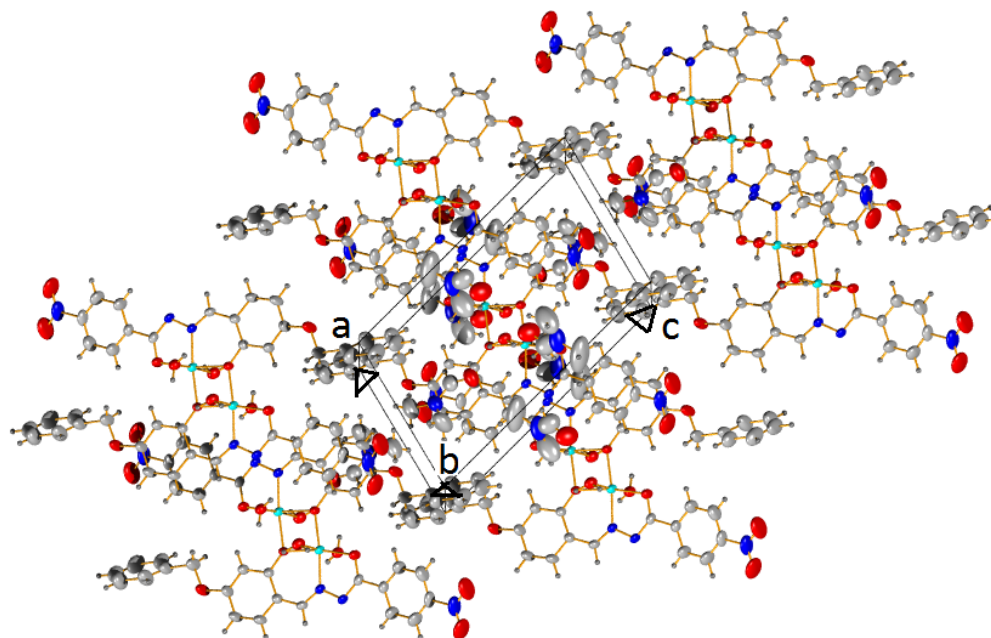


Fig. 5.13. Packing diagram of complex viewed along *b* axis.

5.3.6. Thermogravimetric analyses

Thermogravimetric methods are based on the measurement of the dynamic relationship between change in weight of the substance with respect to temperature. TG-DTG measurements under N_2 atmosphere in the 50-700 °C temperature range help to study the thermal stability and nature of water molecules in complexes. The TGA curve for the complex $[NiL^1(H_2O)_2]_2 \cdot 4C_3H_7NO$ (**13**) shows initially a weight loss of 22.29% in the 56-107 °C range in two steps corresponding to loss of four DMF molecules (calcd. 23.17%). This suggests that DMF molecules are present outside the coordination sphere. The second weight loss of 30.30% (calcd 29.23%) has been observed in the temperature range of 320 °C to 410 °C corresponds to loss of four coordinated water molecules together with $C_{14}H_{11}O_2$ fragment of the ligand. After 420 °C, oxidative decomposition

of the remaining part of the complex takes place gradually to give NiO as the ultimate residue [29].

In complex $[(\text{NiL}^2)_2] \cdot \text{H}_2\text{O}$ (**16**), the first weight loss of 2.04% in the 66-139 °C range (calcd. 2.16%) corresponds to removal of one molecule of lattice water. The second weight loss from 330 °C to 440 °C corresponds to the loss of the two Br atoms. The observed weight loss of 20.12% is close to the calculated value (19.66%). Beyond 450 °C, a gradual weight loss occurs due to the decomposition of the remaining contents of the ligand and the formation of NiO as the end product. The thermograms of complexes $[\text{NiL}^1(\text{H}_2\text{O})_2]_2 \cdot 4\text{C}_3\text{H}_7\text{NO}$ (**13**) and $[(\text{NiL}^2)_2] \cdot \text{H}_2\text{O}$ (**16**) are presented in Figs. 5.14 and 5.15 respectively.

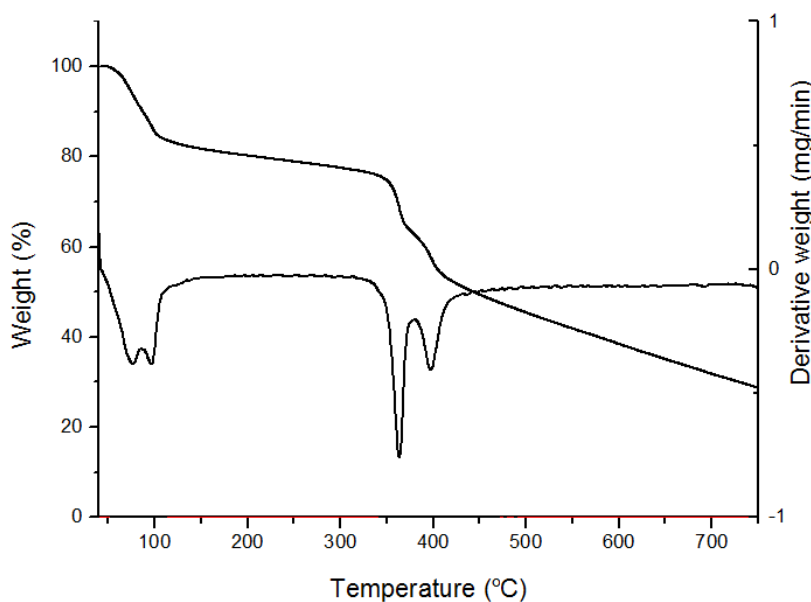


Fig. 5.14. Thermogram of $[\text{NiL}^1(\text{H}_2\text{O})_2]_2 \cdot 4\text{C}_3\text{H}_7\text{NO}$ (13**).**

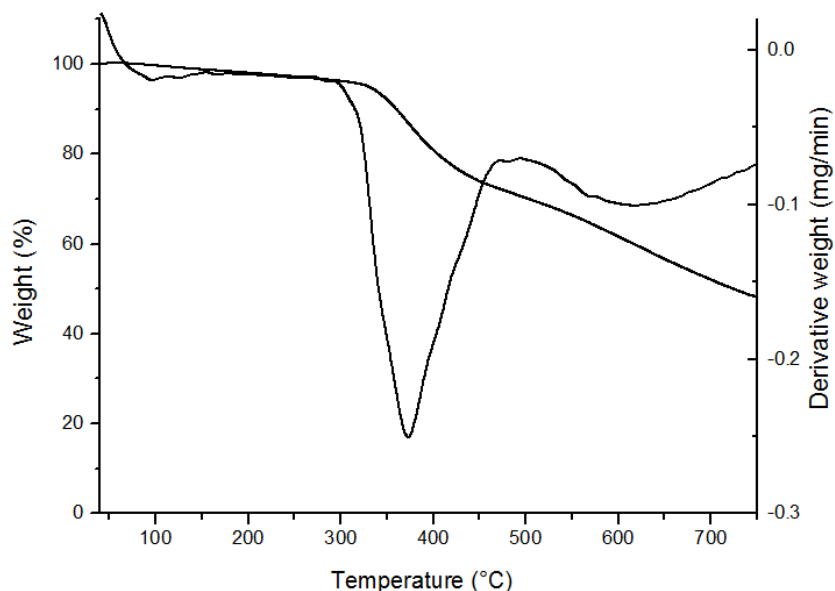
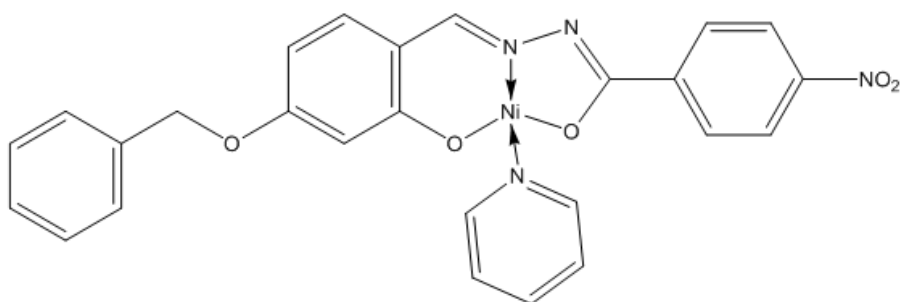
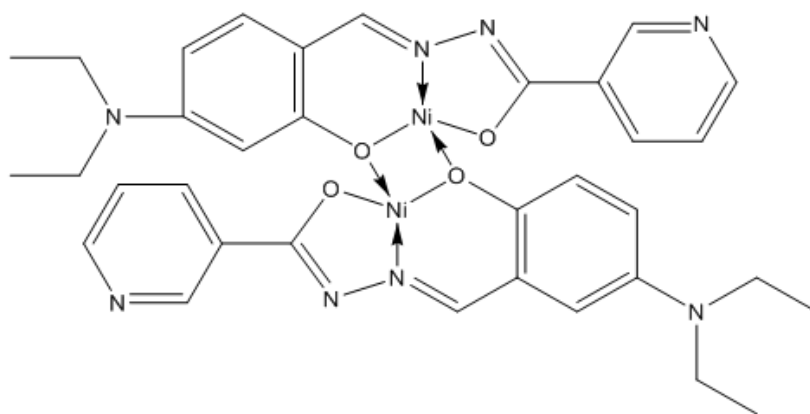


Fig. 5.15. Thermogram of $[(\text{NiL}^2)_2] \cdot \text{H}_2\text{O}$ (16).

Based on the above physico-chemical data, the proposed structures for some Ni(II) complexes are shown in Fig. 5.16. Complexes **13**, **16** and **17** are binuclear and the remaining two (**14** and **15**) are mononuclear mixed ligand metal chelates. Out of the five Ni(II) complexes synthesized, complex **13** has got octahedral geometry, while others have been assigned tetrahedral geometry. In all the complexes hydrazones exist in the iminolate form and act as dideprotonated ONO donor ligands.



[NiL¹py] (15)



[(NiL³)₂] (17)

Fig. 5.16. Tentative structures of some of the Ni(II) complexes.

References

- [1] K.M. Rahulan, N. Padmanathan, R. Philip, S. Balamurugan, C.C. Kanakam, *Appl. Surf. Sci.* 282 (2013) 656.
- [2] A. Volbeda, M.H. Charon, C. Piras, E.C. Hatchikian, M. Frey, J.C.F. Camps, *Nature* 373 (1995) 580.
- [3] A.L.D. Lacey, E.C. Hatchikian, A. Volbeda, M. Frey, J.C.F. Camps, V.M. Fernandez, *J. Am. Chem. Soc.* 119 (1997) 7181.
- [4] D.G. Krishna, N. Devanna, K.B. Chandrasekhar, *J. Pharm. Biomed. Sci.* 1 (2010) 1.
- [5] B. Singh, K.K. Narang, R. Srivastava, *Synth. React. Inorg. Met.-Org. Chem.* 33 (2003) 1025.
- [6] I. Babahan, E.P. Coba, H. Biyik, *Maejo Int. J. Sci. Technol.* 7 (2013) 26.
- [7] Y. Harinath, D.H.K. Reddy, B.N. Kumar, K. Lakshmi, K. Sessaiah, *J. Chem. Pharm. Res.* 3 (2011) 698.
- [8] P. Krishnamoorthy, P. Sathyadevi, R.R. Butorac, A.H. Cowley, N.S.P. Bhuvanesh, N. Dharmaraj, *Dalton Trans.* 41 (2012) 4423.
- [9] W. Luo, X. Meng, X. Sun, F. Xiao, J. Shen, Y. Zhou, G. Cheng, Z. Ji, *Inorg. Chem. Commun.* 10 (2007) 1351.
- [10] P. Krishnamoorthy, P. Sathyadevi, R.R. Butorac, A.H. Cowley, N.S.P. Bhuvanesh, N. Dharmaraj, *Dalton Trans.* 41 (2012) 6842.
- [11] G. Soras, N. Psaroudakis, G.A. Mousdis, M.J. Manos, A.J. Tasiopoulos, P. Aloukos, S. Couris, P. Labeguerie, J. Lipinski, A. Avramopoulos, M.G. Papadopoulos, *Chem. Phys.* 372 (2010) 33.

- [12] A. Trujillo, M. Fuentealba, D. Carrillo, C. Manzur, I.L. Rak, J.R. Hamon, J.Y. Saillard, *Inorg. Chem.* 49 (2010) 2750.
- [13] L. Pilia, M. Pizzotti, F. Tessore, N. Robertson, *Inorg. Chem.* 53 (2014) 4517.
- [14] S.M. Devi, A.M. Singh, *Int. J. Res. Chem. Environ.* 2 (2012) 290.
- [15] V.M. Naik, M.I. Sambrani, N.B. Mallur, *Indian J. Chem.* 47 (2008) 1793.
- [16] M.P. Teotia, J.N. Gurtu, V.B. Rana, *J. Inorg. Nucl. Chem.* 42 (1980) 821.
- [17] K.M. Ibrahim, M.M. Bekheit, G.M.A. Reash, M.M. Mostafa, *Polyhedron* 5 (1986) 1635.
- [18] N. Nawar, N.M. Hosny, *Chem. Pharm. Bull.* 47 (1999) 944.
- [19] B.N.B. Raj, M.R.P. Kurup, E. Suresh, *Struct. Chem.* 17 (2006) 201.
- [20] A.J M. Xavier, M. Thakur, J.M. Marie, *J. Chem. Pharm. Res.* 4 (2012) 986.
- [21] M. Kuriakose, M.R.P. Kurup, E. Suresh, *Struct. Chem.* 18 (2007) 579.
- [22] N. Chitrapriya, V. Mahalingam, M. Zeller, K. Natarajan, *Inorg. Chim. Acta* 363 (2010) 3685.
- [23] M. Calinescu, E. Ion, A.M. Stadler, *Rev. Roum. Chim.* 53 (2008) 903.
- [24] SMART and SAINT, Area Detector Software Package and SAX Area Detector Integration Program, Bruker Analytical X-ray; Madison, WI, USA, 1997.
- [25] Bruker, SADABS, APEX2, XPREP and SAINT, Bruker AXS Inc., Madison, Wisconsin, USA, 2004.
- [26] G.M. Sheldrick, *Acta Cryst. Sect. A* 64 (2008) 112.

- [27] R.N. Patel, V.P. Sondhiya, D.K. Patel, K.K. Shukla, Y. Singh, *Indian J. Chem.* 51 (2012) 1695.
- [28] A. Datta, J.H. Huang, B. Machura, *J. Chem. Crystallogr.* 42 (2012) 691.
- [29] P.K. Singh, D.N. Kumar, *Spectrochim. Acta A* 64 (2006) 853.

.....❧.....

**SYNTHESES AND SPECTRAL CHARACTERIZATION OF
COPPER(II) CHELATES OF TRIDENTATE AROYLHYDRAZONES**

Contents	6.1 Introduction
	6.2 Experimental
	6.3 Results and discussion
	References

6.1. Introduction

Copper's unique combination of beauty and usability together with its excellent corrosion resistance has made it one of our most widely used industrial and architectural metals. The use of copper is of such importance in our societies that its usage is often considered as a key indicator of various major economies. The physical properties of copper including malleability and workability, corrosion resistance and durability, high electrical and thermal conductivity and ability to alloy with other metals have made it an important metal to a number of diverse industries. Among the common oxidation states of copper (+1 and +2), Cu(II) complexes have been extensively studied. These complexes have tetrahedral, octahedral, square planar and trigonal bipyramidal geometries.

Coordination chemistry of copper has been studied extensively due to its occurrence in the active site of several enzymes and proteins. The biological functions of copper proteins/enzymes include electron transfer, dioxygen transport, oxygenation, oxidation, reduction and disproportionation [1-3]. Copper is essential to all living organisms as a trace dietary mineral because it is a key constituent of the respiratory enzyme complex, cytochrome c oxidase. In molluscs and crustacea copper is a constituent of the blood pigment hemocyanin. Copper compounds are used as bacteriostatic substances, fungicides and wood preservatives.

Aroylhydrazones with two or more donor groups are used as versatile ligands because they can coordinate to metal ions in various chelating modes and bridge two or more metal centers through the imine N atom, iminolate O atom and substituent donor groups. A wide variety of copper complexes of hydrazones have been reported because of their excellent biological applications and their uses in various fields. The coordination of copper by hydrazone ligands is an efficient way to design highly effective drug candidates [4,5]. The low value of the Cu(II)/Cu(I) redox potential in hydrazone complexes has been identified as a possible factor for their biological activity. They also have potential applications as antitubercular and antibacterial agents [6,7]. Krishnamoorthy and co-workers have shown that copper hydrazone complexes have better potential than other metal complexes in the conversion of DNA from supercoiled form to the nicked circular form [8]. The role of copper(I/II) and O₂ in the cytotoxic activity of several alkaloids such as tambjamine and prodigiosin has recently been recognized and explained by the ability of the latter to bind the metal ion [9,10]. Recently copper complexes of hydrazones are gaining prominence in medicinal chemistry due to its great chemotherapeutic

application [11]. There are numerous copper complexes of hydrazones which possess anticancer properties [12,13]. Therefore, copper complexes of hydrazones are one of the important candidates in metal based drugs research. They also act as catalyst for many reactions [14]. Recently Shi *et al.* have shown that copper complexes of hydrazones catalyze the aerobic oxidation of benzyl alcohol under solvent less and room temperature conditions [15]. N-Aroyl-N-salicylidene-hydrazine copper(II) complexes and their adducts with monodentate neutral Lewis bases have been studied for second order nonlinear optical properties. The use of square planar coordinating metals like Cu(II) should force the organic ligand in a planar conformation so as to maximize conjugation and increase the second order nonlinear optical property [16].

Keeping all these facts in mind, we have synthesized five copper(II) complexes of ONO donor aroylhydrazones.

6.2. Experimental

6.2.1. Materials

4-Benzyloxy-2-hydroxybenzaldehyde (Sigma-Aldrich), 5-bromo-2-hydroxy-3-methoxybenzaldehyde (Sigma-Aldrich) 4-diethylamino-2-hydroxybenzaldehyde (Sigma-Aldrich), nicotinic hydrazide (Sigma-Aldrich), 4-nitrobenzoic hydrazide (Sigma-Aldrich), copper(II) acetate monohydrate (Merck), pyridine (S.D. Fine) and 3-picoline (Sigma-Aldrich) were of Analar grade and were used as received. Solvents used were methanol and dimethylformamide.

6.2.2. Syntheses of hydrazones

The syntheses of hydrazones 4-benzyloxy-2-hydroxybenzaldehyde-4-nitrobenzoylhydrazone dimethylformamide monosolvate ($H_2L^1 \cdot C_3H_7NO$),

5-bromo-2-hydroxy-3-methoxybenzaldehyde nicotinoylhydrazone dihydrate methanol monosolvate ($\text{H}_2\text{L}^2 \cdot 2\text{H}_2\text{O} \cdot \text{CH}_3\text{OH}$) and 4-diethylamino-2-hydroxybenzaldehyde nicotinoylhydrazone monohydrate ($\text{H}_2\text{L}^3 \cdot \text{H}_2\text{O}$) have already discussed in Chapter 2.

6.2.3. Syntheses of Cu(II) complexes

6.2.3.1. $[(\text{CuL}^1)_2]$ (18)

This complex was synthesized by refluxing a methanolic solution of $\text{H}_2\text{L}^1 \cdot \text{C}_3\text{H}_7\text{NO}$ (0.464 g, 1 mmol) with a methanolic solution of copper(II) acetate monohydrate (0.199 g, 1 mmol) for 3 h. and cooled. The green colored complex separated was filtered, washed thoroughly with methanol followed by ether and dried over P_4O_{10} *in vacuo*.

$[(\text{CuL}^1)_2]$ (18): Yield: 72%, μ_{eff} (B.M.): 1.45, Elemental Anal. Found (Calcd.) (%): C: 55.11 (55.69); H: 3.74 (3.34); N: 8.93 (9.28).

6.2.3.2. $[\text{CuL}^1\text{pic}]$ (19)

This complex was prepared by refluxing 1:1:1 ratio of $\text{H}_2\text{L}^1 \cdot \text{C}_3\text{H}_7\text{NO}$ (0.464 g, 1 mmol), 3-picoline (0.093 g, 1 mmol) and copper(II) acetate monohydrate (0.199 g, 1 mmol) in methanolic medium for 3 h. The brown colored complex formed was filtered, washed with methanol followed by ether and dried over P_4O_{10} *in vacuo*.

$[\text{CuL}^1\text{pic}]$ (19): Yield: 72%, λ_{m} (DMF): 21 $\text{ohm}^{-1} \text{cm}^2 \text{mol}^{-1}$, μ_{eff} (B.M.): 1.81, Elemental Anal. Found (Calcd.) (%): C: 59.19 (59.39); H: 3.74 (4.06); N: 9.68 (10.26).

6.2.3.3. [CuL¹py] (20)

A hot solution of H₂L¹·C₃H₇NO (0.464 g, 1 mmol) in methanol was mixed with pyridine (0.079 g, 1 mmol). To this a methanolic solution of copper(II) acetate monohydrate (0.199 g, 1 mmol) was added and refluxed for 3 h. The brown colored product formed was filtered, washed with methanol followed by ether and dried over P₄O₁₀ *in vacuo*.

[CuL¹py] (20): Yield: 71%, λ_m (DMF): 18 ohm⁻¹ cm² mol⁻¹, μ_{eff} (B.M.): 1.79, Elemental Anal. Found (Calcd.) (%): C: 58.40 (58.70); H: 3.57 (3.79); N: 10.35 (10.53).

6.2.3.4. [(CuL²)₂]·2H₂O (21)

This complex was synthesized by refluxing a methanolic solution of H₂L²·2H₂O·CH₃OH (0.418 g, 1 mmol) with a methanolic solution of copper(II) acetate monohydrate (0.199 g, 1 mmol) for 3 h. The dark green colored complex formed was filtered, washed with methanol and dried over P₄O₁₀ *in vacuo*.

[(CuL²)₂]·2H₂O (21): Yield: 63%, μ_{eff} (B.M.): 1.34, Elemental Anal. Found (Calcd.) (%): C: 39.53 (39.13); H: 2.66 (2.81); N: 9.22 (9.78).

6.2.3.5. [(CuL³)₂] (22)

This complex was synthesized by refluxing a methanolic solution of H₂L³·H₂O (0.330 g, 1 mmol) with a methanolic solution of Cu(OAc)₂·H₂O (0.199 g, 1 mmol) for 3 h. The green colored product formed was filtered, washed with methanol followed by ether and dried over P₄O₁₀ *in vacuo*.

[(CuL³)₂] (22): Yield: 59%, μ_{eff} (B.M.): 1.32, Elemental Anal. Found (Calcd.) (%): C: 54.12 (54.61); H: 4.45 (4.85); N: 14.44 (14.98).

6.3. Results and discussion

The copper(II) complexes **18**, **21** and **22** were synthesized by refluxing methanolic solutions of the respective hydrazones and copper acetate monohydrate in 1:1 ratio. The complexes **19** and **20** were synthesized by refluxing the methanolic solutions of hydrazones, copper acetate monohydrate and heterocyclic bases in 1:1:1 ratio. Out of the five complexes prepared, **18**, **21** and **22** are binuclear, while the remaining two are mixed ligand metal chelates. The complexes **18**, **21** and **22** are green in color and are partially soluble in solvents like DMSO, DMF and CH₃CN while complexes **19** and **20** are brown in color and are soluble in solvents like DMSO and DMF. In all the complexes synthesized, the hydrazones are coordinated to the metal centre in the iminolic form and act as dideprotonated tridentate ligands. The synthesized compounds are characterized by the following physico-chemical methods. Attempts to grow single crystals suitable for crystal structure determination were unsuccessful.

6.3.1. Elemental analyses

Elemental (C, H, N) analyses of all the samples were carried out using a Vario EL III CHNS elemental analyzer at the SAIF, Kochi, India and the values are given in Section 6.2.3. The analytical data indicate that all the complexes are analytically pure.

6.3.2. Molar conductivity and magnetic susceptibility measurements

The molar conductivity values of 10⁻³ M DMF solutions of the metal complexes are in the 18-21 ohm⁻¹ cm² mol⁻¹ range, indicating the non-electrolytic nature of these complexes [17]. The observed values of magnetic moment for complexes (Section 6.2.3) are generally diagnostic of the

coordination geometry about the metal ion. The room temperature magnetic moments of the mononuclear complexes **19** and **20** in the polycrystalline state are in the 1.79-1.81 B.M. range which is very close to the spin only value of 1.73 B.M. for d^9 copper system. The copper(II) complexes **18**, **21** and **22** exhibit μ_{eff} values in the 1.32-1.45 B.M. range and this low magnetic moment may be attributed to considerable antiferromagnetic interaction between metal centres suggesting dimeric nature of these complexes [18,19].

6.3.3. Infrared spectra

The IR spectra provide valuable information regarding the coordination modes of hydrazones. The prominent infrared spectral data of the hydrazones and their Cu(II) complexes are given in Table 6.1. The characteristic IR bands of the complexes show significant changes when compared with those of the proligands and these changes in the characteristic vibrational frequencies of the ligands upon complexation provide evidence for the mode of their binding to the metal ion. IR spectra of some complexes are presented in Figs. 6.1-6.3.

The spectra of the proligands show $\nu(\text{C}=\text{N})$ bands in the 1603-1609 cm^{-1} region which are shifted to lower frequencies in the spectra of all the complexes (1600-1604 cm^{-1}) indicating the involvement of azomethine nitrogen in coordination to the metal ion. The $\nu(\text{C}=\text{O})$ and $\nu(\text{N}-\text{H})$ bands present in the IR spectra of hydrazones are absent in complexes but new band appears in the 1233-1339 cm^{-1} region due to $\nu(\text{C}-\text{O})$ stretching vibration, indicating that the deprotonated ligand is in the iminolate form in the complexes. The appearance of bands in the 1514-1534 cm^{-1} range in the complexes are due to the asymmetric stretching vibration of the newly formed

C=N bond as a result of the iminolization of the ligands. In the case of free hydrazones broad bands in the 3377-3505 cm^{-1} region are due to the stretching mode of phenolic O–H group. This band is found to be absent in all the complexes, indicating deprotonation of phenolic –OH and its coordination to the central metal ion. In complex **21**, a broad band at 3448 cm^{-1} is due to the presence of lattice water which is further confirmed from its thermogravimetric analysis. The bands due to heterocyclic bases are observed in the 724-1426 cm^{-1} range for complexes **19** and **20**. Assignment of the proposed coordination sites is further supported by the appearance of medium bands in the 462-495 cm^{-1} and 415-428 cm^{-1} regions which could be attributed to the stretching modes of the metal to ligand bonds, $\nu(\text{Cu-O})$ and $\nu(\text{Cu-N})$ respectively. Accordingly, the ligands act as tridentate chelating agent with azomethine nitrogen, phenolate and iminolate oxygen atoms as donor sites [20-22].

Table 6.1. The important IR frequencies (cm^{-1}) of hydrazones and their Cu(II) complexes

Compound	$\nu(\text{C=N})$	$\nu(\text{C=N})^a$	$\nu(\text{C=O})/$ $\nu(\text{C-O})$	$\nu(\text{N-H})$	$\nu(\text{Cu-O})$	$\nu(\text{Cu-N})$
$\text{H}_2\text{L}^1 \cdot \text{C}_3\text{H}_7\text{NO}$	1604	----	1661	3186	----	----
$[(\text{CuL}^1)_2]$ (18)	1601	1529	1339	----	464	427
$[\text{CuL}^1\text{pic}]$ (19)	1602	1525	1335	----	464	415
$[\text{CuL}^1\text{py}]$ (20)	1600	1524	1334	----	495	420
$\text{H}_2\text{L}^2 \cdot 2\text{H}_2\text{O} \cdot \text{CH}_3\text{OH}$	1609	----	1669	3067	----	----
$[(\text{CuL}^2)_2] \cdot 2\text{H}_2\text{O}$ (21)	1604	1534	1233	----	462	428
$\text{H}_2\text{L}^3 \cdot \text{H}_2\text{O}$	1603	----	1632	3075	----	----
$[(\text{CuL}^3)_2]$ (22)	1600	1514	1242	----	486	418

^aNewly formed C=N

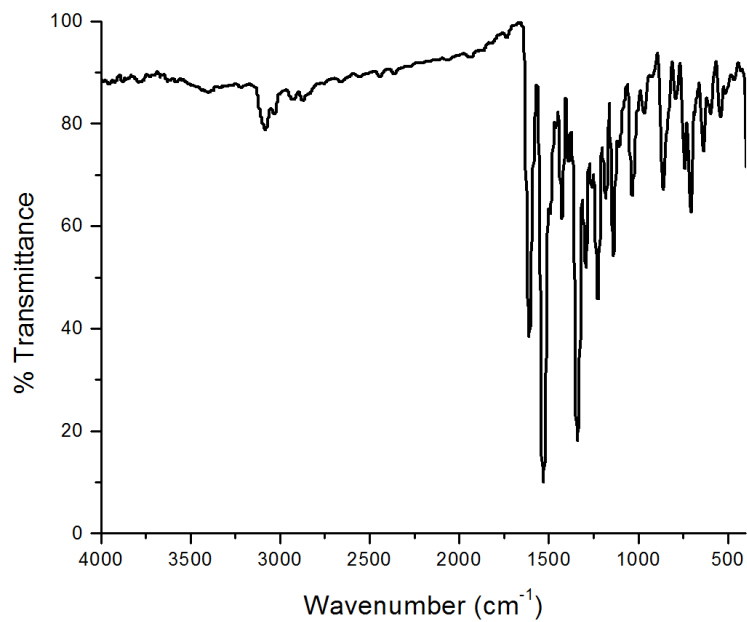


Fig. 6.1. IR spectrum of $[(CuL^1)_2]$ (18).

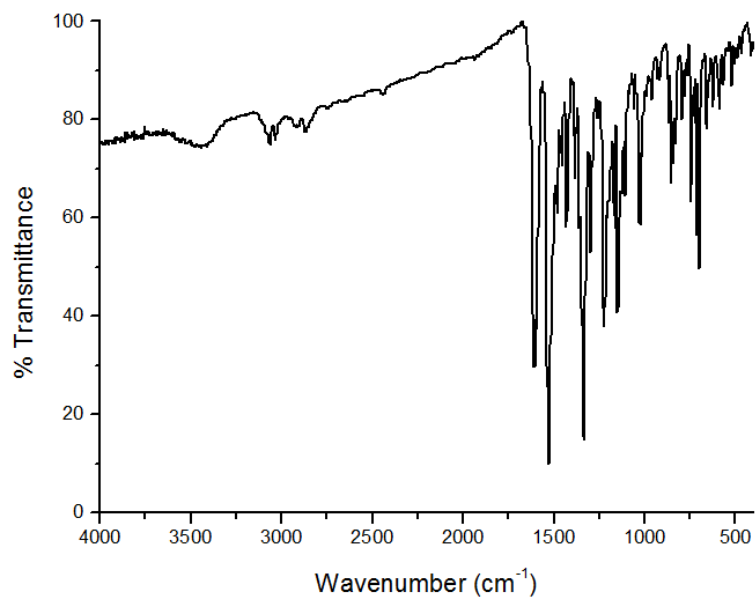


Fig. 6.2. IR spectrum of $[CuL^1pic]$ (19).

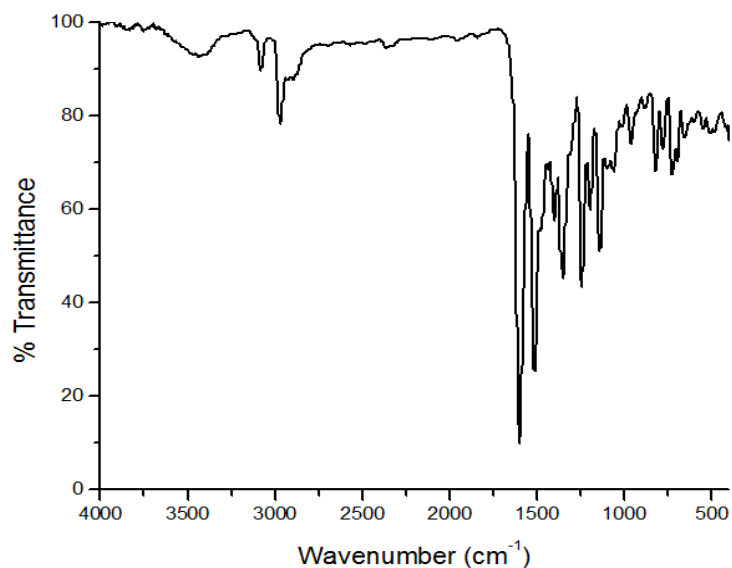


Fig. 6.3. IR spectrum of $[(\text{CuL}^3)_2]$ (**22**).

6.3.4. Electronic spectra

The electronic absorption spectra are often very helpful in the evaluation of results furnished by other methods of structural investigation. The electronic spectral measurements are used for assigning the stereochemistry of metal ions in the complexes based on the position and number of *d-d* transition peaks. The electronic spectra of the complexes **21** and **22** were taken in solid state and the rest in DMF. The electronic spectral data are presented in Table 6.2.

The intraligand transitions of complexes are assigned to bands in the 41340-26070 cm^{-1} range. It is observed that $n \rightarrow \pi^*$ and $\pi \rightarrow \pi^*$ transitions of hydrazones suffered a marginal shift up on complexation. The shift of the bands due to intraligand transitions is the result of the weakening of the C=N bond and extension of conjugation upon complexation. The shift is also due to coordination *via* phenolate and iminolate oxygen and is an indication of the

iminolization followed by the deprotonation of the ligands during complexation. The charge transfer bands are observed as intense bands in the 18210-23730 cm^{-1} region and the broadness of these bands is due to the combination of $\text{O} \rightarrow \text{Cu}$ and $\text{N} \rightarrow \text{Cu}$ LMCT transitions [23]. Electronic spectra of some complexes are presented in Figs. 6.4 and 6.5.

Copper(II) has the spectroscopic ground state term 2D which will be split by an octahedral field into two levels, $^2T_{2g}$ and 2E_g . However, in lower symmetry copper(II) complexes, the energy levels again split and more transitions will be observed. For square planar complexes with $d_{x^2-y^2}$ ground state, three transitions are possible viz., $d_{x^2-y^2} \rightarrow d_{xy}$, $d_{x^2-y^2} \rightarrow d_z^2$ and $d_{x^2-y^2} \rightarrow d_{xz}, d_{yz}$ ($^2B_{2g} \leftarrow ^2B_{1g}, ^2A_{1g} \leftarrow ^2B_{1g}$ and $^2E_g \leftarrow ^2B_{1g}$). Since the four d orbitals lie very close together, each transition cannot be distinguished by its energy and hence it is very difficult to resolve the three bands into separate components. The visible spectra of the complexes were recorded in DMF and exhibit $d-d$ bands in the 14060-19640 cm^{-1} range. However we could not locate any $d-d$ bands for $[(\text{CuL}^2)_2] \cdot 2\text{H}_2\text{O}$ (**21**), probably due to masking by the high intensity charge transfer bands [24,25].

Table 6.2. Electronic spectral assignments (cm^{-1}) of hydrazones and their Cu(II) complexes

Compound	$n \rightarrow \pi^* / \pi \rightarrow \pi^*$	LMCT	$d-d$
$\text{H}_2\text{L}^1 \cdot \text{C}_3\text{H}_7\text{NO}$	36990, 34130, 28970	----	----
$[(\text{CuL}^1)_2]$ (18)	36940, 30840	23730	19320
$[\text{CuL}^1\text{pic}]$ (19)	36140, 31330	23570	19640
$[\text{CuL}^1\text{py}]$ (20)	36290, 31030	23310	14090
$\text{H}_2\text{L}^2 \cdot 2\text{H}_2\text{O} \cdot \text{CH}_3\text{OH}$	33240, 29350	----	----
$[(\text{CuL}^2)_2] \cdot 2\text{H}_2\text{O}$ (21)	28950	22390	----
$\text{H}_2\text{L}^3 \cdot \text{H}_2\text{O}$	36780, 27020	----	----
$[(\text{CuL}^3)_2]$ (22)	41340, 26070	18210	14060

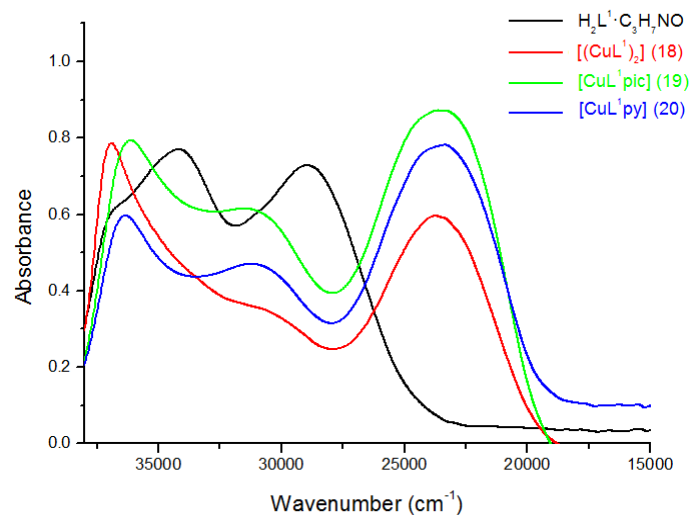


Fig. 6.4. UV spectra of $H_2L^1 \cdot C_3H_7NO$ and its Cu(II) complexes.

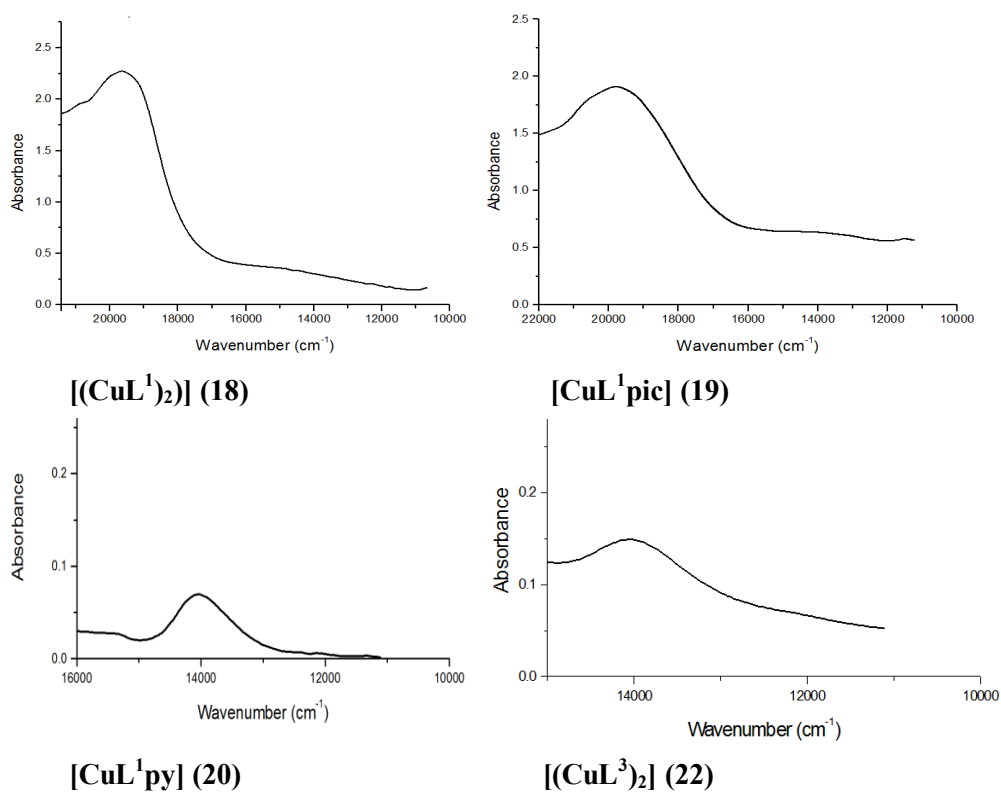


Fig. 6.5. Visible spectra of Cu(II) complexes.

6.3.5. Electron paramagnetic resonance spectra

Electron paramagnetic resonance is a branch of absorption spectroscopy in which radiation of microwave frequency is absorbed by a molecule or ion having unpaired electron(s). Thus it is a convenient and effective way to probe the electronic structure of paramagnetic molecules.

The copper(II) ion with a d^9 configuration has an effective spin of $S = 1/2$ and is associated with a spin angular momentum $m_s = \pm 1/2$ leading to a doubly degenerate spin state in the absence of magnetic field. In a magnetic field this degeneracy is lifted and the energy difference between these states is given by $\Delta E = h\nu = g\beta B$ where h is the Planck's constant, ν is the microwave frequency for transition from $m_s = +1/2$ to $m_s = -1/2$, g is the Lande splitting factor (equal to 2.0023 for a free electron), β is the Bohr magneton and B is the magnetic field strength. The copper(II) ion, with an effective spin of $S = 1/2$ couples with nuclear spin of ^{63}Cu ($I = 3/2$) and give rise to four ($2I+1 = 4$) hyperfine lines.

EPR spectroscopy plays an important role in determining the stereochemistry of copper complexes. For coordination geometries corresponding to an elongated octahedron, a square pyramid or square planar, the ground state is $d_{x^2-y^2}$. When the coordination around Cu(II) ion is a compressed octahedron or a trigonal bipyramid, the ground state is d_z^2 . EPR spectroscopy can distinguish the ground states $d_{x^2-y^2}$ and d_z^2 on the basis of the principal values of the g tensor in the anisotropic spectra [26]. For copper(II) in most environments, the ground state magnetism is essentially spin only and orbital motion is said to be quenched. The g factors are shifted from the free electron value of 2.0023 by spin-orbit coupling of the ground state to excited states [27].

The EPR spectra of complexes **18-22** in polycrystalline state at 298 K and in frozen DMF at 77 K were recorded in the X band using 100 kHz field modulation and 9.4 GHz microwave frequency; g factors were quoted relative to the standard marker TCNE ($g = 2.00277$). Some of the EPR spectra are simulated and the experimental (red) and simulated (blue) best fits are included [28].

In polycrystalline state at 298 K, $[(\text{CuL}^1)_2]$ (**18**) displays a typical axial spectrum with $g_{\parallel} = 2.197$ and $g_{\perp} = 2.052$ (Fig. 6.6). In polycrystalline state, since it is magnetically concentrated the anisotropy may be lost. Dilution of the solid isolates the electron spin of the given complex from that of another paramagnetic molecule.

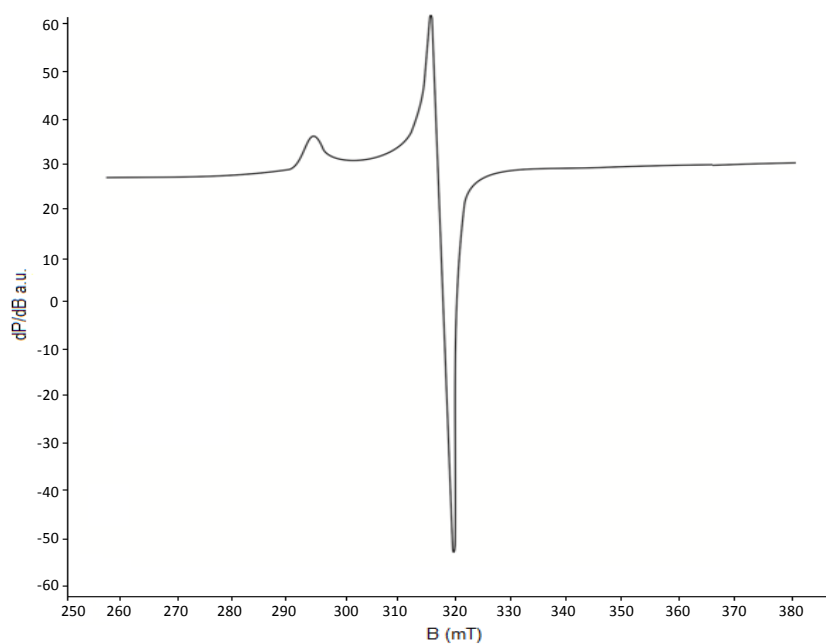


Fig. 6.6. EPR spectrum of $[(\text{CuL}^1)_2]$ (**18**) in polycrystalline state at 298 K.

In frozen DMF at 77 K, complex **18** displays a well resolved axial spectrum with four hyperfine lines in both the perpendicular and parallel regions ($g_{\parallel} = 2.225$, $g_{\perp} = 2.030$, $A_{\parallel} = 196 \times 10^{-4} \text{ cm}^{-1}$ and $A_{\perp} = 21 \times 10^{-4} \text{ cm}^{-1}$) and is presented in Fig. 6.7. The trend $g_{\parallel} > g_{\perp} > 2.0023$ is consistent with $d_{x^2-y^2}$ ground state in a square planar geometry [29]. But the expected superhyperfine splittings due to azomethine nitrogen are missing in this complex.

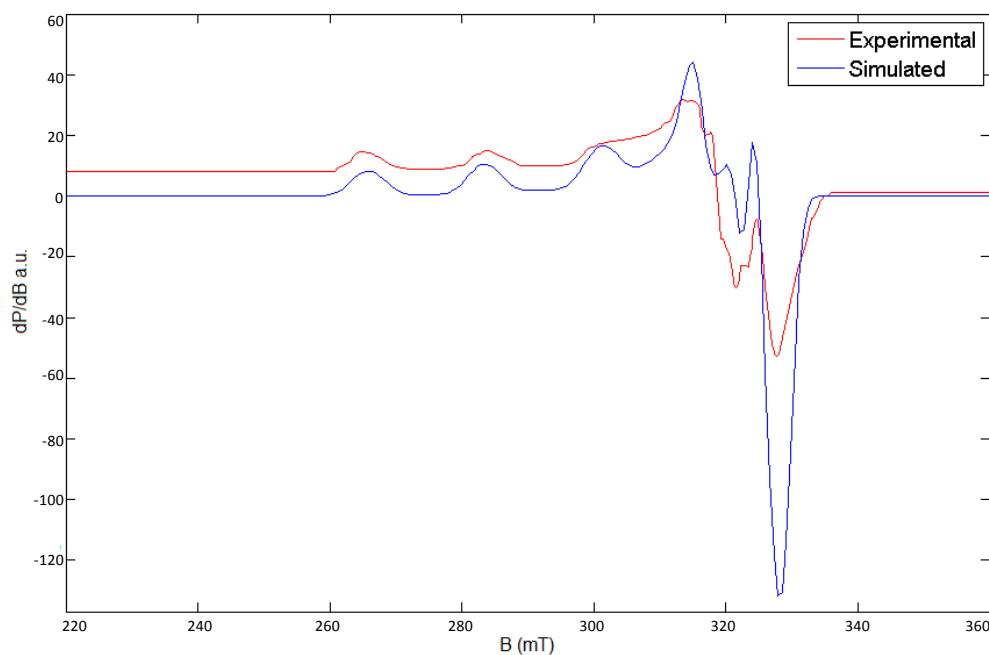


Fig. 6.7. EPR spectrum of $[(\text{CuL}^1)_2]$ (**18**) in DMF at 77 K.

The complex $[\text{CuL}^1\text{pic}]$ (**19**) exhibits an axial spectrum in the polycrystalline state at 298 K with $g_{\parallel} = 2.192$ and $g_{\perp} = 2.071$ (Fig. 6.8). In frozen DMF, it displays well-resolved axial anisotropy with four hyperfine splittings resulting from coupling of the electron spin with the spin of the ^{63}Cu

nucleus ($I = 3/2$) (Fig. 6.9). The pattern observed for g values, $g_{\parallel} > g_{\perp} > 2.0023$ ($g_{\parallel} = 2.210$, $g_{\perp} = 2.061$) suggests square planar geometry with unpaired electron in $d_{x^2-y^2}$ orbital.

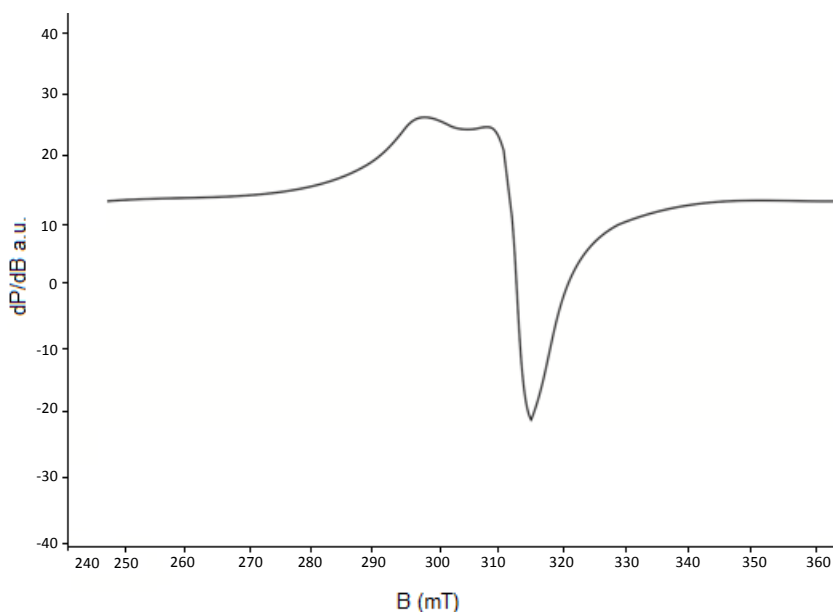


Fig. 6.8. EPR spectrum of $[\text{CuL}^1\text{pic}]$ (19) in polycrystalline state at 298 K.

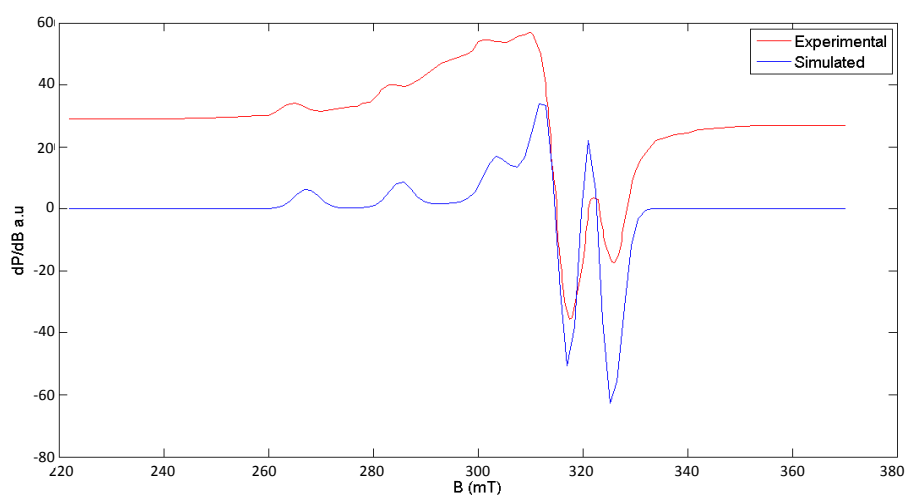


Fig. 6.9. EPR spectrum of $[\text{CuL}^1\text{pic}]$ (19) in DMF at 77 K.

The spectrum of [CuL¹py] (**20**) is axial in nature in polycrystalline state at 298 K (Fig. 6.10) with well defined g_{\parallel} and g_{\perp} features ($g_{\parallel} = 2.192$, $g_{\perp} = 2.054$). In DMF at 77 K, it shows well resolved axial spectrum ($g_{\parallel} = 2.210$, $g_{\perp} = 2.059$ and $A_{\parallel} = 206 \times 10^{-4} \text{ cm}^{-1}$) with four hyperfine lines in the parallel region (Fig. 6.11). Since $g_{\parallel} > g_{\perp} > 2.0023$, a square planar geometry can be assigned to this complex. The g_{\parallel} values are nearly the same for all the complexes indicating that the bonding is dominated by the hydrazone moiety rather than the heterocyclic base [30].

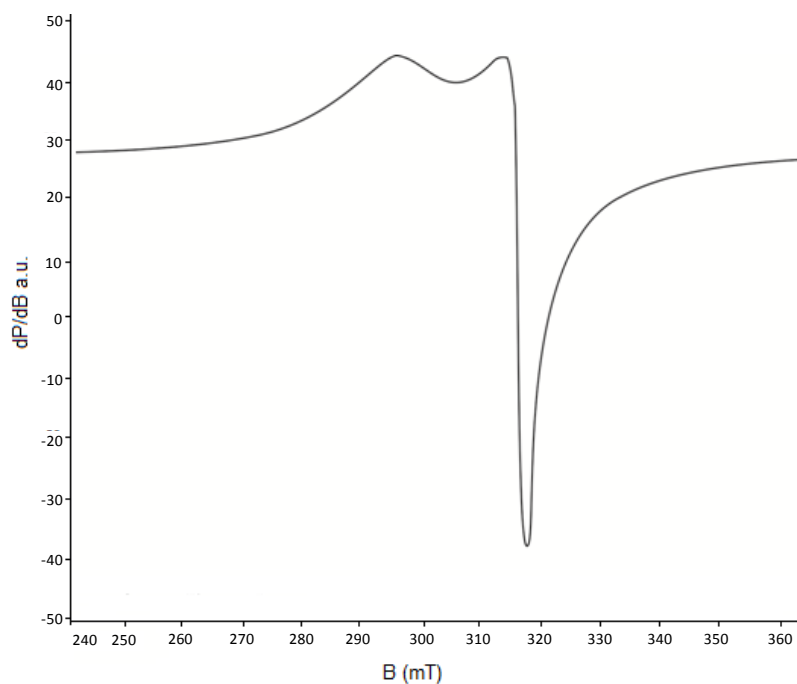


Fig. 6.10. EPR spectrum of [CuL¹py] (**20**) in polycrystalline state at 298 K.

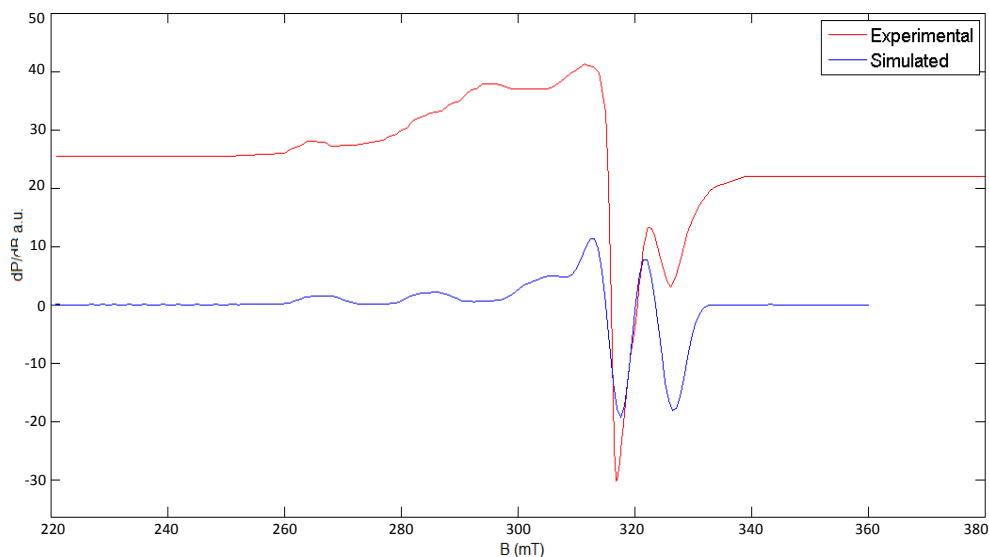


Fig. 6.11. EPR spectrum of [CuL¹py] (20) in DMF at 77 K.

The complex $[(\text{CuL}^2)_2] \cdot 2\text{H}_2\text{O}$ (**21**) exhibits an isotropic spectrum ($g_{\text{iso}} = 2.103$) in the polycrystalline state at 298 K (Fig. 6.12). Such isotropic spectrum consisting of only one broad signal and hence only one g value (g_{iso}) arises from extensive exchange coupling through misalignment of the local molecular axes between different molecules in the unit cell (dipolar broadening) and enhanced spin lattice relaxation. This type of spectra unfortunately give no information on the electronic ground state of copper(II) ion present in the complex. The complex **21** in frozen DMF at 77 K exhibits an axial spectrum with four hyperfine lines in the parallel region ($g_{\parallel} = 2.250$, $g_{\perp} = 2.063$, $A_{\parallel} = 201 \times 10^{-4} \text{ cm}^{-1}$) and in addition to this three superhyperfine signals are also observed (Fig. 6.13) which arise from the coupling of the electron spin with the nuclear spin of the azomethine nitrogen atom.

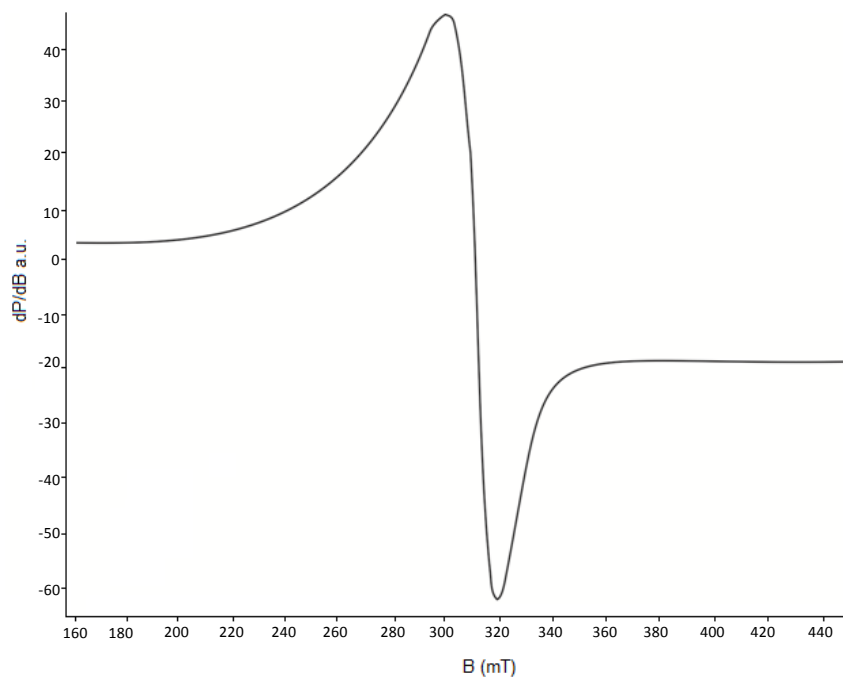


Fig. 6.12. EPR spectrum of $[(\text{CuL}^2)_2] \cdot 2\text{H}_2\text{O}$ (21) in polycrystalline state at 298 K.

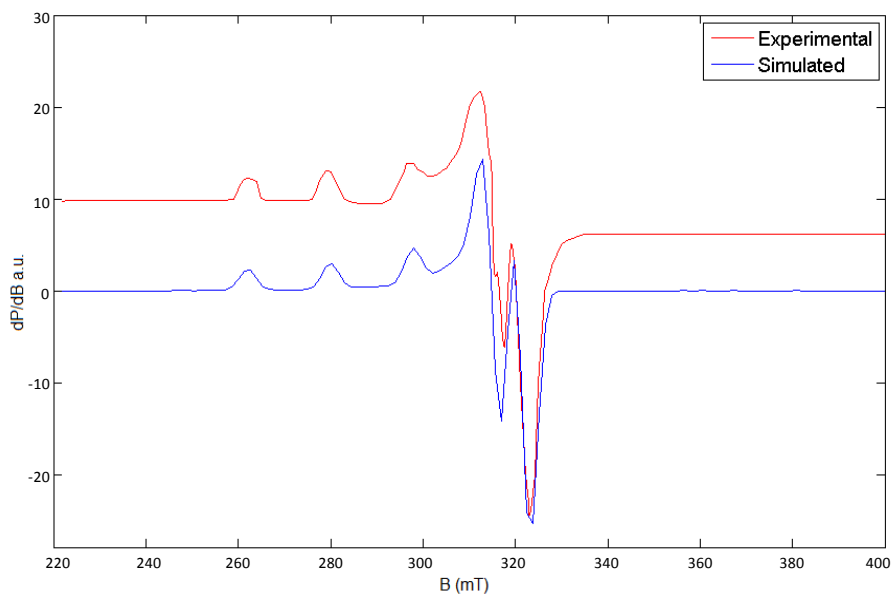


Fig. 6.13. EPR spectrum of $[(\text{CuL}^2)_2] \cdot 2\text{H}_2\text{O}$ (21) in DMF at 77 K.

In polycrystalline state at 298 K, the EPR spectrum of complex $[(\text{CuL}^3)_2]$ (**22**) is found to be axial in nature (Fig. 6.14) with $g_{\parallel} = 2.097$ and $g_{\perp} = 2.026$. In frozen DMF at 77 K, the complex **22** displays well-resolved axial anisotropy with four hyperfine splittings in the parallel region ($g_{\parallel} = 2.200$, $g_{\perp} = 2.060$, $A_{\parallel} = 190 \times 10^{-4} \text{ cm}^{-1}$) resulting from coupling of the electron spin with the spin of the ^{63}Cu nucleus ($I = 3/2$) (Fig. 6.15). The trend of g values $g_{\parallel} > g_{\perp} > 2.0023$ observed for the complex indicates that the unpaired electron most likely resides in the $d_{x^2-y^2}$ orbital which is consistent with proposed planar stereochemistry.

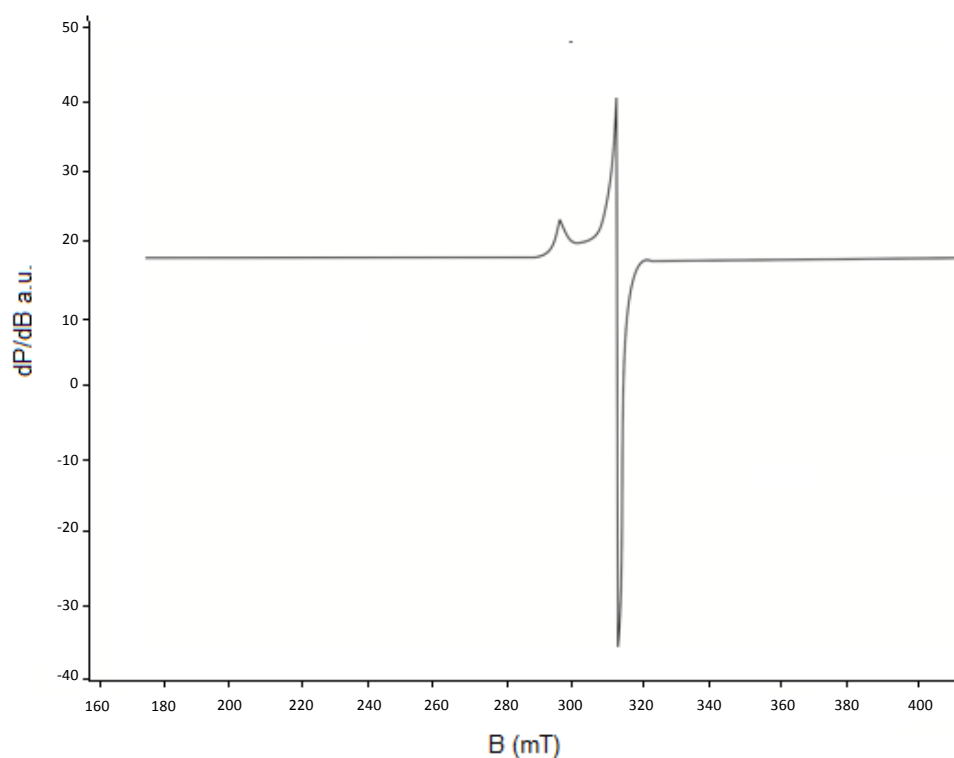


Fig. 6.14. EPR spectrum of $[(\text{CuL}^3)_2]$ (**22**) in polycrystalline state at 298 K.

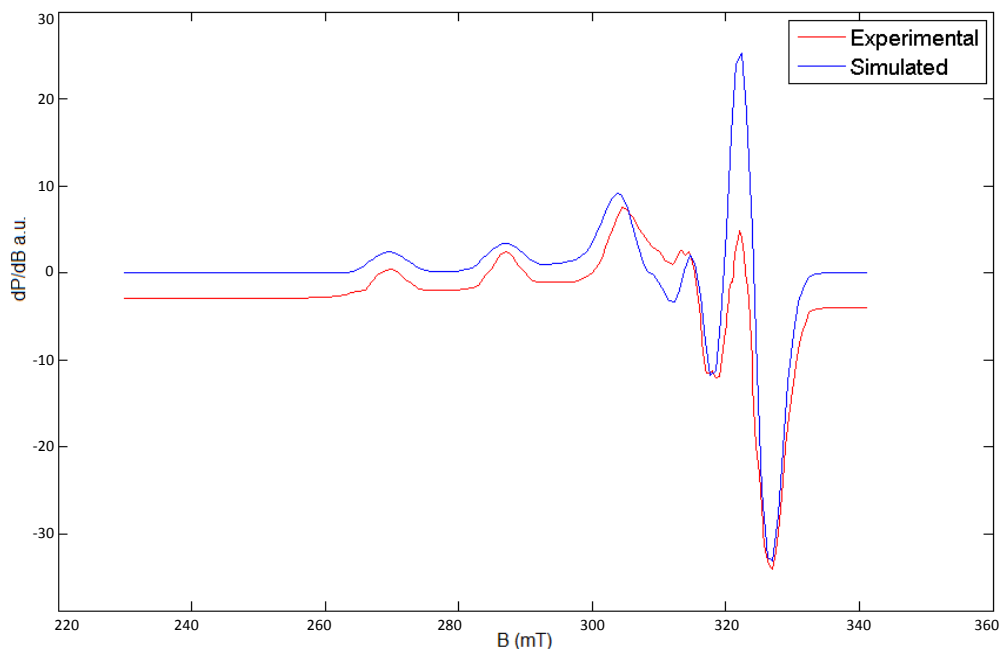


Fig. 6.15. EPR spectrum of $[(\text{CuL}^3)_2]$ (22) in DMF at 77 K.

All the complexes show well resolved axial spectra in frozen DMF at 77 K with $g_{\parallel} > g_{\perp} > 2.0023$ relationship consistent with $d_{x^2-y^2}$ ground state in a square planar geometry. The empirical factor, $f = g_{\parallel} / A_{\parallel}$ (cm^{-1}) is an index of tetragonal distortion and it may be vary from 105 to 135 for small to extreme distortion and that depends on the nature of the coordinated atoms. In all the complexes f falls in the 107-115 cm range corresponding to small to medium distortion from planarity [31,32]. The EPR spectral parameters of the copper(II) complexes are presented in the Table 6.3.

Table 6.3. EPR spectral parameters of copper(II) complexes in polycrystalline state at 298 K and in DMF at 77 K

Compound	Polycrystalline state (298 K)				DMF (77 K)								
	$g_{\text{iso}}/g_{\parallel}, g_{\perp}$	g_{\parallel}	g_{\perp}	g_{av}	A_{\parallel}^a	A_{\perp}^a	A_{av}^a	f	α^2	β^2	γ^2	K_{\parallel}	K_{\perp}
$[(\text{CuL})_2]$ (18)	2.197, 2.052	2.225	2.030	2.095	196	21	79	113	0.818	0.984	0.694	0.805	0.568
$[\text{CuL}^{\text{pic}}]$ (19)	2.192, 2.071	2.210	2.061	2.111	198	-	-	111	0.823	0.938	0.996	0.772	0.820
$[\text{CuL}^{\text{py}}]$ (20)	2.192, 2.054	2.210	2.059	2.109	206	29	88	107	0.844	0.786	0.822	0.664	0.694
$[(\text{CuL}^2)_2] \cdot 2\text{H}_2\text{O}$ (21)	2.103	2.250	2.063	2.125	201	-	-	111	0.872	-	-	-	-
$[(\text{CuL}^3)_2]$ (22)	2.097, 2.026	2.200	2.060	2.107	190	-	-	115	0.790	0.818	0.884	0.647	0.699

^a Expressed in units of cm^{-1} multiplied by a factor of 10^4

Kivelson and Neiman showed that for an ionic environment $g_{\parallel} \geq 2.3$ but for a covalent environment $g_{\parallel} < 2.3$. The fact that g_{\parallel} values are less than 2.3 for all the complexes is an indication of significant covalent bond in them. The higher g values observed in case of these complexes, when compared to the g value of a free electron, 2.0023, also indicate the covalent nature of the bond between the metal ion and the ligand. The g_{av} value of the complex **21** in solution state is consistent with the g_{iso} value suggesting that it is not undergoing any kind of dissociation in the solution state [33,34]. The EPR spectra of dimeric complexes **18**, **21** and **22** do not exhibit any half field signals typical for coupled binuclear complexes which may be due to the lack of enough intensity [35]. The geometric parameter G which is a measure of the exchange interaction between the copper centers in the polycrystalline state is calculated using the equation: $G = g_{\parallel} - 2.0023 / g_{\perp} - 2.0023$ for axial spectra. The G value in copper(II) complexes are less than 4.4 suggesting $d_{x^2-y^2}$ ground state with considerable exchange coupling [35,36].

The EPR parameters g_{\parallel} , g_{\perp} , A_{\parallel} and the energies of $d-d$ transitions are used to evaluate the bonding parameters α^2 , β^2 and γ^2 which may be regarded as measures of the covalency of the in-plane σ bonds, in-plane π bonds and out-of-plane π bonds respectively. The fraction of the unpaired electron density located on the copper ion i.e., value of in-plane σ -bonding parameter α^2 is estimated from the expression,

$$\alpha^2 = -A_{\parallel} / 0.036 + (g_{\parallel} - 2.0023) + 3/7(g_{\perp} - 2.0023) + 0.04$$

The orbital reduction factors, $K_{\parallel}^2 = \alpha^2\beta^2$ and $K_{\perp}^2 = \alpha^2\gamma^2$ are calculated using the following expressions

$$K_{\parallel}^2 = (g_{\parallel} - 2.0023) E_{d-d} / 8\lambda_o$$

$$K_{\perp}^2 = (g_{\perp} - 2.0023) E_{d-d} / 2\lambda_o$$

where λ_o represents the spin orbit coupling constant with a value of -828 cm^{-1} [37,38].

Hathaway has pointed out that for pure σ bonding, $K_{\parallel} \approx K_{\perp} \approx 0.77$, and for in-plane π bonding, $K_{\parallel} < K_{\perp}$, while for out-of-plane π bonding, $K_{\perp} < K_{\parallel}$ [39]. Here in compounds **19**, **20** and **22** it is observed that $K_{\parallel} < K_{\perp}$ which indicates the presence of significant in-plane π bonding. In complex **18**, $K_{\perp} < K_{\parallel}$, *i.e.*, out-of-plane π bonding is significant. The values of bonding parameters α^2 , β^2 and $\gamma^2 < 1.0$ (value of 1.0 for 100% ionic character) indicate that the metal-ligand bonds in the complexes under investigation are partially ionic and partially covalent in nature.

6.3.6. Thermogravimetric analysis

The thermogravimetric analysis was carried out within the temperature range from room temperature to $700 \text{ }^{\circ}\text{C}$. The main aim of the thermal analysis is to obtain information concerning the thermal stability of the complex, the number of water molecules present in the complex and to decide whether they are inside or outside the coordination sphere [40]. Thermogram of $[(\text{CuL}^2)_2] \cdot 2\text{H}_2\text{O}$ (**21**) shows a weight loss of 4.48% (calcd. 4.19%) due to the removal of two molecules of lattice water in the $61\text{-}120 \text{ }^{\circ}\text{C}$ range. Further degradation of the complex takes place between $218\text{-}420 \text{ }^{\circ}\text{C}$ with a weight loss of 42.68% (calcd.

42.28%) corresponds to the elimination of one of the hydrazone ligands. Beyond 490 °C a gradual weight loss occurs due to the thermal degradation of the remaining part of the complex and the decomposition is not completed up to 700 °C indicating strong ligand to metal bond.

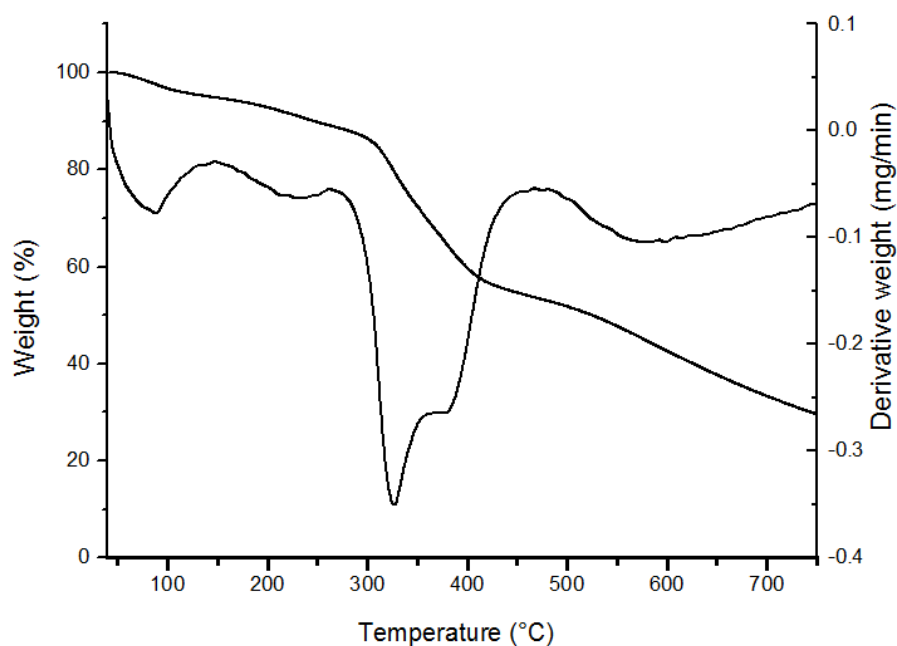
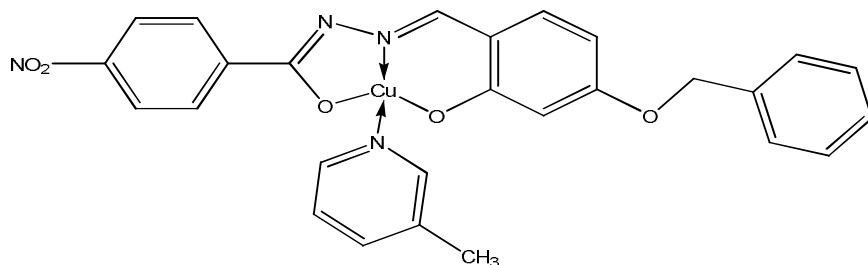
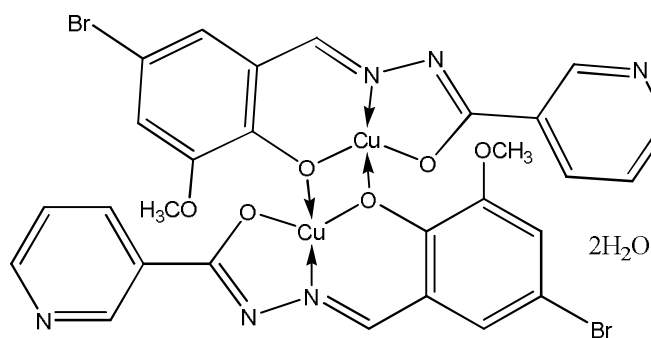


Fig. 6.16. Thermogram of $[(CuL^2)_2] \cdot 2H_2O$ (21).

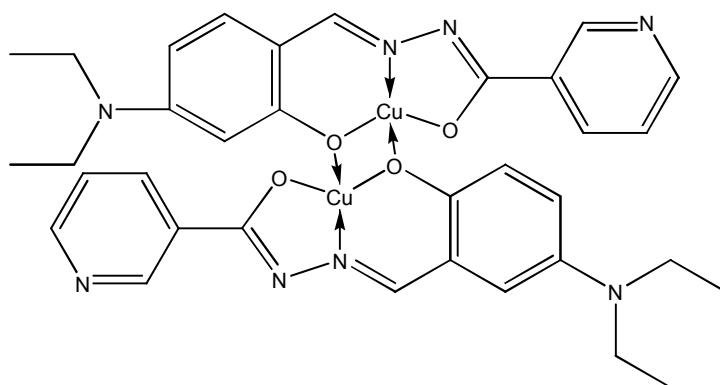
Thus, based on the above analytical and physico-chemical data, the proposed structures for some complexes are shown in Fig. 6.17. Out of the five complexes synthesized, complexes **18**, **21** and **22** are binuclear and the remaining two (**19** and **20**) are mononuclear mixed ligand metal chelates. EPR study suggests a distorted square-planar structure for these complexes.



[CuL¹pic] (19)



[(CuL²)₂]·2H₂O (21)



[(CuL³)₂] (22)

Fig. 6.17. Tentative structures of some of the Cu(II) complexes.

References

- [1] R.N. Mukherjee, *Indian J. Chem.* 42 (2003) 2175.
- [2] R.H. Holm, P. Kennepohl, E.I. Solomon, *Chem. Rev.* 96 (1996) 2239.
- [3] R.N. Mukherjee, *Comprehensive Coordination Chemistry II: From Biology to Nanotechnology* 5 (2003).
- [4] J. Patole, U. Sandbhor, S. Padhye, D.N. Deobagkar, C.E. Anson, A. Powell, *Bioorg. Med. Chem. Lett.* 13 (2003) 51.
- [5] S.T. Chew, K.M. Lo, S.K. Lee, M.P. Heng, W.Y. Teoh, K.S. Sim, K.W. Tan, *Eur. J. Med. Chem.* 76 (2014) 397.
- [6] M. Singh, N. Raghav, *Int. J. Pharm. Pharm. Sci.* 3 (2011) 26.
- [7] A. Jamadar, A.K.D. Klair, K. Vemuri, M. Sritharan, P. Dandawate, S. Padhye, *Dalton Trans.* 41 (2012) 9192.
- [8] P. Krishnamoorthy, P. Sathyadevi, A.H. Cowley, R.R. Butorac, N. Dharmaraj, *Eur. J. Med. Chem.* 46 (2011) 3376.
- [9] M.S. Melvin, J.T. Tomlinson, G.R. Saluta, G.L. Kucera, N. Lindquist, R.A. Manderville, *J. Am. Chem. Soc.* 122 (2000) 6333.
- [10] S.R. Hermida, C. Wende, A.B. Lago, R. Carballo, N. Kulak, E.M.V. Lopez, *Eur. J. Inorg. Chem.* 2013 (2013) 5843.
- [11] M. Alagesan, N.S.P. Bhuvanesh, N. Dharmaraj, *Dalton Trans.* 42 (2013) 7210.
- [12] D.S. Raja, E. Ramachandran, N.S.P. Bhuvanesh, K. Natarajan, *Eur. J. Med. Chem.* 64 (2013) 148.
- [13] D.S. Raja, N.S.P. Bhuvanesh, K. Natarajan, *Eur. J. Med. Chem.* 47 (2012) 73.
- [14] A. Mizar, M.F.C.G. Silva, M.N. Kopylovich, S. Mukherjee, K.T. Mahmudov, A.J.L. Pombeiro, *Eur. J. Inorg. Chem.* (2012) 2305.

- [15] H. Shi, Y. Yin, *Inorg. Chim. Acta* 421 (2014) 446.
- [16] F. Cariati, U. Caruso, R. Centore, W. Marcolli, A.D. Maria, B. Panunzi, A. Roviello, A. Tuzi, *Inorg. Chem.* 41 (2002) 6597.
- [17] P.K. Singh, D.N. Kumar, *Spectrochim. Acta* 64 (2006) 853.
- [18] S. Bootwala, M. Tariq, S. Somasundaran, K. Aruna, *Int. J. Pharm. Bio. Sci.* 3 (2013) 345.
- [19] D. Matoga, J. Szklarzewicz, R. Grybos, K. Kurpiewska, W. Nitek, *Inorg. Chem.* 50 (2011) 3501.
- [20] J. Chakraborty, S. Thakurta, G. Pilet, D. Luneau, S. Mitra, *Polyhedron* 28 (2009) 819.
- [21] D. Nagakavitha, K.H. Reddy, *Res. J. Pharm. Biol. Chem. Sci.* 5 (2014) 1806.
- [22] M.V. Angelusiu, S.F. Barbuceanu, C. Draghici, G.L. Almajan, *Eur. J. Med. Chem.* 45 (2010) 2055.
- [23] P.R. Chetana, M.N. Somashekar, B.S. Srinatha, R.S. Policegoudra, S.M. Aradhya, *Int. J. Pharm. Sci. Rev. Res.* 26 (2014) 284.
- [24] B. Jain, M. Verma, S. Malik, *Int. J. Pharm. Res. Sci.* 02 (2014) 155.
- [25] M.K. Prasanna, K.Pradeepkumar, *Int. J. Pharm. Biomed. Sci.* 4 (2013) 24.
- [26] E. Garribba, G. Micera, *J. Chem. Educ.* 83 (2006) 1229.
- [27] M. Valko, P. Pelikan, S. Biscupic, M. Mazur, *Chem. Papers* 44 (1990) 805.
- [28] S. Stoll, *Spectral Simulations in Solid-State Electron Paramagnetic Resonance*, Ph. D. thesis, ETH, Zurich, 2003.
- [29] N.A. Mangalam, S. Sivakumar, M.R.P. Kurup, E. Suresh, *Spectrochim. Acta* 75 (2010) 686.
- [30] L. Latheef, M.R.P. Kurup, *Spectrochim. Acta* 70 (2008) 86.

- [31] S.I. Findone, K.W.H. Stevens, Proc. Phys. Soc. 73 (1959) 116.
- [32] A. Diaz, R. Pogni, R. Cao, R. Basosi, Inorg. Chim. Acta 275 (1998) 552.
- [33] J.R. Wasson, C. Trapp, J. Phys. Chem. 73 (1969) 3763.
- [34] D. Kivelson, R. Neiman, J. Chem. Soc., Dalton Trans. 35 (1961) 149.
- [35] E. Manoj, M.R.P. Kurup, A. Punnoose, Spectrochim. Acta 72 (2009) 474.
- [36] B.J. Hathaway, D.E. Billing, Coord. Chem. Rev. 5 (1970) 143.
- [37] B.J. Hathaway, Structure and Bonding, Springer Verlag, Heidelberg (1973) 60.
- [38] U.L. Kala, S. Suma, S. Krishnan, M.R.P. Kurup, R.P. John, Polyhedron 26 (2007) 1427.
- [39] B.J. Hathaway, J. Chem. Soc. Dalton Trans. (1972) 1196.
- [40] O.M.I. Adly, Spectrochim. Acta 79 (2011) 1295.

..........

**SYNTHESES, SPECTRAL CHARACTERIZATION AND CRYSTAL
STRUCTURES OF ZINC(II) AND CADMIUM(II) CHELATES OF
TRIDENTATE AROYLHYDRAZONES**

Contents	7.1 Introduction
	7.2 Experimental
	7.3 Results and discussion
	References

7.1. Introduction

Zinc and its congener cadmium are different from the typical transition metals, which do not have partially filled *d* or *f* electron shells in the elemental or in its common oxidation states. Similar to zinc, cadmium prefers +2 oxidation state in most of its complexes (only very rare examples of +1 are known). Zinc and cadmium are two heavy metals naturally occurring in small amounts in soil. Zinc was named by the Swiss alchemist Theophrastus Bombastus von Hohenheim (1493-1541), who coined the new Latin word *zincum* from antecedents that are not clear. Cadmium was discovered in 1817 as an impurity in zinc by Stromeyer, who studied the deposits in lead and zinc furnaces called *cadmiaforncis* and accordingly the metal was called cadmium. Zinc is a bluish-white metal of moderate strength, hardness and ductility. Cadmium is a soft, malleable, ductile, bluish-white divalent metal.

As a micronutrient, zinc is an essential element to maintain metabolic functions of living organisms. Cadmium is a very toxic divalent heavy metal and is non-essential for plants. For a long time, cadmium was used in fluorescence microscopy, semiconductor and chemical battery although the toxicity of cadmium largely limits its potential applications. Zinc is the only metal known to be required for at least one enzyme in each of the major classes of enzymatic activities. Zinc can function as an active site of hydrolytic enzymes, where it is ligated by hard donors (N or O). It has long been recognized as an important co-factor in biological molecules, either as a structural template in protein folding or as a Lewis acid catalyst that can readily adopt the coordination numbers 4, 5 or 6 [1-3].

The chemical similarity of zinc(II) and cadmium(II) suggests that the latter may displace the former from the active site in enzymes containing zinc(II). Elements having similar physical and chemical characteristics, such as Cd and Zn, might have biologically antagonistic impact on each other: Zn inhibits Cd intake and accumulation in plants and prevents Cd toxicity [4]. Accordingly, Zn enhances antioxidant enzyme activities of zinc containing enzyme superoxide dismutase and competes Cd to bind –SH groups and membrane proteins of enzymes to protect plants against Cd toxicity [5]. Cadmium is a known carcinogen that inactivates the DNA mismatch repair pathway. Even though cadmium has been known as a toxic metal, the Cd(II) ion has recently been found to serve as the catalytic centre in a newly discovered carbonic anhydrase [6,7]. Cadmium can induce the synthesis of cadmium binding protein, in fact, the administration of cadmium and zinc to animals induce the synthesis of these proteins called metallothioneins, which play an important role in the metabolism of these elements [8].

The coordination chemistry of zinc and cadmium in both non-biological and biological areas has been the subject of intensive studies. Complexes of d^{10} metal ions, such as zinc(II) and cadmium(II) are of great interest because of their involvement in various biological processes [10-13]. Zn(II) and Cd(II) complexes have been very interesting in the context of their structural diversity and photophysical properties. Noncentrosymmetric compounds of zinc and cadmium are promising materials for optical second harmonic generation as they possess wide transparent window in the visible and near infrared regions [14,15]. Zn(II) and Cd(II) complexes have also attracted considerable interest due to potential applications of their fluorescence properties [16,17].

The varieties of possible metal complexes with wide choice of hydrazone ligands, and coordination environments, have prompted us to undertake research in this area. As a part of our continuing work on tridentate aroylhydrazones containing N and O donor atoms and in the light of the importance of Cd and Zn metals, we have synthesized and characterized five zinc(II) and five cadmium(II) complexes of the tridentate aroylhydrazones and studied the coordination behavior of hydrazones with these metals.

7.2. Experimental

7.2.1. Materials

4-Benzyloxy-2-hydroxybenzaldehyde (Sigma-Aldrich), 5-bromo-2-hydroxy-3-methoxybenzaldehyde (Sigma-Aldrich), 2-benzoylpyridine (Sigma-Aldrich), nicotinic hydrazide (Sigma-Aldrich), 4-nitrobenzoic hydrazide (Sigma-Aldrich), cadmium(II) acetate dihydrate (Merck), cadmium(II) bromide tetrahydrate (Sigma-Aldrich), zinc(II) acetate dihydrate (Sigma-Aldrich),

zinc(II) chloride (Sigma-Aldrich), pyridine (S.D.Fine) and 3-picoline (Sigma-Aldrich) were of Analar grade and were used as received. Solvents used were methanol, ethanol and DMF.

7.2.2. Syntheses of hydrazones

The syntheses of hydrazones 4-benzyloxy-2-hydroxybenzaldehyde-4-nitrobenzoylhydrazone dimethylformamide monosolvate ($H_2L^1 \cdot C_3H_7NO$), 5-bromo-2-hydroxy-3-methoxybenzaldehyde nicotinoylhydrazone dihydrate methanol monosolvate ($H_2L^2 \cdot 2H_2O \cdot CH_3OH$) and 2-benzoylpyridine-4-nitrobenzoylhydrazone (HL^4) have already discussed in Chapter 2.

7.2.3. Syntheses of Zn(II) complexes

7.2.3.1. $[(ZnL^1)_2]$ (23)

A methanolic solution of $H_2L^1 \cdot C_3H_7NO$ (0.464 g, 1 mmol) was treated with a methanolic solution of zinc(II) acetate dihydrate (0.218 g, 1 mmol). The solution was refluxed for 4 h. and the yellow colored complex separated out was collected, washed with methanol followed by ether and dried over P_4O_{10} *in vacuo*.

$[(ZnL^1)_2]$ (23): Yield: 57%, $\lambda_m(DMF)$: $9 \text{ ohm}^{-1} \text{ cm}^2 \text{ mol}^{-1}$, Elemental Anal. Found (Calcd.) (%): C: 55.00 (55.46); H: 3.45 (3.32); N: 9.37 (9.24).

7.2.3.2. $[ZnL^1 \text{pic}]$ (24)

To a hot methanolic solution of $H_2L^1 \cdot C_3H_7NO$ (0.464 g, 1 mmol), a methanolic solution of zinc(II) acetate dihydrate (0.218 g, 1 mmol) and 3-picoline (0.093 g, 1 mmol) were added. The mixture was refluxed for 4 h. and kept overnight for cooling. The yellow colored product formed was filtered, washed with methanol followed by ether and then dried over P_4O_{10} *in vacuo*.

[ZnL¹pic] (**24**): Yield: 55%, λ_m (DMF): 14 ohm⁻¹ cm² mol⁻¹, Elemental Anal. Found (Calcd.) (%): C: 59.37 (59.19); H: 4.43 (4.05); N: 10.45 (10.23).

7.2.3.3. [ZnL¹py] (**25**)

To a hot methanolic solution of H₂L¹·C₃H₇NO (0.464 g, 1 mmol), a methanolic solution of zinc(II) acetate dihydrate (0.218 g, 1 mmol) was added followed by pyridine (0.079 g, 1 mmol). The resulting solution was refluxed for 4 h. The yellow colored complex separated out was filtered, washed with methanol followed by ether and dried over P₄O₁₀ *in vacuo*.

[ZnL¹py] (**25**): Yield: 68%, Elemental Anal. Found (Calcd.) (%): C: 58.14 (58.49); H: 3.40 (3.78); N: 10.34 (10.49).

7.2.3.4. [(ZnL²)₂]·H₂O (**26**)

A methanolic solution of H₂L²·2H₂O·CH₃OH (0.418 g, 1 mmol) was treated with a methanolic solution of zinc(II) acetate dihydrate (0.218 g, 1 mmol). The solution was heated under reflux for 4 h. The yellow colored complex formed was filtered, washed with methanol followed by ether and dried over P₄O₁₀ *in vacuo*.

[(ZnL²)₂]·H₂O (**26**): Yield: 61%, λ_m (DMF): 15 ohm⁻¹ cm² mol⁻¹, Elemental Anal. Found (Calcd.) (%): C: 39.46 (39.79); H: 2.93 (2.62); N: 10.10 (9.94).

7.2.3.5. [Zn(L⁴)₂]·0.5CH₃OH·0.5CH₃CH₂OH (**27**)

Methanolic solutions of HL⁴ (0.346 g, 1 mmol) and ZnCl₂ (0.136 g, 1 mmol) were mixed and the reaction mixture was refluxed for 4 h. The resulting solution was allowed to evaporate at room temperature and the yellow precipitate obtained was filtered, washed with methanol, followed by ether and

dried over P_4O_{10} *in vacuo*. Single crystals of the complex suitable for X-ray diffraction were obtained by recrystallization from a mixture of ethanol and methanol (1:1 v/v).

$[Zn(L^4)]_2 \cdot 0.5CH_3OH \cdot 0.5CH_3CH_2OH$ (**27**): Yield: 67%, λ_m (DMF): 13 $ohm^{-1} cm^2 mol^{-1}$, Elemental Anal. Found (Calcd.) (%): C: 60.05 (59.67); H: 3.76 (3.93); N: 14.49 (14.09).

7.2.4. Syntheses of Cd(II) complexes

7.2.4.1. $[CdL^1(H_2O)]_2$ (**28**)

Methanolic solutions of $H_2L^1 \cdot C_3H_7NO$ (0.464 g, 1 mmol) and $Cd(CH_3COO)_2 \cdot 2H_2O$ (0.266 g, 1 mmol) were mixed and heated under reflux for 4 h. The product formed was yellow colored and it was filtered, washed with methanol followed by ether and dried over P_4O_{10} *in vacuo*.

$[CdL^1(H_2O)]_2$ (**28**): Yield: 61%, Elemental Anal. Found (Calcd.) (%): C: 49.02 (48.52); H: 3.17 (3.30); N: 8.54 (8.08).

7.2.4.2. $[CdL^1pic]$ (**29**)

This complex was synthesized by refluxing hot methanolic solutions of $H_2L^1 \cdot C_3H_7NO$ (0.464 g, 1 mmol), $Cd(CH_3COO)_2 \cdot 2H_2O$ (0.266 g, 1 mmol) and 3-picoline (0.093 g, 1 mmol) for 4 h. The yellow colored product formed was filtered, washed with methanol followed by ether and dried over P_4O_{10} *in vacuo*.

$[CdL^1pic]$ (**29**): Yield: 59%, Elemental Anal. Found (Calcd.) (%): C: 55.01 (54.51); H: 4.23 (3.73); N: 8.98 (9.42).

7.2.4.3. [CdL¹py] (30)

This complex was synthesized by refluxing hot methanolic solutions of H₂L¹·C₃H₇NO (0.464 g, 1 mmol), Cd(CH₃COO)₂·2H₂O (0.266 g, 1 mmol) and pyridine (0.079 g, 1 mmol) for 4 h. On slow evaporation, yellow colored solid formed was separated, washed with methanol followed by ether and dried over P₄O₁₀ *in vacuo*.

[CdL¹py] (30): Yield: 62%, Elemental Anal. Found (Calcd.) (%): C: 53.25 (53.76); H: 3.82 (3.47); N: 9.45 (9.65).

7.2.4.4. [(CdL²)₂]·H₂O (31)

A solution of H₂L²·2H₂O·CH₃OH (0.418 g, 1 mmol) in methanol was mixed with a methanolic solution of cadmium(II) acetate dihydrate (0.266 g, 1 mmol) and the mixture was heated under reflux for 4 h. and cooled. The yellow colored complex formed was filtered, washed with methanol followed by ether and dried over P₄O₁₀ *in vacuo*.

[(CdL²)₂]·H₂O (31): Yield: 67%, λ_m(DMF): 10 ohm⁻¹ cm² mol⁻¹, Elemental Anal. Found (Calcd.) (%): C:36.02 (35.81); H: 2.45 (2.36); N: 8.68 (8.95).

7.2.4.5. [Cd(HL⁴)Br₂]·C₃H₇NO (32)

Methanolic solutions of HL⁴ (0.346 g, 1 mmol) and CdBr₂·4H₂O (0.344 g, 1 mmol) were mixed and heated under reflux for 4 h. It was allowed to stand at room temperature and upon slow evaporation the light yellow colored crystalline product separated out was filtered, washed with methanol followed by ether and dried over P₄O₁₀ *in vacuo*. Single crystals of the complex suitable for X-ray diffraction were obtained by recrystallization from a mixture of methanol and DMF (1:1 v/v).

$[\text{Cd}(\text{HL}^4)\text{Br}_2] \cdot \text{C}_3\text{H}_7\text{NO}$ (**32**): Yield: 75%, $\lambda_m(\text{DMF})$: $18 \text{ ohm}^{-1} \text{ cm}^2 \text{ mol}^{-1}$, Elemental Anal. Found (Calcd.) (%): C: 38.27 (38.20); H: 2.88 (3.06); 10.39 (10.13).

7.3. Results and discussion

The complexes **23**, **26**, **27**, **28**, **31** and **32** were prepared by refluxing the hydrazones and the corresponding metal(II) salts in 1:1 ratio, while the complexes **24**, **25**, **29** and **30** were prepared by refluxing corresponding hydrazones, metal salts and heterocyclic bases in 1:1:1 ratio. Complexes **25**, **28**, **29** and **30** are partially soluble in solvents like DMSO and DMF, while others are completely soluble in these solvents. In complex **32**, hydrazone coordinates in the neutral amido form while in others they are in the iminolate form. Single crystals of compounds **27** and **32** could be isolated and the structures were established by single crystal XRD studies. The complexes were characterized by the following physico-chemical methods.

7.3.1. Elemental analyses

Elemental analyses data (C, H, N) of all complexes are given in Section 7.2.3-7.2.4. The observed C, H, N values show that all the complexes are analytically pure and are consistent with the stoichiometry of the formula given in Section 7.2.3 and 7.2.4.

7.3.2. Molar conductivity measurements

The synthesized complexes $[\text{ZnL}^1\text{py}]$ (**25**), $[\text{CdL}^1(\text{H}_2\text{O})_2]$ (**28**), $[\text{CdL}^1\text{pic}]$ (**29**) and $[\text{CdL}^1\text{py}]$ (**30**) are partially soluble in most of the common solvents like DMSO, DMF, ethanol, methanol etc. and therefore, conductance measurements of these complexes were not carried out. The molar

conductivities of the soluble complexes **23**, **24**, **26**, **27**, **31** and **32** in DMF (10^{-3} M) were measured at 298 K with a Systronic model 303 direct reading conductivity bridge. The molar conductance values of these complexes lie in the 4-18 $\text{ohm}^{-1} \text{cm}^2 \text{mol}^{-1}$ range which is much less than the value of 65-90 $\text{ohm}^{-1} \text{cm}^2 \text{mol}^{-1}$ obtained for a 1:1 electrolyte in the same solvent. These low values indicate their non-electrolytic nature as expected [18].

7.3.3. Infrared spectra

The comparison of the IR spectra of the complexes with that of the parent aroylhydrazones helps to establish the mode of coordination of the ligands to the metal center. The tentative infrared spectral assignments of the complexes are listed in Table 7.1. In principle, the hydrazone can exhibit amido-iminol tautomerism since it contains $-\text{NH}-\text{C}=\text{O}$ functional group. In all the complexes synthesized for our present study, except in complex **32**, the hydrazone coordinates in the iminolate form, while in complex **32**, it is in the amido form. The $\nu(\text{C}=\text{O})$ bands observed in the 1632-1683 cm^{-1} region in the infrared spectra of the free hydrazones disappear in those of the complexes, except in **32**, but new bands appear in the 1210-1313 cm^{-1} region probably due to $\nu(\text{C}-\text{O})$ stretching, suggesting the iminolization followed by deprotonation of hydrazones and chelation of iminolate oxygen with the metal ion. Correspondingly $\nu(\text{N}-\text{H})$ bands disappear and new $\nu(\text{C}=\text{N})$ bands are appeared in the 1515-1534 cm^{-1} region, due to the stretching frequency of the newly formed $\text{C}=\text{N}$ group which results by the iminolization of the ligands, except in complex **32** [19]. In complex **32**, $\nu(\text{C}=\text{O})$ band is shifted to lower frequency by 4 cm^{-1} indicating coordination through the carbonyl oxygen and suggesting the existence of ligand in the amido form [20]. The stretching frequencies of the azomethine ($\text{C}=\text{N}$) group of the free hydrazones observed in the 1597-1609 cm^{-1}

region are shifted to 1593-1606 cm^{-1} region in complexes, in agreement with coordination of the azomethine nitrogen in their complexes. The bands at 3488 and 3505 cm^{-1} ascribed to phenolic $-\text{OH}$ group for H_2L^1 and H_2L^2 respectively have disappeared, giving evidence for deprotonation of phenolic $-\text{OH}$ and its coordination to the central metal ion. The ligand coordination to the metal center is substantiated by bands in the 480-565 cm^{-1} and 412-480 cm^{-1} regions, attributable to stretching modes of the metal to ligand bonds, $\nu(\text{M}-\text{O})$ and $\nu(\text{M}-\text{N})$ respectively. For the complexes **24**, **25**, **27**, **29**, **30** and **32** the bands in the 753-1462 cm^{-1} region are assigned to coordinated pyridine ring. The complexes **26**, **28** and **31** also show broad bands centered at 3437, 3430 and 3420 cm^{-1} respectively due to the presence of water molecules in these complexes [19-22]. IR spectra of some complexes are presented in Figs. 7.1-7.5.

Table 7.1. The important IR frequencies (cm^{-1}) of Zn(II) and Cd(II) complexes of hydrazones

Compound	$\nu(\text{C}=\text{N})$	$\nu(\text{C}=\text{N})^a$	$\nu(\text{C}=\text{O})/\nu(\text{C}-\text{O})$	$\nu(\text{M}-\text{O})$	$\nu(\text{M}-\text{N})$
$[(\text{ZnL}^1)_2]$ (23)	1599	1534	1218	530	431
$[\text{ZnL}^1\text{pic}]$ (24)	1601	1525	1210	502	469
$[\text{ZnL}^1\text{py}]$ (25)	1600	1529	1217	480	417
$[(\text{ZnL}^2)_2]\cdot\text{H}_2\text{O}$ (26)	1606	1515	1225	565	445
$[\text{Zn}(\text{L}^4)_2]\cdot 0.5\text{CH}_3\text{OH}\cdot 0.5\text{CH}_3\text{CH}_2\text{OH}$ (27)	1594	1519	1313	513	412
$[\text{CdL}^1(\text{H}_2\text{O})_2]$ (28)	1597	1533	1217	512	466
$[\text{CdL}^1\text{pic}]$ (29)	1600	1530	1220	511	466
$[\text{CdL}^1\text{py}]$ (30)	1593	1534	1216	513	468
$[(\text{CdL}^2)_2]\cdot\text{H}_2\text{O}$ (31)	1600	1522	1239	537	480
$[\text{Cd}(\text{HL}^4)\text{Br}_2]\cdot\text{C}_3\text{H}_7\text{NO}$ (32)	1593	----	1673	521	416

^a Newly formed C=N

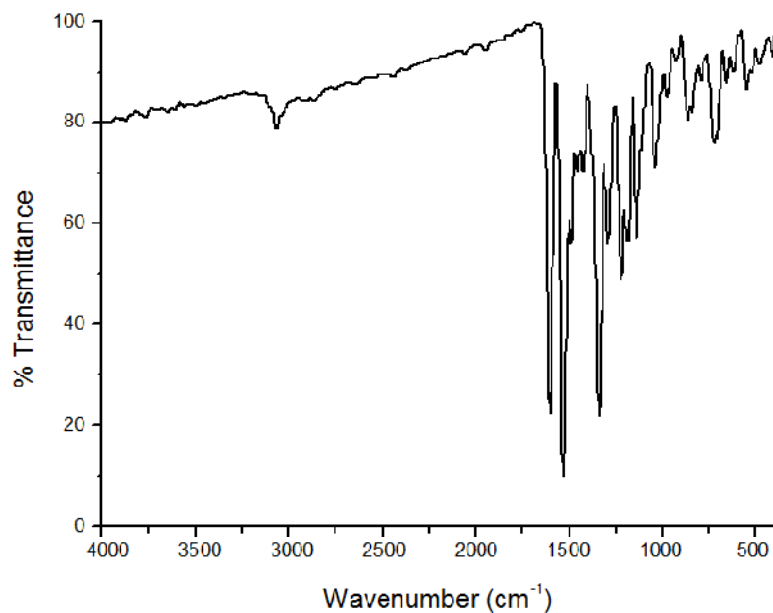


Fig. 7.1. IR spectrum of [ZnL¹pic] (24) .

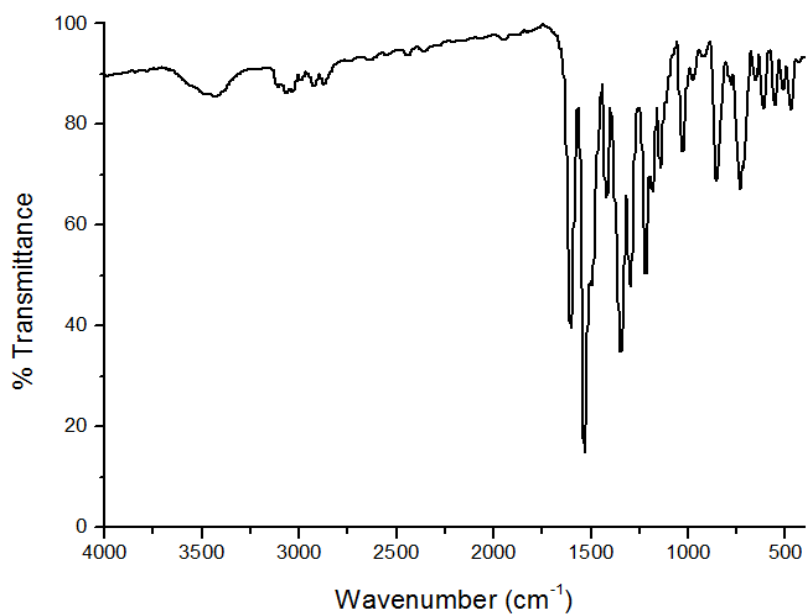


Fig. 7.2. IR spectrum of [ZnL¹py] (25).

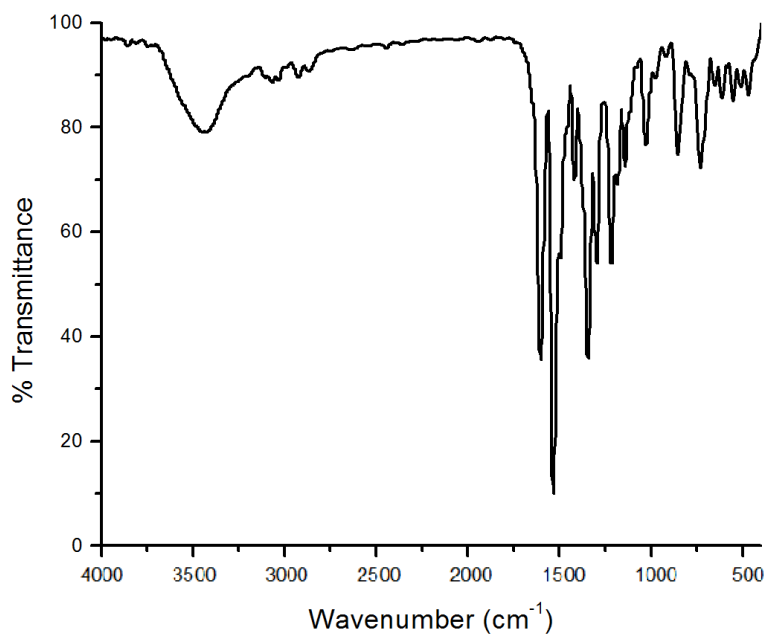


Fig. 7.3. IR spectrum of $[\text{CdL}^1(\text{H}_2\text{O})]_2$ (28).

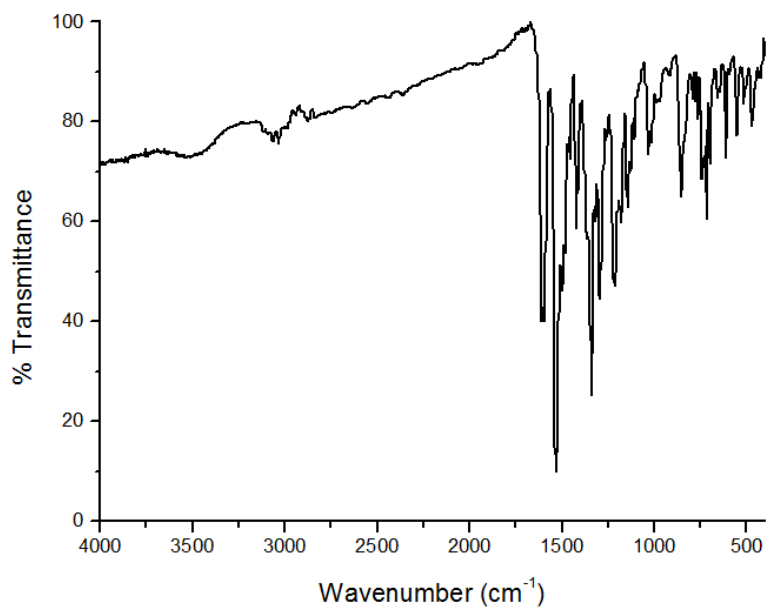


Fig. 7.4. IR spectrum of $[\text{CdL}^1\text{py}]$ (30).

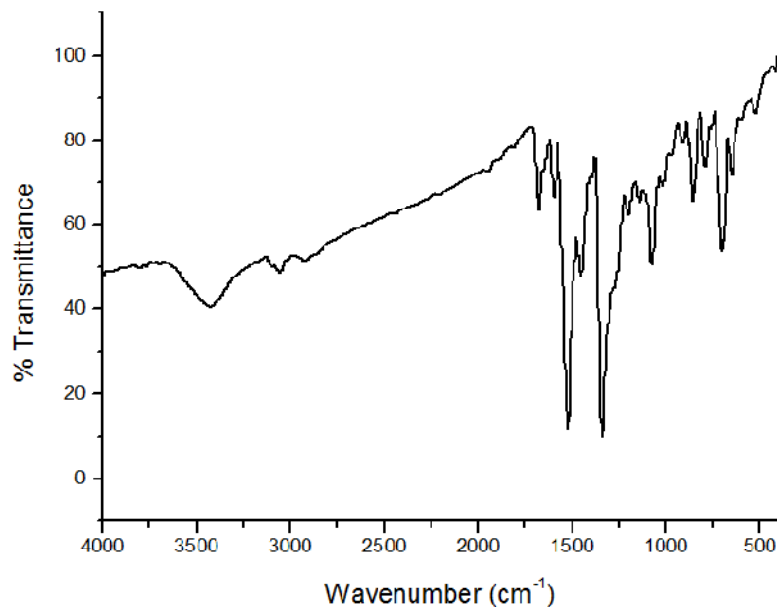


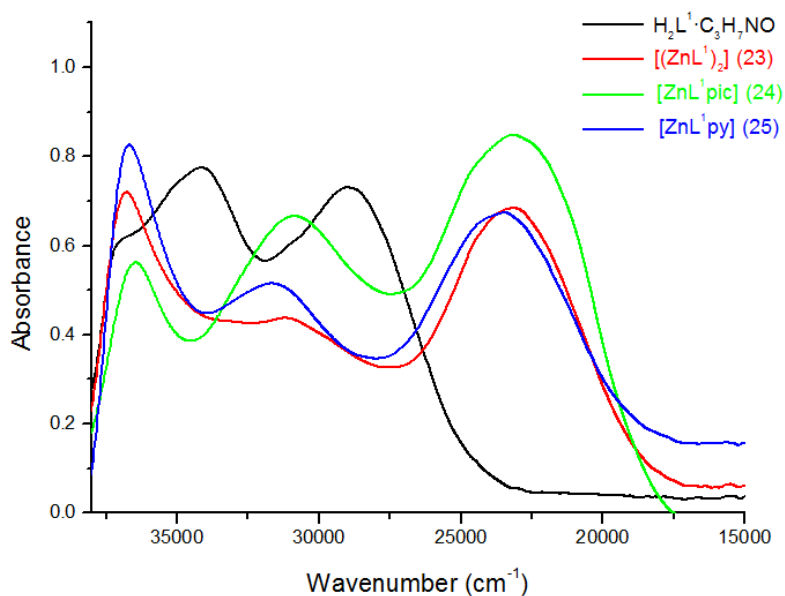
Fig. 7.5. IR spectrum of $[\text{Cd}(\text{HL}^4)\text{Br}_2]\cdot\text{C}_3\text{H}_7\text{NO}$ (32).

7.3.4. Electronic spectra

The electronic spectra of the Zn(II) and Cd(II) complexes were recorded in DMF and spectral data are given in Table 7.2. Electronic spectra of some of the complexes are presented in Figs.7.6-7.9. The absorption bands due to $n\rightarrow\pi^*$ and $\pi\rightarrow\pi^*$ transitions of free hydrazones suffered considerable shift upon complexation. This is due to the weakening of the C=O bond and the extension of conjugation upon complexation. This may also be due to the involvement of phenolate oxygen atom and azomethine nitrogen atom in coordination. The new bands observed for complexes in the 22060-24820 cm^{-1} region can be assigned to the metal to ligand charge transfer transitions. No appreciable absorptions occurred below 20000 cm^{-1} indicating the absence of $d-d$ bands which is in accordance with d^{10} configuration of Zn(II) and Cd(II) ions [23,24].

Table 7.2. Electronic spectral assignments (cm^{-1}) of Zn(II) and Cd(II) complexes of hydrazones

Compound	$n \rightarrow \pi^*/\pi \rightarrow \pi^*$	MLCT
$[(\text{ZnL}^1)_2]$ (23)	36780, 31250	23210
$[\text{ZnL}^1\text{pic}]$ (24)	36450, 30930	23110
$[\text{ZnL}^1\text{py}]$ (25)	36660, 31630	23470
$[(\text{ZnL}^2)_2] \cdot \text{H}_2\text{O}$ (26)	36540, 31590	24400
$[\text{Zn}(\text{L}^4)] \cdot 0.5\text{CH}_3\text{OH} \cdot 0.5\text{CH}_3\text{CH}_2\text{OH}$ (27)	36480	24820
$[\text{CdL}^1(\text{H}_2\text{O})_2]$ (28)	36830, 29310	22500
$[\text{CdL}^1\text{pic}]$ (29)	36430, 29480	22060
$[\text{CdL}^1\text{py}]$ (30)	36340, 30360	22540
$[(\text{CdL}^2)_2] \cdot \text{H}_2\text{O}$ (31)	36570, 32980	24820
$[\text{Cd}(\text{HL}^4)\text{Br}_2] \cdot \text{C}_3\text{H}_7\text{NO}$ (32)	36400	24640

**Fig. 7.6. Electronic spectra of $\text{H}_2\text{L}^1 \cdot \text{C}_3\text{H}_7\text{NO}$ and its Zn(II) complexes.**

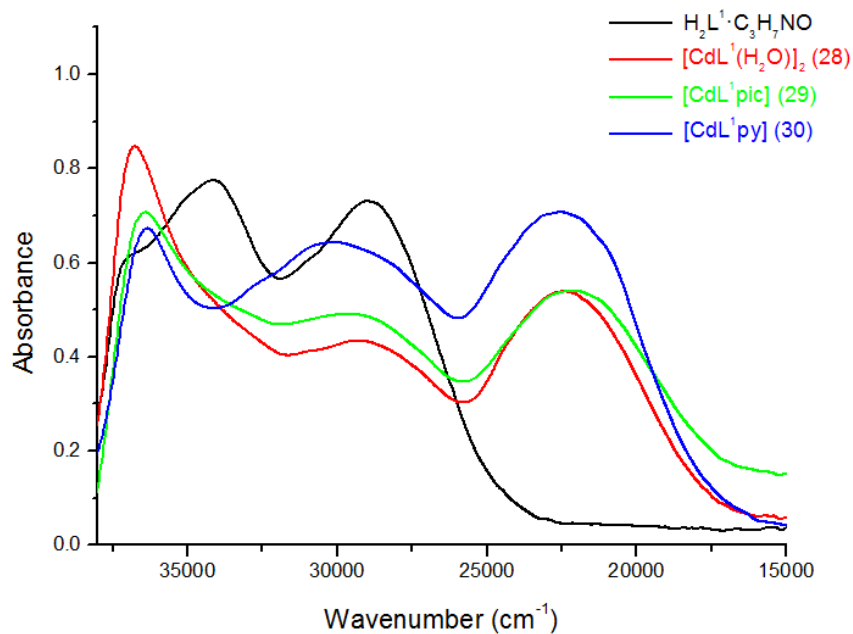


Fig. 7.7. Electronic spectra of $H_2L^1 \cdot C_3H_7NO$ and its Cd(II) complexes.

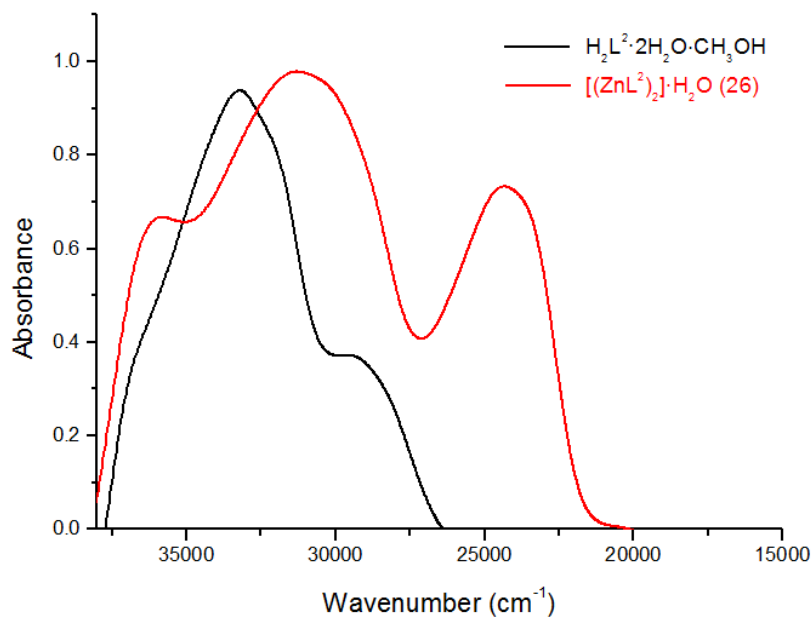


Fig. 7.8. Electronic spectra of $H_2L^2 \cdot 2H_2O \cdot CH_3OH$ and its Zn(II) complex.

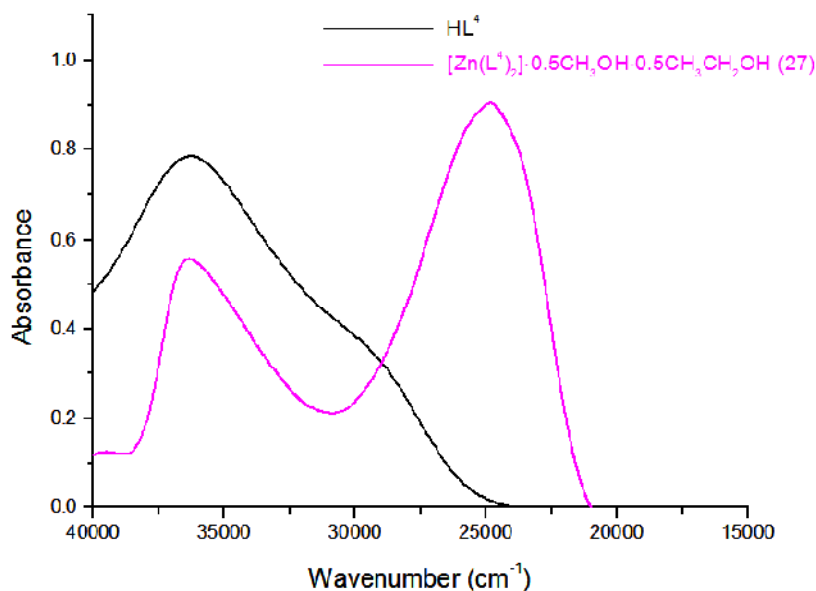


Fig. 7.9. Electronic spectra of HL⁴ and its Zn(II) complex.

7.3.5. X-ray crystallography

Single crystals of complex [Zn(L⁴)₂]·0.5CH₃OH·0.5CH₃CH₂OH (**27**) suitable for X-ray diffraction studies were obtained by recrystallization from a mixture of ethanol and methanol (1:1 v/v) while that of complex [Cd(HL⁴)Br₂]·C₃H₇NO (**32**) were obtained by recrystallization from a mixture of DMF and methanol (1:1 v/v). Single crystals of dimensions 0.30 × 0.20 × 0.20 mm³ of the complex **27** and 0.30 × 0.25 × 0.20 mm³ of the complex **32** were selected and mounted on a Bruker SMART APEXII CCD diffractometer with graphite-monochromated Mo K α ($\lambda = 0.71073 \text{ \AA}$) radiation at the Sophisticated Analytical Instruments Facility (SAIF), Cochin University of Science and Technology, Kochi-22, Kerala, India. The crystallographic data and structure refinement parameters for the complexes **27** and **32** are given in Tables 7.3 and 7.5 respectively. Bruker SMART software was used for data acquisition and Bruker SAINT software for data integration [25]. The

structure was solved by direct methods using SHELXS97 and refined by full-matrix least-squares refinement on F^2 using SHELXL97 [26]. The molecular and crystal structures were plotted using DIAMOND version 3.2g [27].

In $[\text{Zn}(\text{L}^4)_2] \cdot 0.5\text{CH}_3\text{OH} \cdot 0.5\text{CH}_3\text{CH}_2\text{OH}$ (**27**) and $[\text{Cd}(\text{HL}^4)\text{Br}_2] \cdot \text{C}_3\text{H}_7\text{NO}$ (**32**) all non-hydrogen atoms were refined anisotropically and all H atoms on C were placed in calculated positions, guided by difference maps, with C–H bond distances 0.93–0.96 Å. The H atoms were assigned as $U_{\text{iso}}=1.2U_{\text{eq}}$ (1.5 for Me). In complex **27**, H atoms of O13–H13 and O14–H14 were located from difference maps and the bond distances were restrained using DFIX instructions. N3–H3' H atom of complex **32** was located from difference maps and refined isotropically.

7.3.5.1. Crystal structure of $[\text{Zn}(\text{L}^4)_2] \cdot 0.5\text{CH}_3\text{OH} \cdot 0.5\text{CH}_3\text{CH}_2\text{OH}$ (**27**)

The molecular structure of the bis-ligated complex, $[\text{Zn}(\text{L}^4)_2] \cdot 0.5\text{CH}_3\text{OH} \cdot 0.5\text{CH}_3\text{CH}_2\text{OH}$ (**27**) (Fig.7.10) shows that it is monomeric, with each tridentate ligand coordinating to the Zn(II) ion in a monodeprotonated iminolate form. The selected bond lengths and angles are given in Table 7.4. The complex crystallizes in to a monoclinic space group $P2_1/c$. The Zn(II) centre is hexacoordinated and the coordination around the Zn(II) ion can be best described as a distorted octahedron with a ZnO_2N_4 chromophore. Each Zn atom is coordinated by azomethine nitrogen, iminolate oxygen and pyridyl nitrogen from two monodeprotonated hydrazone ligands. The *cis* angles O(4)–Zn(1)–N(1), N(6)–Zn(1)–N(1), O(1)–Zn(1)–N(5) and N(2)–Zn(1)–N(1) are $91.1(8)^\circ$, $90.6(9)^\circ$, $94.2(8)^\circ$ and $75.1(8)^\circ$ and *trans* angles N(6)–Zn(1)–N(2), O(1)–Zn(1)–N(1), O(4)–Zn(1)–N(5) are $165.3(9)^\circ$, $150.0(8)^\circ$, $147.0(9)^\circ$ respectively indicating that the complex **27** has large distortion from

octahedral geometry. All the angles subtended at the Zn(II) ion by donor atoms show marked deviation from that expected for an ideal octahedral geometry. The torsion angle of 178.04° observed for C(5)–C(6)–N(2)–N(3) supports *E* configuration with respect to N(2)=C(6) bond. It is interesting to note that the proligand changes from *Z* configuration to *E* (with respect to N(2)=C(6) bond) upon complexation. The asymmetric unit consists of two molecules of Zn(II) complexes with one ethanol and methanol molecules as solvates (Fig. 7.11). Each of the two molecules in the asymmetric unit of **27** have very similar structural parameters and are comparable to those observed in other similar Zn(II) complexes [28].

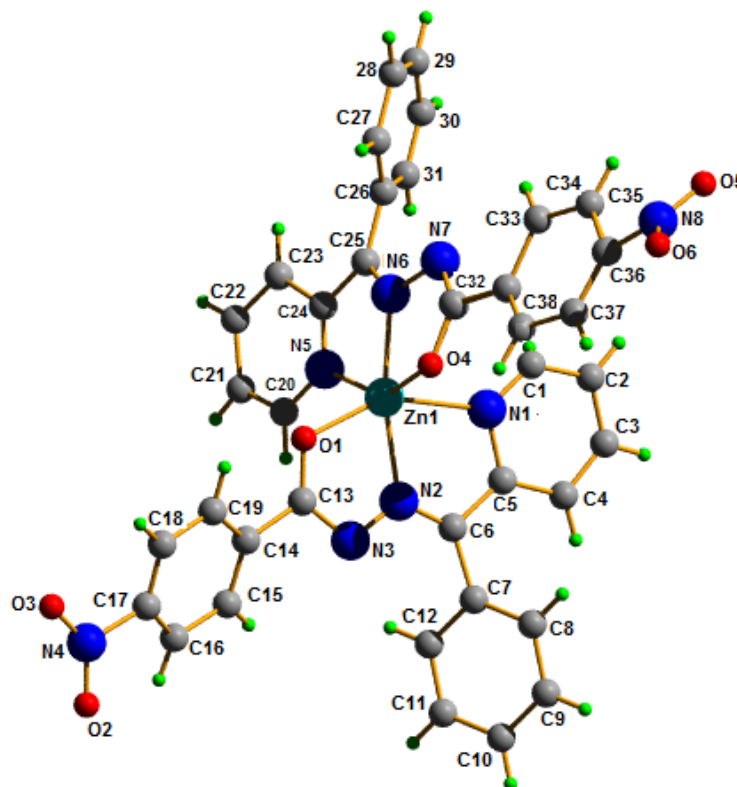


Fig. 7.10. Molecular structure of $[\text{Zn}(\text{L}^4)] \cdot 0.5\text{CH}_3\text{OH} \cdot 0.5\text{CH}_3\text{CH}_2\text{OH}$ (**27**) (solvent molecules are omitted for clarity).

Table 7.3. Crystal data and structure refinement parameters for [Zn(L⁴)₂]·0.5CH₃OH·0.5CH₃CH₂OH (27)

Parameters	[Zn(L ⁴) ₂]·0.5CH ₃ OH·0.5CH ₃ CH ₂ OH (27)
Empirical formula	C ₇₉ H ₆₂ N ₁₆ Zn ₂ O ₁₄
Formula weight	1590.25
Temperature	293 K
Wavelength	0.71073 Å
Crystal system	Monoclinic
Space group	<i>P</i> 2 ₁ / <i>c</i>
Unit cell dimensions	<i>a</i> = 28.874(4) Å <i>b</i> = 14.442(2) Å <i>c</i> = 18.019(2) Å <i>α</i> = 90.00° <i>β</i> = 90.12(5)° <i>γ</i> = 90.00°
Volume	7513.9(18) Å ³
Z	4
Density (calculated)	1.371 mg/m ³
Absorption coefficient	0.715 mm ⁻¹
<i>F</i> (000)	3192
Crystal size	0.30 x 0.20 x 0.20 mm ³
θ range for data collection	1.33 to 25.00°
Limiting indices	-30 ≤ <i>h</i> ≤ 34 -17 ≤ <i>k</i> ≤ 10 -21 ≤ <i>l</i> ≤ 14
Reflections collected	23962
Unique Reflections (<i>R</i> _{int})	13178 [<i>R</i> (int) = 0.1060]
Refinement method	Full-matrix least-squares on <i>F</i> ²
Data / restraints / parameters	13178 / 2452 / 1188
Goodness-of-fit on <i>F</i> ²	0.938
Final <i>R</i> indices [<i>I</i> > 2σ(<i>I</i>)]	<i>R</i> ₁ = 0.0857, <i>wR</i> ₂ = 0.1859
<i>R</i> indices (all data)	<i>R</i> ₁ = 0.2997, <i>wR</i> ₂ = 0.3058
Largest diff. peak and hole	0.620 and -0.486 e Å ⁻³

$$R_1 = \frac{\sum ||F_o| - |F_c||}{\sum |F_o|}$$

$$wR_2 = [\sum w(F_o^2 - F_c^2)^2 / \sum w(F_o^2)^2]^{1/2}$$

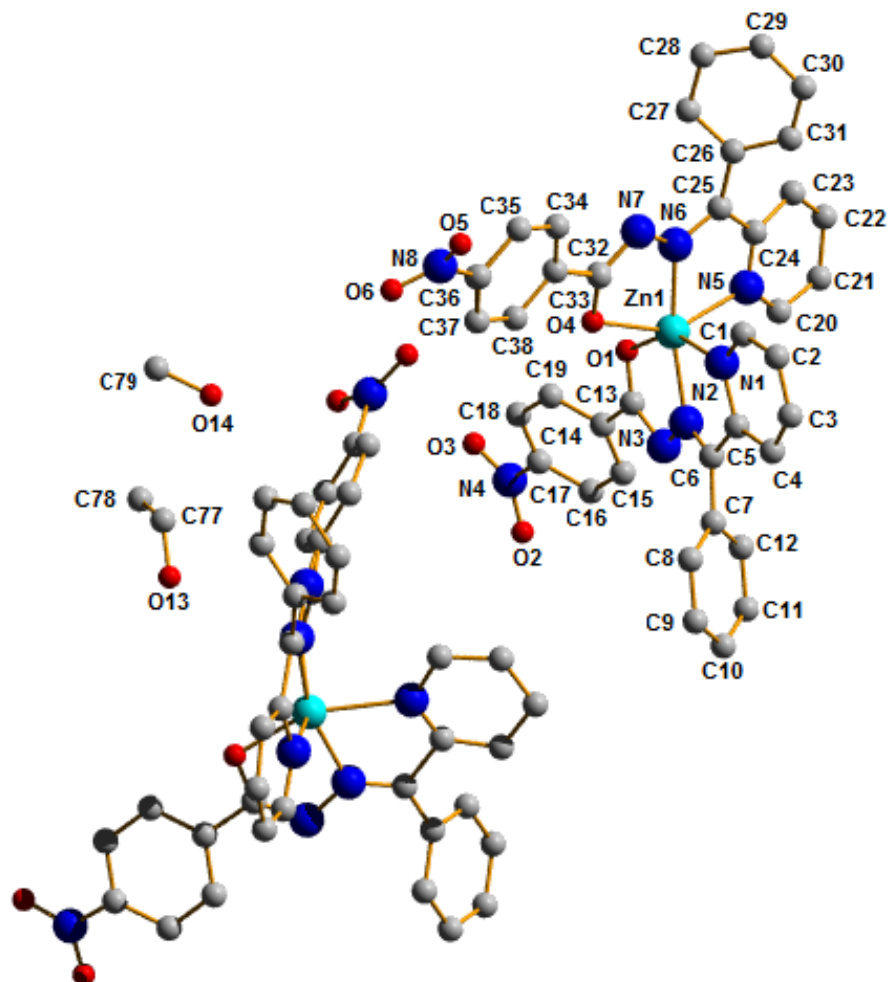


Fig. 7.11. Asymmetric unit of $[\text{Zn}(\text{L}^4)_2] \cdot 0.5\text{CH}_3\text{OH} \cdot 0.5\text{CH}_3\text{CH}_2\text{OH}$ (27).

The Zn(II) center is shared by two fused five membered chelate rings. The bicyclic chelate system $[\text{N}(1), \text{C}(5), \text{C}(6), \text{N}(2), \text{N}(3), \text{C}(13), \text{O}(1), \text{Zn}(1)]$ makes a dihedral angle of 84.87° with its counterpart $[\text{N}(5), \text{C}(24), \text{C}(25), \text{N}(6), \text{N}(7), \text{C}(32), \text{O}(4), \text{Zn}(1)]$ and is approximately planar with a maximum mean plane deviation of 0.088 \AA for Zn(1).

Table 7.4. Selected bond lengths and angles for complex [Zn(L⁴)₂]·0.5CH₃OH·0.5CH₃CH₂OH (27)

Bond lengths (Å)		Bond angles (°)	
Zn(1)–N(1)	2.262(2)	O(4)–Zn(1)–N(1)	91.1(8)
Zn(1)–N(2)	2.080(2)	N(5)–Zn(1)–N(1)	99.1(8)
Zn(1)–O(1)	2.045(19)	N(6)–Zn(1)–N(1)	90.6(9)
Zn(1)–N(5)	2.190(2)	N(2)–Zn(1)–N(1)	75.1(8)
Zn(1)–N(6)	2.060(2)	N(6)–Zn(1)–N(5)	73.0(9)
Zn(1)–O(4)	2.110(2)	O(1)–Zn(1)–N(5)	94.2(8)
C(13)–O(1)	1.240(2)	N(2)–Zn(1)–O(4)	107.6(9)
C(32)–O(4)	1.310(3)	N(6)–Zn(1)–O(4)	75.6(9)
N(2)–C(6)	1.270(3)	N(2)–Zn(1)–N(5)	105.3(9)
N(2)–N(3)	1.333(2)	N(6)–Zn(1)–N(2)	165.3(9)
C(13)–N(3)	1.370(3)	O(4)–Zn(1)–N(5)	147.0(9)
N(7)–C(32)	1.290(3)	O(1)–Zn(1)–N(1)	150.0(8)

The Zn–N(azo) bond lengths are less compared to Zn–N(py) indicating the strength of former bond than the latter. The Zn–N(py), Zn–N(azo) and Zn–O bond lengths observed here are within the range reported for other similar complexes of divalent metal ions [28]. The ligand has undergone amido-iminol tautomerism and coordination through iminolate oxygen is confirmed from the increased bond length of C(13)–O(1) and C(32)–O(4) bonds of complex when compared to the corresponding value in the free ligand. Here packing of the complex is stabilized by weak non-conventional hydrogen bonding interactions. The unit cell packing diagram of the complex **27** viewed along *c* axis is given in Fig. 7.12.

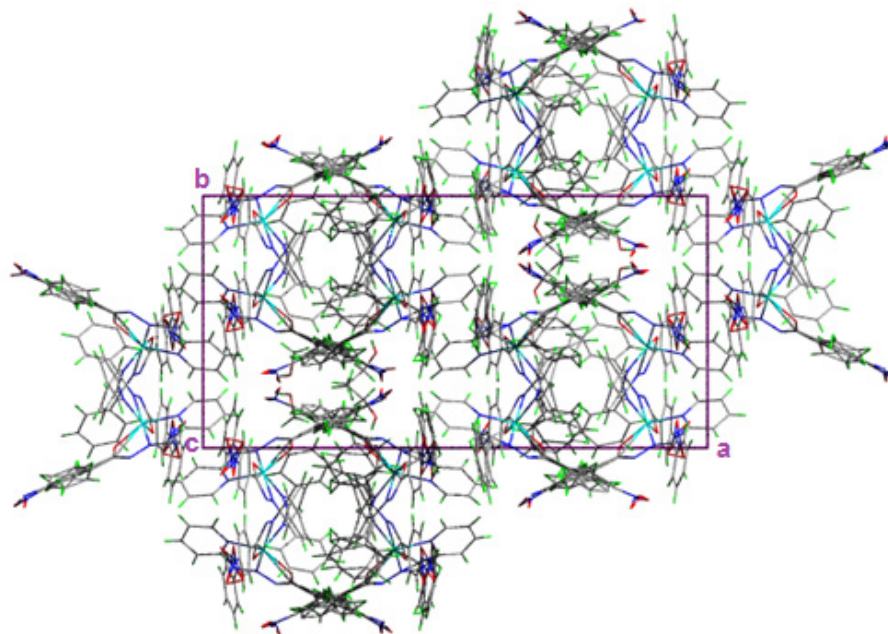


Fig. 7.12. Packing diagram of $\text{Zn}(\text{L}^4)_2 \cdot 0.5\text{CH}_3\text{OH} \cdot 0.5\text{CH}_3\text{CH}_2\text{OH}$ (27) viewed along c axis.

7.3.5.2. Crystal structure of $[\text{Cd}(\text{HL}^4)\text{Br}_2] \cdot \text{C}_3\text{H}_7\text{NO}$ (32)

The molecular structure of the mononuclear Cd(II) complex with the atom numbering scheme is shown in Fig. 7.13. The complex crystallizes as a DMF solvate in the monoclinic space group $P2_1/n$. In this complex, Cd(II) ion is in a pentacoordinated environment and the coordination sites are occupied by azomethine nitrogen N(2), pyridyl nitrogen N(1) and ketoxy oxygen O(1) of the hydrazone ligand and the remaining coordination positions are occupied by two bromide ions. The proligand HL^4 , adjusts in such a fashion that the Z configuration is changed to E upon complexation. The oxygen atom of the hydrazone ligand is coordinated to the metal atom in amido form, which is confirmed by the single bond nature of C(13)–N(3) (1.371 Å) and double bond nature of C(13)–O(1) (1.217 Å) bonds.

The bond lengths, Cd–N_(py), 2.358(4) Å and Cd–N_(azo), 2.360(3) Å are very similar to other Cd(II) complexes of hydrazones [30]. The bond distances to Cd are in the order Cd–N_(py) < Cd–N_(azo) < Cd–O_(ketoxy) < Cd–Br(2) < Cd–Br(1). The basal plane involves either Br(1) or Br(2) with hydrazone moiety and the Cd atom is displaced with a distance of 0.9667 Å above the basal plane. The dihedral angle between the two aromatic rings of 2-benzoylpyridine part of the hydrazone ligand is 62.45° and that between phenyl ring of the hydrazide part and pyridyl ring is 19.42°. The selected bond lengths and bond angles are given in Table 7.6.

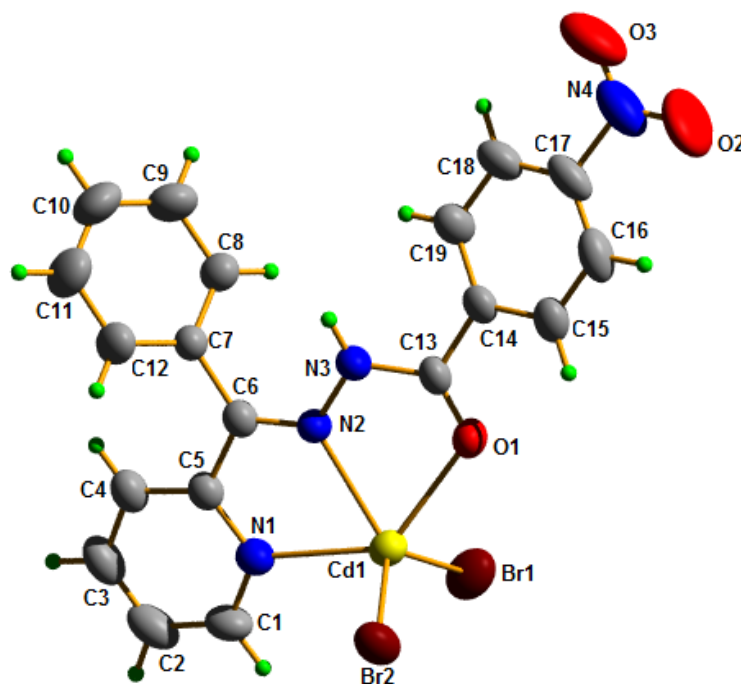


Fig. 7.13. Molecular structure of [Cd(HL⁴)Br₂]·C₃H₇NO (32) (DMF molecule is omitted for clarity).

Table 7.5. Crystal data and structure refinement parameters for [Cd(HL⁴)Br₂]·C₃H₇NO (32)

Parameters	[Cd(HL ⁴)Br ₂]·C ₃ H ₇ NO (32)
Empirical formula	C ₂₂ H ₂₁ Br ₂ CdN ₅ O ₄
Formula weight	691.65
Temperature	293 K
Wavelength	0.71073 Å
Crystal system	Monoclinic
Space group	<i>P</i> 2 ₁ / <i>n</i>
Unit cell dimensions	<i>a</i> = 8.333(7) Å <i>b</i> = 18.789(2) Å <i>c</i> = 16.809(17) Å <i>α</i> = 90.00° <i>β</i> = 97.18(4)° <i>γ</i> = 90.00°
Volume	2611.4(4) Å ³
<i>Z</i>	4
Density (calculated)	1.759 mg/m ³
Absorption coefficient	3.933 mm ⁻¹
<i>F</i> (000)	1352
Crystal size	0.30 x 0.25 x 0.20 mm ³
θ range for data collection	2.67 to 25.00°
Limiting indices	-7 ≤ <i>h</i> ≤ 9 -21 ≤ <i>k</i> ≤ 22 -19 ≤ <i>l</i> ≤ 19
Reflections collected	16940
Unique Reflections (<i>R</i> _{int})	4588 [<i>R</i> (int) = 0.0429]
Refinement method	Full-matrix least-squares on <i>F</i> ²
Data / restraints / parameters	4561 / 0 / 309
Goodness-of-fit on <i>F</i> ²	1.017
Final <i>R</i> indices [<i>I</i> > 2σ(<i>I</i>)]	<i>R</i> ₁ = 0.0350, <i>wR</i> ₂ = 0.0769
<i>R</i> indices (all data)	<i>R</i> ₁ = 0.0631, <i>wR</i> ₂ = 0.0880
Largest diff. peak and hole	741 and -0.482 e Å ⁻³

$$R_1 = \frac{\sum ||F_o| - |F_c||}{\sum |F_o|}$$

$$wR_2 = \left[\frac{\sum w(F_o^2 - F_c^2)^2}{\sum w(F_o^2)^2} \right]^{1/2}$$

Table 7.6. Selected bond lengths and angles for complex [Cd(HL⁴)Br₂]·C₃H₇NO (32)

Bond lengths (Å)		Bond angles (°)	
Cd(1)–N(1)	2.358(4)	N(1)–Cd(1)–N(2)	67.60(12)
Cd(1)–N(2)	2.360(3)	N(1)–Cd(1)–O(1)	133.93(12)
Cd(1)–O(1)	2.401(3)	N(2)–Cd(1)–O(1)	66.88(11)
Cd(1)–Br(1)	2.554(7)	N(1)–Cd(1)–Br(2)	100.83(9)
Cd(1)–Br(2)	2.532(6)	N(2)–Cd(1)–Br(2)	113.28(9)
C(6)–N(2)	2.283(5)	O(1)–Cd(1)–Br(2)	103.09(8)
N(2)–N(3)	1.378(4)	N(1)–Cd(1)–Br(1)	99.99(9)
C(13)–N(3)	1.371(5)	N(2)–Cd(1)–Br(1)	120.84(9)
C(13)–O(1)	1.217(5)	O(1)–Cd(1)–Br(1)	96.99(9)

According to Addison *et al.*, for five coordinated complexes, the angular structural parameter (τ) is used to propose an index of trigonality. The value of τ is defined by an equation represented by $\tau = (\beta - \alpha)/60$, where β is the greatest basal angle and α is the second greatest angle; τ is 0 for square pyramidal forms and 1 for trigonal bipyramidal forms [30,31]. However, in the case of the five coordinate systems, the structures vary from near regular trigonal bipyramidal (RTB) to near square based pyramidal (SBP). The value of τ for the complex **32** is 0.21 indicating that the coordination geometry around Cd(II) is best described as distorted square based pyramidal geometry. The *cis* angles N(1)–Cd(1)–Br(2) and N(1)–Cd(1)–Br(1) are 100.83(9)° and 99.99(9)° and *trans* angles N(1)–Cd(1)–O(1) and N(2)–Cd(1)–Br(1) are 133.93(12)° and 120.84(9)° respectively indicating that the complex **32** has large distortion from square pyramidal geometry. The coordination polyhedra present in a unit cell is shown in Fig. 7.14.

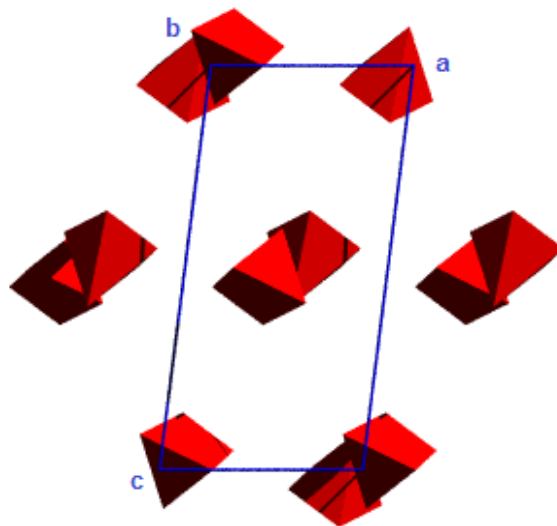


Fig. 7.14. Coordination polyhedra in a unit cell.

In the unit cell, $\pi \cdots \pi$ and hydrogen bonding interactions are observed (Figs. 7.15-7.16). A strong conventional N(3)–H(3') \cdots O(4) hydrogen bond is present in the crystal structure in which the oxygen atom of the solvent dimethylformamide acts as the acceptor. The $\pi \cdots \pi$ interaction is present between Cg(3) rings [N(1), C(1), C(2), C(3), C(4), C(5)] of neighboring molecules at a Cg \cdots Cg distance of 3.711(3) Å. The intermolecular hydrogen bonding interactions supported with $\pi \cdots \pi$ interactions establish a supramolecular linkage among the molecules in the crystal system. The unit cell packing diagram of the complex **32** viewed along *c* axis is given in Fig. 7.17.

Table 7.7. Interaction parameters of [Cd(HL⁴)Br₂]·C₃H₇NO (32)

Hydrogen bonding interaction				
D–H···A	D–H (Å)	H···A (Å)	D···A (Å)	D–H···A (°)
N(3)–H(3')···O(4) ^a	0.86	1.98	2.744(5)	146.6
π···π interactions				
Cg(I)···Cg(J)	Cg···Cg (Å)	α (°)	β (°)	
Cg(3)···Cg(3) ^b	3.711(3)	0	22.60	

Equivalent position codes : a = x-1, y, z; b = 1-x, 1-y, 2-z
 Cg(3) = N(1), C(1), C(2), C(3), C(4), C(5)
 D, Donor; A, acceptor; Cg, Centroid; α, dihedral angle between planes I & J; β, angle between Cg···Cg and Cg(J) perp.

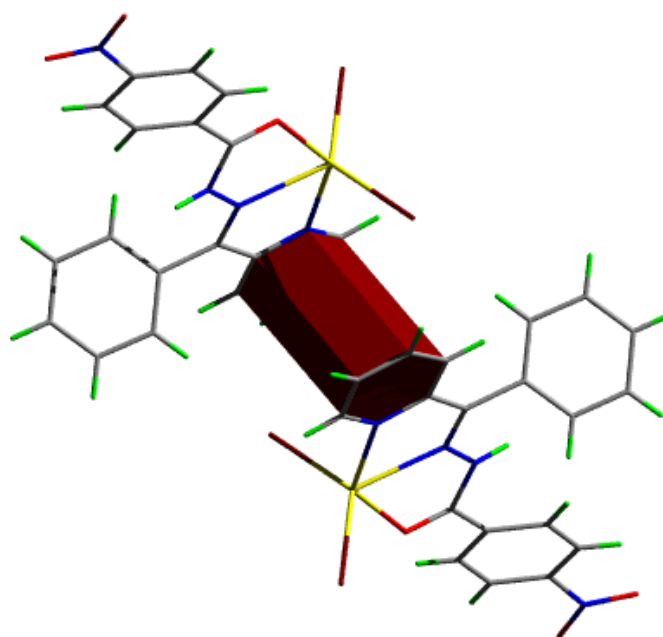


Fig. 7.15. The π···π interaction in [Cd(HL⁴)Br₂]·C₃H₇NO (32).

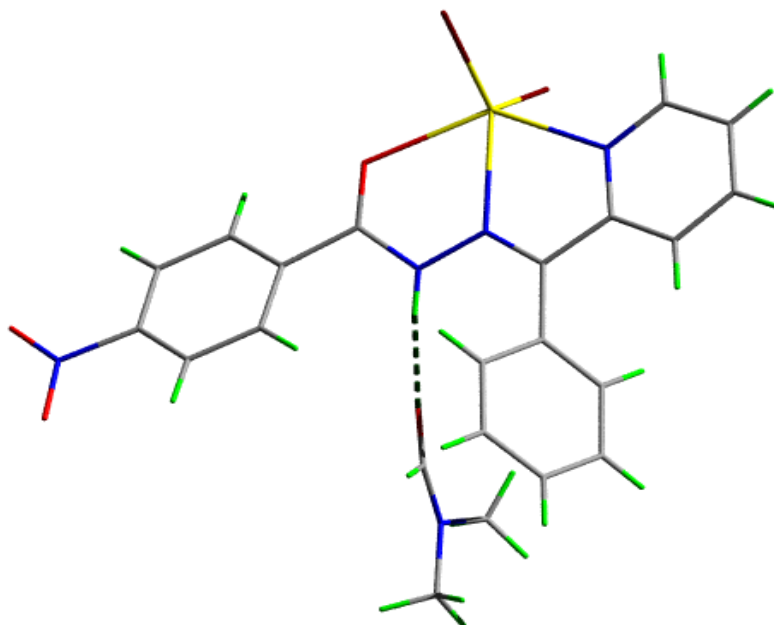


Fig. 7.16. Hydrogen bonding interaction shown as dotted line.

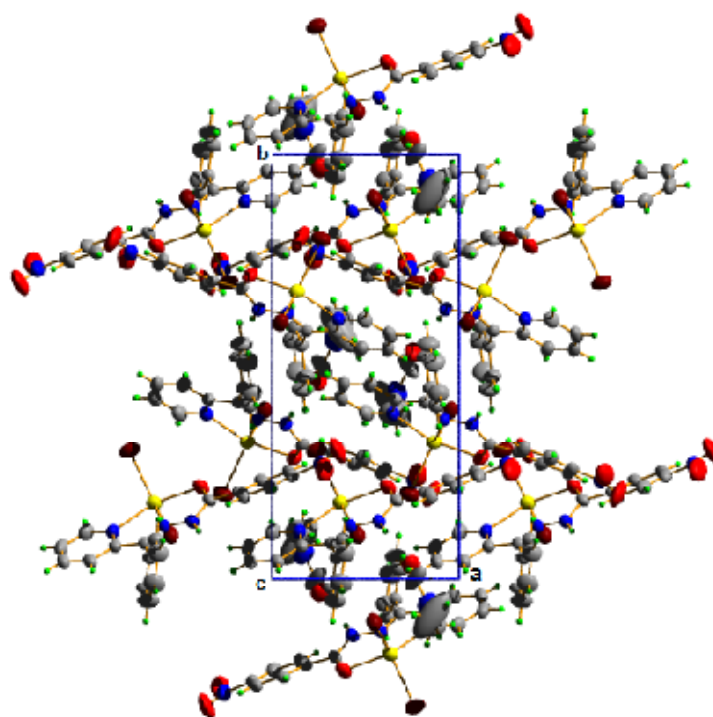


Fig. 7.17. Packing diagram of complex viewed along *c* axis.

7.3.6. Thermogravimetric analyses

Thermogravimetry is a powerful method for determining complex stoichiometries. The thermal analyses of the complexes **26**, **28** and **31** were carried out in the 50-700 °C range in dynamic nitrogen atmosphere. The complexes show a gradual weight loss indicating decomposition by fragmentation with increasing temperature. Thermogravimetric analyses of the complexes gave information concerning the thermal stability and the nature of water molecules in the complexes [32,33]. It was observed that the hydrated complexes lose water of hydration in the first step, followed by decomposition of ligand molecules in the subsequent steps. Analyses show that the weight loss for lattice water are observed below 200 °C and weight loss due to coordinated water molecules are in the 200-350 °C range. The thermograms of complexes **26**, **28** and **31** are presented in Figs. 7.18-7.20.

For the complex $[(ZnL^2)_2] \cdot H_2O$ (**26**), the first step in the decomposition sequence within the temperature range of 70-94 °C corresponds to the loss of one molecule of lattice water present in the complex. The observed weight loss of 1.93% is in good agreement with the calculated value of 2.13%. The anhydrous complex is stable up to 210 °C. The decomposition of the ligands take place in the 210-601 °C range and after this temperature a plateau is obtained, which indicates the formation of stable metal oxide (Fig. 7.18).

In $[CdL^1(H_2O)]_2$ (**28**), the first weight loss of 3.96% (calcd. 3.46%) is observed in the 220-250 °C range indicating the presence of two coordinated water molecules. Above 350 °C, the compound decomposes gradually due to the removal of the organic part of the complex (Fig. 7.19).

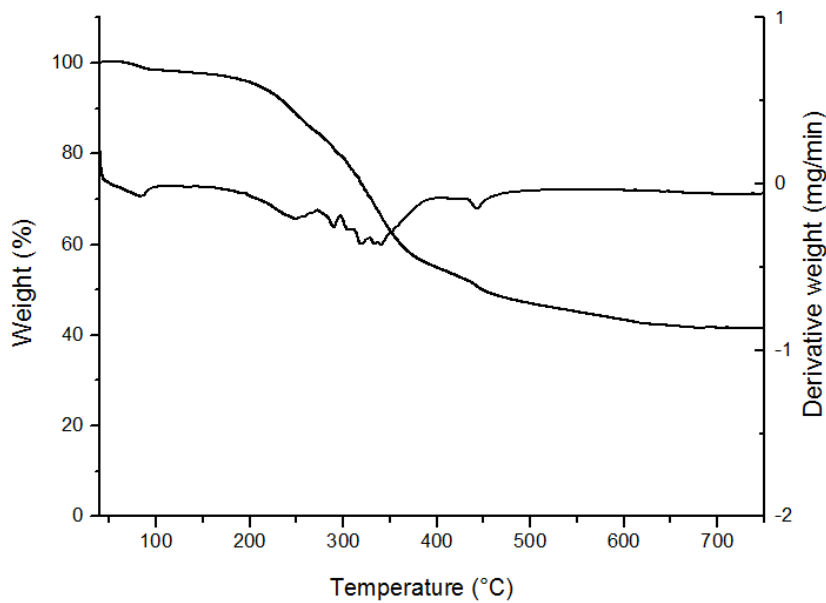


Fig. 7.18. Thermogram of $[(ZnL^2)_2] \cdot H_2O$ (26).

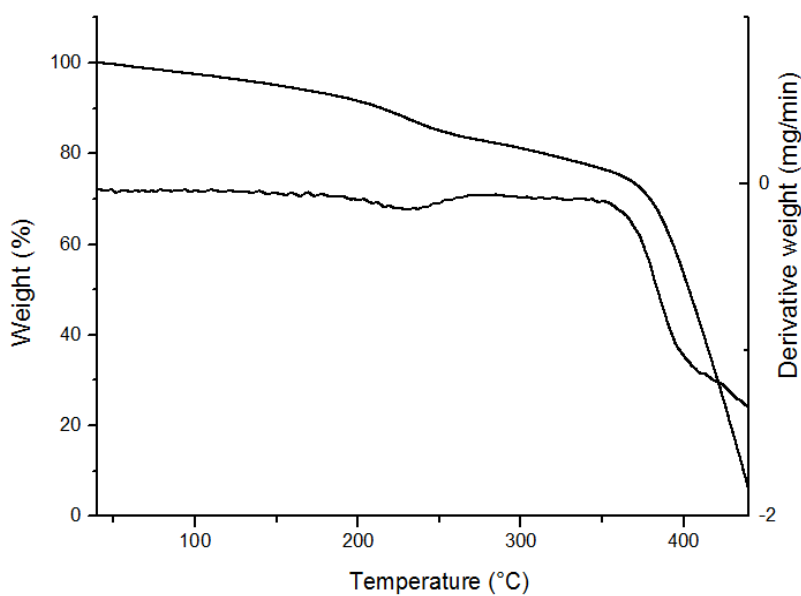


Fig. 7.19. Thermogram of $[CdL^1(H_2O)]_2$ (28).

In $[(CdL^2)_2] \cdot H_2O$ (**31**), a weight loss of 1.87% is observed in the 65-97 °C range due to the loss of one molecule of water from its lattice (calcd. 1.91%). The anhydrous complex is stable up to 294 °C. After this temperature, the complex undergoes two step degradation in the 294-707 °C range corresponding to the degradation of two molecules of ligands and finally reduces to cadmium oxide. The observed weight loss of 79.00% is close to the calculated value (75.57%) (Fig. 7.20).

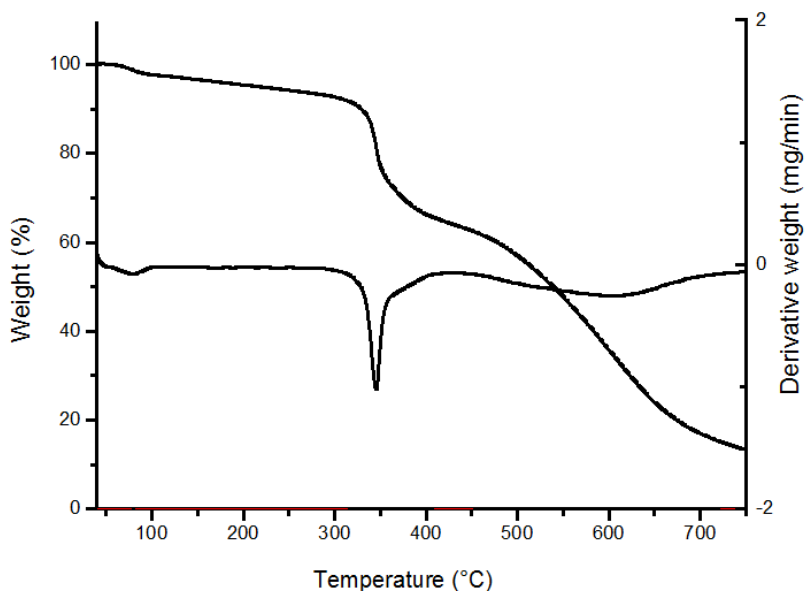
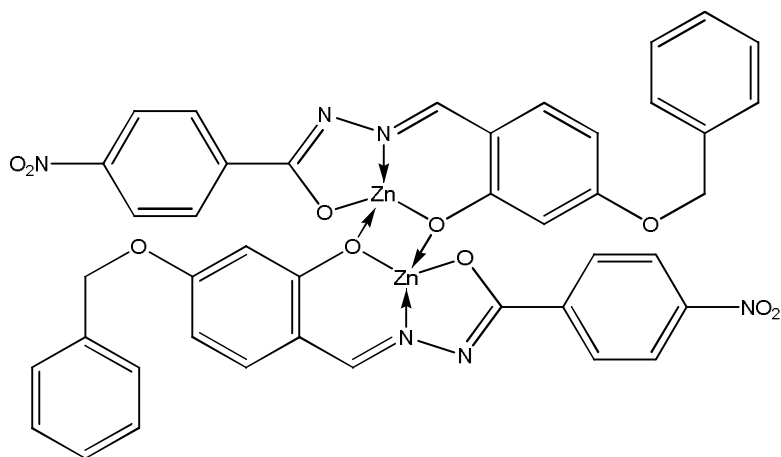
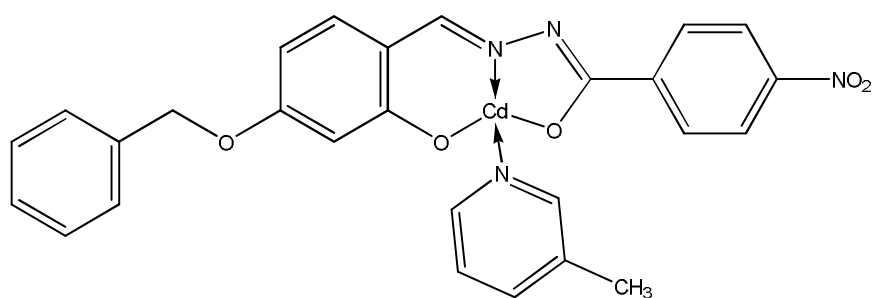
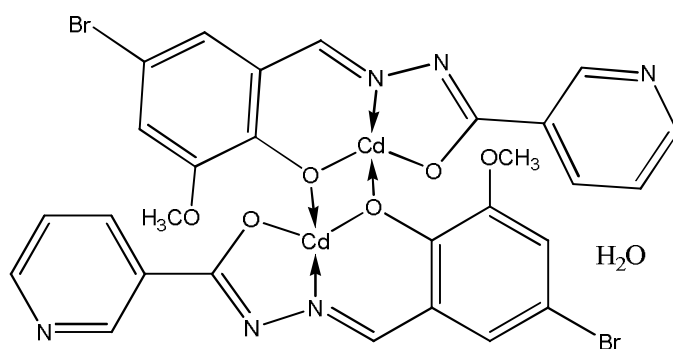


Fig. 7.20. Thermogram of $[(CdL^2)_2] \cdot H_2O$ (31**).**

On the basis of the physico-chemical measurements discussed above, the tentative structures proposed for some Zn(II) and Cd(II) complexes are presented below. In all complexes except **32**, the hydrazones exist in the iminolate form, while in **32** it is in the amido form. Compounds **23**, **26**, **28** and **31** are dimeric in nature while others are monomeric metal chelates.

 $[(ZnL^1)_2]$ (23) $[CdL^1pic]$ (29) $[(CdL^2)_2] \cdot H_2O$ (31)**Fig. 7.21.** Tentative structures of some of the Zn(II) and Cd(II) complexes.

References

- [1] W.N. Lipscomb, N. Strater, *Chem. Rev.* 96 (1996) 2375.
- [2] B.L. Vallee, D.S. Auld, *Acc. Chem. Res.* 26 (1993) 543.
- [3] X.X. Sun, C.M. Qi, S.L. Ma, H.B. Huang, W.X. Zhu, Y.C. Liu, *Inorg. Chem. Commun.* 9 (2006) 911.
- [4] P. Das, S. Samantaray, G.R. Rout, *Environ. Pollut.* 98 (1997) 29.
- [5] F.B. Wu, G.P. Zhang, *J. Plant Nutr.* 25 (2002) 2745.
- [6] T.W. Lane, F.M.M. Morel, *Proc. Natl. Acad. Sci., USA* 97 (2000) 4627.
- [7] E.T. Dikkaya, N. Ergun, *Euro. J. Exp. Bio.* 4 (2014) 288.
- [8] G. Wilkinson, R.D. Gillard, J.A. McCleverty, *Comprehensive Coordination Chemistry*, Pergamon Press, England 5 (1987).
- [9] C.P. Li, M. Du, *Inorg. Chem. Commun.* 14 (2011) 502.
- [10] B. Singh, K.K. Narang, R. Srivastava, *Synth. React. Inorg. Met-Org. Chem.* 33 (2003) 1025.
- [11] K.M. Ibrahim, R.R. Zaky, E.A. Gomaa, M.N.A. Hady, *Spectrochim. Acta A* 107 (2013) 133.
- [12] O.A.E. Gammal, T.H. Rakha, H.M. Metwally, G.M.A. Reash, *Spectrochim. Acta A* 127 (2014) 144.
- [13] Y. Harinath, D.H.K. Reddy, B.N. Kumar, C. Apparao, K. Seshaiiah, *Spectrochim. Acta A* 101 (2013) 264.
- [14] T. Balakrishnan, K. Ramamurthi, *Mater. Lett.* 62 (2008) 65.
- [15] H.T. Ye, C.Y. Ren, G.F. Hou, Y.H. Yu, X. Xu, J.S. Gao, P.F. Yan, S.W. Ng, *Cryst. Growth Des.* 14 (2014) 3309.

- [16] A. Ray, S. Banerjee, S. Sen, R.J. Butcher, G.M. Rosair, M.T. Garland, S. Mitra, *Struct. Chem.* 19 (2008) 209.
- [17] F. Liu, W.P. Zhang, S.Y. He, *Russ. J. Coord. Chem.* 36 (2010) 105.
- [18] Z.H. Chohan, K.M. Khan, C.T. Supuran, *Appl. Organometal. Chem.* 18 (2004) 305.
- [19] S. Naskar, D. Mishra, R.J. Butcher, S.K. Chattopadhyay, *Polyhedron* 26 (2007) 3703.
- [20] M.K. Prasanna, K. Pradeepkumar, *Int. J. Pharm. Biomed. Sci.* 4 (2013) 24.
- [21] V.P. Singh, S. Singh, D.P. Singh, P. Singh, K. Tiwari, M. Mishra, R.J. Butcher, *Polyhedron* 56 (2013) 71.
- [22] S. Sen, P. Talukder, G. Rosair, S. Mitra, *Struct. Chem.* 16 (2005) 605.
- [23] M.M. Wang, H. Wang, G.Q. Gan, Y. Qu, H. Chen, Z.D. Lin, *J. Macromol. Sci., Part A: Pure Appl. Chem.* 49 (2012) 355.
- [24] M.M.A. Neaimi, M.M.A. Khuder, *Spectrochim. Acta A* 105 (2013) 365.
- [25] SMART and SAINT, Area Detector Software Package and SAX Area Detector Integration Program, Bruker Analytical X-ray; Madison, WI, USA, 1997.
- [26] G.M. Sheldrick, *Acta Cryst. Sect. A* 64 (2008) 112.
- [27] K. Brandenburg, Diamond Version 3.2g, Crystal Impact GbR, Bonn, Germany, 2010.
- [28] A.S. Pedrares, N. Camina, J. Romero, M.L. Duran, J.A.G. Vazquez, *Polyhedron* 27 (2008) 3391.
- [29] M. Akkurt, A.A. Khandar, M.N. Tahir, F.A. Afkhamib, S.A.H. Yazdi, *Acta Cryst. E* 70 (2014) m213.

- [30] A.W. Addison, T.N. Rao, J. Reedijk, J.V. Rijn, G.C. Verschoor, J. Chem. Soc., Dalton Trans. 7 (1984) 1349.
- [31] M. Vaidyanathan, R. Balamurugan, U. Sivagnanam, M. Palaniandavar, J. Chem. Soc., Dalton Trans. 23 (2001) 3498.
- [32] A.A.A. Emara, B.A.E. Sayed, E.A.E. Ahmed, Spectrochim. Acta A 69 (2008) 757.
- [33] B. Hollo, J. Magyari, V.Z. Radovanovic, G. Vuckovic, Z.D. Tomic, I.M. Szilagyi, G. Pokol, K.M. Szecsenyi, Polyhedron 80 (2014) 142.

.....❧.....

**SYNTHESES, SPECTRAL CHARACTERIZATION AND CRYSTAL
STRUCTURE OF DIOXIDOMOLYBDENUM(VI) CHELATES OF
TRIDENTATE AROYLHYDRAZONES**

Contents	8.1 Introduction
	8.2 Experimental
	8.3 Results and discussion
	References

8.1. Introduction

Molybdenum is a hard, silver-white transition metal discovered by Swedish chemist Carl Wilhelm Scheele in 1778. Molybdenum is a biologically important trace metal that occurs in the redox-active sites of molybdoenzymes involved in nitrogen, carbon or sulfur metabolism. Among the second series of transition metals, only molybdenum represents a biometal important for microorganisms, plants and animals [1]. The biochemical importance of molybdenum is due to its ability to provide facile electron-transfer pathways, a consequence of the easy inter-convertibility of the different oxidation states and to form bonds with nitrogen and oxygen donors, which are sufficiently strong to permit the existence of stable complexes but also sufficiently labile to permit facile ligand exchange reactions or changes in the molybdenum coordination number. The mononuclear molybdoenzymes containing terminal oxo group(s) are believed to be obligatory for the oxotransferase activity of

these enzymes. The mechanism of molybdenum oxotransferase has extensively been investigated for a long time. Some of the complexes possess oxygen atom transfer properties as they were found to oxidize thiols, hydrazine, polyketones and tertiary phosphines [2,3].

Coordination chemistry of molybdenum still engages the attention of researchers due to the chemistry of its oxidation state, coordination number, ligating atoms, their impact on structure, reactivity and also because of the potential applications of molybdenum compounds [4-7]. Studies on oxidomolybdenum and dioxidomolybdenum complexes have opened up a new vista of research and analysis of uncharted biochemical significance [8-13]. Molybdenum complexes with hydrazone ligands have been reported to possess interesting antibacterial activities [14]. The molybdenum complexes of hydrazones show remarkable catalytic activities in several industrial processes such as epoxidation of olefins [15], oxidation of sulfides [16-17], olefin metathesis [18], ammoxidation of propene [19] and isomerization of allylic alcohols [20].

Molybdenum is a versatile transition metal with a large number of stable and accessible oxidation states, the oxidation states +4, +5 and +6 have received much attention recently. It has been reported that dioxidomolybdenum(VI) and oxidomolybdenum(V) complexes are stable, whereas oxidomolybdenum(IV) complexes are unstable, but stable at vacuum condition [21]. Complexes containing the oxidomolybdenum and dioxidomolybdenum groups dominate the higher oxidation state of molybdenum [22]. Most simple dioxidomolybdenum(VI) coordination complexes contain the *cis*-MoO₂²⁺ cation. The studies on dioxidomolybdenum complexes of the type MoO₂L

derived from dianionic tridentate ligand system are particularly significant because they provide an open coordination site that can be utilized for substrate binding [23]. For that reason dioxidomolybdenum(VI) complexes with dibasic tridentate ligands occupy a significant place within the scope of fundamental chemistry of this metal.

8.2. Experimental

8.2.1. Materials

4-Benzyloxy-2-hydroxybenzaldehyde (Sigma-Aldrich), 5-bromo-2-hydroxy-3-methoxybenzaldehyde (Sigma-Aldrich), 4-diethylamino-2-hydroxybenzaldehyde (Sigma-Aldrich), nicotinic hydrazide (Sigma-Aldrich), 4-nitrobenzoic hydrazide (Sigma-Aldrich) and $\text{MoO}_2(\text{acac})_2$ (Sigma-Aldrich) were of Analar grade and were used as received. Solvents used were methanol and dimethylformamide.

8.2.2. Syntheses of hydrazones

The syntheses of hydrazones 4-benzyloxy-2-hydroxybenzaldehyde-4-nitrobenzoylhydrazone dimethylformamide monosolvate ($\text{H}_2\text{L}^1 \cdot \text{C}_3\text{H}_7\text{NO}$), 5-bromo-2-hydroxy-3-methoxybenzaldehyde nicotinoylhydrazone dihydrate methanol monosolvate ($\text{H}_2\text{L}^2 \cdot 2\text{H}_2\text{O} \cdot \text{CH}_3\text{OH}$) and 4-diethylamino-2-hydroxybenzaldehyde nicotinoylhydrazone monohydrate ($\text{H}_2\text{L}^3 \cdot \text{H}_2\text{O}$) have already discussed in Chapter 2.

8.2.3. Syntheses of $\text{MoO}_2(\text{VI})$ complexes

8.2.3.1. $[(\text{MoO}_2\text{L}^1)_2]$ (33)

The complex $[(\text{MoO}_2\text{L}^1)_2]$ (33) was prepared by refluxing methanolic solutions of $\text{H}_2\text{L}^1 \cdot \text{C}_3\text{H}_7\text{NO}$ (0.464 g, 1 mmol) and $\text{MoO}_2(\text{acac})_2$ (0.326 g, 1 mmol) for 4 h. The resulting solution was allowed to evaporate at room

temperature and the orange colored product formed was filtered, washed with methanol followed by ether and dried over P_4O_{10} *in vacuo*.

$[(MoO_2L^1)_2]$ (**33**): Yield: 69%, λ_m (DMF): $8 \text{ ohm}^{-1} \text{ cm}^2 \text{ mol}^{-1}$, Elemental Anal. Found (Calcd.) (%): C: 48.51 (48.76); H: 3.03 (2.92); N: 7.70 (8.12).

8.2.3.2. $[MoO_2L^1DMF]$ (**34**)

To a solution of $H_2L^1 \cdot C_3H_7NO$ (0.464 g, 1 mmol) in DMF, $MoO_2(acac)_2$ (0.326 g, 1 mmol) in DMF was added. The resultant solution was refluxed for 4 h. This was cooled and the orange colored crystalline complex formed was collected, washed with methanol followed by ether and dried over P_4O_{10} *in vacuo*.

$[MoO_2L^1DMF]$ (**34**): Yield: 67%, λ_m (DMF): $11 \text{ ohm}^{-1} \text{ cm}^2 \text{ mol}^{-1}$, Elemental Anal. Found (Calcd.) (%): C: 48.98 (48.82); H: 3.93 (3.76); N: 9.87 (9.49).

8.2.3.3. $[(MoO_2L^2)_2] \cdot 2H_2O$ (**35**)

A solution of $H_2L^2 \cdot 2H_2O \cdot CH_3OH$ (0.418 g, 1 mmol) in methanol was treated with a methanolic solution of $MoO_2(acac)_2$ (0.326 g, 1 mmol) and refluxed for 4 h. The resulting orange solution was allowed to stand at room temperature and after slow evaporation the orange colored complex formed was filtered, washed with methanol followed by ether and dried over P_4O_{10} *in vacuo*.

$[(MoO_2L^2)_2] \cdot 2H_2O$ (**35**): Yield: 65%, λ_m (DMF): $9 \text{ ohm}^{-1} \text{ cm}^2 \text{ mol}^{-1}$, Elemental Anal. Found (Calcd.) (%): C: 34.33 (34.03); H: 2.98 (2.45); N: 8.29 (8.50).

8.2.3.4. [(MoO₂L³)₂] (36)

Methanolic solutions of H₂L³·H₂O (0.330 g, 1 mmol) and MoO₂(acac)₂ (0.326 g, 1 mmol) were mixed and the resulting mixture was refluxed for 4 h. The orange colored complex separated out was filtered, washed with methanol followed by ether and dried over P₄O₁₀ *in vacuo*.

[(MoO₂L³)₂] (**36**): Yield: 65%, λ_m (DMF): 3 ohm⁻¹ cm² mol⁻¹, Elemental Anal. Found (Calcd.) (%): C: 46.33 (46.59); H: 4.32 (4.14); N: 12.58 (12.78).

8.3. Results and discussion

Out of the four Mo(VI) complexes presented here, complexes **33**, **35** and **36** were synthesized by refluxing methanolic solutions of the hydrazones and bis(acetylacetonato)dioxomolybdenum(VI) in 1:1 ratio. The stoichiometric reaction of bis(acetylacetonato)dioxomolybdenum(VI) with 4-benzyloxy-2-hydroxybenzaldehyde-4-nitrobenzoylhydrazone in N,N-dimethylformamide afforded the six coordinate complex [MoO₂L¹DMF] (**34**). All the complexes are orange in color and are soluble in solvents like DMSO, DMF and acetonitrile. Single crystals of complex **34** could be isolated and the structure was established by single crystal XRD studies. The synthesized complexes are characterized by the following physico-chemical methods.

8.3.1. Elemental analyses

The elemental analyses data indicate that the complexes are analytically pure. The observed C, H, N values of the complexes are in close agreement with that of the formula suggested and are given in Section 8.2.3.

8.3.2. Molar conductivity and magnetic susceptibility measurements

The molar conductivity values of 10^{-3} M DMF solutions of all the four complexes are found to be in the $3\text{-}12\text{ ohm}^{-1}\text{ cm}^2\text{ mol}^{-1}$ range which is much less than the value of $65\text{-}90\text{ ohm}^{-1}\text{ cm}^2\text{ mol}^{-1}$ obtained for uni-univalent electrolytes in this solvent [24]. Thus it can be concluded that these complexes are undissociated in DMF which indicates the non-electrolytic nature of these complexes. Magnetic susceptibility measurements indicate the diamagnetic nature of these complexes and it is a clear evidence for the +6 oxidation state of molybdenum.

8.3.3. Infrared spectra

In order to study the binding modes of the hydrazones to the metal in the complexes, the IR spectrum of the proligand was compared with the spectra of the complexes. Important infrared frequencies of the hydrazones and complexes along with their tentative assignments are given in Table 8.1.

Table 8.1. The important IR frequencies (cm^{-1}) of hydrazones and their dioxidomolybdenum(VI) complexes

Compound	$\nu(\text{C}=\text{N})$	$\nu(\text{C}=\text{N})^{\text{a}}$	$\nu(\text{C}=\text{O})/\nu(\text{C}-\text{O})$	$\nu(\text{N}-\text{H})$	$\nu(\text{Mo}=\text{O})$
$\text{H}_2\text{L}^1 \cdot \text{C}_3\text{H}_7\text{NO}$	1604	----	1661	3186	----
$[(\text{MoO}_2\text{L}^1)_2]$ (33)	1599	1538	1283	----	897, 935
$[\text{MoO}_2\text{L}^1\text{DMF}]$ (34)	1594	1538	1335	----	903, 940
$\text{H}_2\text{L}^2 \cdot 2\text{H}_2\text{O} \cdot \text{CH}_3\text{OH}$	1609	----	1669	3067	----
$[(\text{MoO}_2\text{L}^2)_2] \cdot 2\text{H}_2\text{O}$ (35)	1608	1554	1336	----	912, 938
$\text{H}_2\text{L}^3 \cdot \text{H}_2\text{O}$	1603	----	1632	3075	----
$[(\text{MoO}_2\text{L}^3)_2]$ (36)	1599	1574	1345	----	894, 970

^aNewly formed C=N

The aroylhydrazones show stretching bands attributed to $\nu(\text{C}=\text{O})$, $\nu(\text{C}=\text{N})$ and $\nu(\text{N}-\text{H})$ at 1661, 1604 and 3186 cm^{-1} for H_2L^1 , 1669, 1609 and 3067 cm^{-1} for H_2L^2 and at 1632, 1603 and 3075 cm^{-1} for H_2L^3 respectively. The bands due to $\nu(\text{C}=\text{O})$ and $\nu(\text{N}-\text{H})$ are absent in the complexes, suggesting the occurrence of amido-iminol tautomerization followed by deprotonation of the ligands during complexation. The $\nu(\text{C}=\text{N})$ absorption observed in the 1603-1609 cm^{-1} region for the proligands are shifted to lower frequency in all the complexes indicating the coordination of azomethine nitrogen to the metal. The broad band occurs at 3434 cm^{-1} for the complex **35** indicating the presence of lattice water. All the complexes exhibit two bands in the 894-912 and 935-970 cm^{-1} regions assigned to symmetric and asymmetric vibrations respectively of the *cis*- MoO_2 cores [25]. The weak bands in the 550-585 and 460-470 cm^{-1} regions in the metal complexes have been assigned to $\nu(\text{Mo}-\text{O})$ and $\nu(\text{Mo}-\text{N})$ modes respectively. Figs. 8.1-8.2 depict the infrared spectra of some of the dioxidomolybdenum complexes of aroylhydrazones.

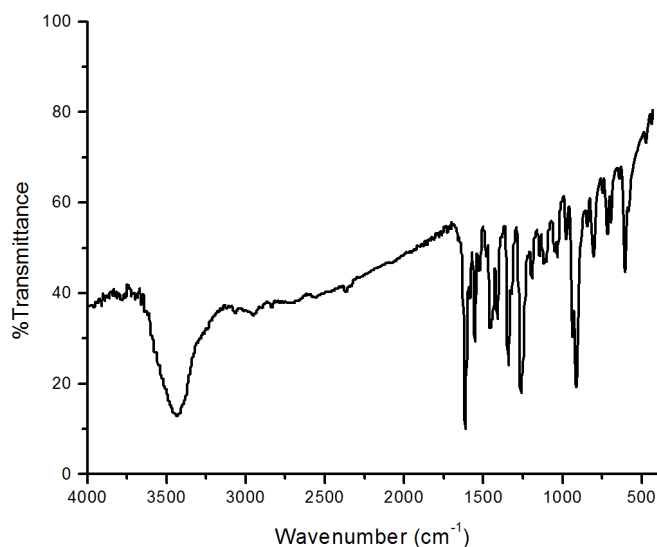


Fig. 8.1. IR spectrum of $[(\text{MoO}_2\text{L}^2)_2] \cdot 2\text{H}_2\text{O}$ (**35**).

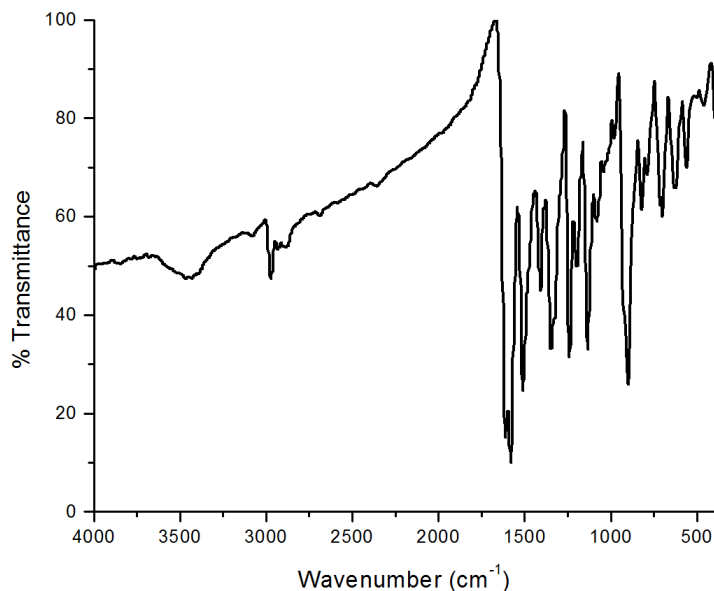


Fig. 8.2. IR spectrum of $[(\text{MoO}_2\text{L}^3)_2]$ (36).

8.3.4. Electronic spectra

The electronic spectra of the hydrazones and the complexes were recorded in DMF and the electronic spectral assignments are given in Table 8.2. The electronic spectra of the hydrazones show bands in the 27020-36990 cm^{-1} region due to $n \rightarrow \pi^*/\pi \rightarrow \pi^*$ transitions. These bands suffered considerable shift in intensity and wavelength on coordination. The complexes show broad bands in the 21110-23620 cm^{-1} region which may be assigned to ligand to metal charge transfer transitions and the absence of any bands in the visible region suggests that the oxidation state of molybdenum is +6 which indicates the diamagnetic behaviour of the complexes. Fig. 8.3 represents the electronic spectra of some of the complexes.

Table 8.2. Electronic spectral assignments (cm^{-1}) of hydrazones and their $\text{MoO}_2(\text{VI})$ complexes

Compound	$n \rightarrow \pi^*/\pi \rightarrow \pi^*$	LMCT
$\text{H}_2\text{L}^1 \cdot \text{C}_3\text{H}_7\text{NO}$	36990, 34130, 28970	----
$[(\text{MoO}_2\text{L}^1)_2]$ (33)	36680, 34140, 29270	23010
$[\text{MoO}_2\text{L}^1\text{DMF}]$ (34)	36950, 29810	23340
$\text{H}_2\text{L}^2 \cdot 2\text{H}_2\text{O} \cdot \text{CH}_3\text{OH}$	33240, 29350	----
$[(\text{MoO}_2\text{L}^2)_2] \cdot 2\text{H}_2\text{O}$ (35)	33090	23620
$\text{H}_2\text{L}^3 \cdot \text{H}_2\text{O}$	36780, 27020	----
$[(\text{MoO}_2\text{L}^3)_2]$ (36)	36740, 27650	21110

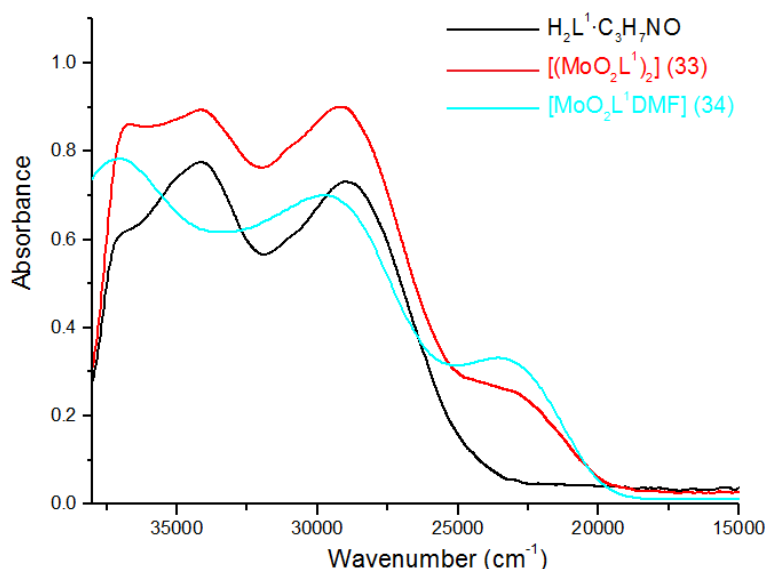


Fig. 8.3. Electronic spectra of $\text{H}_2\text{L}^1 \cdot \text{C}_3\text{H}_7\text{NO}$ and its dioxidomolybdenum(VI) complexes.

8.3.5. X-ray crystallography

Orange block shaped crystals of $[\text{MoO}_2\text{L}^1\text{DMF}]$ (**34**) were obtained by recrystallization from DMF. A single crystal with approximate dimensions of $0.40 \times 0.35 \times 0.30 \text{ mm}^3$ was mounted on a Bruker SMART APEXII CCD

diffractometer equipped with a graphite crystal, incident-beam monochromator and a fine focus sealed tube with Mo K α radiation ($\lambda = 0.71073 \text{ \AA}$) as the X-ray source. The unit cell dimensions were measured and the data collection was performed at 296 K. Bruker SMART software was used for data acquisition and Bruker SAINT software for data integration [26]. Absorption corrections were carried out using SADABS based on Laue symmetry using equivalent reflections [27]. The structure was solved with direct methods and refined with full-matrix least-squares calculations using the SHELXS97 and SHELXL97 [28] software programs respectively. The molecular and crystal structures were plotted using DIAMOND version 3.2g [29]. The crystallographic data and structure refinement parameters for the complex at 296 K are given in Table 8.3. All non-hydrogen atoms were refined anisotropically and all H atoms on C were placed in calculated positions guided by difference maps with C–H bond distances 0.93-0.96 \AA . H atoms were assigned as $U_{\text{iso}}=1.2U_{\text{eq}}$ (1.5 for Me).

The molecular structure of the complex with atom numbering scheme is shown in Fig. 8.4 and relevant bond distances and angles are presented in Table 8.4. The complex crystallizes into a triclinic space group $P\bar{1}$. There are two crystallographically independent molecules in the asymmetric unit of the compound (Fig. 8.5) with bond lengths and angles which agree with each other and are within the normal ranges and are comparable to those observed in other similar dioxidomolybdenum(VI) complexes [30,31]. The coordination geometry around molybdenum can be described as distorted octahedral with phenolate oxygen, imino nitrogen, iminolate oxygen and one oxo oxygen defining the equatorial plane and with DMF and the other oxo oxygen occupying axial positions.

Table 8.3. Crystal data and structure refinement parameters for complex 34

Parameters	[MoO ₂ L ¹ DMF] (34)
Empirical formula	C ₂₄ H ₂₂ MoN ₄ O ₈
Formula weight	590.40
Temperature	296 K
Wavelength	0.71073 Å
Crystal system	Triclinic
Space group	$P\bar{1}$
Unit cell dimensions	$a = 14.0681(12)$ Å $b = 14.0982(12)$ Å $c = 15.2049(12)$ Å $\alpha = 95.301(3)^\circ$ $\beta = 114.053(3)^\circ$ $\gamma = 111.047(3)^\circ$
Volume	2467.2(4) Å ³
Z	4
Density (calculated)	1.589 mg/m ³
Absorption coefficient	0.588 mm ⁻¹
$F(000)$	1200
Crystal size	0.40 × 0.35 × 0.30 mm ³
θ range for data collection	1.80 to 27.00°
Limiting indices	-14 ≤ h ≤ 17 -18 ≤ k ≤ 12 -19 ≤ l ≤ 19
Reflections collected	17880
Unique Reflections (R _{int})	10768 [R(int) = 0.0204]
Refinement method	Full-matrix least-squares on F ²
Data / restraints / parameters	10548 / 0 / 672
Goodness-of-fit on F ²	1.031
Final R indices [I > 2σ(I)]	R ₁ = 0.0377, wR ₂ = 0.0919
R indices (all data)	R ₁ = 0.0573, wR ₂ = 0.1059
Largest diff. peak and hole	1.063 and -0.649 e Å ⁻³

$$R_1 = \frac{\sum ||F_o| - |F_c||}{\sum |F_o|}$$

$$wR_2 = [\sum w(F_o^2 - F_c^2)^2 / \sum w(F_o^2)^2]^{1/2}$$

The hydrazone ligand is coordinated in its dianionic iminolate form which is evident from the C(15)–N(2) and C(15)–O(3) bond lengths with values of 1.292(4) and 1.316(3) Å respectively. In the complex, the dianionic hydrazone ligand is bonded to the MoO₂ core in a planar fashion without changing its *E* configuration with respect to C(14)=N(1) bond. The atoms O(2), N(1), O(3) and O(6) in the complex define a plane with high degree of planarity and the Mo atom is displaced by 0.3264 Å from this plane. The tridentate hydrazone ligand coordinate to Mo atom in a meridional fashion forming five and six membered metallocycles involving the MoO₂²⁺ moiety.

The angular distortion in the octahedral environment around Mo comes from the five and six membered chelate rings taken by the hydrazone ligand so that the *trans* angles and *cis* angles significantly deviate from the ideal values of 180° and 90° respectively. The rings Cg(4) [C(8), C(9), C(10), C(11), C(12), C(13)] and Cg(5) [C(16), C(17), C(18), C(19), C(20), C(21)] make a dihedral angle of 17.10(11)° with each other. The Mo(1)–O(8) bond is longer than the other Mo–O bonds indicating that the DMF molecule is weakly coordinated to the MoO₂ core and this position holds the possibility of functioning as a substrate binding site.

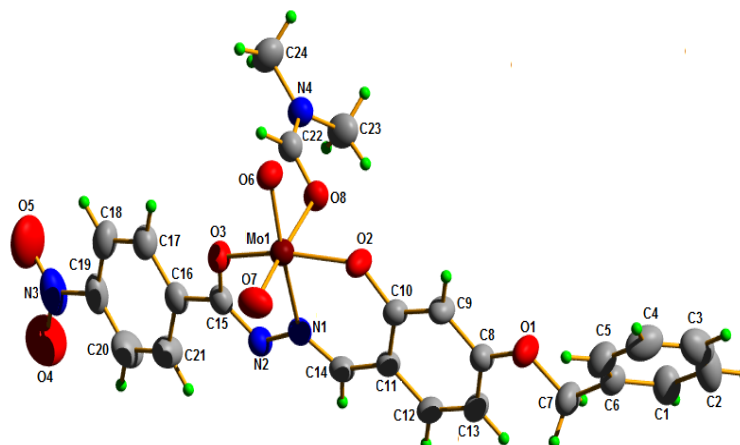


Fig. 8.4. Structure and labelling diagram for $[\text{MoO}_2\text{L}^1\text{DMF}]$ (34).

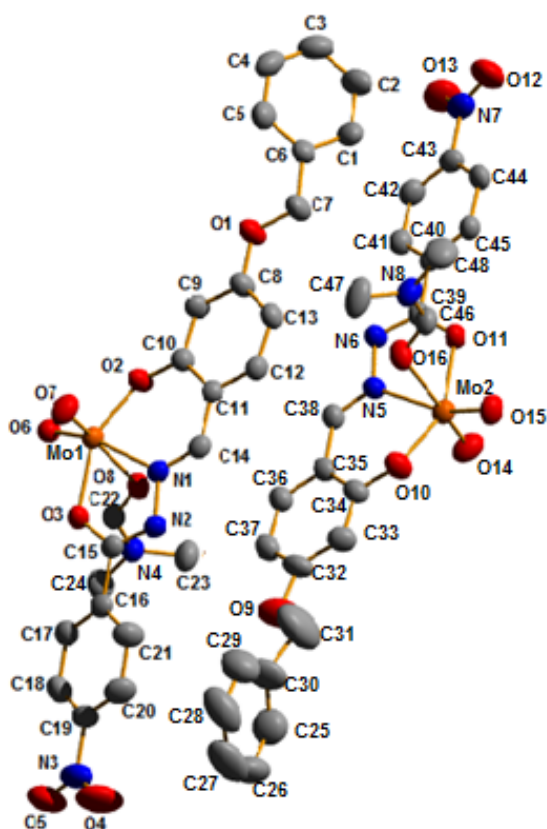


Fig. 8.5. Asymmetric unit of $[\text{MoO}_2\text{L}^1\text{DMF}]$ (34) (hydrogen atoms are omitted for clarity).

Table 8.4. Selected bond lengths and angles for [MoO₂L¹DMF] (34)

Bond lengths (Å)		Bond angles (°)	
Mo(1)–O(7)	1.689(2)	O(7)–Mo(1)–O(6)	104.84(11)
Mo(1)–O(6)	1.705(2)	O(7)–Mo(1)–O(2)	99.95(12)
Mo(1)–O(2)	1.923(2)	O(6)–Mo(1)–O(2)	102.31(9)
Mo(1)–O(3)	2.009(2)	O(7)–Mo(1)–O(3)	97.10(11)
Mo(1)–N(1)	2.217(2)	O(6)–Mo(1)–O(3)	97.19(9)
Mo(1)–O(8)	2.341(2)	O(7)–Mo(1)–N(1)	95.07(10)
Mo(2)–O(14)	1.682(2)	O(2)–Mo(1)–O(3)	149.74(9)
Mo(2)–O(15)	1.701(2)	O(7)–Mo(1)–O(8)	170.90(9)
Mo(2)–O(10)	1.923(2)	O(6)–Mo(1)–N(1)	158.54(10)
Mo(2)–O(11)	2.007(2)	O(14)–Mo(2)–O(15)	104.87(12)
Mo(2)–N(5)	2.218(2)	O(15)–Mo(2)–O(10)	102.52(10)
Mo(2)–O(16)	2.351(2)	O(14)–Mo(2)–O(10)	100.83(12)
C(15)–O(3)	1.316(3)	O(15)–Mo(2)–O(11)	97.47(10)
C(10)–O(2)	1.353(4)	O(14)–Mo(2)–O(11)	96.23(11)
N(1)–C(14)	1.289(4)	O(14)–Mo(2)–N(5)	94.12(10)
C(39)–O(11)	1.313(3)	O(10)–Mo(2)–O(11)	149.27(9)
C(34)–O(10)	1.348(4)	O(14)–Mo(2)–O(16)	170.79(10)
N(5)–C(38)	1.292(4)	O(15)–Mo(2)–N(5)	159.40(11)

There are no conventional hydrogen bonds present in the molecular system. However some weak interactions like $\pi \cdots \pi$, C–H $\cdots\pi$ and C–H \cdots O nonconventional hydrogen bonding interactions are observed in the crystal structure. The adjacent molecules are linked into chains by nonconventional hydrogen bonding interactions as shown in Fig. 8.6. Rings Cg(9) and Cg(10) of neighboring molecules are involved in $\pi \cdots \pi$ stacking with a distance of 3.808(2) Å (Fig. 8.7). C–H $\cdots\pi$ interactions exist between H(1) and Cg(10) [C(40), C(41), C(42), C(43), C(44), C(45)] and H(42) and Cg(3) [C(1), C(2),

C(3), C(4), C(5), C(6)] (Fig. 8.8). The $\pi \cdots \pi$ and C–H $\cdots\pi$ interactions can support the packing stability in the absence of strong conventional hydrogen bonds. The interaction parameters are shown in Table 8.5.

Table 8.5. Interaction parameters of [MoO₂L¹DMF] (34)

Hydrogen bonding interactions				
D–H \cdots A	D–H (Å)	H \cdots A (Å)	D \cdots A (Å)	D–H \cdots A (°)
C(3)–H(3) \cdots O(6) ^a	0.93	2.49	3.330(5)	150
C(22)–H(22) \cdots O(6)	0.93	2.43	2.910(4)	112
C(22)–H(22) \cdots O(15) ^b	0.93	2.51	3.403(4)	161
C(23)–H(23A) \cdots O(8)	0.96	2.39	2.784(5)	104
C(38)–H(38) \cdots O(14) ^c	0.93	2.49	3.181(5)	132
C(46)–H(46) \cdots O(6) ^d	0.93	2.48	3.400(5)	168
C(46)–H(46) \cdots O(15)	0.93	2.55	2.936(5)	105
C(48)–H(48C) \cdots O(16)	0.96	2.39	2.776(6)	104
$\pi \cdots \pi$ interactions				
Cg(I) \cdots Cg(J)	Cg \cdots Cg (Å)	α (°)	β (°)	
Cg(9) \cdots Cg(10) ^e	3.808(2)	8.39(19)	21.41	
C–H$\cdots\pi$ interactions				
C–H(I) \cdots Cg(J)	H \cdots Cg (Å)	C–H \cdots Cg (°)	C \cdots Cg (Å)	
C(1)–H(1) \cdots Cg(10) ^f	2.74	135	3.465(5)	
C(42)–H(42) \cdots Cg(3) ^g	2.83	138	3.577(5)	

Equivalent position codes : a = 1-x, 1-y, -z; b = x, -1+y, z; c = 2-x, 2-y, 1-z; d = x, 1+y, z; e = 2-x, 2-y, 1-z; f = x, y, z; g = 1-x, 2-y, -z
 Cg(3) = C(1), C(2), C(3), C(4), C(5), C(6); Cg(9) = C(32), C(33), C(34), C(35), C(36), C(37);
 Cg(10) = C(40), C(41), C(42), C(43), C(44), C(45)
 D, Donor; A, acceptor; Cg, Centroid; α , dihedral angle between planes I & J; β , angle between Cg \cdots Cg and Cg(J) perp.

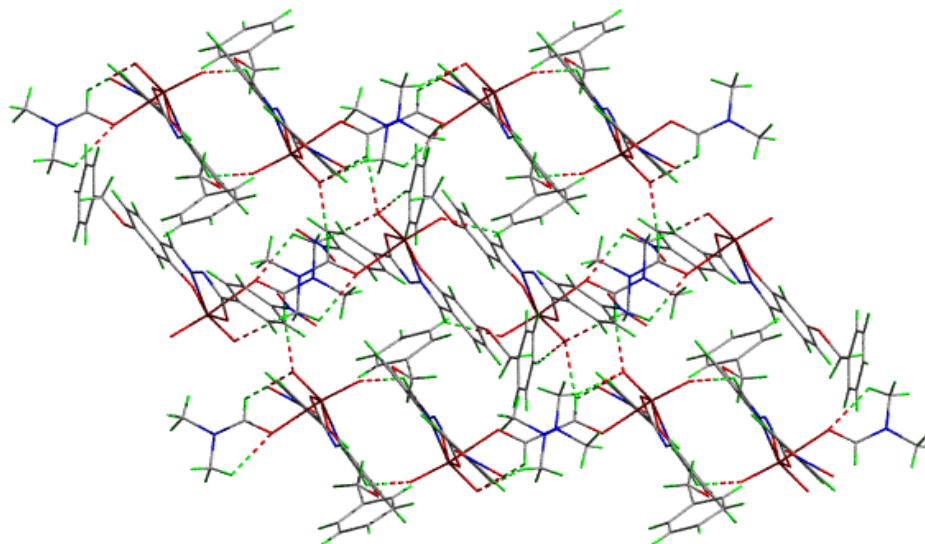


Fig. 8.6. Supramolecular chain mediated by nonconventional hydrogen bonding interactions.

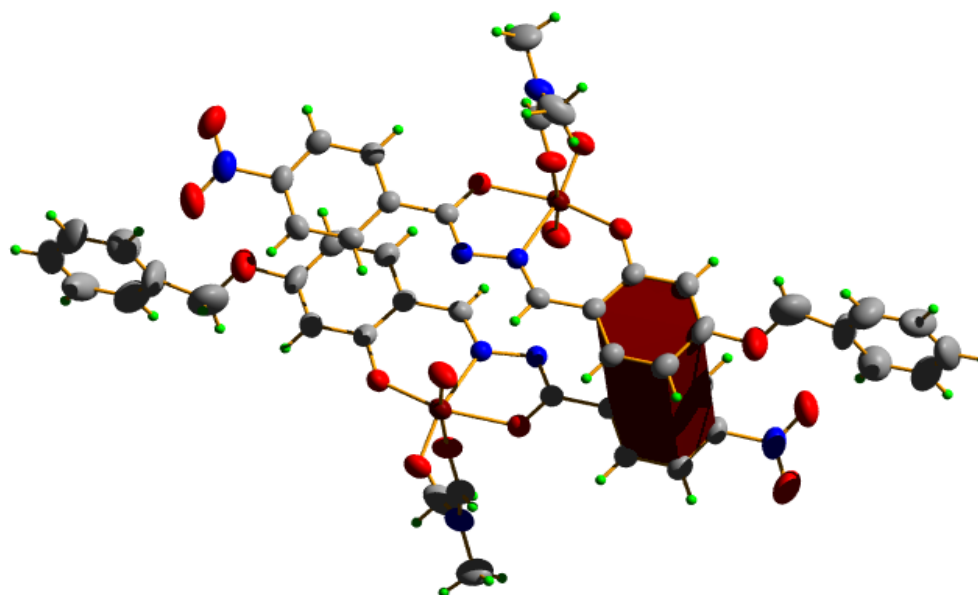


Fig. 8.7. The $\pi \cdots \pi$ interaction present in [MoO₂L¹DMF] (34).

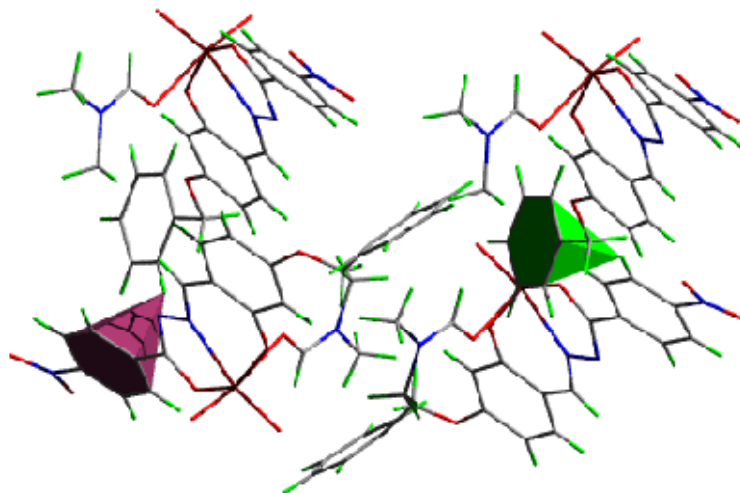


Fig. 8.8. C–H··· π interactions present in [MoO₂L¹DMF] (34).

The unit cell packing diagram of the complex viewed along *b* axis is shown in Fig. 8.9. The coordination polyhedra present in a super cell is shown in Fig. 8.10.

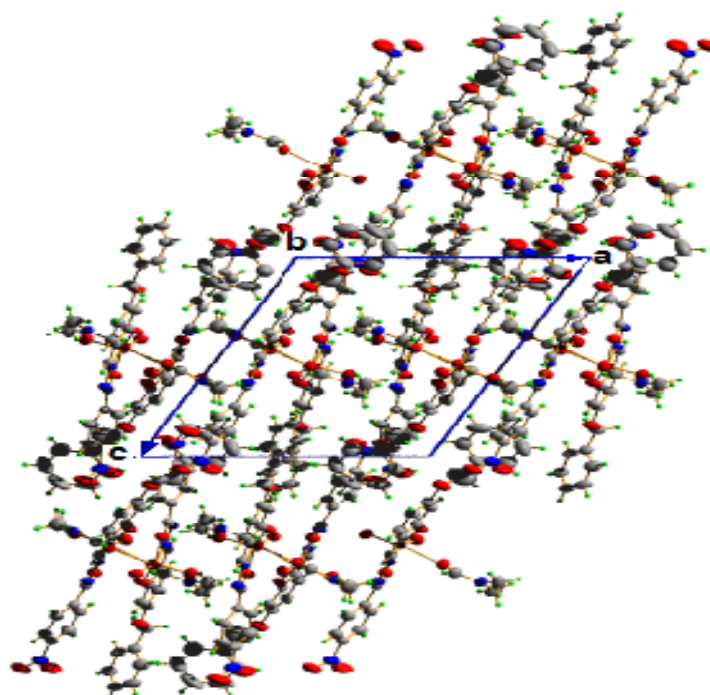


Fig. 8.9. Packing diagram of complex viewed along *b* axis.

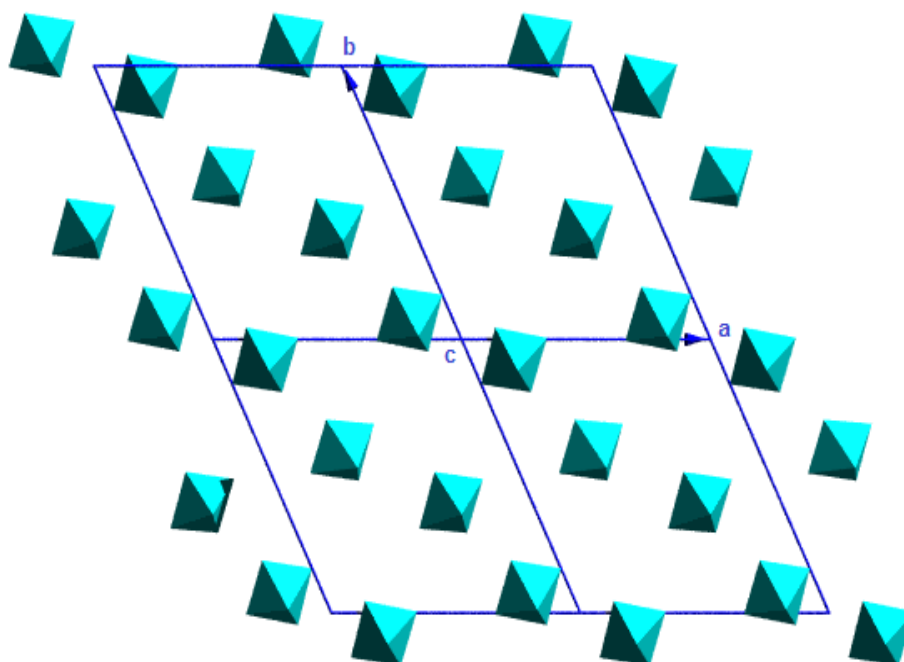


Fig. 8.10. Coordination polyhedra of $[\text{MoO}_2\text{L}^1\text{DMF}]$ (**34**) in a super cell.

8.3.6. Thermogravimetric analysis

The thermogravimetric analysis will give information concerning the thermal stability and nature of water molecules in complexes. Reports show that the weight loss for lattice water are observed below 200 °C and weight loss due to coordinated water are in the 200-350 °C range. The TG curve for the complex $[(\text{MoO}_2\text{L}^2)_2]\cdot 2\text{H}_2\text{O}$ (**35**) shows initially a weight loss of 3.55% in the 162-183 °C range corresponding to the loss of two lattice water molecules (Fig. 8.11). The observed weight loss of 3.55% is close to the calculated value (3.64%). The second weight loss from 284 °C to 321 °C corresponds to the loss of the two Br atoms. The observed weight loss of 16.34% agrees well with the calculated value (16.80%). Beyond 321 °C gradual weight loss

occurs due to the thermal degradation of the remaining contents of the hydrazone ligand and the formation of MoO₃ as the end product [32-34].

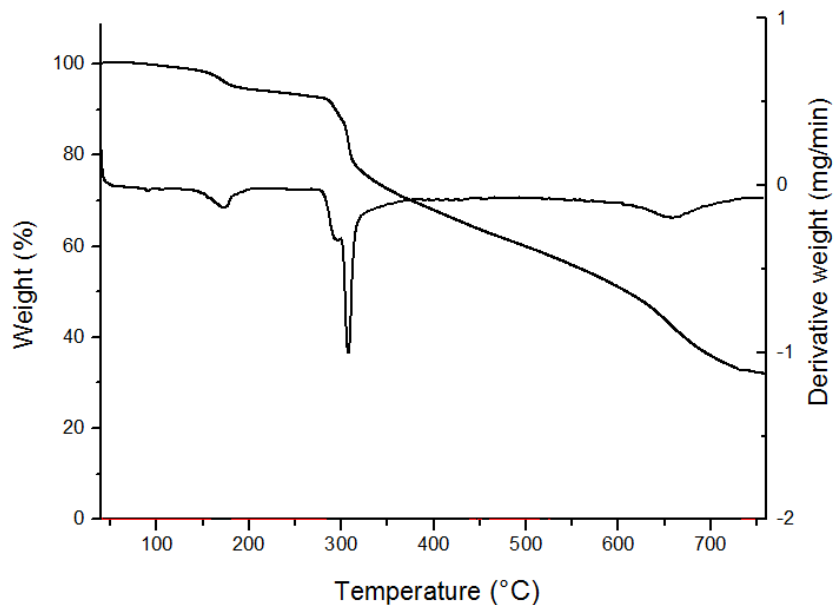
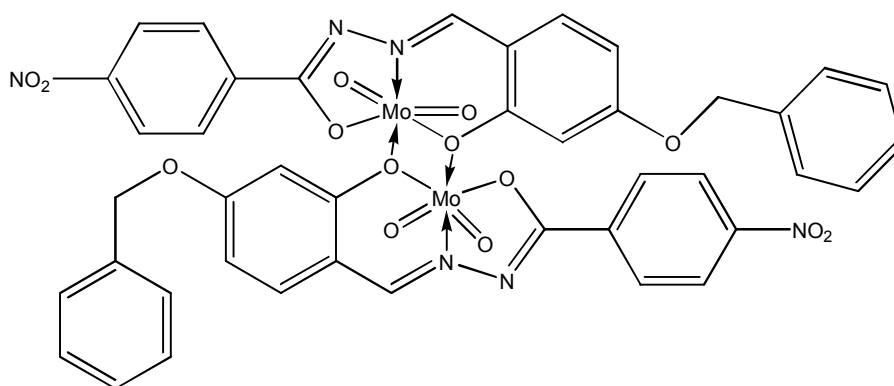
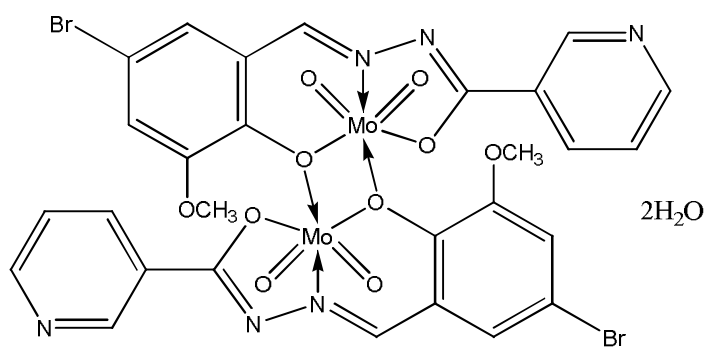


Fig. 8.11. Thermogram of [(MoO₂L²)₂·2H₂O (35).

On the basis of the physico-chemical characterizations discussed above, the tentative structures proposed for some MoO₂(VI) complexes are given below. The MoO₂(VI) complexes synthesized have got octahedral geometry and in all complexes the hydrazones exist in the dideprotonated iminolate form.



$[(\text{MoO}_2\text{L}^1)_2]$ (33)



$[(\text{MoO}_2\text{L}^2)_2] \cdot 2\text{H}_2\text{O}$ (35)

Fig. 8.12. Tentative structures of some of the $\text{MoO}_2(\text{VI})$ complexes.

References

- [1] M.L.H. Nair, D. Thankamani, *Indian J. Chem.* 48 (2009) 1212.
- [2] I. Sheikhsoaie, A. Rezaeffard, N. Monadi, S. Kaafi, *Polyhedron* 28 (2009) 733.
- [3] S.N. Rao, N. Kathale, N.N. Rao, K.N. Munshi, *Inorg. Chim. Acta* 360 (2007) 4010.
- [4] S.D. Perera, B.L. Shaw, M.T. Pett, *Inorg. Chim. Acta* 236 (1995) 7.
- [5] S. Gupta, A.K. Barik, S. Pal, A. Hazra, S. Roy, R.J. Butcher, S.K. Kar, *Polyhedron* 26 (2007) 133.
- [6] A.A. Soliman, S.A. Ali, A. Orabi, *Spectrochim. Acta A* 65 (2006) 841.
- [7] M. Tamm, B. Drebel, V. Urban, T. Lugger, *Inorg. Chem. Commun.* 5 (2002) 837.
- [8] S.A. Roberts, C.G. Young, C.A. Kipke, W.E. Cleland, K. Yamanouchi, M.D. Carducci, J.H. Enemark, *Inorg. Chem.* 29 (1990) 3650.
- [9] N. Mathew, M.R.P. Kurup, *Spectrochim. Acta A* 78 (2011) 1424.
- [10] M. Saleem, M. Sharma, H.N. Sheikh, B.L. Kalsotra, *Indian J. Chem.* 46 (2007) 1423.
- [11] W.X. Xu, W.H. Li, *Russ. J. Coord. Chem.* 38 (2012) 92.
- [12] S. Pasayat, S.P. Dash, S. Majumder, R. Dinda, E. Sinn, H.S. Evans, S. Mukhopadhyay, S.K. Bhutia, Mitra, *Polyhedron* 80 (2014) 198.
- [13] N.K. Ngan, K.M. Lo, C.S.R. Wong, *Polyhedron* 33 (2012) 235.
- [14] S. Pasayat, S.P. Dash, Saswati, P.K. Majhi, Y.P. Patil, M. Nethaji, H.R. Dash, S. Das, R. Dinda, *Polyhedron* 38 (2012) 198.
- [15] V. Vrdoljak, J. Pisk, D. Agustin, P. Novak, J.P. Vukovic, D.M. Calogovic, *New J. Chem.* 38 (2014) 6176.
- [16] R. Debel, A. Buchholz, W. Plass, *Z. Anorg. Allg. Chem.* 634 (2008) 2291.

- [17] M. Mancka, W. Plass, *Inorg. Chem. Commun.* 10 (2007) 677.
- [18] K.J. Ivin, J.C. Mol, *Olefin Metathesis Polymerization*, Academic Press, London (1997).
- [19] R.K. Grasselli, *Catal. Today* 49 (1999) 141.
- [20] J. Belgacem, J. Kress, J.A. Osborn, *J. Am. Chem. Soc.* 114 (1992) 1501.
- [21] S.K. Patil, V.M. Naik, N.B. Mallur, *Der Pharma Chemica* 4 (2012) 1812.
- [22] M.L.H. Nair, M.S. Pramila, *Asian J. Chem.* 20 (2008) 2504.
- [23] K. Andjelkovic, M. Sumar, I.I. Burmazovic, *J. Therm. Anal. Cal.* 66 (2001) 759.
- [24] W.J. Geary, *Coord. Chem. Rev.* 7 (1971) 81.
- [25] S.B. Ding, W.H. Li, *J. Coord. Chem.* 66 (2013) 2023.
- [26] SMART and SAINT, Area Detector Software Package and SAX Area Detector Integration Program, Bruker Analytical X-ray; Madison, WI, USA, 1997.
- [27] Bruker, SADABS, APEX2, XPREP and SAINT, Bruker AXS Inc., Madison, Wisconsin, USA, 2004.
- [28] G.M. Sheldrick, *Acta Cryst. A* 64 (2008) 112.
- [29] K. Brandenburg, Diamond Version 3.2g, Crystal Impact GbR, Bonn, Germany, 2010.
- [30] Q.S. Zong, *Synth. React. Inorg. Met-Org. Nano-Met. Chem.* 43 (2013) 1423.
- [31] S.X. Wang, *Acta Cryst. E* 68 (2012) m358.
- [32] S. Kavlak, H.K. Can, Z.M.O. Rzaev, A. Guner, *J. Appl. Polym. Sci.* 100 (2006) 3926.
- [33] S.S. Qian, X.S. Cheng, Z.L. You, H.L. Zhu, *Acta Chim. Slov.* 60 (2013) 870.
- [34] W. Jingping, H. Qiuxia, N. Jingyang, *J. Coord. Chem.* 57 (2004) 33.

..........

**STUDIES ON SECOND ORDER NONLINEAR OPTICAL
PROPERTIES OF AROYLHYDRAZONES AND SOME TRANSITION
METAL CHELATES**

Contents	9.1 Introduction
	9.2 Experimental
	9.3 Results and discussion
	References

9.1. Introduction

Nonlinear optics (NLO) is concerned with the nonlinear relationship between dielectric polarization P and electric field E in optical media. Nonlinear optics is a cornerstone of the emerging field of photonics in which photons instead of electrons are used for signal transmission and processing [1,2]. The field of nonlinear optics is complex and encompasses myriads of interesting effects and applications in the field of laser technology, fiber optic communication and optoelectronics [3-6]. Nonlinear optical materials play an important role in nonlinear optics and in particular they have a great impact on information technology and industrial applications. Nonlinear optical materials have been used in electro-optic devices for more efficient processing and transmitting information in the field of fiber optic communications. In a series of developments ranging from the use of wires to send signals along

wire telegraphy to wireless or radio telegraphy, science has achieved an increase of communication rates as measured in bits per second by a factor of one billion. The latest in this series of advances is an optical fibre system in which large amounts of information coded as light pulses are passed along optical fibres. The phenomenon of optical power limiting, a nonlinear optical effect has attracted much attention due to its application to the protection of eyes and sensitive optical devices from high power laser pulses [7].

In order to satisfy the day-to-day technological requirements, many scientists focused their attention on the growth of materials which have a good nonlinear optical behavior and be optically transparent in the visible region. Nonlinear optical phenomena occur only on the application of intense electromagnetic fields. The advent of laser has led to the systematic studies of several nonlinear optical phenomena as laser is sufficiently intense to make changes in the optical properties of the molecular systems. Nonlinear optical materials have a nonlinear response to the electric field associated with the light of a laser beam leading to the transformation of light of one wavelength to the light of another wavelength. Second harmonic generation (SHG) is one of the major nonlinear optical processes in which a nonlinear optical material mediates the adding-up of two photons to form new one with twice the frequency [8]. After this discovery, numerous nonlinear optical phenomena have been studied and a number of NLO-active materials have been developed [9-12].

9.1.1. Theoretical explanation of nonlinear optics

Nonlinear optics is concerned with the alterations in frequency, phase or other physical properties of intense applied electromagnetic fields on

interaction with various materials. The interaction of intense electromagnetic field with a nonlinear optical material will cause the material properties to change and the next photon that arrives will see a different material. The propagation of a wave through a material causes changes in the spatial distribution of electric charges as the charged species in the material (ions or electrons) interact with the electric field of the wave. In a nonlinear optical material, strong interactions can exist among the various fields. The main effect of these interactions is the displacement of the valence electrons from their normal orbits. This perturbation develops electric dipoles whose macroscopic manifestation is the polarization. The displacement of the electron density away from the nucleus results in a charge separation which produces induced dipoles with moment μ . This results in new fields, created by oscillating dipoles within the materials.

At moderate field strength the displacement of charge from the equilibrium position is proportional to the electric field and a linear relationship of the induced polarization with the applied field is observed.

$$\text{Polarization, } P = \epsilon_0 \chi E \dots\dots\dots(1)$$

where χ is the linear polarizability of the material, E is the electric field component of the incident light and ϵ_0 is the permittivity of free space.

At sufficiently intense fields such as electric fields from pulsed laser beams which can approach the magnitude of typical internal fields in crystals, polarization becomes independent of the field and a nonlinear optical phenomenon is observed. Therefore, this nonlinear response is expressed by writing the induced polarization as a power series in the field.

$$P = \sum \epsilon_0 \chi^{(n)} E^{(n)} \dots\dots\dots (2)$$

$$P = \epsilon_0 (\chi_{ij}^{(1)} E_j + \chi_{ijk}^{(2)} E_j E_k + \chi_{ijkl}^{(3)} E_j E_k E_l + \dots) \dots\dots\dots (3)$$

where $\chi^{(2)}$, $\chi^{(3)}$ are the nonlinear susceptibilities of the medium. $\chi^{(1)}$ is the linear term responsible for material's linear optical properties like refractive index, dispersion and absorption. $\chi^{(2)}$ is the quadratic term which describes second harmonic generation in noncentrosymmetric materials. $\chi^{(3)}$ is the cubic term responsible for third harmonic generation. Hence the induced polarization is capable of multiplying the fundamental frequency to second, third and even higher harmonics.

9.1.2. Second harmonic generation

Second harmonic generation (SHG) is a nonlinear optical process in which photons interacting with nonlinear optical materials are effectively combined to form new photons with twice the energy and therefore, twice the frequency and half the wavelength of the initial photons. The compound should have high second order hyperpolarizability (β) to exhibit large NLO properties. The hyperpolarizability can be enhanced by increasing intramolecular charge transfer interaction by extending the π -conjugated system. The generation of second harmonic phenomenon is represented in Fig. 9.1.

Second harmonic generation was first demonstrated by Franken *et al.* in 1961 [13]. The demonstration was made possible by the invention of the laser which created the required high intensity monochromatic light. They focused a ruby laser with a wavelength of 694 nm into a quartz sample that results in the conversion of 694 nm wavelength into an output light of 347 nm wavelength (Fig. 9.2). This phenomenon occurs only within a noncentrosymmetric medium, usually a crystal.

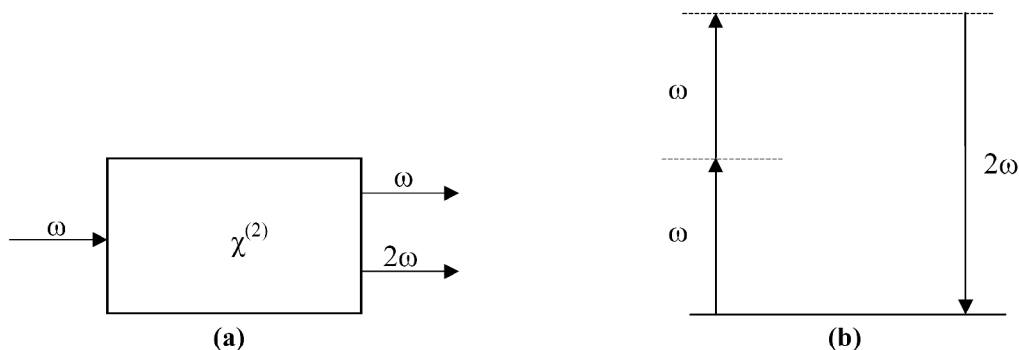


Fig. 9.1.(a). Geometry of second harmonic generation (b). Energy level diagram describing second harmonic generation.

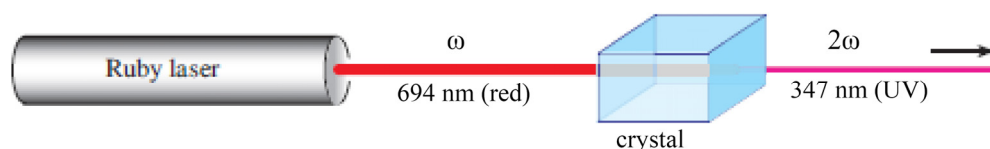


Fig. 9.2. Schematic illustration of optical frequency doubling.

The light propagated through a noncentrosymmetric crystalline medium generates light at second harmonics of the applied frequency. Such frequency doubling processes are generally used to produce green light (532 nm) from a Nd-YAG laser operating at 1064 nm. This important nonlinear property of noncentrosymmetric crystals is called second harmonic generation and this phenomenon is useful in optical communications, photonics and electro-optic devices, enriching the development of new nonlinear optical materials of inorganic and organic types.

9.1.3. Second order nonlinear optical materials

9.1.3.1. Design of molecules for second order nonlinear optics

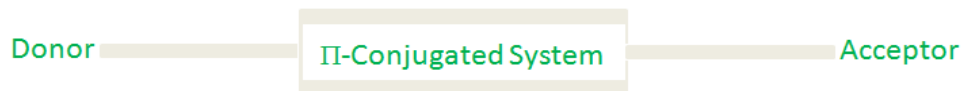
In recent years, there has been a growing interest in the studies of the nonlinear optical properties of different materials because of their practical use

in optoelectronic devices. Second harmonic generation (SHG) is one of the major nonlinear optical processes and is extensively explored. Second harmonic generation exists only in noncentrosymmetric materials. If the molecule is centrosymmetric, then $\chi^{(2)}$ in eqn. (3) is zero. The response of centrosymmetric molecules to an external field is given by $P(-E) = -P(E)$. This relation expresses the requirement that the induced polarization of centrosymmetric molecules is opposite and of equal magnitude when the field is reversed. In order to satisfy this condition, all coefficients of even power of E in eqn. (3) have to be zero. Hence only noncentrosymmetric molecules have a nonzero $\chi^{(2)}$ value, since then $P(-E) \neq -P(E)$.

However, for a noncentrosymmetric compound to be used as NLO material, the essential requirements are that the molecules possess a large NLO response, good mechanical strength, chemical stability and be optically transparent in the visible and near IR regions [14].

The preliminary step for the syntheses of a second order nonlinear optical material involves the identification of suitable NLO chromophores. NLO chromophores are molecules with electron donor and acceptor conjugated π -systems. The design strategy for NLO chromophores used by many with success involves connecting donor and acceptor groups at the terminal position of a π -bridge to create highly polarized molecules which could exhibit large molecular nonlinearity [15]. This indicates that optical nonlinearity of molecules can be enhanced by adding strong electron donating and withdrawing entities as well as adjusting the distance between donor and acceptor groups. This creates a highly polarizable charge transfer compound with an asymmetric electron distribution in either or both the ground and

excited states, thus leading to an increased optical nonlinearity. Several authors have pointed out the importance of charge delocalization in highly conjugated systems and emphasized the importance of charge transfer between donor and acceptor substituents on extended π -electron systems such as substituted benzene molecules. The types of π bridges investigated for developing efficient NLO materials and molecules are acetylenes, azobridges, hydrazones, semicarbazones, aromatic and heteroaromatic rings [16-21]. The magnitude of molecular polarizability and hyperpolarizability coefficients are found to increase linearly with an increase in conjugation length between donor and acceptor groups. The strength of donor and acceptor groups and the packing of molecules to build a noncentrosymmetric crystal structure plays important roles in determining the magnitude of nonlinear optical efficiency [22].



For NLO active metal complexes the primary role played by the metal is that of generating the actual push-pull chromophore. The use of some transition metals should force the ligand in a planar conformation so as to maximize conjugation [23]. Proper choice of the ligand, metal and its oxidation state allows the compound to show excellent NLO activity.

It has also been established that hydrogen bonds play a vital role in governing the NLO property [24]. Pure inorganic NLO materials, potassium dihydrogen phosphate (KDP) and its isomorphs are representative of hydrogen bonded materials which possess important electro-optic and nonlinear optical properties with excellent mechanical strength and thermal stability. The effect

of hydrogen bonding will increase the hyperpolarizability value which is essential and required property for a system to exhibit SHG efficiency. Another requirement for a good nonlinear optical material is that it should have excellent optical quality. This means that for new materials for which single crystals are not available it is necessary to grow single crystals of optical quality. Thus in many cases the search for new and better nonlinear optical materials is very largely a crystal growing effort. During the last two decades, a large number of nonlinear optical molecules have been synthesized and investigated allowing researchers to gain insight into the chemistry and physics of optical hyperpolarizabilities.

9.1.3.2. Inorganic materials as second order NLO materials

In the beginning, NLO studies were concentrated on inorganic materials such as quartz, potassium dihydrogen phosphate (KDP), potassium titanyl phosphate (KTP), beta barium borate and cadmium sulfide [25-27]. These compounds are found to exhibit very good SHG response. Even though inorganic crystals are used as nonlinear optical materials, they have several drawbacks such as difficulty to grow high quality single crystals, their higher expenses and the difficulty in incorporating them into electronic devices.

9.1.3.3. Organic molecules as second order NLO materials

It has been shown that certain classes of organic molecules have large second order nonlinear hyperpolarizabilities [28]. Organic nonlinear materials have a number of potential advantages over inorganic materials. Specifically they have been investigated due to their small dielectric constants, good optical properties, large nonlinear optical susceptibilities and rapid response in electro-optic effect. Considerable studies have been done in order to

understand the origin of nonlinear behavior of organic NLO materials. Rentzepis and Pao observed SHG in 3,4-benzopyrene in 1964 [29]. These materials offer many possibilities to tailor materials with the desired properties through optimization of the microscopic hyperpolarizabilities and the incorporation of molecules in a crystalline lattice and polymers [30].

9.1.3.4. Hydrazones as second order NLO materials

There is currently a considerable effort to develop materials with large second order nonlinear optical susceptibilities because of their potential applications in optical signal processing and frequency conversion. For nonlinear optical materials with large second order nonlinearities, noncentrosymmetry is a prerequisite for nonvanishing molecular hyperpolarizabilities and macroscopic susceptibilities. Among organic materials, hydrazones and their derivatives have recently attracted much attention due to their high tendency to crystallize in asymmetric structure and for their synthetic flexibility that can offer the modification of nonlinear properties. Nonlinear optical properties shown by some hydrazones and their metal complexes offer their use in optoelectronic devices [31]. To date, compounds that have been developed for applications in nonlinear optics are built from donor-acceptor conjugated molecules. It is well established that the extension of the conjugation path (transmitter) between the electron donating and withdrawing groups strongly increases the molecular nonlinearity. Serbutoviez *et al.* prepared some compounds based on push-pull derivatives of benzaldehyde phenylhydrazone and thiophenecarboxaldehyde phenylhydrazone. Since the hydrazone backbone is an asymmetric transmitter it allows for a given donor and acceptor group, the preparation of two different types of compounds: I and II, which are potentially active for second order nonlinear optics (Fig. 9.3). The hydrazone backbone can be considered as a

9.1.4. NLO measurements

Kurtz and Perry powder method is an important tool for studying nonlinear optical properties of organic and inorganic NLO materials [35]. It is a popular method to evaluate the second harmonic generation efficiencies of nonlinear optical materials. The experimental arrangement for the nonlinear optical studies utilizes a Quanta-Ray DCR II Nd: YAG laser. The well powdered sample was illuminated by a laser beam of fundamental wavelength 1064 nm, with pulse width of 10 ns and repetition rate 10 Hz. An output signal of 532 nm (green) was measured in a 90° geometry using KDP as the standard.

9.2. Experimental

9.2.1. Syntheses of hydrazones

The syntheses of hydrazones 4-benzyloxy-2-hydroxybenzaldehyde-4-nitrobenzoylhydrazone dimethylformamide monosolvate ($H_2L^1 \cdot C_3H_7NO$), 5-bromo-2-hydroxy-3-methoxybenzaldehyde nicotinoylhydrazone dihydrate methanol monosolvate ($H_2L^2 \cdot 2H_2O \cdot CH_3OH$), 4-diethylamino-2-hydroxybenzaldehyde nicotinoylhydrazone monohydrate ($H_2L^3 \cdot H_2O$) and 2-benzoylpyridine-4-nitrobenzoylhydrazone (HL^4) have already discussed in Chapter 2.

9.2.2. Syntheses of transition metal chelates

The syntheses of transition metal chelates have already discussed in Chapters 3-8.

9.2.3. Second harmonic generation studies

The relative SHG efficiency of hydrazones and complexes with respect to KDP was made by the Kurtz and Perry powder technique. The finely

powdered sample was packed in capillary tube having 0.8 mm thickness. The experimental arrangement for the nonlinear optical studies utilizes a Quanta-Ray DCR II Nd: YAG laser. The sample was illuminated by a laser beam of fundamental wavelength 1064 nm, with pulse width of 10 ns and repetition rate 10 Hz. The output from the sample was monochromated to collect the intensity of 532 nm components and the fundamental was eliminated. The second harmonic radiation generated by the randomly oriented sample was focused by a lens and detected by a photo multiplier tube. A strong bright green emission emerging from the mounted sample shows that the sample exhibits good NLO property. KDP was used as a reference material for the present measurements.

9.3. Results and discussion

The nonlinear optical properties of $H_2L^1 \cdot C_3H_7NO$, $H_2L^2 \cdot 2H_2O \cdot CH_3OH$, $H_2L^3 \cdot H_2O$, HL^4 and transition metal chelates of $H_2L^1 \cdot C_3H_7NO$ were studied in powder form by Kurtz and Perry powder technique. The second harmonic generation efficiencies of the compounds were determined using Nd: YAG laser of fundamental wavelength 1064 nm and microcrystalline powder of KDP as the reference material. Second harmonic radiation generated by the sample was focussed by a lens and detected by a photomultiplier tube. The second harmonic generation in the compounds is confirmed by the emission of green light from the samples. Only $H_2L^1 \cdot C_3H_7NO$, $[CdL^1(H_2O)]_2$ (**28**), $[CdL^1pic]$ (**29**) and $[CdL^1py]$ (**30**) are found to possess SHG activity. For a laser input of 6 mJ/pulse, the SHG signal (532 nm) of 25.2 mV, 111 mV, 22 mV, 23.2 mV and 24.0 mV were obtained for KDP, $H_2L^1 \cdot C_3H_7NO$, $[CdL^1(H_2O)]_2$ (**28**), $[CdL^1pic]$ (**29**) and $[CdL^1py]$ (**30**) respectively. The results indicate that the second harmonic generation efficiency of $H_2L^1 \cdot C_3H_7NO$ is

about 4.40 times that of potassium dihydrogen phosphate (KDP). The high value of SHG efficiency of $\text{H}_2\text{L}^1\cdot\text{C}_3\text{H}_7\text{NO}$ may be attributed to the contributions from the donor- π -acceptor benzyloxy-nitro functionality and hydrogen bonding interactions in the crystal system. The second harmonic generation efficiencies of the samples with respect to KDP are summarized in the Table 9.1.

Table 9.1. Second harmonic generation efficiency of the compounds with respect to KDP

Compound	SHG efficiency w.r. to KDP
$\text{H}_2\text{L}^1\cdot\text{C}_3\text{H}_7\text{NO}$	4.40
$[\text{CdL}^1(\text{H}_2\text{O})]_2$ (28)	0.87
$[\text{CdL}^1\text{pic}]$ (29)	0.92
$[\text{CdL}^1\text{py}]$ (30)	0.95

SHG activity of KDP = 1

Conclusion

Kurtz-Perry powder SHG test confirms the frequency doubling of the samples $\text{H}_2\text{L}^1\cdot\text{C}_3\text{H}_7\text{NO}$, $[\text{CdL}^1(\text{H}_2\text{O})]_2$ (**28**), $[\text{CdL}^1\text{pic}]$ (**29**) and $[\text{CdL}^1\text{py}]$ (**30**). It is observed that the efficiency of $\text{H}_2\text{L}^1\cdot\text{C}_3\text{H}_7\text{NO}$ is 4.40 times as large as KDP. The second harmonic generation efficiencies of $[\text{CdL}^1(\text{H}_2\text{O})]_2$ (**28**), $[\text{CdL}^1\text{pic}]$ (**29**) and $[\text{CdL}^1\text{py}]$ (**30**) are 0.87, 0.92 and 0.95 times respectively that of KDP.

References

- [1] D.N. Nikogosian, *Nonlinear Optical Crystals: A Complete Survey*; Springer-Science, New York, 2005.
- [2] K. Jain, G.W. Pratt, *Appl. Phys. Lett.* 28 (1976) 719.
- [3] P.N. Prasad, D.J. Williams, *Introduction to Nonlinear Optical Effects in Molecules and Polymers*, Wiley-Interscience, New York, 1991.
- [4] X.Q. Wang, D. Xu, D.R. Yuan, Y.P. Tian, W.T. Yu, S.Y. Sun, Z.H. Yang, Q. Fang, M.K. Lu, Y.X. Yan, F.Q. Meng, S.Y. Guo, G.H. Zhang, M.H. Jiang, *Mater. Res. Bull.* 34 (2003) 199.
- [5] I. Ledoux, *Synth. Metal* 54 (1993) 123.
- [6] M. Iwai, T. Kobayashi, H. Fuyra, Y. Mori, T. Sasaki, *Jpn. J. Appl. Phys.* 36 (1997) 276.
- [7] L. Vivien, N. Izard, D. Riehl, F. Hache, E. Anglaret, *AIP Conf Proc.* 685 (2003) 559.
- [8] C. Wang, T. Zhang, W. Lin, *Chem. Rev.* 112 (2012) 1084.
- [9] N.J. Long, *Angew. Chem. Int. Ed. Engl.* 34 (1995) 21.
- [10] I.C. Khoo, *Liquid Crystals-Physical Properties and Nonlinear Optical Phenomena*, Wiley, New York, 1995.
- [11] B.A.E. Saleh, M.C. Teich, *Fundamentals of Photonics*, Wiley, New York, 1991.
- [12] D.S. Chemla, J. Zyss, *Nonlinear Optical Properties of Organic Molecules and Crystals*, Academic Press, New York, 1987.
- [13] P.A. Franken, A.E. Hill, C.W. Peters, G. Weinreich, *Phys. Rev. Lett.* 7 (1961) 118.
- [14] J.T.J. Prakash, L.R. Nirmala, *Int. J. Comput. Appl.* 6 (2010) 7.

- [15] K. Naseema, K.V. Sujith, K.B. Manjunatha, B. Kalluraya, G. Umesh, V. Rao, *Optic. Laser Tech.* 42 (2010) 741.
- [16] L.T. Cheng, W. Tam, S.H. Stevenson, G.R. Meredith, G. Rikken, S.R. Marder, *J. Phys. Chem.* 95 (1991) 10631.
- [17] C.R. Moylan, R.J. Tweig, V.Y. Lee, S.A. Swanson, K.M. Betterton, R.D. Miller, *J. Am. Chem. Soc.* 115 (1993) 12599.
- [18] G.A. Babu, R.P. Ramasamy, P. Ramasamy, S. Natarajan, *J. Cryst. Growth* 311 (2009) 3461.
- [19] N. Vijayan, R. Ramesh Babu, R. Gopalakrishnan, S. Dhanuskodi, P. Ramasamy, *J. Cryst. Growth* 233 (2001) 863.
- [20] L.T. Cheng, W. Tam, S.R. Marder, A.E. Steigman, G. Rikken, C.W. Spangler, *J. Phys. Chem.* 95 (1991) 10643.
- [21] V.P. Rao, Y.M. Cai, A.K.Y. Jen, *Chem. Commun.* (1994) 1689.
- [22] T. Dhanabal, G. Amirthaganesan, M. Dhandapani, S.K. Das, *J. Mol. Struct.* 1035 (2013) 483.
- [23] J. Buey, S. Coco, L. Diez, P. Espinet, J.M.M. Alvarez, J.A. Miguel, *Organomet.* 17 (1998) 1750.
- [24] C. Lei, Z. Yang, B. Zhang, M.H. Lee, Q. Jing, Z. Chen, X.C. Huang, Y. Wang, S. Pan, M.R.S.A. Janjua, *Phys. Chem. Chem. Phys.* 16 (2014) 20089.
- [25] C. Loth, D. Bruneau, E. Fabre, *Appl. Opt.* 19 (1980) 1022.
- [26] M.E. Hagerman, K.R. Poepelmeier, *Chem. Mater.* 7 (1995) 602.
- [27] L.J. Bromley, A. Guy, D.C. Hanna, *Opt. Commun.* 67 (1988) 316.
- [28] P.C. Ray, *Chem. Rev.* 110 (2010) 5332.
- [29] P.M. Rentzepis, Y.H. Pao, *Appl. Phys. Lett.* 5 (1964) 156.
- [30] A.H. Reshak, H. Kamarudin, S. Auluck, *J. Phys. Chem.* 116 (2012) 4677.

- [31] S.Y. Ebrahimipour, I. Sheikhshoae, A. Crochet, M. Khaleghi, K.M. Fromm, *J. Mol. Struct.* 1072 (2014) 267.
- [32] C. Serbutoviez, C. Bosshard, G. Knopfle, P. Wyss, P. Pretre, P. Gunter, K. Schenk, E. Solari, G. Chapuis, *Chem. Mater.* 7 (1995) 1198.
- [33] P. Gu, X. Xu, F. Zhou, T. Zhao, G. Ye, G. Liu, Q. Xu, J. Ge, J. Lu, *Chin. J. Chem.* 32 (2014) 205.
- [34] F. Cariati, U. Caruso, R. Centore, W. Marcolli, A. De Maria, B. Panunzi, M.A. Roviello, A. Tuzi, *Inorg. Chem.* 41 (2002) 6597.
- [35] S.K. Kurtz, T.T. Perry, *J. Appl. Phys.* 39 (1968) 3798.

.....✂.....

SUMMARY AND CONCLUSIONS

Aroylhydrazones are a class of azomethines with the structure $\text{Ar-CO-NH-N=CR}_1\text{R}_2$. They are distinguished from other members of this family by the presence of two interlinking nitrogen atoms and are formed usually by the condensation of aroylhydrazides with ketones or aldehydes. Amido-iminol tautomerism occurs readily in hydrazones and has an important role in determining the overall charge on the ligands coordinating the metal ions. Thus coordination complexes derived from hydrazones contain either neutral amido form or deprotonated iminolate form. The coordination mode adopted by a hydrazone can be altered by the use of suitable substituents both in the carbonyl and hydrazide part.

There is a growing interest in the structural studies of aroylhydrazones as they show a broad spectrum of applications in pharmaceutical and industrial fields. The aroylhydrazones show a variety of biological activities with potential uses in antibacterial, antifungal and anticancer studies. In addition, their varied coordinating behavior makes them interesting candidates for metal-based drugs. In many cases it was reported that metal chelates possess better biological activities than their corresponding ligands. Hydrazones and their metal complexes have found applications in chemical processes like non linear optics, sensors etc. Donor- π -Acceptor type aroylhydrazones play an

important role in the second harmonic generation efficiency. The wide transparency window in the visible region makes them ideal candidates for NLO applications.

The ability of aroylhydrazones to bind with transition metals is a developing area of research interest and the coordinating properties of hydrazones can be tuned by the appropriate choice of parent aldehyde or ketone and the hydrazide. So in the present work we selected four different aroylhydrazones as principal ligands. Introduction of heterocyclic bases like 1,10-phenanthroline, 2,2'-bipyridine, 3-picoline and pyridine leads to the syntheses of mixed ligand metal chelates which can cause different bonding modes, spectral properties and geometries in coordination compounds. The importance of aroylhydrazones and their complexes in various fields and their interesting coordinating properties stimulate our interest in the investigation of transition metal chelates with four different aroylhydrazones. The aroylhydrazones selected are 4-benzyloxy-2-hydroxybenzaldehyde-4-nitrobenzoylhydrazone dimethylformamide monosolvate, 5-bromo-2-hydroxy-3-methoxybenzaldehyde nicotinoylhydrazone dihydrate methanol monosolvate, 4-diethylamino-2-hydroxybenzaldehyde nicotinoylhydrazone monohydrate and 2-benzoylpyridine-4-nitrobenzoylhydrazone. The selection of 4-benzyloxy-2-hydroxybenzaldehyde-4-nitrobenzoylhydrazone was based on the idea of developing ligands having D- π -A general structure, so that the proligand and metal complexes exhibit NLO activity. Hence it is interesting to explore the coordinating capabilities of the synthesized hydrazones and to study the NLO activity of hydrazones and some of the metal complexes.

The work presented in this thesis is divided into nine chapters.

Chapter 1

Chapter 1 entitled 'A brief outline on aroylhydrazones' involves a general introduction to aroylhydrazones, coordination diversity of aroylhydrazones and their applications in various fields. The objectives of the present work and the details of different physico-chemical techniques used for the characterization of aroylhydrazones and their metal complexes are also discussed in this chapter.

Chapter 2

Chapter 2 deals with the syntheses of four different aroylhydrazones and their characterization by elemental analyses, mass, FT-IR, UV-Vis and ^1H NMR spectral studies. X-ray quality single crystals of all the four aroylhydrazones were grown and their molecular structures were established by single crystal X-ray diffraction studies. The single crystal X-ray diffraction studies of the compounds reveal that aroylhydrazones exist in amido form in the solid state.

The aroylhydrazones synthesized are

- 1) 4-benzyloxy-2-hydroxybenzaldehyde-4-nitrobenzoylhydrazone dimethylformamide monosolvate ($\text{H}_2\text{L}^1 \cdot \text{C}_3\text{H}_7\text{NO}$)
- 2) 5-bromo-2-hydroxy-3-methoxybenzaldehyde nicotinoylhydrazone dihydrate methanol monosolvate ($\text{H}_2\text{L}^2 \cdot 2\text{H}_2\text{O} \cdot \text{CH}_3\text{OH}$)
- 3) 4-diethylamino-2-hydroxybenzaldehyde nicotinoylhydrazone monohydrate ($\text{H}_2\text{L}^3 \cdot \text{H}_2\text{O}$)
- 4) 2-benzoylpyridine-4-nitrobenzoylhydrazone (HL^4)

Chapter 3

Chapter 3 discusses the syntheses and characterization of seven oxidovanadium(IV) complexes with ONO donor aroylhydrazones. These include three binuclear oxidovanadium(IV) complexes and four mononuclear mixed ligand chelates with heterocyclic bases like 1,10 phenanthroline, 2,2'-bipyridine, 3-picoline and pyridine as coligands. All the complexes are characterized by various physico-chemical methods such as elemental analyses, molar conductivity studies, magnetic susceptibility measurements, FT-IR, UV-Vis and EPR spectral studies. In all the complexes, hydrazones are coordinated to the metal centre in the iminolate form and hence act as dideprotonated tridentate ligands as evidenced from the shift of characteristic IR bands of the complexes from the proligands. Magnetic susceptibility measurements clearly indicate that all the complexes are paramagnetic in nature with vanadium in +4 oxidation state. Some complexes exhibit subnormal magnetic moments due to the strong antiferromagnetic exchange, suggesting dimeric nature of these complexes. In the EPR spectra, the g values are typically less than the free electron value and in DMF at 77 K, they displayed well resolved axial anisotropy with two sets of eight line pattern with $g_{\parallel} < g_{\perp}$ and $A_{\parallel} > A_{\perp}$ relationship characteristic of an axially compressed d_{xy}^1 configuration.

Chapter 4

This chapter deals with the syntheses and characterization of five cobalt(II) complexes of aroylhydrazones. The coligands used here are heterocyclic bases like 3-picoline and pyridine. The complexes are characterized by elemental analyses, molar conductivity studies, magnetic susceptibility

measurements, thermogravimetric analyses, FT-IR and electronic spectral studies. In all the complexes, the tridentate hydrazones are coordinated to metal in the iminolate form which was well supported by IR spectral data. All the complexes are found to be non-electrolytic in nature. Magnetic susceptibility measurements indicate that all the complexes are paramagnetic with cobalt in the +2 oxidation state.

Chapter 5

Chapter 5 describes the syntheses of five nickel(II) complexes followed by their characterization using various physico-chemical techniques such as elemental analyses, molar conductivity studies, magnetic susceptibility measurements, thermogravimetric analyses, FT-IR and electronic spectral studies and single crystal X-ray diffraction studies. The IR spectral studies show that aroylhydrazones coordinate in the iminolate form in all the complexes and act as dideprotonated tridentate ligands. All the complexes are found to be paramagnetic excluding the possibility of square planar geometry. One of the complexes was recrystallized from a mixture of methanol and dimethylformamide (1:1 v/v) and the dimeric complex has a distorted octahedral geometry.

Chapter 6

Chapter 6 explains the syntheses of five copper(II) complexes along with their characterization using various physico-chemical techniques including elemental analyses, molar conductivity studies, magnetic susceptibility measurements, FT-IR, EPR, electronic spectral studies and thermal analyses. Heterocyclic bases like 3-picoline and pyridine were used as coligands. In all the complexes the hydrazone exists in iminolate form and gets coordinated

through azomethine nitrogen, phenolate oxygen and iminolate oxygen. The magnetic susceptibility measurements reveal that all the complexes are paramagnetic. Some complexes have low the magnetic moment values indicating their dimeric nature. EPR spectra of the complexes were taken in polycrystalline state at 298 K and in frozen DMF at 77 K. The $g_{\parallel} > g_{\perp} > 2.0023$ indicate that the unpaired electron in Cu(II) resides in the $d_{x^2-y^2}$ orbital. The g_{\parallel} values in all these complexes are less than 2.3 which is an indication of covalent character for M–L bond in these complexes.

Chapter 7

Chapter 7 includes the syntheses and characterization of some zinc and cadmium complexes of aroylhydrazones. Five Zn(II) and five Cd(II) complexes have been synthesized and characterized by conductivity studies, magnetic susceptibility measurements, thermal analyses, infrared and electronic spectral studies and single crystal X-ray diffraction studies. In one of the complexes the hydrazone moiety is coordinated in the amido form while in others it is in the iminolate form as evidenced from IR spectral data. One of the zinc complexes was crystallized in monoclinic space group $P2_1/c$ and the Zn(II) complex has a distorted octahedral geometry. The disposition of the two ligand moieties is in such a way that the meridional isomer is obtained. The structure of one of the cadmium complexes has been resolved using single crystal X-ray diffraction studies. The Cd(II) complex crystallizes into a monoclinic space group $P2_1/n$. The complex adopts a distorted square pyramidal geometry with pyridyl nitrogen, azomethine nitrogen and ketoxy oxygen atom of the principal ligand and one of the Br atoms from the metal salt occupying the square plane and the other Br atom of metal salt occupying the axial position.

Chapter 8

Chapter 8 explains the syntheses and characterization of four dioxidomolybdenum(VI) complexes. The characterization techniques include elemental analyses, molar conductivity studies, magnetic susceptibility measurements, thermal analyses, infrared and electronic spectral studies and single crystal X-ray diffraction studies. All the complexes are non-electrolytic as well as diamagnetic in nature. The molecular structure of one of the complexes has been resolved using single crystal X-ray diffraction studies. The coordination geometry around molybdenum is distorted octahedral in which the tridentate ligand coordinates to the metal in a meridional fashion forming five membered and six membered metallocycles involving the MoO_2^{2+} moiety. Phenolate oxygen, azomethine nitrogen and iminolate oxygen of the ligand and one of the terminal oxo atoms occupy the equatorial positions of the complex. The axial positions are occupied by the other terminal oxygen and oxygen atom of the solvent, N,N-dimethylformamide. The DMF molecule is weakly coordinated to the MoO_2 core and this position holds the possibility of functioning as a substrate binding site.

Chapter 9

Chapter 9 discusses the nonlinear optical studies of synthesized aroylhydrazones and transition metal complexes of 4-benzyloxy-2-hydroxybenzaldehyde-4-nitrobenzoylhydrazone dimethylformamide monosolvate. The second harmonic generation studies of the compounds were carried out using Kurtz and Perry powder technique. In this experiment, Q-switched pulses were obtained from a Q-switched Nd: YAG laser of fundamental wavelength 1064 nm and the SHG efficiency of the sample was evaluated by

taking the microcrystalline powder of KDP as the reference material. The output from the sample was monochromated to collect the intensity of 532 nm components and the fundamental was eliminated. Only $\text{H}_2\text{L}^1\cdot\text{C}_3\text{H}_7\text{NO}$, $[\text{CdL}^1(\text{H}_2\text{O})]_2$, $[\text{CdL}^1\text{pic}]$ and $[\text{CdL}^1\text{py}]$ are found to possess SHG activity. The results indicate that the second harmonic generation efficiency of $\text{H}_2\text{L}^1\cdot\text{C}_3\text{H}_7\text{NO}$ is about 4.40 times that of potassium dihydrogen phosphate (KDP). The second harmonic generation efficiency of $[\text{CdL}^1(\text{H}_2\text{O})]_2$, $[\text{CdL}^1\text{pic}]$, $[\text{CdL}^1\text{py}]$ are 0.87, 0.92 and 0.95 times respectively that of KDP.

..........

Abbreviations

H ₂ L ¹	4-benzyloxy-2-hydroxybenzaldehyde-4-nitrobenzoylhydrazone
H ₂ L ²	5-bromo-2-hydroxy-3-methoxybenzaldehyde nicotinoylhydrazone
H ₂ L ³	4-diethylamino-2-hydroxybenzaldehyde nicotinoylhydrazone
HL ⁴	2-benzoylpyridine-4-nitrobenzoylhydrazone
bipy	2,2'-bipyridine
phen	1,10-phenanthroline
pic	3-picoline
py	pyridine
DMF	N,N-dimethylformamide
Complex 1	[(VOL ¹) ₂]
Complex 2	[VOL ¹ pic]
Complex 3	[VOL ¹ py]
Complex 4	[(VOL ²) ₂]
Complex 5	[VOL ² phen]
Complex 6	[VOL ² bipy]
Complex 7	[(VOL ³) ₂]
Complex 8	[(CoL ¹) ₂]
Complex 9	[CoL ¹ pic]
Complex 10	[CoL ¹ py]·2H ₂ O
Complex 11	[(CoL ²) ₂]·2H ₂ O
Complex 12	[(CoL ³) ₂]·4H ₂ O
Complex 13	[NiL ¹ (H ₂ O) ₂] ₂ ·4C ₃ H ₇ NO
Complex 14	[NiL ¹ pic]
Complex 15	[NiL ¹ py]
Complex 16	[(NiL ²) ₂]·H ₂ O
Complex 17	[(NiL ³) ₂]
Complex 18	[(CuL ¹) ₂]
Complex 19	[CuL ¹ pic]
Complex 20	[CuL ¹ py]

Complex 21	$[(\text{CuL}^2)_2] \cdot 2\text{H}_2\text{O}$
Complex 22	$[(\text{CuL}^3)_2]$
Complex 23	$[(\text{ZnL}^1)_2]$
Complex 24	$[\text{ZnL}^1\text{pic}]$
Complex 25	$[\text{ZnL}^1\text{py}]$
Complex 26	$[(\text{ZnL}^2)_2] \cdot \text{H}_2\text{O}$
Complex 27	$[\text{Zn}(\text{L}^4)_2] \cdot 0.5\text{CH}_3\text{OH} \cdot 0.5\text{CH}_3\text{CH}_2\text{OH}$
Complex 28	$[\text{CdL}^1(\text{H}_2\text{O})_2]$
Complex 29	$[\text{CdL}^1\text{pic}]$
Complex 30	$[\text{CdL}^1\text{py}]$
Complex 31	$[(\text{CdL}^2)_2] \cdot \text{H}_2\text{O}$
Complex 32	$[\text{Cd}(\text{HL}^4)\text{Br}_2] \cdot \text{C}_3\text{H}_7\text{NO}$
Complex 33	$[(\text{MoO}_2\text{L}^1)_2]$
Complex 34	$[\text{MoO}_2\text{L}^1\text{DMF}]$
Complex 35	$[(\text{MoO}_2\text{L}^2)_2] \cdot 2\text{H}_2\text{O}$
Complex 36	$[(\text{MoO}_2\text{L}^3)_2]$

..........

Curriculum Vitae



Bibitha Joseph

Email: bibithajosephbj@gmail.com

bibitha2004@yahoo.co.in

Mob: 9961617875

Areas of Interest: Teaching and Research

Academic Profile

Pursuing Ph. D. (Inorganic Chemistry)
(2009-present)
Area of research – Coordination Chemistry
Supervising guide – Prof. M.R. Prathapachandra Kurup
Department of Applied Chemistry
Cochin University of Science & Technology, Kochi.

M.Sc. (2002-2004)
School of Chemical Sciences
Mahatma Gandhi University, Kerala.
Percentage of marks – 73.4%

B.Sc. (1999- 2002)
Devamatha College, Kuravilangad
Mahatma Gandhi University, Kerala.
Percentage of marks – 89.8%

Pre-Degree (1997- 1999)
Devamatha College, Kuravilangad
Mahatma Gandhi University, Kerala.
Percentage of marks – 77.4%

S.S.L.C (1997)
St. Mary's G.H.S., Kuravilangad, Kerala
Percentage of marks – 84.66%

Achievements

Qualified CSIR-JRF - 2008 December

Work Experience

- February 2005 - November 2007
Organization : Hulhudhuffaaruu School, Republic of Maldives
Designation : Chemistry Teacher
- July 2008 – June 2009
Organization : Devamatha College, Kuravilangad
Designation : Guest Lecturer

Research Experience

- Nearly five years of research experience in the field of coordination chemistry

Professional Skills

- Familiar with MS Office
- Familiar with chemistry software packages like ChemsSketch, Origin, EPR simulation packages
- Familiar with crystallographic softwares
- Experienced in using instruments like UV-Vis spectrometer, FT-IR spectrometer, Thermogravimetric analyzer, Gouy balance etc.

Personal Profile

Father's name : Joseph Mathew
Husband's name : Gilson Scaria
Date of Birth : 26th February 1982
Nationality : Indian
Gender : Female
Marital Status : Married

Permanent address

Purackal
Kuravilangad P.O.
Kottayam – 686633

Contact address

Pottananiyil
Malipara P.O.
Kothamangalam-686691

Paper Published

- N'-[(E)-4-Benzyloxy-2-hydroxybenzylidene]-4-nitrobenzohydrazide monohydrate, Bibitha Joseph, M. Sithambaresan and M. R. P. Kurup, Acta Cryst. (2012), E68, o1421–o1422.
- N'-[(E)-4-Benzyloxy-2-hydroxybenzylidene]-4-nitrobenzohydrazide dimethylformamide monosolvate, Bibitha Joseph, M. Sithambaresan and M. R. P. Kurup, Acta Cryst. (2013), E69, o1160–o1161.

3. Syntheses, spectral characterization and structure of a zinc(II) complex of 2-benzoylpyridine-4-nitrobenzoylhydrazone , J. Bibitha, M.C. Vineetha, M.R.P. Kurup and Babu Varghese, 23rd Swadeshi Science Congress-2013, 164.
4. Syntheses and spectroscopic characterization of novel transition metal complexes with a tridentate aroylhydrazone, J. Bibitha and M.R.P. Kurup, 23rd Swadeshi Science Congress-2013, 179.
5. Bis { μ -N-[(E)-4-benzyloxy-2-oxidobenzylidene]-4-nitrobenzenecarbohydrazidato} bis[diaquanickel(II)] dimethylformamide tetrasolvate, Bibitha Joseph, M. Sithambaresan, M. R. P. Kurup and Seik Weng Ng, Acta Cryst. (2014), E70, m211-m212.

Conferences

1. Participated in the International Conference on Materials for the New Millennium (MATCON-2010), held at the Department of Applied Chemistry, Cochin University of Science and Technology, Kochi-22 during 10-13 January 2010.
2. Participated in the National Conference “Current Trends in Chemistry” (CTriC-2012) held at the Department of Applied Chemistry, Cochin University of Science and Technology, Kochi during 20-21 January 2012.
3. Participated and presented a poster in the National Conference “Current Trends in Chemistry” (CTriC-2013) held at the Department of Applied Chemistry, Cochin University of Science and Technology, Kochi during 22-23 March 2013.
4. Participated and presented a paper in the 23rd Swadeshi Science Congress. held at the Department of Applied Chemistry, M. G. University, Kottayam during 6-8 November 2013.
5. Participated and presented a poster in the International Conference ICEFCC 2014 held at the All Saints’ College, Thiruvananthapuram during 17-18 February 2014.
6. Participated and presented a poster in the National Conference “Current Trends in Chemistry” (CTriC-2014) held at the Department of Applied Chemistry, Cochin University of Science and Technology, Kochi during 22-23 March 2014.